



University of Tennessee, Knoxville  
**TRACE: Tennessee Research and Creative  
Exchange**

---

Doctoral Dissertations

Graduate School

---

5-2022

## Cat COVID, CMV and Chemokines, Oh My!

Trevor Hancock

*University of Tennessee, Knoxville*, [thancoc5@vols.utk.edu](mailto:thancoc5@vols.utk.edu)

Follow this and additional works at: [https://trace.tennessee.edu/utk\\_graddiss](https://trace.tennessee.edu/utk_graddiss)



Part of the [Immunopathology Commons](#), [Pathogenic Microbiology Commons](#), [Virology Commons](#), and the [Virus Diseases Commons](#)

---

### Recommended Citation

Hancock, Trevor, "Cat COVID, CMV and Chemokines, Oh My!". " PhD diss., University of Tennessee, 2022. [https://trace.tennessee.edu/utk\\_graddiss/7185](https://trace.tennessee.edu/utk_graddiss/7185)

This Dissertation is brought to you for free and open access by the Graduate School at TRACE: Tennessee Research and Creative Exchange. It has been accepted for inclusion in Doctoral Dissertations by an authorized administrator of TRACE: Tennessee Research and Creative Exchange. For more information, please contact [trace@utk.edu](mailto:trace@utk.edu).

To the Graduate Council:

I am submitting herewith a dissertation written by Trevor Hancock entitled "Cat COVID, CMV and Chemokines, Oh My!". I have examined the final electronic copy of this dissertation for form and content and recommend that it be accepted in partial fulfillment of the requirements for the degree of Doctor of Philosophy, with a major in Microbiology.

Tim E. Sparer, Major Professor

We have read this dissertation and recommend its acceptance:

Todd B. Reynolds, Jonathan Wall, Sarah Lebeis, Jeremiah G. Johnson

Accepted for the Council:

Dixie L. Thompson

Vice Provost and Dean of the Graduate School

(Original signatures are on file with official student records.)

# **Cat Covid, CMV and Chemokines, Oh My!**

A Dissertation Presented for the  
Doctor of Philosophy  
Degree  
The University of Tennessee, Knoxville

Trevor J. Hancock  
May 2022

Copyright © 2022 by Trevor J. Hancock  
All rights reserved.

## ACKNOWLEDGEMENTS

There are many people outside the university without whom I would likely not have reached this point today. I would like to thank my friends and family. My parents for instilling a drive to succeed and apply myself to the best of my abilities, and always being there for me. I must thank my wife Elizabeth Hancock for her support throughout my graduate career. She has seen the highs and lows that come with this process, and always encouraged me to stay the course. She has endured late days and long distance, and “I need to go to work for 30 minutes” turning into 3 hours of unexpected experiments. She has graciously handled it all, and I do not know where I’d be without her.

I have a lot of gratitude for my boss, Dr. Tim Sparer, for his mentorship and the opportunity to work in his lab. Tim, your passion for the field and emphasis on scientific rigor/controls has shaped me into the scientist I am today. You allowed me the space to explore and learn new ideas, make mistakes, and grow as an independent researcher. I am grateful for the opportunity to work for you and the friendship we have developed. My committee members (Doctors Todd Reynolds, Sarah Lebeis, Jon Wall, and Jeremiah Johnson) have also been an invaluable asset throughout my tenure. They have provided all kinds of assistance and insight, as well as friendship and support. I thank them all for taking me on and freely giving their time.

Over the years in the Sparer lab, we have had a veritable army of undergraduates volunteer their time and energy. All of their contributions were appreciated, but I would like to especially highlight and thank Madison Keelty, Andrea Ramirez, and Peyton Hickman. You helped lessen the burden and set a great example for others who followed. I must also thank my fellow former Sparer lab member, Dr. Joseph Jackson. You played an instrumental role in my graduate career. You helped train me, challenged me, and became a great friend. I appreciate all that you have done for me both during your tenure at UT and after. To my current Sparer lab mate, Morgan thank you for helping finish out my tenure at UT. I look forward to seeing the scientist you develop into.

The Johnson lab has been close to the Sparer lab since inception, and I want to thank Sean Callahan and Dr. Brittni Kelley for always being there and being supportive

friends. The same applies to Andy Wagner and Bridget O'Banion. You have both been there from day one at UT, and require special acknowledgement for commiserating with me, spit balling crazy ideas, and helping keep me sane. Dr. Tom Masi is a wealth of knowledge, and I am indebted to him for educating me on protein production and purification. I need to thank my mentors from Lipscomb University for helping provide the scientific foundation I built upon at UT. Doctors Kent Gallaher, Bonny Millimaki, and Jon Lowrance; you each provided valuable mentorship from teaching philosophy, research approach, and fortitude. You helped set me on the path to where I am today and cultivated the skills and mindset to succeed.

## ABSTRACT

Cytomegalovirus (CMV) is an important pathogen infecting most humans worldwide. CMV infection within immunocompromised individuals can cause severe morbidity and potential mortality. Disease during CMV infection is due to virus dissemination and subsequent inflammation. Host immune cells lie at the intersection potentially mediating both. The CMV-encoded viral chemokine vCXCL-1 is a proposed virulence factor in mouse models increasing immune cell recruitment and disease. However, the primary immune cell mediator is undetermined. To identify targets, Chapter 2 examines CXCR2 expression (receptor for vCXCL-1) among various mouse tissues and human peripheral blood under steady-state conditions. *In vitro*, isoforms of HCMV's vCXCL-1 induce differential outcomes even when acting upon the same cells/receptors (termed functional selectivity), the *in vivo* consequences of which are unknown. In Chapter 3, recombinant MCMVs expressing vCXCL-1 *in vivo*, as well as purified chemokine *in vitro*, and protein modeling *in silico* help further characterize functional differences between viral and host chemokines. We additionally identified a conserved, unique region within the C-terminus of vCXCL-1. These observations provide the basis for future studies of CMV pathogenesis.

Following recruitment to a site of infection, viral uptake occurs infecting migrated cells. Prevention of viral entry is an attractive therapeutic target to lessen viral burden and disease. However, there are limitations in relating *in vitro* assays to *in vivo*, as MCMV derived *in vivo* displays altered entry phenotypes rendering attachment and entry inhibitors less effective. In Chapters 4 and 5 we further characterized differences between *in vitro* and *in vivo* derived MCMV. In Chapter 4, *in vitro* and *in vivo* virus display different dependencies on cell surface heparan sulfate proteoglycans (HS) for attachment, with *in vivo* virus less dependent on HS and potentially utilizing different moieties. Chapter 5 further demonstrates *in vivo* virus' reduced HS interaction. *In vivo* virus was additionally found to be of a uniform size and contain submicron particle distributions (potentially extracellular vesicles) different from *in vitro* derived virus. While submicron particles did

not appear to play a role to enhance infection *in vitro*, their exact role is unknown. These advances can hopefully better inform development of anti-CMV therapeutics.

## TABLE OF CONTENTS

|   |    |
|---|----|
| Chapter 1 - Introduction.....   | 1  |
| Abstract.....   | 2  |
| Cytomegalovirus Background .....  | 2  |
| Clinical Disease Characteristics.....   | 3  |
| CMV Treatment .....   | 4  |
| Animal Models of CMV .....  | 5  |
| Cytomegalovirus Viral Chemokines and Receptors .....                            | 6  |
| Viral Chemokine Receptors .....   | 6  |
| Viral Chemokine vIL-10.....   | 9  |
| Dual-function Viral Chemokines UL128 and UL130 .....                            | 9  |
| The alpha-chemokines UL146 and UL147.....                                       | 10 |
| Neutrophils and their Relationship to Cytomegalovirus Infections.....           | 12 |
| Neutrophil Recruitment to Sites of Infection.....                               | 15 |
| Neutrophil Recognition of Virally Infected Cells.....                           | 16 |
| Typical Neutrophil Functions .....  | 16 |
| Neutrophils as Antigen Presenting Cells .....                                   | 18 |
| Neutrophils Call the Shots: Influencing Follow-up Responses .....               | 19 |
| Protection vs. Pathogenesis.....  | 21 |
| Neutrophils Enhancing Viral Dissemination .....                                 | 23 |
| Trogoctosis/Trogoptosis as a Potential Viral Uptake Mechanism.....              | 24 |
| Reverse Transmigration .....  | 25 |
| Neutrophil-Mediated Enhancement of Infection .....                              | 26 |
| Conclusion .....  | 29 |
| References.....   | 32 |
| Chapter 2 - Immunophenotyping cxcr2 expression across a variety of immune cells |    |
| Derived from various tissues .....  | 52 |
| Abstract: .....   | 53 |
| Introduction:.....  | 53 |
| Results:.....   | 56 |

|   |     |
|---|-----|
| Discussion: .....   | 60  |
| Materials and Methods:.....   | 65  |
| IACUC and IRB approval.....   | 65  |
| Isolation of cells from murine tissues .....  | 65  |
| Isolation of human peripheral blood cells.....  | 65  |
| Staining cells and flow cytometry.....  | 66  |
| Statistics .....  | 66  |
| References.....   | 68  |
| Chapter 3 - Functional and Structural Characteristics of <i>ULI46</i> from Distinct Human               |     |
| CMV Strains .....   | 74  |
| Abstract.....   | 75  |
| Introduction.....   | 76  |
| Results.....  | 78  |
| Discussion.....   | 89  |
| Materials and Methods.....  | 94  |
| Cells and Viruses .....   | 94  |
| Animals.....  | 95  |
| Production and Purification of Recombinant Chemokines.....  | 95  |
| Anti-Chemokine ELISAs.....  | 96  |
| Western Blots.....  | 96  |
| Isothermal Titration Calorimetry .....  | 97  |
| Protein Structural Prediction.....  | 97  |
| Protein Alignments .....  | 97  |
| Statistics .....  | 97  |
| Acknowledgements.....   | 98  |
| References.....   | 99  |
| Chapter 4 - Heparan sulfate utilization differs between <i>in vivo</i> and <i>in vitro</i> derived mcmv |     |
| .....   | 105 |
| Abstract:.....  | 106 |
| Introduction:.....  | 106 |

|   |     |
|---|-----|
| Results:.....   | 109 |
| Discussion: .....   | 116 |
| Materials and Methods:.....   | 120 |
| Cells and viruses: .....  | 120 |
| Flow cytometry detection of infection.....                                | 120 |
| Plaque assays .....   | 121 |
| CRISPR-Cas9 generation of HS mutants .....                                | 121 |
| Animals.....  | 122 |
| Statistics .....  | 122 |
| References.....   | 123 |
| Chapter 5 - MCMV Centrifugal Enhancement: A New Spin on an Old Topic..... | 129 |
| Abstract: .....   | 130 |
| Introduction:.....  | 130 |
| Results:.....   | 134 |
| Discussion .....  | 146 |
| Methods: .....  | 153 |
| Cells and Viruses .....   | 153 |
| Animals.....  | 153 |
| Plaque Assays and Centrifugal Enhancement.....                            | 154 |
| Flow Virometry.....   | 154 |
| Exosome Inhibition.....   | 155 |
| Statistics .....  | 155 |
| References.....   | 156 |
| Chapter 6 - Conclusions and Recommendations .....                         | 164 |
| Conclusions.....  | 165 |
| Chapter 2.....  | 165 |
| Chapter 3.....  | 165 |
| Chapter 4 & 5.....  | 166 |
| Future Directions .....   | 166 |
| CXCR2 Expression.....   | 166 |

|  |     |
|--|-----|
| vCXCL-1's Role in CMV Infection .....  | 167 |
| vCXCL-1 C-terminus function and CXCR2 interaction .....  | 168 |
| Viral Entry of TCV and SGV .....   | 168 |
| References .....   | 170 |
| Appendix - Possible Cross Reactivity of Feline and White-tailed Deer Samples Towards<br>the RBD of SARS-CoV-2..... | 173 |
| Abstract.....  | 174 |
| Importance .....   | 175 |
| Introduction.....  | 175 |
| Materials and methods .....  | 179 |
| Recombinant RBD production and purification .....  | 179 |
| Serum and Plasma samples.....  | 180 |
| Anti-RBD ELISA.....  | 181 |
| Western and dot blots.....   | 182 |
| Neutralization assays .....  | 182 |
| Fecal coronavirus PCR screen and sequence alignments .....   | 183 |
| Statistics .....   | 184 |
| Results.....   | 184 |
| Discussion.....  | 195 |
| Limitations of this study .....  | 203 |
| Conclusion .....   | 203 |
| Acknowledgments.....   | 204 |
| References.....  | 205 |
| Vita.....  | 212 |

## LIST OF TABLES

|  |     |
|--|-----|
| <b>Table A.1:</b> Characteristics of Feline Samples.....       | 189 |
| <b>Table A.2:</b> Fecal Coronavirus Screening Information..... | 196 |

## LIST OF FIGURES

|  |     |
|--|-----|
| <b>Figure 1.1:</b> CMV viral chemokine and chemokine receptor immune manipulation. ....  | 7   |
| <b>Figure 1.2:</b> Neutrophil recruitment and effector functions. ....   | 14  |
| <b>Figure 1.3:</b> Potential hijacking of neutrophil functions for CMV gain. ....  | 28  |
| <b>Figure 2.1:</b> CXCR2 expression in various mouse tissues. ....   | 59  |
| <b>Figure 2.2:</b> CXCR2 expression in human peripheral blood. ....  | 61  |
| <b>Figure 3.1:</b> Characterization of a recombinant MCMV expressing vCXCL-1 from the<br>Towne strain of HCMV. ....                    | 79  |
| <b>Figure 3.2:</b> Recombinant MCMV's expressing vCXCL-1's differentially affect virulence<br>in immunocompromised mice. ....          | 81  |
| <b>Figure 3.3:</b> Alignments of HCMV vCXCL-1's reveals extended C-terminus. ....  | 83  |
| <b>Figure 3.4:</b> Expression of recombinant chemokines using <i>Pichia pastoris</i> . ....  | 84  |
| <b>Figure 3.5:</b> vCXCL-1 <sub>Toledo</sub> has diminished heparin binding. ....  | 86  |
| <b>Figure 3.6:</b> <i>Ab initio</i> modeling of vCXCL-1 from Toledo and Towne strains of HCMV.<br>.....                                | 88  |
| <b>Figure 3.7:</b> Extended C-terminus of vCXCL-1 <sub>Toledo</sub> and vCXCL-1 <sub>Towne</sub> is not present in<br>host CXCL8. .... | 90  |
| <b>Figure 3.8:</b> CXCR2 chemokine ligand models. ....   | 91  |
| <b>Figure 4.1:</b> MCMV Entry is HS-dependent, irrespective of viral MCK2 status. ....   | 110 |
| <b>Figure 4.2:</b> Fibroblasts with HS mutations point to variable HS utilization by TCV and<br>SGV. ....                              | 112 |
| <b>Figure 4.3:</b> Sulfation and negative charge on HS chains are responsible for MCMV<br>infection. ....                              | 113 |
| <b>Figure 4.4:</b> HS mutants alter entry kinetics. ....   | 115 |
| <b>Figure 4.5:</b> SGV has lowered affinity/attachment to fibroblasts. ....  | 117 |
| <b>Figure 4.6:</b> Loss of HS leads to equal attachment for TCV and SGV. ....  | 118 |
| <b>Figure 5.1:</b> Centrifugal enhancement is predominantly an in vitro phenotype. ....  | 136 |
| <b>Figure 5.2:</b> Centrifugal enhancement relies upon heparan sulfate proteoglycans and is<br>MCK2/endocytosis independent. ....      | 137 |

|  |     |
|--|-----|
| <b>Figure 5.3:</b> Enhancement is not due to >200 nm particles. ....                                     | 139 |
| <b>Figure 5.4:</b> Flow virometry of MCMV identifies distinct TCV vs. SGV particle<br>distributions..... | 140 |
| <b>Figure 5.5:</b> MCMV infection alters MEF 10.1-secreted extracellular vesicles (EVs). .               | 142 |
| <b>Figure 5.6:</b> In vivo MCMV infection alters EV composition within the salivary gland.<br>.....      | 143 |
| <b>Figure 5.7:</b> TCV and SGV differ in extracellular particle composition. ....                        | 145 |
| <b>Figure 5.8:</b> Exosome inhibition alters EVs produced by uninfected MEF 10.1 cells....               | 147 |
| <b>Figure 5.9:</b> Exosome inhibition does not impact centrifugal enhancement.....                       | 148 |
| <b>Figure A.1:</b> Anti-SARS-CoV-2 ELISA Sensitivity and Specificity.....                                | 186 |
| <b>Figure A.2:</b> Pre-Pandemic Feline Antibodies Cross-React with SARS-CoV-2<br>RBD.....                | 188 |
| <b>Figure A.3:</b> Dog Serum Cross-reacts to a Co-Purified Protein.....                                  | 191 |
| <b>Figure A.4:</b> Serological Testing of Other Regional Animals.....                                    | 192 |
| <b>Figure A.5:</b> Neutralization Assays.....  | 194 |
| <b>Figure A.6:</b> Pan Coronavirus Screen of East Tennessee Felines.....                                 | 197 |
| <b>Figure A.7:</b> RBD Coronavirus Screen of East Tennessee Felines.....                                 | 198 |

# **CHAPTER 1 - INTRODUCTION**

This work was performed by: Trevor J. Hancock and Tim E. Sparer

Author Contributions: Conceptualization, T.E.S. and T.J.H.; Writing—original draft preparation, T.J.H.; Writing—review and editing, T.E.S. and T.J.H.; Visualization, T.J.H.; Funding Acquisition, T.E.S.

### **Abstract**

Cytomegalovirus (CMV) is a ubiquitous and important pathogen infecting a majority of adults. Like all herpesviruses, CMVs are highly evolved and adapted to their host species, establishing latency and maintaining life-long infection of its host. CMV's immune manipulation is important for both acute and latent infections. CMV-encoded homologs of host chemokines and chemokine receptors carry out a portion of this immune manipulation. These viral chemokines and chemokine homologs are important for establishing and maintaining latency as well as enhancing viral spread from the initial site of infection *in vivo*. A prime target for both of these strategies are the cells of the myeloid lineage (i.e., neutrophils, monocytes/macrophages, and dendritic cells). While these cells can, and typically do, perform host-protective functions, contributing to clearance of viral infections, CMVs utilize cells of the myeloid lineage as viral shuttles and sites of latency. For the purposes of this review, we focus on the role of neutrophils in CMV infections, as well as how CMV subverts their natural immune function for pro-viral outcomes.

### **Cytomegalovirus Background**

The virus responsible for causing cytomegalic inclusion disease (CID) of human salivary glands was isolated by Margaret Smith in 1956 and subsequently named human cytomegalovirus (HCMV) [1], with a murine counterpart (MCMV) identified and isolated 2 years later. This initial isolate of MCMV is still in modern day use as the Smith strain of MCMV [2]. As a member of the herpesvirus family, it shares many structural and genetic similarities to herpes simplex virus (HSV). Both are similarly sized (~150-200nm) enveloped viruses with a large dsDNA genome conferring a large coding potential [3-5]. Like many herpesviruses, HCMV is spread by contact with infected bodily secretions [5]. CMVs are highly adapted to their host, resulting in species-specificity for all CMVs [5].

This species-specificity is due to differences in viral manipulation of programmed cell death pathways, and differences in the regulation of these processes among mammalian species [6, 7]. This intimate relationship between the virus and host allows CMVs to establish a lifelong infection, undergoing latency with sporadic periods of reactivation [8]. Unlike viruses such as human immunodeficiency virus (HIV), CMVs do not integrate into the host genome to establish latency [8]. Instead, viral latency is likely achieved by epigenetic silencing of lytic genes, with reactivation induced by re-expression of them [8]. Because of its nuanced control of host processes at both the cellular and tissue/organ level, CMV has earned the moniker “master immune-manipulator.”

### *Clinical Disease Characteristics*

HCMV infects roughly 40-90% of adults worldwide with seropositivity rates influenced by factors such as socio-economic status, age, and sex [5, 9, 10]. Infection in many instances is asymptomatic with mild to no illness [5]. Individuals are typically exposed as youths from either shedding family members or childcare centers [11], and seronegative adults are often infected after having children, with additional children increasing the likelihood [12]. Maternal transfer of CMV represents one of the most significant sources of CMV disease, resulting in congenital infection and disorders [13-15]. In America, 1 in 200 neonates are congenitally infected with a further 1 in 5 developing long-term sequelae [13-15]. Congenital CMV induces a variety of symptoms, but typically manifests as neurological issues such as sensorineural hearing loss and intellectual disabilities, in spite of not infecting neurons [13-15]. Congenital CMV transmission rates are dependent on previous exposure, with infection of seronegative mothers more likely to cause severe congenital disease [15]. Along with serostatus, timing of infection is thought to influence the occurrence of congenital disease [15]. Infections during the first trimester are associated with increased incidence of congenital disorders [15]. While an important susceptible population for CMV-induced disease, neonates and pregnant women are not the only population at risk of CMV-induced disease.

Immunosuppressed individuals such as those undergoing chemotherapy, late-stage HIV/AIDS patients, and organ transplant recipients are also highly susceptible to CMV

disease [5, 16, 17]. Disease can be induced by either primary infection or reactivation of latent virus [5, 8]. Immunosuppressive treatment during chemotherapy allows for reactivation of latent CMV, and subsequent viral replication results in tissue/organ damage [5, 18]. Similarly, loss of T cells in late-stage AIDS stops adaptive immune cell control of CMV-replicative cells enabling reactivation [19]. For both solid organ transplantation and hematopoietic stem cell transplantation, serostatus of donor and recipient is considered [17, 20]. Solid organ recipients that are seronegative and receiving an organ from seropositive individual have the greatest risk of developing disease [17]. Reactivation or transfer of infection from seropositive organs, can result in transplant rejection and death [17]. As a result of the potential transplant rejection and mortality, CMV antiviral prophylaxis is widely adopted to control viral replication [20]. With hematopoietic stem cell transplantation, seropositive donor/seronegative recipient (D+/R-) has been associated with the worst clinical outcomes followed by seropositive donor/recipient (D+/R+) [20]. Along with the potential for transfer of infection from CMV+ donor to recipient, CMV+ hematopoietic transplants have an increased risk of developing complications such as graft vs host disease (GVHD) [20]. The profound effects of CMV disease within susceptible individuals provides the rationale for development of effective and minimally toxic CMV antivirals and vaccines.

### ***CMV Treatment***

There is currently no clinically approved vaccine for HCMV. As such, treatment centers around one of four FDA-approved antiviral compounds (i.e., cidofovir, ganciclovir, letermovir, and foscarnet). While effective in many instances (such as immunosuppressed adults and prophylaxis of organ transplant recipients), poor oral availability, severe cytotoxic side effects, and antiviral resistance have been documented with many of these drugs limiting their use [21]. Additionally, none of these drugs can be used to treat or prevent congenital infections. In order to better protect susceptible populations, development of effective CMV vaccines is a high priority [22]. However, recent efforts have highlighted the difficulty of CMV vaccine development. A subunit vaccine developed against the fusion protein of HCMV (gB) showed initial promise to reduce maternal

transmission by producing high titers of anti-gB antibodies and was ~40-50% efficacious at reducing primary infection of women [23, 24]. Unfortunately, this was not sufficient to secure FDA approval [25]. However, anti-gB based vaccines may provide some promise for CMV disease associated with organ transplantation, reducing viral load and duration within the highest risk group [26]. These successes have revived interest and paved the way for over 10 additional potential vaccines currently in Phase I or II clinical trials [27]. Indeed, Moderna developed an mRNA vaccine for use against CMV, laying the foundation for SARS-CoV-2 vaccine trials [28]. Unfortunately, rapid development of antivirals and study of *in vivo* processes is complicated by the species-specificity of CMVs. Consequently, there exists a plethora of model systems to study general CMV processes *in vivo* and extrapolate these conclusions back to HCMV infections and disease.

### ***Animal Models of CMV***

Owing to the species-specific nature of CMVs, animal models of CMV are commonly utilized to evaluate *in vivo* functions. The most utilized system is the mouse model and MCMV [29, 30]. Mouse models are a particularly attractive system owing to the high availability of diverse and flexible host genotypes, disease similarities to HCMV infection of humans, availability of well-characterized recombinant viruses, and relatively low cost [29-31]. While non-human primate models such as Rhesus macaques and RhCMV have greater genetic similarity to HCMV [31, 32], studies involving RhCMV are limited by cost and availability of CMV-free animals. Additionally, development and maintenance of RhCMV-free populations is difficult and time consuming. Guinea pig CMV (GPCMV) has proven to be a suitable model for studying vertical transmission of CMV and resultant infection of neonates [33]. However, limitations in host genetic models, reagents, and recombinant viruses is a detriment to their widespread use. Rat CMV faces similar challenges as GPCMV limiting its adoption as the prominent CMV animal model. As such, mouse models have come to dominate the CMV field as a cost-effective solution with translatability to human disease [30].

## **Cytomegalovirus Viral Chemokines and Receptors**

Cytomegaloviruses encode immunomodulatory molecules to evade host recognition [34, 35], inhibit or delay programmed cell death [36], or influence antiviral functions [37]. Large DNA viruses (such as poxviruses and herpesviruses) have substantial coding potential. As such, it is unsurprising that many contain viral homologs for host immune proteins as a strategy to manipulate and fine tune host antiviral responses. Herpesviruses in particular encode numerous homologs to host chemokines and chemokine receptors [38]. Chemokines are chemotactic proteins used to recruit cells to a site within the body. Expression of chemokines and their receptors are tightly controlled by the host to ensure homeostasis. Chemokine receptor expression is a potential mechanism by which viruses can direct virally infected cells to target tissues [39], or maintain latency within reservoirs [40, 41] (Fig. 1.1). Soluble viral chemokines are thought to act as specific homing signals to attract susceptible cells to the site of infection [42, 43] or alter the function of responding antiviral cells [44, 45] (Fig. 1.1).

### ***Viral Chemokine Receptors***

HCMV contains four G-protein coupled receptors with similarity to chemokine receptors (US27, US28, UL33, UL78) [38]. US28 is the most well characterized of the GPCR/chemokine receptors and is a constitutively active receptor capable of binding a diverse array of host chemokines such as CCL5, CX3CL1, MCP-1 [46, 47]. Recently, both US27 and US28 have been proposed to function as sinks for G $\alpha$  subunits, dampening GPCR signaling [48]. US28 is also important for both infection of target cells and driving migration/chemotaxis of infected cells [39]. As such, it is thought to play a role in the spread of HCMV *in vivo* and the resultant viral pathology. Expression of US28 in a mouse model of CMV resulted in dendritic cell-dependent migration of virus to salivary glands following intranasal infection [39], whereas US28 (or the MCMV homolog M33 [49]) deletion significantly impaired viral migration out of lungs into the blood and subsequent infection of the salivary glands [39]. Similarly to US28, M33 is capable of inducing migration of infected or transfected cells [50]. M33-deleted viruses display lowered titer in salivary glands and spleens [50, 51]. However, in immunocompromised mice (NSGs) M33

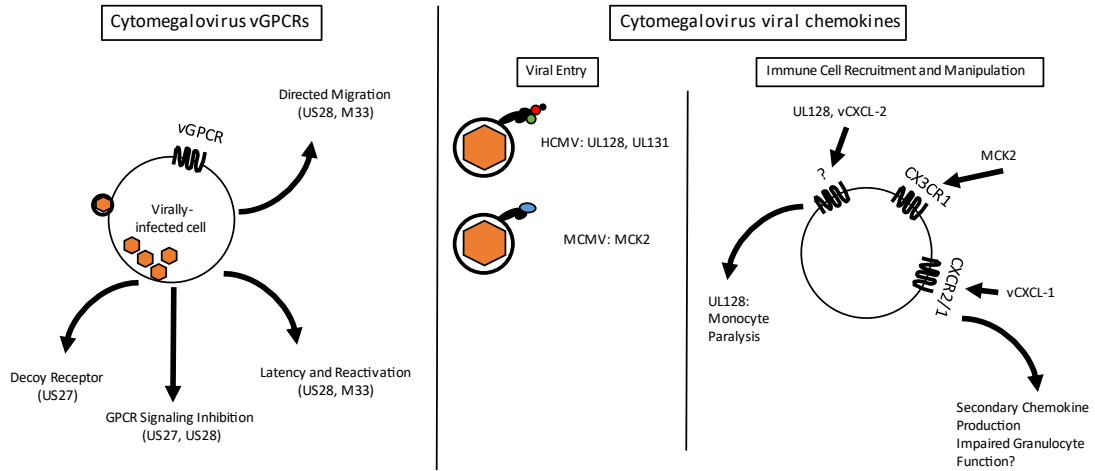


**Figure 1.1:** CMV viral chemokine and chemokine receptor immune manipulation. CMV-encoded viral GPCRs (vGPCRs) can play a variety of functions manipulating GPCR signaling or establishing viral latency and reactivation. Virally-encoded chemokine homologs play roles in viral entry and immune manipulation.

deficiency resulted in normal viral replication within the spleen and liver [52]. The M33-mutant virus had ~400-fold reduction of virus within the salivary gland following NSG infection, but virus was able to replicate within the tissue [52]. This reduction in salivary gland infection for M33-deficient viruses is likely due to decreased trafficking to the organ, and not a replication defect as M33 expression was not necessary for infection of SG explants [52]. CMV GPCR homologs appear vital for proper trafficking of virally infected cells to secretory organs.

While US28 plays a function in directing migration of infected cells, it is also required for HCMV latency [41, 53]. US28 signaling suppresses lytic protein expression by repressing the major immediate early protein (MIEP) [54]. US28 mediated suppression of HCMV lytic infection failed when CD34<sup>+</sup> cells were differentiated, pointing to a role in maintaining latency within hematopoietic progenitors and not differentiated cells [54]. US28's maintenance of latency is dependent on ligand binding [40], as constitutive signaling without ligand binding induced reactivation [40]. While the murine counterpart to US28 (M33) functions similarly for directing chemotaxis, M33 mutants display impaired reactivation from latency [50]. One would expect M33 mutants to display increased reactivation or decreased establishment of latency. This could be due to differences in M33 and US28, differences in latent reservoirs between MCMV and HCMV, or differences in the mechanisms for the establishment and maintenance of latency between the two.

Along with its roles in latency, US28 signaling within humanized mouse models of HCMV altered hematopoiesis, increasing CD3<sup>+</sup> T cells and CD14<sup>+</sup> monocytes while decreasing CD19<sup>+</sup> B cells [40]. US28 is also commonly found in glioblastoma cells where its constitutive activity helps drive proliferation of tumor cells [55]. M78, another GPCR/chemokine receptor with no identified ligands, binds and internalizes major histocompatibility class-II (MHC-II) on infected cells reducing recognition of virally infected cells [34]. As such, M78 decreases MHC-II levels to avoid T cell recognition and viral clearance, promoting infection of the salivary gland [34]. Altogether, CMV encoded GPCR/chemokine receptors have nuanced functions in viral infection, directing migration of infected cells and playing vital roles in the establishment and maintenance of latency.

### ***Viral Chemokine vIL-10***

HCMV *UL111A* (vIL-10) encodes a viral homolog of human IL-10, an immunosuppressive cytokine that binds to host IL-10 receptor (hIL-10R) [56]. Like host IL-10, vIL-10 is capable of inhibiting proinflammatory cytokine production and DC maturation [57, 58]. There are multiple isoforms of vIL-10, with the initially described vIL-10A expressed during lytic infection of cells [56]. The second vIL10 (vIL-10B) was detected during infection of progenitor cells typically used to study HCMV latency leading to speculation that it is a latency associated protein [59]. Other vIL-10 isoforms have also been identified with their function still to be determined [60]. HCMV vIL-10 is also thought to upregulate human monocyte expression of hIL-10, further propagating its immunosuppressive effects [61]. vIL-10 can additionally form heterodimers with hIL-10 further modulating signaling [60]. In a rhesus macaque model of CMV, neutralization of RhCMV vIL-10 reduced horizontal transmission of CMV potentially through reduced shedding of virus in saliva [62]. RhCMV strains lacking a vIL-10 homolog had increased innate immune responses at early timepoints post infection [63], with increased myeloid and dendritic cell levels by 2 weeks post infection [63]. Loss of vIL-10 corresponded with increased proinflammatory cytokines and activation markers of helper T cells [63]. Adaptive immune responses were dampened in the presence of vIL-10, lowering anti-RhCMV antibody titers and numbers of CMV-specific CD4<sup>+</sup> and CD8<sup>+</sup> T cells [63]. vIL-10 appears to have pro-viral functions by diminishing anti-viral responses. However, hIL-10 signaling during CMV infection may play a protective effect by limiting virally induced immunopathology [64]. Overall, vIL-10A plays a broad role in controlling the magnitude of the immune response during acute CMV infection, with an additional isoform (vIL-10B) important for latency within CD34<sup>+</sup> hematopoietic progenitor cells.

### ***Dual-function Viral Chemokines UL128 and UL130***

UL128 and UL130 are key components of an HCMV viral entry complex termed the pentameric complex [65]. The pentameric complex consists of the herpesvirus conserved glycoproteins gL and gH, along with the HCMV specific UL128, UL130, and UL131 proteins responsible for infection of cells *via* endocytosis [65]. Along with its role in viral entry, UL128 has sequence similarity to host CC chemokines [66]. Soluble UL128

is capable of blocking migration of monocytes (induced by CCL2 or CCL5) and reduction of surface chemokine receptors (CCR1, CCR2, CCR5) [44]. UL128 is also reported to function as a beta chemokine to recruit peripheral blood mononuclear cells (analogous to host MIP-1 $\alpha$ ) [67], and potentially responsible for the arrest/paralysis of monocytes [44]. UL130 also has sequence similarity to chemokines, with a signal peptide and single N-terminal cysteine residue placing it as a viral C chemokine [66, 68]. However, UL130 is a luminal glycoprotein typically only found within the viral envelope or interior of infected cells [69]. Based on this, UL130 is not a functional chemokine. The closest homolog for UL128 and UL130 within MCMV is the viral product MCK2. MCK2 is a spliced gene product of *m129* and *m131* [70], with sequence similarity to CC chemokines. Analogous to UL128-131, MCK2 plays a role as both chemotactic protein [71] and viral entry complex [72]. MCK2 is important for infection of acinar salivary glands as well as promoting T cell evasion and maintenance of virus within the salivary gland [69]. Multiple CMVs utilizing proteins with chemokine homology and function for dual purposes points to conserved strategy and convergent evolution.

#### ***The alpha-chemokines UL146 and UL147***

HCMV contains two genes (*UL146* and *UL147*) with similarity to CXC chemokines and possessing an N-terminal ELR motif, which classifies them as alpha-chemokines [42]. *UL147* encodes for a putative protein called vCXCL-2 [42]. Other than its predicted similarity to CXC chemokines, not much is known about *UL147*. *UL146*, on the other hand, produces vCXCL-1 a chemokine that binds host CXCR2 and CX3CR, with some isolates additionally able to bind CXCR1 [42, 45, 73, 74]. vCXCL-1 stimulates CXCR2 on primary human neutrophils, inducing chemotaxis and calcium flux [45, 73, 74]. Initial work by Penfold et al. and Lüttichau demonstrated a clear preference for CXCR2 signaling over CXCR1 [42, 73], and while CXCR1 has been reported to be stimulated by vCXCL-1, not all genotypes of *UL146* can induce receptor activation *in vitro* [45]. Along with activation of host chemokine receptors, vCXCL-1 was thought to function as an autocrine by binding to and signaling through a virally encoded GPCR/chemokine receptor such as US28. However, no evidence has been found for an interaction between US28 and

vCXCL-1 [73]. Yamin et al. reported vCXCL-1 binding to both CXCR2 and CX3CR1, preferentially recruiting CXCR2<sup>+</sup> neutrophils, but still capable of inducing migration of CX3CR1<sup>+</sup> NK cells [74]. Contradictory reports exist for the involvement of the fractalkine receptor, CX3CR1, and vCXCL-1. Lüttichau investigated numerous chemokine receptors, including CX3CR1, and reported that vCXCL-1 induces calcium flux within CXCR1 and CXCR2 expressing cells only [73]. The presence of CXCR2 on naïve NK cells could explain the findings of Yamin et al. [74]. While the involvement of CX3CR1 cannot be entirely excluded, CXCR2 is likely still the dominant receptor target of vCXCL-1 inducing the greatest calcium flux and activation.

As many cell types express CXCR2, vCXCL-1 may play a complex role in modulating the host immune response. While recruitment of cells capable of recognizing and clearing infected cells appears counterintuitive, vCXCL-1's interaction with CXCR2 may cause distinct pro-viral outcomes based on the cell type stimulated. While the consequences of CXCR2 engagement and stimulation in many cell types is unknown, in NK cells and DCs CXCL8 stimulation of CXCR2 can play a pro-viral role by blunting immune responses of recruited cells. Conceivably, vCXCL-1 could directly inhibit the antiviral function of NK cells and indirectly inhibit antiviral functions by preventing DC antigen presentation in the draining lymph nodes [75, 76]. It may also play a role in reactivation, driving differentiation of infected monocytes, where virus replication is stalled, to macrophages, where productive virus replication occurs, which can lead to both reactivation and disseminated disease within the host [77]. Recruitment of neutrophils, monocytes, and/or DCs to infected tissues may also allow for infection of target cells and dissemination to distal organs such as the spleen, liver, lungs, or salivary glands [78].

*UL146* is a hypervariable region within the HCMV genome with 14 genotypes reported [79]. Structural differences in chemokines can result in drastically different functions/signaling outcomes. This is referred to as functional selectivity or biased agonism. A prime example of functional selectivity is the chemokine receptor CCR7 which binds both the ligands CCL19 and CCL21 [80]. CCL19 and CCL21 are secreted by discrete as well as overlapping cell types, and even though they interact with the same receptor, subtle differences in structure results in different functional and signaling outcomes [80,

81]. Purified HCMV vCXCL-1's stimulation of human peripheral neutrophils *in vitro* demonstrated differential binding and receptor stimulation between the genotypes [45]. Along with differences in binding and receptor stimulation, vCXCL-1s displayed functional selectivity in human peripheral neutrophils, inducing chemotaxis and secondary chemokine production to differing levels [45]. This has potential implications on *in vivo* function/activity of vCXCL-1 and resulting disease. vCXCL-1 *in vivo* studies are limited as there is no predicted homolog within MCMV for either *ULI46* or *ULI47*. Conflicting evidence exists for a correlation between the *ULI46* genotype and disease severity/outcome in congenital CMV infections and organ transplant recipients [82-87]. More recently, expression of vCXCL-1 within a mouse model under control of the MCK2 promoter resulted in increased viral burden, and enhanced mortality within immunocompromised animals [43]. This provided the first direct *in vivo* evidence for vCXCL-1 as a virulence factor. Within rhesus CMV, there are six predicted homologs for alpha-chemokines [88]. Presence of *ULI46* homologs in a vaccine strain of RhCMV against SIV ablated T cell mediated protection towards SIV [89]. *ULI46* homologs in rhesus thus alter T cell responses; whether this is through direct stimulation of CXCR2<sup>+</sup> T cells [90] or an indirect bystander mechanism remains to be identified. Varied cell types express CXCR2 [91], and with the differing outcomes of CXCR2 stimulation in each cell type, vCXCL-1 may function more broadly as an overarching immune manipulator interacting with multiple cell types to manipulate host immune responses into a pro-viral state.

### **Neutrophils and their Relationship to Cytomegalovirus Infections**

Neutrophils are granulocytic cells comprising the majority of circulating leukocytes [92]. These abundant and essential innate immune cells are typically associated with and studied in the context of bacterial and fungal infections. As the first infiltrating cell type during sterile or infectious inflammation, they set the stage for disease progression or resolution. Neutrophils are readily mobilized and pre-equipped with a variety of antimicrobial functions, allowing them to efficiently clear infections and damaged tissue [92]. Along with their direct effector functions, they produce cytokines and exocytose

inflammatory mediators to modulate subsequent immune responses, helping shape the course and outcome of disease [92]. Despite the focus on their role and function in bacterial and fungal infections, they are highly adept members of the innate immune system who also serve important roles during viral infections [93]. This is despite their relatively short lifespan and inability to develop traditional immunological memory. Neutrophilic responses to many viral infections walk a fine line between immunopathology which results in tissue and organ damage and pathogen clearance. General neutrophils functions are represented in Figure 1.2.

There is a storied history of polymorphonuclear cells (neutrophils) and CMV. CMV was found in mononuclear cells and granulocytic cells as far back as 1977 [94]. It was noted that patients who received granulocyte/neutrophils transfusions during bone marrow transplantation had a higher incidence of CMV infection [95]. The incidence of CMV infection was only significantly elevated when granulocytes/neutrophils were transferred from CMV+ donor to CMV- recipient [96]. Extracted peripheral Neutrophils were more likely to have CMV DNA than mononuclear cells, and virus was culturable from all neutrophil fractions [97, 98]. Additionally, early viral transcripts were detected in neutrophils isolated from patients, suggesting virus uncoating and initiation of immediate-early transcription [97]. Despite initiation of viral transcription and early gene products, complete replication and production of infectious progeny did not occur within infected human granulocytes [99]. Neutrophils are thought to pick up the virus at endothelial:neutrophil interfaces via small pores and microfusions to shuttle virus across [99]. These infected neutrophils are then capable of transferring infection to uninfected cell types such as fibroblasts [100]. Neutrophils are also capable of *ex vivo* acquisition of CMV from infected fibroblasts and endothelial cells [100, 101]. Neutrophils are thus thought to be at least one cell type capable of disseminating virus *in vivo* [43, 102].

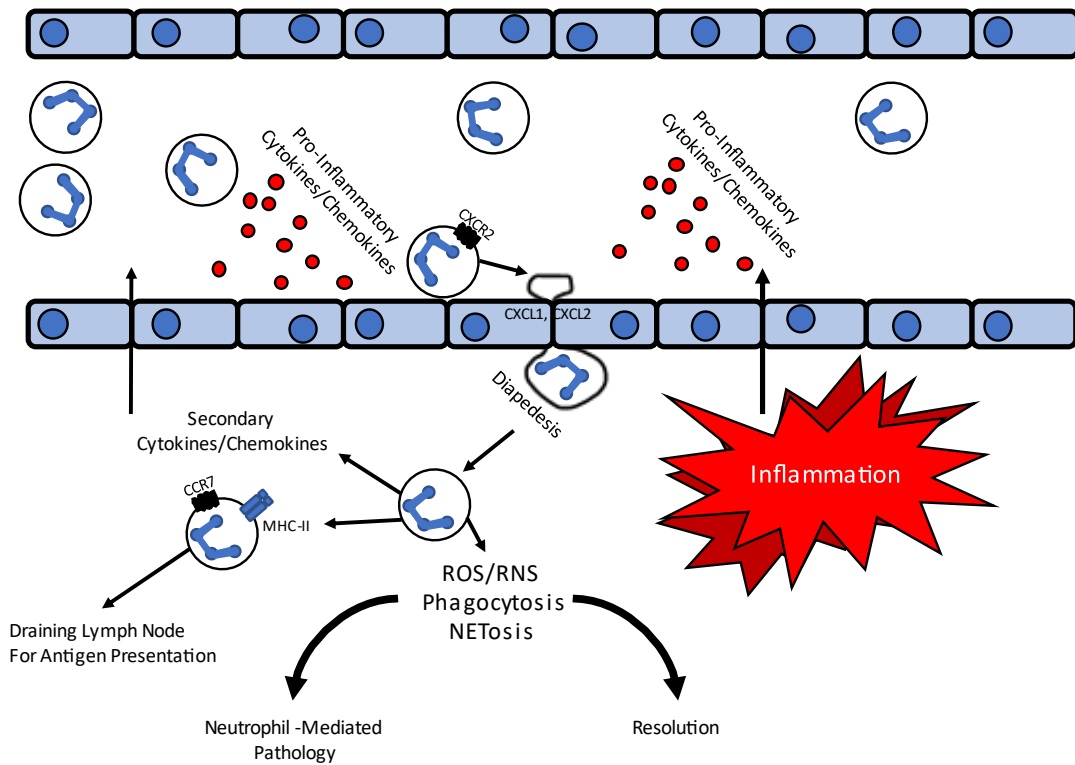


**Figure 1.2:** Neutrophil recruitment and effector functions.

Neutrophil recruitment into tissues is driven by pro-inflammatory cytokine and chemokine secretion. Neutrophils that have adhered to the endothelium undergo diapedesis and tissue extravasation based on CXCR2 signaling and the host chemokines CXCL1 and CXCL2. Neutrophils within the tissue can undergo a variety of effector functions to promote clearance or recruit additional immune cell types. Neutrophil activity can lead to resolution of inflammation and tissue protection, or neutrophil-mediated tissue damage.

### ***Neutrophil Recruitment to Sites of Infection***

Neutrophil levels in circulation and bone marrow are a result of a finely tuned balance of CXCR2 and CXCR4 signaling [103-105]. SDF-1/CXCR4 signaling maintains immature neutrophils within the bone marrow [103-105]. Granulopoiesis is the result of CXCR2 stimulation overriding pro-retention signals from CXCR4 and the migration of neutrophils into circulation. Both bone marrow and circulating neutrophils express the chemokine receptors CXCR1/CXCR2, which allow for chemotaxis in response to a variety of CXC- chemokines [104, 106, 107]. Not all neutrophils may express CXCR2, though. In mice, CXCR2-negative neutrophils represent an alternative subset of neutrophils that still migrate to a stimulus, albeit delayed [108]. What chemokines and receptors this CXCR2-deficient neutrophil subset uses for tissue homing is still unknown. For classical neutrophils, engagement and activation of CXCR1/2, typically *via* the pro-inflammatory cytokines CXCL-8, CXCL-1, and CXCL-2, attract neutrophils to the infection site where they subsequently migrate into the tissue [106, 109]. Neutrophils also recognize and respond to common inflammatory stimuli such as proteins of the IL-1 family, TNF, and IL-6, which signal through IL-1R, TNFR, and IL-6R, respectively [92]. Neutrophils activated in tissue are suspected to expand their receptor profile and respond to additional stimuli such as IFN- $\gamma$  and CC chemokines [110-113]. Expression of the expanded chemokine receptors is functional as they were shown to migrate in response to these other ligands [110-113].

Following stimulation, granulocytes rapidly migrate to the site of inflammation. Selectins and integrins on the surface help slow and tether neutrophils, which subsequently leads to their extravasation into the tissue [114]. The chemokines CXCL1 and CXCL2 secreted by endothelial cells/pericytes and neutrophils control extravasation [109]. CXCL1 secretion from stimulated endothelial cells establishes gradients for luminal and sub-luminal crawling, guiding neutrophils towards inflammatory stimuli. Localized CXCL2 secreted from activated neutrophils binds to endothelial atypical chemokine receptor 1 (ACKR1) and guides them towards cellular junctions for diapedesis into the sub-luminal space, after which CXCL1 again drives them towards the stimulus [109]. Other inflammatory stimuli such as CXCL5 and leukotriene B4 (LTB4) can also help drive

neutrophil migration [115-117]. Once within the tissue, neutrophils can then recognize and carry out effector functions to respond to the source of inflammation.

### ***Neutrophil Recognition of Virally Infected Cells***

Neutrophils are decorated with a diverse array of PRRs (pattern recognition receptors) allowing them to recognize infectious agents within an infected or inflamed tissue [118]. PRRs are positioned externally and internally for recognition of damage associated molecular patterns and pathogen associated molecular patterns (DAMPs and PAMPs, respectively). Globally, toll-like receptors (TLRs) and C-type lectin receptors (CLRs) recognize bacterial, fungal, and viral products in the extracellular space [118]. Internally, TLRs, NOD-like receptors (NLRs), and RIG-I like receptors (RLRs) contribute to recognition of foreign endosomal and cytoplasmic molecules [118]. Neutrophils have been shown to recognize a variety of virally infected cells. Neutrophil TLR8, a ssRNA sensing receptor, recognizes Coxsackie B, influenza, and HIV viruses [119, 120]. Influenza virus and HIV are also recognized by endosomal TLR7, another ssRNA sensing TLR [119-121]. Along with the recognition of conserved epitopes via PRRs, neutrophils express surface Fc-receptors enabling recognition of antibody targeted opsonized particles and participation in antibody-dependent cellular cytotoxicity (ADCC) [122]. They are also able to recognize complement fixed cells and undertake effector and cytotoxic activity against target cells [92].

### ***Typical Neutrophil Functions***

Neutrophils are equipped with a variety of antimicrobial and antiviral tools for efficient clearance of pathogens and damaged tissue. Traditional neutrophil effector functions are covered in an excellent review [92]. Following activation and recognition of damage and pathogen associated molecular patterns, neutrophils can undertake a variety of effector functions: reactive oxygen species (ROS) production, phagocytosis of bacteria/fungi, phagocytosis of dead/infected cells, release of neutrophil extracellular traps (NETs), and production/release of inflammatory cytokines. The characteristic granules of neutrophils are pre-packaged with antimicrobial peptides, reactive species (ROS/RNS), and cytokines allowing for rapid, robust responses to inflammation and infection.

Neutrophil pathogen recognition and activation causes the secretion of these granules, spilling their cytotoxic payload into the injured tissue. Accumulation of these neutrophil-derived products leads to cellular toxicity for both pathogens and local host tissues [93].

Neutrophil-derived reactive species from degranulation or oxidative burst has several inflammatory and anti-inflammatory properties [123]. Aside from ROS/RNS pre-packaged within granules, neutrophils can efficiently generate reactive species to combat infectious agents [92]. However, accumulation of high ROS is damaging to host tissue [123], and RNS/ROS accumulation may interfere with immune responses. Nitration of MHC-TCR complexes by excess reactive species interferes with T cell activation which can modulate adaptive immune responses [124]. In contrast, neutrophil-derived ROS helps convert macrophages from a pro-inflammatory state towards tissue repair and resolution of inflammation [125]. ROS accumulation also appears to be central to determining the nature of some anti-microbial responses [126]. High extracellular ROS during *C. albicans* coculture with neutrophils favors NETosis over phagocytosis as the mechanism for clearance of fungus [126].

The primary mechanism to deal with infections for many immune cells, including neutrophils, is phagocytosis followed by internal destruction/degradation [92]. Phagocytosis and engulfment of infectious agents, infected cells, or dying cells allows for their degradation and clearance from local tissues. Phagocytosis during viral infections requires opsonization and Fc-mediated recognition to clear virally-infected cells. Internalization is followed by fusion with lysosomes containing degrading enzymes causing the destruction of phagocytosed particles. However, some microbes can hijack the phagosome-lysosome pathway and persist within the interior of neutrophils [127]. Hence, uptake of pathogens via phagocytosis does not necessarily result in their clearance.

The final major effector function of neutrophils is NETosis. NETosis (i.e., the act of extruding NETs) is a form of programmed cell death where neutrophils secrete their decondensed chromatin complexed with antimicrobial proteins [128]. Thought to be driven by distinct stimuli such as localized accumulation of ROS, neutrophils will extrude their nuclear contents coated in antimicrobial proteins derived from neutrophil granules [128]. Chromatin decondensation induced by histone citrullination causes NETosis and protein-

arginine deiminase type 4 (PAD4) and neutrophil elastase lead to further degradation [128]. However, alternative NET-induction pathways likely exist as demonstrated with *C. albicans* infections [129]. Astonishingly, enucleation does not appear to spell the end of the neutrophil “lifecycle”, nor their utility *in vivo*. Even after ejecting their nuclear contents, “ghost” neutrophils, formally called neutrophil cytoplasts, are still able to recognize pathogens and perform effector functions like ROS generation and phagocytosis at levels comparable to intact neutrophils [130-132]. Thought to primarily be a mechanism to control bacterial and fungal infections, NETs have also been implicated in the control and pathology of viral infections [110, 133, 134]. For example, HIV incubation with neutrophils generated NETs which protected susceptible cells [135]. Chikungunya virus induced NETs results in virus neutralization, while *in vivo* inhibition of NETosis contributed to increased virulence and viral loads [133]. Additionally, respiratory viruses such as respiratory syncytial virus and influenza virus (IAV) induce NETs [110, 134, 136]. Some viruses such as hepatitis B have been shown to evade and oppose NET formation by decreasing ROS accumulation with a resultant diminution of NETosis [137]. While NET formation is potentially helpful by neutralizing infectious particles and reducing local virus loads, NETosis could also drive local tissue damage and inflammation, as seen in a simian immunodeficiency virus (SIV) model of non-human primate infection where high levels of NETosis biomarkers correlated with tissue damage and depletion of local CD4<sup>+</sup> T cells [138]. Granulocytes have multiple effector functions capable of neutralizing virus or eliminating virally infected cells. These functions constitute a double-edged sword either contributing to viral control and clearance or inducing immunopathology.

### ***Neutrophils as Antigen Presenting Cells***

Long considered as pure effector cells, neutrophils have more recently been described as having antigen presentation functions [139]. Neutrophil expression of MHC-II, which presents antigens to CD4 T cells to initiate the adaptive immune response, is atypical, and they are not considered “professional” antigen presenting cells (APCs) [140]. However, subsets of neutrophils were shown to efficiently upregulate MHC-II and present antigen to T cells [139, 141]. As an atypical APC, they may be less efficient compared to

their professional counterparts [140]. Neutrophils potentially can overcome this disparity just by their sheer numbers. However, murine neutrophils respond to influenza infection very efficiently within the lung interstitial space calling to question their inefficiency [141]. The exact stimulus and signals necessary to induce neutrophil MHC-II expression is an as-of-yet unanswered question, but neutrophil phagocytosis of red blood cells leads to expression of MHC-II [142]. Along with direct antigen presentation, granulocytes increase the efficiency of nearby APCs to present antigens [143]. Vaccination of neutrophil-depleted mice lessened adaptive immune responses leading to fewer activated T cells and lower serum antibody titers [143]. This was potentially through reduction in professional APC's antigen uptake, as well as diminution of DC and macrophage antigen presentation in a neutrophil-dependent manner [143]. Activated neutrophils ROS production also inhibits T cell receptor signaling by nitration of the receptor and preventing recognition of cognate antigen presented on MHC molecules [124]. This can further dampen T cell responses by failing to activate/license them. Overall, neutrophils directly and indirectly contribute to antigen presentation, affecting the innate-adaptive immunity cross-talk.

### ***Neutrophils Call the Shots: Influencing Follow-up Responses***

As the first cell type to arrive at sites of inflammation, the neutrophil response can greatly influence disease course and outcome. Activated neutrophils are potent sources of both pro- (ex. IL-1 $\alpha$ , IL-1 $\beta$ , CXCL8, IL-12) and anti-inflammatory (ex. IL-1Ra, IL-10, TGF- $\beta$ ) chemokines and cytokines [144], revealing complexity and duality to their responses. Neutrophils form interactions with many members of the innate immune system [92, 145]. Neutrophils both recruit and instruct DC maturation within inflamed tissues [146, 147]. Similarly, neutropenic mice have impaired NK cell maturation and impairment of cytotoxic function [148]. As innate cells, neutrophils and monocytes/macrophages have closely coordinated functions, and influence the activity of each other. Inflammatory cytokines/chemokines mediate the initial influx of neutrophils, many of which are secreted by tissue resident macrophages [145]. Tissue infiltrated neutrophils lead to the secretion of chemokines which serve to recruit monocytic cells from circulation and results in monocyte/macrophage accumulation within the inflamed tissue [145]. Additional signaling

can skew the immune response and generate M1/Type 1 versus M2/Type 2 differentiation and monocytic immune responses [145].

Neutrophils have recently been highlighted as a potential point of cross-talk between the innate and adaptive immune system. As discussed above, neutrophils can present antigen to T cells [139, 141]. Along with APC functions, neutrophils are suspected to play multiple roles in recruiting T cells into tissues. As neutrophils migrate into tissues, they may create local chemokine gradients or membranous deposits termed “trails” which cytotoxic T cells can subsequently follow to an infection site [149]. These “trails” seem to establish a localized gradient that specifically guides CD8<sup>+</sup> T cells and the loss of CXCL12 from the granulocytic compartment ablated T cell recruitment. Additionally, neutropenic mice display increased morbidity and mortality during influenza infection due to decreased recruitment of both cytotoxic and helper T cells [149]. Granulocytes can also play suppressive roles, inhibiting T cell proliferation and IFN- $\gamma$  secretion, despite adequate T cell activation or antigen recognition [150]. Neutrophil-mediated T cell inhibition can occur through multiple mechanisms. Activated neutrophils often produce ROS, but overabundant ROS production and arginase-1 activity inhibits T cell proliferation [150]. Suppressive neutrophils express programmed death ligand-1 (PD-L1) which induces checkpoint inhibition and exhaustion of activated T cells [150-152]. Neutrophil immunosuppression results in decreased IL-2R blocking T cell responsiveness to typical IL-2 signaling/activation [150, 153].

Neutrophils impact not just the T cell arm of the adaptive immune system, but B cell induced humoral immunity, as well [153]. While small in number, a unique population of splenic neutrophils promotes the maturation of marginal zone B cells, promoting plasma cell generation, and allowing for the production of T cell independent immunoglobulins [154, 155]. This is potentially mediated through their production of B cell maturation signals such as B cell activating factor (BAFF) and a proliferation-inducing ligand (APRIL) [154-156]. Increased B cell proliferation and activation signals can come at a cost. Neutrophil overproduction of APRIL and BAFF can lead to B cell neoplasia [157, 158]. As with T cells, granulocytes can also suppress B cell activity. Neutrophil secretion of TGF- $\beta$  suppresses B cell antibody production [159, 160]. ROS, nitric oxide, and arginase-

1 production by an immunosuppressive neutrophil subtype similarly suppresses B cell responses [159, 160]. The end result is that neutrophils can play roles in both directing and enhancing innate and adaptive cell function as well as inhibiting their activity. This is related to the heterogeneity of the neutrophil population containing both distinct pro- and anti-inflammatory populations which can exist in equilibrium. As high-dimensional and unbiased data analysis techniques mature, identification of phenotypically distinct pro- and anti-inflammatory neutrophils will follow. This will allow for a further dissection and characterization of the role and relationship of neutrophil subtypes to other immune cells.

### ***Protection vs. Pathogenesis***

A major question of neutrophil responses during viral infection is the benefit or detriment to the host. Neutrophil responses are tightly controlled to ensure an appropriate response to avoid immunopathology while still providing protection. This balancing act is heavily influenced by the relative survival of neutrophils within infected tissues. Accumulation and maintenance of neutrophils within tissues leads to increased levels of cytotoxic proteins, tissue damage, and delays tissue remodeling and repair [161]. As a result, neutrophil apoptosis and clearance by tissue phagocytes represents an important mechanism of tissue protection and initiates resolution of inflammation and tissue repair [161]. Resolution of inflammation occurs via apoptosis and subsequent efferocytosis of dead/dying neutrophils by other phagocytes (primarily macrophages) [162]. By undergoing a controlled, non-lysis form of programmed cell death, neutrophils prevent release of cytotoxic molecules and unnecessary inflammation [161]. Moreover, neutrophil apoptosis and efferocytosis by phagocytes transitions cells into an anti-inflammatory profile and signal tissue repair and remodeling [161, 163]. In addition to the removal of inflammatory neutrophils, phagocytosis of neutrophils alters tissue macrophages to secrete the anti-inflammatory cytokine IL-10 [164] helping amplify this resolution of inflammation. Along with their ability to influence neighboring cells, neutrophils play important roles in the healing process in a variety of tissues [165-167]. Granulocytes are potential sources of the anti-inflammatory cytokine IL-10 enabling them to directly resolve acute inflammation [168-170]. Immature/immunosuppressive neutrophils are also neuro-regenerative and

secrete growth factors leading to increased ocular and central nervous system (CNS) recovery following traumatic nerve damage [108].

Pro-inflammatory cytokine secretion (such as TNF- $\alpha$ , IL-6, IL-1 $\beta$ ) induces neutrophil-driven tissue damage, neutrophil extracellular traps in local tissues, and the accumulation of ROS [92, 128]. Activation and accumulation of neutrophils is associated with pathology for a variety of viruses. Coxsackievirus infection inhibits neutrophil apoptosis, while also increasing activation and is, to some degree, responsible for myocarditis in mice [171]. Neutrophil-depletion decreases Coxsackievirus-induced myocarditis [171]. SARS-CoV-2 infected patients with severe COVID, a coronavirus disease, simultaneously have lymphopenia and neutrophilia. This results in a significantly elevated neutrophil:lymphocyte ratios in the blood, which may drive lung inflammation and damage [172-174]. Neutrophils isolated from COVID patients also have increased pro-inflammatory cytokine production (i.e., IL-6, IL-1 $\beta$ , TNF- $\alpha$ , IFN- $\alpha$ ) when stimulated [175] and show increased signatures of NETosis [176]. Neutrophil-depleted or CXCR2-knockout mice display reduced airway inflammation upon rhinovirus challenge [177]. Granulocyte TNF- $\alpha$  release drives rhinovirus hyperinflammation, as decreased neutrophil accumulation led to lowered TNF- $\alpha$  and MIP-2 in bronchioalveolar lavage fluid. Similar studies with influenza demonstrate neutrophil driven immunopathology. Neutrophils from IAV infected animals display increased NETosis in response to CXCL8 stimulation *ex vivo* [178]. Inhibition of NETosis, a byproduct of CXCR2 inhibition, in combination with neuraminidase inhibitors during lethal IAV challenge led to increased animal survival [178]. Conversely, loss of neutrophils in IAV exacerbates disease increasing morbidity and mortality [179]. In support of this, CD11b knockout mice have increased immunopathology in murine IAV infection due to loss of lung-infiltrated neutrophils which appear to control T cell influx and subsequent tissue damage [179].

Along with respiratory infections, proper modulation of neutrophil recruitment appears to be crucial for viral CNS infections. Based on herpes simplex virus CNS infections, astrocytes and neurons express CXCL1 (KC) during infection to recruit neutrophils [180]. These neutrophils perturb the blood brain barrier integrity, leading to viral encephalitis [180]. Mice deficient in CXCR2 display decreased neutrophil

recruitment and blood brain barrier permeability and increased survival [180]. In opposition, when mice infected with a neurotropic strain of the murine gammaherpesvirus MHV-68 were treated with blocking antibodies against CXCR2, there was 100% mortality despite the generation of virus specific T-cells [181]. This was due to decreased BBB degradation (i.e., an intact blood brain barrier), which limited T-cell recruitment to the brain. Neutrophil recruitment and subsequent pathology or protection varies for different infections and tissues.

### **Neutrophils Enhancing Viral Dissemination**

As the most abundant circulating immune cell, neutrophils represent prime targets for viral manipulation. Multiple viruses infect them [99, 171, 182, 183] and in many cases these infections are non-productive, resulting in the death of the infected cell prior to viral replication and release of infectious progeny [99, 171, 183]. However, infection of granulocytes is non-trivial, as infected neutrophils transfer infection [43, 96, 100, 102, 182]. For CMV specifically, both HCMV and MCMV have been associated with the granulocytic fraction [43, 97, 99, 101]. These infected neutrophils are capable of transferring infection *in vitro/ex vivo*, and adoptive transfer of neutrophils from MCMV-infected animals transmits infection to naïve mice [43].

Perhaps unsurprising given the CMV's immune manipulation and its historical relationship with neutrophils, CMV is capable of modulating neutrophil responses and function during infections. CMV infection is known to impair neutrophil migration, oxidative burst, and phagocytosis [184-186]. This impairment lasts for 2-3 weeks post-infection [186]. Functionally, this reduces neutrophil responsiveness and ability to kill/clear other pathogens. Co-infection models of MCMV and bacterial and fungal pathogens results in a significant increase in mortality even when using sub-lethal concentrations of virus and bacteria/fungi [187-190]. MCMV's manipulation of immune responses could render the host susceptible to subsequent infections [187]. Clinical observations support this idea as immunocompromised individuals who develop CMV disease have increased rates of invasive fungal infections [191]. The neutrophil represents an overlooked cell type with historical ties to acute disease and a potential target of viral

immune evasion strategies. As such, the role(s) neutrophils play in the immune response to CMV infection is relevant, whether it is involved in control and clearance or subverted for viral purposes.

### ***Trogocytosis/Trogoptosis as a Potential Viral Uptake Mechanism***

Phagocytosis of target cells is an important effector function of neutrophils. However, novel non-phagocytic “eating” can also occur. Trogocytosis is a process whereby immune cells form microfusion events with a target cell, removing portions of the membrane or intracellular contents [192]. This sampling or eating of a target cell can be cytotoxic and non-cytotoxic. Neutrophils utilize trogocytosis on the large extracellular parasite, *Trichomonas vaginalis*, gradually eating their opponent to death [193]. Additionally, neutrophils use antibody-dependent cellular cytotoxicity of cancer cells in an altered process known as trogoptosis where membrane microfusion and transfer of cytoplasmic material leads to a leaky membrane and necrotic cell death of the cancerous cell [194]. While further studies on the mechanisms driving trogoptosis and trogocytosis are required, the cytotoxic mechanism appears to require complement fixation and/or antibody targeting [194]. Once initiated, neutrophil serine proteases play a role in “taking a bite” out of the target cell [193, 194].

Trogocytosis and trogoptosis membrane microfusions and transfer of cellular content between target cell and immune cell potentially serves as an intracellular sampling method [192]. Sampling of membrane and intracellular contents may play important roles in the generation of immune responses. For instance, cross-dressing of MHC onto DCs and subsequent antigen presentation occurs via a trogocytosis mechanism [195]. Non-professional antigen presenting cells can also cross-dress MHC molecules for presentation to helper T cells [192]. Trogocytosis likely occurs both *in vitro* and *in vivo*, as Yamanaka et al. found that NOD/SCID mice repopulated with human leukocytes displayed both human and murine MHC-I and CD45 molecules [196, 197]. Nearly 100% of adoptively transferred cells displayed mouse surface molecules without chromosomal chimerism, demonstrating an abundant swapping of surface proteins [196]. If trogocytosis and membrane microfusions are abundant processes *in vivo*, it raises the question: could

infectious agents take advantage of this process to enhance infection or broaden its tropism?

The trogocytosis sampling of the intracellular contents of cells potentially contributes to the spread of infections. Indeed, macrophages can transfer *Francisella tularensis*, and *Salmonella enterica* can spread from infected to uninfected macrophages *via* trogocytosis [198]. Trogocytosis is shown or suspected to be involved in infections for multiple viruses. During co-culture of HCMV-infected endothelial cells with neutrophils, microfusions and trogocytosis are implicated in the transfer of virus to the granulocytic fraction [99]. This potentially represents another pathway for cell-to-cell transfer of cytomegaloviruses [99]. Monocytes were able to make B cells susceptible to H5N1 influenza virus infection *via* trogocytosis and transfer of IAV receptor (i.e.,  $\alpha$ 2,3-sialic acid) [199]. Additionally, cell-to-cell contact is implicated in the spread of HIV *via* multiple potential mechanisms with trogocytosis among them. CD8<sup>+</sup> T-cells can “capture” CD4 molecules potentially *via* trogocytosis, making them capable of binding HIV [200]. However, this does result in their infection [200]. It is also unclear whether CD8<sup>+</sup> T-cells “cross-dressed” with CD4 are capable of transferring HIV to another susceptible cell type. Whether trogocytic transfer of infection is a pathogen-directed or stochastic process is yet to be determined, but represents a potentially immunologically covert mechanism of cell-to-cell transmission. As CMV infection *in vivo* and infection of many immune cells such as neutrophils is thought to be predominantly mediated by cell-to-cell transmission, trogocytosis could play a prominent role in the uptake of virus by granulocytic cells.

### ***Reverse Transmigration***

Migration into a tissue was once thought to be the final resting place of activated neutrophils. The observation of reverse migrated neutrophils has challenged this traditional paradigm in recent years. Reverse transendothelial migration (rTEM) is the counter to the traditional transendothelial migration (TEM) path of activated neutrophils. This process involves the migration of activated neutrophils that have made the luminal-to-subluminal transition back into circulation [201]. These recirculating activated granulocytes disseminate inflammation throughout the host and cause distant organ damage [202].

Neutrophils that have undergone rTEM downregulate the chemokine receptors CXCR1 and CXCR2, the two major receptors responsible for guiding neutrophil chemotaxis into inflamed tissues, making them incapable of migrating into secondary sites/areas of inflammation [203]. These rTEM neutrophils display delayed apoptosis and initially accumulate within the lungs where they can lead to organ damage due to enhanced oxidative burst [201, 203, 204]. Ultimately increased expression of CXCR4 on rTEM neutrophils homes them back to the bone marrow where they undergo apoptosis and clearance [205]. rTEM is pertinent to CMV as neutrophils are capable of viral uptake and transfer of infection *in vitro* and *in vivo* [43, 100]. Reverse migration represents a potential strategy for neutrophil-mediated dissemination of infection.

### ***Neutrophil-Mediated Enhancement of Infection***

Along with immunopathological responses, neutrophils enhance spread of infections. Infected neutrophils could function as a “Trojan horse”, shielding intracellular pathogens from immune recognition and allowing transference of infection (Fig. 1.3). Acting as pathogen shuttles, neutrophils enhance the spread of intracellular bacteria such as *Leishmania major*, which allows for bacterial transfer and infection of monocytic cells [206]. In addition, if neutrophils are capable of recirculation, they may act as dissemination vehicles/shuttles to carry infectious agents to other tissues and initiate infection. For example, neutrophils serve as vehicles for replication and dissemination of H5N1 influenza virus *in vivo* [182]. They can also pick up and disseminate MCMV, as adoptive transfer of MCMV-harboring neutrophils led to productive infection of recipient mice [43]. Infection of granulocytic cells either within the tissue, who subsequently reverse migrate, or at the endothelial-leukocyte interface of the lumen could serve to shuttle the virus, seeding the lungs, hematopoietic compartment, and potentially other blood filtering organs with virus [78]. Neutrophils may also play a role in viral reactivation (Fig. 1.3). One site of latency for CMV is within myeloid hematopoietic progenitor cells within the bone marrow. Neutrophils are abundant within the bone marrow and respond to CXCR2 signaling for release. As such, it is possible that vCXCL-1 or host chemokine stimulation of CXCR2

may recruit infected neutrophils from the bone marrow and disseminate infection to distal organs.

Neutrophils are potent sources of cytokines/chemokines, coordinating the initial response to infection [92, 150]. Activation of neutrophils causes the release of many signaling molecules, enforcing and amplifying pre-existing recruitment signals as well as providing stimulus for migration of additional cell types. A properly controlled recruitment of effector cells is important to both host and virus. Towards this end, many viruses have developed their own strategies to manipulate innate and adaptive immunity [207]. CMV may utilize neutrophils as signal amplifiers to recruit desired immune cells to the site of infection (Fig. 1.3). CMV manipulation of neutrophils and vCXCL-1 stimulation of CXCR2 induces secondary chemokine expression [45]. HCMV-infected cells stimulate neutrophils to secrete IL-6 to recruit CMV-susceptible monocytes [208]. On its own, neutrophil recruitment of monocytic cells to an active site of CMV replication creates an opportunity for infection of the monocytic cell. Migration of infected monocytes to distal organs could disseminate infection and disease. Monocytes are also a potential site of latency *in vivo* [8, 209]. CMV's manipulation of neutrophils may serve to recruit a desired cell type for efficient dissemination and latency.

Monocytic cells will often phagocytose dying/apoptotic neutrophils to protect tissues and to mediate tissue repair and resolution of inflammation. Infected neutrophils could potentially serve as a decoy for infection of the replication-permissive cells of the monocytic lineage. Alternatively, neutrophils could serve as a "tether" for CMV, enhancing infection of other cell types. During HIV infection, neutrophils bind virus to their surface and transfer it to cocultured lymphocytes [210]. This method of viral infection/transfer was more efficient than cell-free infection and activation of neutrophils or recipient peripheral blood mononuclear cells further increased the infection rate [210].

There is evidence for neutrophils serving as both signal amplifiers recruiting target cells and intra-organ shuttles/Trojan horses disseminating infection. Acting as signal amplifiers, they can recruit susceptible cells to sites of infection, contributing to their infection and indirectly spreading the virus. Alternatively, as viral shuttles they can directly transfer infection from a site of infection to uninfected cells/tissue. Regardless of the role

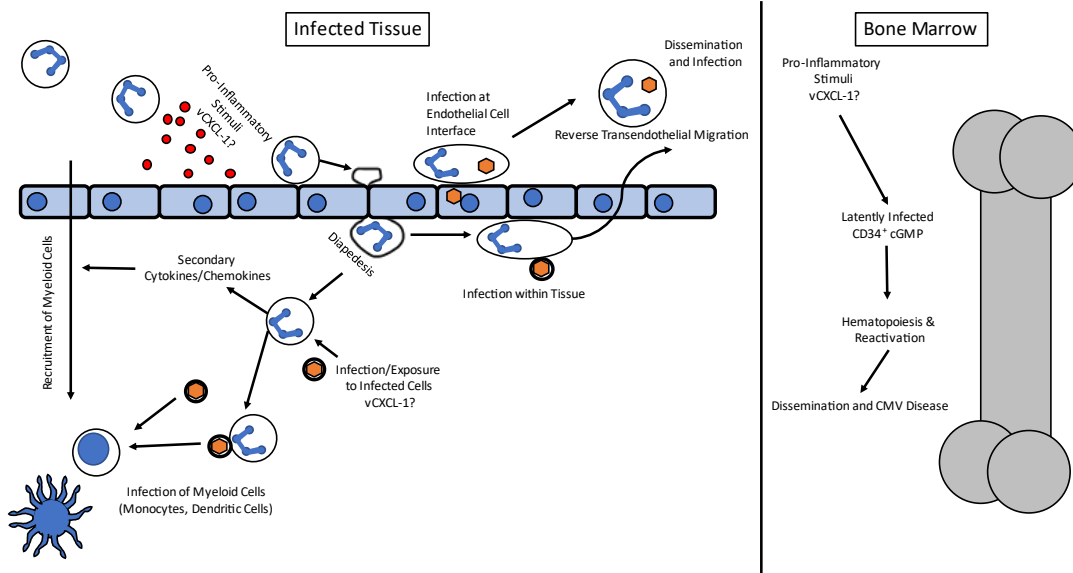


**Figure 1.3:** Potential hijacking of neutrophil functions for CMV gain.

Neutrophil recruitment to sites of CMV infection can allow for infection of neutrophils and potential neutrophil-mediated dissemination of virus (Trojan horse model). In addition to direct spread of virus, neutrophils at the site of infection could also serve as signal amplifiers to recruit preferred cell types for subsequent CMV infection and dissemination. Alternatively, infected myeloid precursor cells in the bone marrow (a major site of latency) could serve as both sites of latency and dissemination vehicle.

neutrophils play in CMV-induced disease, the vCXCL1-CXCR2 axis is potentially an important mediator to establish a pro-viral outcome.

### Conclusion

CMV has garnered a reputation as an adept puppeteer, refining immune responses conducive to its own benefit. CMV encoded viral chemokines such as *UL146/vCXCL-1* are one arm of this process. Infection of immunocompromised mice with MCMVs expressing vCXCL-1 implicates the viral chemokine as a virulence factor [43]. vCXCL-1 represents an attractive target for development of novel antiviral therapeutics, a high priority for CMV clinicians. Neutrophils express functional CXCR2 [91] and are prominent targets for manipulation by the viral chemokine vCXCL-1 [43, 45]. Neutrophils are associated *in vivo* with inflammation and dissemination and can transfer virus *in vitro* and *in vivo* [43, 100]. Despite this, neutrophils are probably not the only target of vCXCL-1 and may not constitute the main cell type either. vCXCL-1 expression increased dissemination and spread of MCMV *in vivo* [43]. However, depletion of neutrophils in mice infected with a vCXCL-1 expressing virus failed to reduce viral burden to WT levels [43]. While there was a significant reduction when neutropenic mice were infected, the still-elevated levels of infection points to an additional cell type responding to vCXCL-1 *in vivo* and enhancing dissemination. What cell type is the major driver of vCXCL-1 induced disease was not readily apparent, but CXCR2 expression may be key to home in on potential candidates.

A global expression profile of CXCR2 by leukocytes in naïve animals is lacking. Immunophenotyping of CXCR2 expression has been limited to specific cell types and tissues within certain disease states. This lack of characterization limits our ability to determine the primary target of vCXCL-1 *in vivo*. However, there are several cell types commonly reported to be CXCR2 positive which could potentially be recruited to sites of infection by vCXCL-1 secretion. Subsets of monocytes and dendritic cells express CXCR2 in mice [76, 91, 211]. Infection of both can lead to carriage of virus out of initial sites and into secondary tissues [212, 213]. DC infection and limited dissemination of virus is thought to reduce viral-induced disease [213]. Infection of monocytic cells results in

disseminated infection of organs such as spleen and liver causing tissue damage and disease [213]. More typically associated with viral recognition and clearance of CMV infection, natural killer cells also express CXCR2. NK cells are likely not a target for CMV infection, as neither infection of NK cells nor transfer of infection have been reported. However, CXCL8 stimulation of CXCR2 in NK cells impairs antiviral functions [75]. vCXCL-1 may play a similar role in CMV infection to impair infiltrating NK cells and prevent clearance. Similarly, T cells and B cells express CXCR2 [90, 214], but viral dissemination is typically associated with myeloid cells *in vivo*. vCXCL-1 stimulation of adaptive cells expressing CXCR2 may still influence subsets of T and B cells, but the functional consequences are unknown.

Along with a more in-depth map of leukocyte expression of CXCR2, further work will determine the consequences of the functional selectivity of vCXCL-1. Along with limited clinical data, *in vitro* screens of vCXCL-1's demonstrated differential affinity for CXCR2, as well as variable stimulation of the receptor to induce variable calcium flux and chemotaxis [45]. Hence, vCXCL-1 engagement of a host chemokine receptor causes biased agonism and distinct outcomes. However, the *in vivo* consequences of the functional selectivity of vCXCL-1 are unknown. While there have been many advances in CMV and neutrophil biology, there is still much to learn at the intersection of the two. That neutrophils play a role is abundantly clear, but the exact immune network involved or contribution to CMV protection or pathology is an area requiring further examination.

To understand the function of vCXCL-1 and immune manipulation by CMV, a more thorough picture of CXCR2 expression is required. In Chapter 2 we immunophenotype mouse and human peripheral blood for CXCR2 expression and perform comparisons between the two. We additionally examine other murine tissues for CXCR2<sup>+</sup> cells and characterize the CXCR2 immune landscape under homeostatic conditions. In Chapter 3 we further characterize the viral chemokine vCXCL-1 in murine infection models and provide potential molecular mechanisms behind the biased agonism observed *in vitro* [45]. The potential *in vivo* function of vCXCL-1 secretion is to recruit cells to a local tissue for subsequent infection. Infection proceeds by virus interaction with heparan sulfate proteoglycans (HS) [215]. Deeper understanding of the HS-virus interface will

allow for development of targeted therapeutics, and this characterization is the focus of Chapters 4 and 5.

## References

1. Smith, M.G., *Propagation in tissue cultures of a cytopathogenic virus from human salivary gland virus (SGV) disease*. Proc Soc Exp Biol Med, 1956. **92**(2): p. 424-30.
2. Smith, M.G., *Propagation of Salivary Gland Virus of the Mouse in Tissue Cultures*. Proceedings of the Society for Experimental Biology and Medicine, 1954. **86**(3): p. 435-440.
3. Smith, K.O. and L. Rasmussen, *Morphology of Cytomegalovirus (Salivary Gland Virus)*. J Bacteriol, 1963. **85**: p. 1319-25.
4. Luse, S.A. and M.G. Smith, *Electron microscopy of salivary gland viruses*. J Exp Med, 1958. **107**(5): p. 623-32.
5. Liu, L., *Fields Virology, 6th Edition*. Clinical Infectious Diseases, 2014. **59**(4): p. 613-613.
6. McCormick, A.L., et al., *Differential function and expression of the viral inhibitor of caspase 8-induced apoptosis (vICA) and the viral mitochondria-localized inhibitor of apoptosis (vMIA) cell death suppressors conserved in primate and rodent cytomegaloviruses*. Virology, 2003. **316**(2): p. 221-33.
7. Jurak, I. and W. Brune, *Induction of apoptosis limits cytomegalovirus cross-species infection*. EMBO J, 2006. **25**(11): p. 2634-42.
8. Sinclair, J. and P. Sissons, *Latency and reactivation of human cytomegalovirus*. J Gen Virol, 2006. **87**(Pt 7): p. 1763-79.
9. Dowd, J.B., A.E. Aiello, and D.E. Alley, *Socioeconomic disparities in the seroprevalence of cytomegalovirus infection in the US population: NHANES III*. Epidemiol Infect, 2009. **137**(1): p. 58-65.
10. Lachmann, R., et al., *Cytomegalovirus (CMV) seroprevalence in the adult population of Germany*. PLoS One, 2018. **13**(7): p. e0200267.
11. Pass, R.F., et al., *Increased frequency of cytomegalovirus infection in children in group day care*. Pediatrics, 1984. **74**(1): p. 121-6.
12. Revello, M.G., et al., *Molecular epidemiology of primary human cytomegalovirus infection in pregnant women and their families*. J Med Virol, 2008. **80**(8): p. 1415-25.

13. Demmler, G.J., *Congenital cytomegalovirus infection*. *Semin Pediatr Neurol*, 1994. **1**(1): p. 36-42.
14. Lombardi, G. and M. Stronati, [*Congenital cytomegalovirus infection*]. *Minerva Pediatr*, 2005. **57**(5): p. 213-27.
15. Britt, W.J., *Maternal Immunity and the Natural History of Congenital Human Cytomegalovirus Infection*. *Viruses*, 2018. **10**(8).
16. Cheung, T.W. and S.A. Teich, *Cytomegalovirus infection in patients with HIV infection*. *Mt Sinai J Med*, 1999. **66**(2): p. 113-24.
17. Ramanan, P. and R.R. Razonable, *Cytomegalovirus infections in solid organ transplantation: a review*. *Infect Chemother*, 2013. **45**(3): p. 260-71.
18. Smee, D.F., et al., *Progressive murine cytomegalovirus disease after termination of ganciclovir therapy in mice immunosuppressed by cyclophosphamide treatment*. *J Infect Dis*, 1991. **164**(5): p. 958-61.
19. Cheung, T.W. and S.A. Teich, *Cytomegalovirus infection in patients with HIV infection*. *Mount Sinai Journal of Medicine*, 1999. **66**(2): p. 113-124.
20. Jakharia, N., D. Howard, and D.J. Riedel, *CMV Infection in Hematopoietic Stem Cell Transplantation: Prevention and Treatment Strategies*. *Curr Treat Options Infect Dis*, 2021: p. 1-18.
21. Chen, S.J., S.C. Wang, and Y.C. Chen, *Antiviral Agents as Therapeutic Strategies Against Cytomegalovirus Infections*. *Viruses*, 2019. **12**(1).
22. in *Vaccines for the 21st Century: A Tool for Decisionmaking*, K.R. Stratton, J.S. Durch, and R.S. Lawrence, Editors. 2000: Washington (DC).
23. Bernstein, D.I., et al., *Safety and efficacy of a cytomegalovirus glycoprotein B (gB) vaccine in adolescent girls: A randomized clinical trial*. *Vaccine*, 2016. **34**(3): p. 313-9.
24. Pass, R.F., et al., *Vaccine prevention of maternal cytomegalovirus infection*. *N Engl J Med*, 2009. **360**(12): p. 1191-9.
25. Gomes, A.C., P.D. Griffiths, and M.B. Reeves, *The Humoral Immune Response Against the gB Vaccine: Lessons Learnt from Protection in Solid Organ Transplantation*. *Vaccines (Basel)*, 2019. **7**(3).

26. Griffiths, P.D., et al., *Cytomegalovirus glycoprotein-B vaccine with MF59 adjuvant in transplant recipients: a phase 2 randomised placebo-controlled trial*. Lancet, 2011. **377**(9773): p. 1256-63.
27. Plotkin, S.A., et al., *The Status of Vaccine Development Against the Human Cytomegalovirus*. J Infect Dis, 2020. **221**(Suppl 1): p. S113-S122.
28. John, S., et al., *Multi-antigenic human cytomegalovirus mRNA vaccines that elicit potent humoral and cell-mediated immunity*. Vaccine, 2018. **36**(12): p. 1689-1699.
29. Fisher, M.A. and M.L. Lloyd, *A Review of Murine Cytomegalovirus as a Model for Human Cytomegalovirus Disease-Do Mice Lie?* Int J Mol Sci, 2020. **22**(1).
30. Reddehase, M.J. and N.A.W. Lemmermann, *Mouse Model of Cytomegalovirus Disease and Immunotherapy in the Immunocompromised Host: Predictions for Medical Translation that Survived the "Test of Time"*. Viruses, 2018. **10**(12).
31. Rawlinson, W.D., H.E. Farrell, and B.G. Barrell, *Analysis of the complete DNA sequence of murine cytomegalovirus*. J Virol, 1996. **70**(12): p. 8833-49.
32. Powers, C. and K. Fruh, *Rhesus CMV: an emerging animal model for human CMV*. Med Microbiol Immunol, 2008. **197**(2): p. 109-15.
33. Weisblum, Y., et al., *Models of vertical cytomegalovirus (CMV) transmission and pathogenesis*. Semin Immunopathol, 2014. **36**(6): p. 615-25.
34. Yunis, J., et al., *Murine cytomegalovirus degrades MHC class II to colonize the salivary glands*. PLoS Pathog, 2018. **14**(2): p. e1006905.
35. del Val, M., et al., *Cytomegalovirus prevents antigen presentation by blocking the transport of peptide-loaded major histocompatibility complex class I molecules into the medial-Golgi compartment*. J Exp Med, 1992. **176**(3): p. 729-38.
36. Brune, W. and C.E. Andoniou, *Die Another Day: Inhibition of Cell Death Pathways by Cytomegalovirus*. Viruses, 2017. **9**(9).
37. Picarda, G. and C.A. Benedict, *Cytomegalovirus: Shape-Shifting the Immune System*. J Immunol, 2018. **200**(12): p. 3881-3889.
38. Pontejo, S.M., P.M. Murphy, and J.E. Pease, *Chemokine Subversion by Human Herpesviruses*. J Innate Immun, 2018. **10**(5-6): p. 465-478.

39. Farrell, H.E., et al., *Human cytomegalovirus US28 allows dendritic cell exit from lymph nodes*. J Gen Virol, 2018. **99**(11): p. 1509-1514.
40. Crawford, L.B., et al., *Human Cytomegalovirus US28 Ligand Binding Activity Is Required for Latency in CD34(+) Hematopoietic Progenitor Cells and Humanized NSG Mice*. mBio, 2019. **10**(4).
41. Humby, M.S. and C.M. O'Connor, *Human Cytomegalovirus US28 Is Important for Latent Infection of Hematopoietic Progenitor Cells*. J Virol, 2015. **90**(6): p. 2959-70.
42. Penfold, M.E.T., et al., *Cytomegalovirus encodes a potent alpha chemokine*. Proceedings of the National Academy of Sciences of the United States of America, 1999. **96**(17): p. 9839-9844.
43. Jackson, J.W., et al., *The Human Cytomegalovirus Chemokine vCXCL-1 Modulates Normal Dissemination Kinetics of Murine Cytomegalovirus In Vivo*. MBio, 2019. **10**(3).
44. Straschewski, S., et al., *Protein pUL128 of human cytomegalovirus is necessary for monocyte infection and blocking of migration*. J Virol, 2011. **85**(10): p. 5150-8.
45. Heo, J., et al., *Novel Human Cytomegalovirus Viral Chemokines, vCXCL-1s, Display Functional Selectivity for Neutrophil Signaling and Function*. J Immunol, 2015. **195**(1): p. 227-36.
46. Gao, J.L. and P.M. Murphy, *Human cytomegalovirus open reading frame US28 encodes a functional beta chemokine receptor*. J Biol Chem, 1994. **269**(46): p. 28539-42.
47. Miller, W.E., et al., *US28 is a potent activator of phospholipase C during HCMV infection of clinically relevant target cells*. PLoS One, 2012. **7**(11): p. e50524.
48. Tsutsumi, N., et al., *Atypical structural snapshots of human cytomegalovirus GPCR interactions with host G proteins*. Sci Adv, 2022. **8**(3): p. eabl5442.
49. Waldhoer, M., et al., *Murine cytomegalovirus (CMV) M33 and human CMV US28 receptors exhibit similar constitutive signaling activities*. J Virol, 2002. **76**(16): p. 8161-8.

50. Cardin, R.D., et al., *The M33 chemokine receptor homolog of murine cytomegalovirus exhibits a differential tissue-specific role during in vivo replication and latency*. J Virol, 2009. **83**(15): p. 7590-601.
51. Case, R., et al., *Functional analysis of the murine cytomegalovirus chemokine receptor homologue M33: ablation of constitutive signaling is associated with an attenuated phenotype in vivo*. J Virol, 2008. **82**(4): p. 1884-98.
52. Bittencourt, F.M., et al., *The M33 G protein-coupled receptor encoded by murine cytomegalovirus is dispensable for hematogenous dissemination but is required for growth within the salivary gland*. J Virol, 2014. **88**(20): p. 11811-24.
53. Krishna, B.A., et al., *The Requirement for US28 During Cytomegalovirus Latency Is Independent of US27 and US29 Gene Expression*. Front Cell Infect Microbiol, 2020. **10**: p. 186.
54. Krishna, B.A., et al., *Human cytomegalovirus G protein-coupled receptor US28 promotes latency by attenuating c-fos*. Proc Natl Acad Sci U S A, 2019. **116**(5): p. 1755-1764.
55. Heukers, R., et al., *The constitutive activity of the virally encoded chemokine receptor US28 accelerates glioblastoma growth*. Oncogene, 2018. **37**(30): p. 4110-4121.
56. Kotenko, S.V., et al., *Human cytomegalovirus harbors its own unique IL-10 homolog (cmvIL-10)*. Proc Natl Acad Sci U S A, 2000. **97**(4): p. 1695-700.
57. Chang, W.L., et al., *Human cytomegalovirus-encoded interleukin-10 homolog inhibits maturation of dendritic cells and alters their functionality*. J Virol, 2004. **78**(16): p. 8720-31.
58. Poole, E., et al., *Human Cytomegalovirus Interleukin 10 Homologs: Facing the Immune System*. Front Cell Infect Microbiol, 2020. **10**: p. 245.
59. Jenkins, C., A. Abendroth, and B. Slobedman, *A novel viral transcript with homology to human interleukin-10 is expressed during latent human cytomegalovirus infection*. J Virol, 2004. **78**(3): p. 1440-7.
60. Lin, Y.L., et al., *Identification of novel viral interleukin-10 isoforms of human cytomegalovirus AD169*. Virus Res, 2008. **131**(2): p. 213-23.

61. Avdic, S., et al., *Human Cytomegalovirus-Encoded Human Interleukin-10 (IL-10) Homolog Amplifies Its Immunomodulatory Potential by Upregulating Human IL-10 in Monocytes*. J Virol, 2016. **90**(8): p. 3819-3827.
62. Deere, J.D., et al., *Neutralization of rhesus cytomegalovirus IL-10 reduces horizontal transmission and alters long-term immunity*. Proc Natl Acad Sci U S A, 2019. **116**(26): p. 13036-13041.
63. Chang, W.L. and P.A. Barry, *Attenuation of innate immunity by cytomegalovirus IL-10 establishes a long-term deficit of adaptive antiviral immunity*. Proc Natl Acad Sci U S A, 2010. **107**(52): p. 22647-52.
64. Mutnal, M.B., et al., *Excess neutrophil infiltration during cytomegalovirus brain infection of interleukin-10-deficient mice*. J Neuroimmunol, 2010. **227**(1-2): p. 101-10.
65. Wang, D. and T. Shenk, *Human cytomegalovirus virion protein complex required for epithelial and endothelial cell tropism*. Proc Natl Acad Sci U S A, 2005. **102**(50): p. 18153-8.
66. Pontejo, S.M. and P.M. Murphy, *Chemokines encoded by herpesviruses*. J Leukoc Biol, 2017. **102**(5): p. 1199-1217.
67. Zheng, Q., et al., *HCMV-encoded UL128 enhances TNF-alpha and IL-6 expression and promotes PBMC proliferation through the MAPK/ERK pathway in vitro*. Viral Immunol, 2012. **25**(2): p. 98-105.
68. Malkowska, M., et al., *Alphaherpesvirinae and Gammaherpesvirinae glycoprotein L and CMV UL130 originate from chemokines*. Virol J, 2013. **10**: p. 1.
69. Patrone, M., et al., *Human cytomegalovirus UL130 protein promotes endothelial cell infection through a producer cell modification of the virion*. J Virol, 2005. **79**(13): p. 8361-73.
70. Saederup, N., et al., *Murine cytomegalovirus CC chemokine homolog MCK-2 (m131-129) is a determinant of dissemination that increases inflammation at initial sites of infection*. Journal of Virology, 2001. **75**(20): p. 9966-9976.

71. Noda, S., et al., *Cytomegalovirus MCK-2 controls mobilization and recruitment of myeloid progenitor cells to facilitate dissemination*. *Blood*, 2006. **107**(1): p. 30-8.
72. Wagner, F.M., et al., *The viral chemokine MCK-2 of murine cytomegalovirus promotes infection as part of a gH/gL/MCK-2 complex*. *PLoS Pathog*, 2013. **9**(7): p. e1003493.
73. Lutichau, H.R., *The Cytomegalovirus ULI46 Gene Product vCXCL1 Targets Both CXCR1 and CXCR2 as an Agonist*. *Journal of Biological Chemistry*, 2010. **285**(12): p. 9137-9146.
74. Yamin, R., et al., *HCMV vCXCL1 Binds Several Chemokine Receptors and Preferentially Attracts Neutrophils over NK Cells by Interacting with CXCR2*. *Cell Reports*, 2016. **15**(7): p. 1542-1553.
75. Wu, J., et al., *IL-6 and IL-8 secreted by tumour cells impair the function of NK cells via the STAT3 pathway in oesophageal squamous cell carcinoma*. *J Exp Clin Cancer Res*, 2019. **38**(1): p. 321.
76. Alfaro, C., et al., *Carcinoma-derived interleukin-8 disorients dendritic cell migration without impairing T-cell stimulation*. *PLoS One*, 2011. **6**(3): p. e17922.
77. Min, C.K., et al., *The Differentiation of Human Cytomegalovirus Infected-Monocytes Is Required for Viral Replication*. *Front Cell Infect Microbiol*, 2020. **10**: p. 368.
78. Jackson, J.W. and T. Sparer, *There Is Always Another Way! Cytomegalovirus' Multifaceted Dissemination Schemes*. *Viruses*, 2018. **10**(7).
79. Dolan, A., et al., *Genetic content of wild-type human cytomegalovirus*. *J Gen Virol*, 2004. **85**(Pt 5): p. 1301-1312.
80. Raju, R., et al., *Differential ligand-signaling network of CCL19/CCL21-CCR7 system*. *Database (Oxford)*, 2015. **2015**.
81. Yan, Y., et al., *CCL19 and CCR7 Expression, Signaling Pathways, and Adjuvant Functions in Viral Infection and Prevention*. *Front Cell Dev Biol*, 2019. **7**: p. 212.
82. Arav-Boger, R., *Strain Variation and Disease Severity in Congenital Cytomegalovirus Infection: In Search of a Viral Marker*. *Infect Dis Clin North Am*, 2015. **29**(3): p. 401-14.

83. He, R., et al., *Sequence variability of human cytomegalovirus UL146 and UL147 genes in low-passage clinical isolates*. Intervirology, 2006. **49**(4): p. 215-23.
84. Heo, J., et al., *Polymorphisms within human cytomegalovirus chemokine (UL146/UL147) and cytokine receptor genes (UL144) are not predictive of sequelae in congenitally infected children*. Virology, 2008. **378**(1): p. 86-96.
85. Berg, C., et al., *The frequency of cytomegalovirus non-ELR UL146 genotypes in neonates with congenital CMV disease is comparable to strains in the background population*. BMC Infect Dis, 2021. **21**(1): p. 386.
86. Guo, G., et al., *Polymorphisms and features of cytomegalovirus UL144 and UL146 in congenitally infected neonates with hepatic involvement*. PLoS One, 2017. **12**(2): p. e0171959.
87. Paradowska, E., et al., *Cytomegalovirus alpha-chemokine genotypes are associated with clinical manifestations in children with congenital or postnatal infections*. Virology, 2014. **462-463**: p. 207-17.
88. Oxford, K.L., et al., *Protein coding content of the UL)b' region of wild-type rhesus cytomegalovirus*. Virology, 2008. **373**(1): p. 181-8.
89. Malouli, D., et al., *Cytomegaloviral determinants of CD8(+) T cell programming and RhCMV/SIV vaccine efficacy*. Sci Immunol, 2021. **6**(57).
90. Lippert, U., et al., *Human T lymphocytes and mast cells differentially express and regulate extra- and intracellular CXCR1 and CXCR2*. Exp Dermatol, 2004. **13**(8): p. 520-5.
91. Stadtmann, A. and A. Zarbock, *CXCR2: From Bench to Bedside*. Front Immunol, 2012. **3**: p. 263.
92. Kolaczkowska, E. and P. Kubes, *Neutrophil recruitment and function in health and inflammation*. Nat Rev Immunol, 2013. **13**(3): p. 159-75.
93. Johansson, C. and F.C.M. Kirsebom, *Neutrophils in respiratory viral infections*. Mucosal Immunol, 2021. **14**(4): p. 815-827.
94. Rinaldo, C.R., Jr., P.H. Black, and M.S. Hirsch, *Interaction of cytomegalovirus with leukocytes from patients with mononucleosis due to cytomegalovirus*. J Infect Dis, 1977. **136**(5): p. 667-78.

95. Winston, D.J., et al., *Prophylactic granulocyte transfusions during human bone marrow transplantation*. Am J Med, 1980. **68**(6): p. 893-7.
96. Hersman, J., et al., *The effect of granulocyte transfusions on the incidence of cytomegalovirus infection after allogeneic marrow transplantation*. Ann Intern Med, 1982. **96**(2): p. 149-52.
97. Gerna, G., et al., *Human cytomegalovirus infection of the major leukocyte subpopulations and evidence for initial viral replication in polymorphonuclear leukocytes from viremic patients*. J Infect Dis, 1992. **166**(6): p. 1236-44.
98. Saltzman, R.L., M.R. Quirk, and M.C. Jordan, *Disseminated cytomegalovirus infection. Molecular analysis of virus and leukocyte interactions in viremia*. J Clin Invest, 1988. **81**(1): p. 75-81.
99. Gerna, G., et al., *Human cytomegalovirus replicates abortively in polymorphonuclear leukocytes after transfer from infected endothelial cells via transient microfusion events*. J Virol, 2000. **74**(12): p. 5629-38.
100. Grundy, J.E., et al., *Cytomegalovirus-infected endothelial cells recruit neutrophils by the secretion of C-X-C chemokines and transmit virus by direct neutrophil-endothelial cell contact and during neutrophil transendothelial migration*. J Infect Dis, 1998. **177**(6): p. 1465-74.
101. Braun, B. and C. Sinzger, *Transmission of cell-associated human cytomegalovirus isolates between various cell types using polymorphonuclear leukocytes as a vehicle*. Med Microbiol Immunol, 2021. **210**(4): p. 197-209.
102. van der Strate, B.W., et al., *Dissemination of rat cytomegalovirus through infected granulocytes and monocytes in vitro and in vivo*. J Virol, 2003. **77**(20): p. 11274-8.
103. Eash, K.J., et al., *CXCR2 and CXCR4 antagonistically regulate neutrophil trafficking from murine bone marrow*. J Clin Invest, 2010. **120**(7): p. 2423-31.
104. Martin, C., et al., *Chemokines acting via CXCR2 and CXCR4 control the release of neutrophils from the bone marrow and their return following senescence*. Immunity, 2003. **19**(4): p. 583-93.

105. Suratt, B.T., et al., *Role of the CXCR4/SDF-1 chemokine axis in circulating neutrophil homeostasis*. *Blood*, 2004. **104**(2): p. 565-71.
106. Burdon, P.C., C. Martin, and S.M. Rankin, *Migration across the sinusoidal endothelium regulates neutrophil mobilization in response to ELR + CXC chemokines*. *Br J Haematol*, 2008. **142**(1): p. 100-8.
107. Wengner, A.M., et al., *The coordinated action of G-CSF and ELR + CXC chemokines in neutrophil mobilization during acute inflammation*. *Blood*, 2008. **111**(1): p. 42-9.
108. Sas, A.R., et al., *A new neutrophil subset promotes CNS neuron survival and axon regeneration*. *Nat Immunol*, 2020. **21**(12): p. 1496-1505.
109. Girbl, T., et al., *Distinct Compartmentalization of the Chemokines CXCL1 and CXCL2 and the Atypical Receptor ACKR1 Determine Discrete Stages of Neutrophil Diapedesis*. *Immunity*, 2018. **49**(6): p. 1062-1076 e6.
110. Rudd, J.M., et al., *Neutrophils Induce a Novel Chemokine Receptors Repertoire During Influenza Pneumonia*. *Front Cell Infect Microbiol*, 2019. **9**: p. 108.
111. Hartl, D., et al., *Infiltrated neutrophils acquire novel chemokine receptor expression and chemokine responsiveness in chronic inflammatory lung diseases*. *J Immunol*, 2008. **181**(11): p. 8053-67.
112. Johnston, B., et al., *Chronic inflammation upregulates chemokine receptors and induces neutrophil migration to monocyte chemoattractant protein-1*. *J Clin Invest*, 1999. **103**(9): p. 1269-76.
113. Lionakis, M.S., et al., *Chemokine receptor Ccr1 drives neutrophil-mediated kidney immunopathology and mortality in invasive candidiasis*. *PLoS Pathog*, 2012. **8**(8): p. e1002865.
114. Zarbock, A. and K. Ley, *Neutrophil adhesion and activation under flow*. *Microcirculation*, 2009. **16**(1): p. 31-42.
115. Lammermann, T., et al., *Neutrophil swarms require LTB4 and integrins at sites of cell death in vivo*. *Nature*, 2013. **498**(7454): p. 371-5.

116. Mao, Z., et al., *CXCL5 promotes gastric cancer metastasis by inducing epithelial-mesenchymal transition and activating neutrophils*. *Oncogenesis*, 2020. **9**(7): p. 63.
117. Oyoshi, M.K., et al., *Leukotriene B4-driven neutrophil recruitment to the skin is essential for allergic skin inflammation*. *Immunity*, 2012. **37**(4): p. 747-58.
118. Thomas, C.J. and K. Schroder, *Pattern recognition receptor function in neutrophils*. *Trends Immunol*, 2013. **34**(7): p. 317-28.
119. Saitoh, T., et al., *Neutrophil extracellular traps mediate a host defense response to human immunodeficiency virus-1*. *Cell Host Microbe*, 2012. **12**(1): p. 109-16.
120. Wang, J.P., et al., *Toll-like receptor-mediated activation of neutrophils by influenza A virus*. *Blood*, 2008. **112**(5): p. 2028-34.
121. To, E.E., et al., *Intranasal and epicutaneous administration of Toll-like receptor 7 (TLR7) agonists provides protection against influenza A virus-induced morbidity in mice*. *Sci Rep*, 2019. **9**(1): p. 2366.
122. Wang, Y. and F. Jonsson, *Expression, Role, and Regulation of Neutrophil Fcγ Receptors*. *Front Immunol*, 2019. **10**: p. 1958.
123. Li, H., et al., *Reactive Oxygen Species in Pathogen Clearance: The Killing Mechanisms, the Adaption Response, and the Side Effects*. *Front Microbiol*, 2020. **11**: p. 622534.
124. Nagaraj, S., et al., *Altered recognition of antigen is a mechanism of CD8+ T cell tolerance in cancer*. *Nat Med*, 2007. **13**(7): p. 828-35.
125. Yang, W., et al., *Neutrophils promote the development of reparative macrophages mediated by ROS to orchestrate liver repair*. *Nat Commun*, 2019. **10**(1): p. 1076.
126. Warnatsch, A., et al., *Reactive Oxygen Species Localization Programs Inflammation to Clear Microbes of Different Size*. *Immunity*, 2017. **46**(3): p. 421-432.
127. Kobayashi, S.D., N. Malachowa, and F.R. DeLeo, *Neutrophils and Bacterial Immune Evasion*. *J Innate Immun*, 2018. **10**(5-6): p. 432-441.
128. Papayannopoulos, V., *Neutrophil extracellular traps in immunity and disease*. *Nat Rev Immunol*, 2018. **18**(2): p. 134-147.

129. Guiducci, E., et al., *Candida albicans-Induced NETosis Is Independent of Peptidylarginine Deiminase 4*. Front Immunol, 2018. **9**: p. 1573.
130. Roos, D., A.A. Voetman, and L.J. Meerhof, *Functional activity of enucleated human polymorphonuclear leukocytes*. J Cell Biol, 1983. **97**(2): p. 368-77.
131. Krishnamoorthy, N., et al., *Neutrophil cytoplasts induce TH17 differentiation and skew inflammation toward neutrophilia in severe asthma*. Sci Immunol, 2018. **3**(26).
132. Malawista, S.E., G. Van Blaricom, and M.G. Breitenstein, *Cryopreservable neutrophil surrogates. Stored cytoplasts from human polymorphonuclear leukocytes retain chemotactic, phagocytic, and microbicidal function*. J Clin Invest, 1989. **83**(2): p. 728-32.
133. Hiroki, C.H., et al., *Neutrophil Extracellular Traps Effectively Control Acute Chikungunya Virus Infection*. Front Immunol, 2019. **10**: p. 3108.
134. Muraro, S.P., et al., *Respiratory Syncytial Virus induces the classical ROS-dependent NETosis through PAD-4 and necroptosis pathways activation*. Sci Rep, 2018. **8**(1): p. 14166.
135. Barr, F.D., et al., *Neutrophil extracellular traps prevent HIV infection in the female genital tract*. Mucosal Immunol, 2018. **11**(5): p. 1420-1428.
136. Stacey, H.D., et al., *IgA potentiates NETosis in response to viral infection*. Proc Natl Acad Sci U S A, 2021. **118**(27).
137. Hu, S., et al., *Hepatitis B Virus Inhibits Neutrophil Extracellular Trap Release by Modulating Reactive Oxygen Species Production and Autophagy*. J Immunol, 2019. **202**(3): p. 805-815.
138. Sivanandham, R., et al., *Neutrophil extracellular trap production contributes to pathogenesis in SIV-infected nonhuman primates*. J Clin Invest, 2018. **128**(11): p. 5178-5183.
139. Vono, M., et al., *Neutrophils acquire the capacity for antigen presentation to memory CD4(+) T cells in vitro and ex vivo*. Blood, 2017. **129**(14): p. 1991-2001.
140. Lin, A. and K. Lore, *Granulocytes: New Members of the Antigen-Presenting Cell Family*. Front Immunol, 2017. **8**: p. 1781.

141. Hufford, M.M., et al., *Influenza-infected neutrophils within the infected lungs act as antigen presenting cells for anti-viral CD8(+) T cells*. PLoS One, 2012. **7**(10): p. e46581.
142. Meinderts, S.M., et al., *Neutrophils acquire antigen-presenting cell features after phagocytosis of IgG-opsonized erythrocytes*. Blood Adv, 2019. **3**(11): p. 1761-1773.
143. Yang, C.W., et al., *Neutrophils influence the level of antigen presentation during the immune response to protein antigens in adjuvants*. J Immunol, 2010. **185**(5): p. 2927-34.
144. Tamassia, N., et al., *Cytokine production by human neutrophils: Revisiting the "dark side of the moon"*. Eur J Clin Invest, 2018. **48 Suppl 2**: p. e12952.
145. Prame Kumar, K., A.J. Nicholls, and C.H.Y. Wong, *Partners in crime: neutrophils and monocytes/macrophages in inflammation and disease*. Cell Tissue Res, 2018. **371**(3): p. 551-565.
146. van Gisbergen, K.P., et al., *Neutrophils mediate immune modulation of dendritic cells through glycosylation-dependent interactions between Mac-1 and DC-SIGN*. J Exp Med, 2005. **201**(8): p. 1281-92.
147. Yang, D., et al., *Human neutrophil defensins selectively chemoattract naive T and immature dendritic cells*. J Leukoc Biol, 2000. **68**(1): p. 9-14.
148. Jaeger, B.N., et al., *Neutrophil depletion impairs natural killer cell maturation, function, and homeostasis*. J Exp Med, 2012. **209**(3): p. 565-80.
149. Lim, K., et al., *Neutrophil trails guide influenza-specific CD8(+) T cells in the airways*. Science, 2015. **349**(6252): p. aaa4352.
150. Leliefeld, P.H., L. Koenderman, and J. Pillay, *How Neutrophils Shape Adaptive Immune Responses*. Front Immunol, 2015. **6**: p. 471.
151. de Kleijn, S., et al., *IFN-gamma-stimulated neutrophils suppress lymphocyte proliferation through expression of PD-L1*. PLoS One, 2013. **8**(8): p. e72249.
152. Tak, T., et al., *Similar activation state of neutrophils in sputum of asthma patients irrespective of sputum eosinophilia*. Clin Exp Immunol, 2015. **182**(2): p. 204-12.

153. Costa, S., et al., *Recent advances on the crosstalk between neutrophils and B or T lymphocytes*. Immunology, 2019. **156**(1): p. 23-32.
154. Puga, I., et al., *B cell-helper neutrophils stimulate the diversification and production of immunoglobulin in the marginal zone of the spleen*. Nat Immunol, 2011. **13**(2): p. 170-80.
155. Parsa, R., et al., *BAFF-secreting neutrophils drive plasma cell responses during emergency granulopoiesis*. J Exp Med, 2016. **213**(8): p. 1537-53.
156. Naranjo-Gomez, M., et al., *Neutrophils are essential for induction of vaccine-like effects by antiviral monoclonal antibody immunotherapies*. JCI Insight, 2018. **3**(9).
157. Gatjen, M., et al., *Splenic Marginal Zone Granulocytes Acquire an Accentuated Neutrophil B-Cell Helper Phenotype in Chronic Lymphocytic Leukemia*. Cancer Res, 2016. **76**(18): p. 5253-65.
158. Schwaller, J., et al., *Neutrophil-derived APRIL concentrated in tumor lesions by proteoglycans correlates with human B-cell lymphoma aggressiveness*. Blood, 2007. **109**(1): p. 331-8.
159. Kamenyeva, O., et al., *Neutrophil recruitment to lymph nodes limits local humoral response to Staphylococcus aureus*. PLoS Pathog, 2015. **11**(4): p. e1004827.
160. Lelis, F.J.N., et al., *Myeloid-derived suppressor cells modulate B-cell responses*. Immunol Lett, 2017. **188**: p. 108-115.
161. Greenlee-Wacker, M.C., *Clearance of apoptotic neutrophils and resolution of inflammation*. Immunol Rev, 2016. **273**(1): p. 357-70.
162. Savill, J.S., et al., *Macrophage phagocytosis of aging neutrophils in inflammation. Programmed cell death in the neutrophil leads to its recognition by macrophages*. J Clin Invest, 1989. **83**(3): p. 865-75.
163. Fadok, V.A., et al., *Macrophages that have ingested apoptotic cells in vitro inhibit proinflammatory cytokine production through autocrine/paracrine mechanisms involving TGF-beta, PGE2, and PAF*. J Clin Invest, 1998. **101**(4): p. 890-8.

164. Chung, E.Y., et al., *Interleukin-10 expression in macrophages during phagocytosis of apoptotic cells is mediated by homeodomain proteins Pbx1 and Prep-1*. *Immunity*, 2007. **27**(6): p. 952-64.
165. Cumpelik, A., et al., *Neutrophil microvesicles resolve gout by inhibiting C5a-mediated priming of the inflammasome*. *Ann Rheum Dis*, 2016. **75**(6): p. 1236-45.
166. Headland, S.E., et al., *Neutrophil-derived microvesicles enter cartilage and protect the joint in inflammatory arthritis*. *Sci Transl Med*, 2015. **7**(315): p. 315ra190.
167. Nishio, N., et al., *Neutrophil depletion delays wound repair in aged mice*. *Age (Dordr)*, 2008. **30**(1): p. 11-9.
168. Gonzalez, L.A., et al., *Characterization of the Anti-Inflammatory Capacity of IL-10-Producing Neutrophils in Response to Streptococcus pneumoniae Infection*. *Front Immunol*, 2021. **12**: p. 638917.
169. Kasten, K.R., J.T. Muenzer, and C.C. Caldwell, *Neutrophils are significant producers of IL-10 during sepsis*. *Biochem Biophys Res Commun*, 2010. **393**(1): p. 28-31.
170. Lewkowicz, N., et al., *Induction of human IL-10-producing neutrophils by LPS-stimulated Treg cells and IL-10*. *Mucosal Immunol*, 2016. **9**(2): p. 364-78.
171. Rivadeneyra, L., et al., *Role of neutrophils in CVB3 infection and viral myocarditis*. *J Mol Cell Cardiol*, 2018. **125**: p. 149-161.
172. Liu, L., et al., *Neutrophil-to-lymphocyte ratio, a critical predictor for assessment of disease severity in patients with COVID-19*. *Int J Lab Hematol*, 2021. **43**(2): p. 329-335.
173. Liu, Y., et al., *Neutrophil-to-lymphocyte ratio as an independent risk factor for mortality in hospitalized patients with COVID-19*. *J Infect*, 2020. **81**(1): p. e6-e12.
174. Wang, J., et al., *Excessive Neutrophils and Neutrophil Extracellular Traps in COVID-19*. *Front Immunol*, 2020. **11**: p. 2063.
175. Parackova, Z., et al., *Disharmonic Inflammatory Signatures in COVID-19: Augmented Neutrophils' but Impaired Monocytes' and Dendritic Cells' Responsiveness*. *Cells*, 2020. **9**(10).

176. Zuo, Y., et al., *Neutrophil extracellular traps in COVID-19*. JCI Insight, 2020. **5**(11).
177. Nagarkar, D.R., et al., *CXCR2 is required for neutrophilic airway inflammation and hyperresponsiveness in a mouse model of human rhinovirus infection*. J Immunol, 2009. **183**(10): p. 6698-707.
178. Ashar, H.K., et al., *Administration of a CXC Chemokine Receptor 2 (CXCR2) Antagonist, SCH527123, Together with Oseltamivir Suppresses NETosis and Protects Mice from Lethal Influenza and Piglets from Swine-Influenza Infection*. Am J Pathol, 2021. **191**(4): p. 669-685.
179. Tak, T., et al., *Neutrophil-mediated Suppression of Influenza-induced Pathology Requires CD11b/CD18 (MAC-1)*. Am J Respir Cell Mol Biol, 2018. **58**(4): p. 492-499.
180. Michael, B.D., et al., *Astrocyte- and Neuron-Derived CXCL1 Drives Neutrophil Transmigration and Blood-Brain Barrier Permeability in Viral Encephalitis*. Cell Rep, 2020. **32**(11): p. 108150.
181. Hosking, M.P., et al., *A protective role for ELR+ chemokines during acute viral encephalomyelitis*. PLoS Pathog, 2009. **5**(11): p. e1000648.
182. Zhao, Y., et al., *Neutrophils may be a vehicle for viral replication and dissemination in human H5N1 avian influenza*. Clin Infect Dis, 2008. **47**(12): p. 1575-8.
183. Larochelle, B., et al., *Epstein-Barr virus infects and induces apoptosis in human neutrophils*. Blood, 1998. **92**(1): p. 291-9.
184. Yourtee, E.L., et al., *Neutrophil response and function during acute cytomegalovirus infection in guinea pigs*. Infect Immun, 1982. **36**(1): p. 11-6.
185. Bale, J.F., Jr., M.E. O'Neil, and T. Greiner, *The interaction of murine cytomegalovirus with murine neutrophils: effect on migratory and phagocytic activities*. J Leukoc Biol, 1985. **38**(6): p. 723-34.
186. Lineaweaver, W., R.J. Howard, and S. McMorris, *Duration of murine neutrophil migration impairments after cytomegalovirus infection*. Surg Gynecol Obstet, 1984. **158**(6): p. 555-6.

187. Bale, J.F., Jr., et al., *Enhanced susceptibility of mice infected with murine cytomegalovirus to intranasal challenge with Escherichia coli: pathogenesis and altered inflammatory response*. J Infect Dis, 1982. **145**(4): p. 525-31.
188. Hamilton, J.R. and J.C. Overall, Jr., *Synergistic infection with murine cytomegalovirus and Pseudomonas aeruginosa in mice*. J Infect Dis, 1978. **137**(6): p. 775-82.
189. Hamilton, J.R., J.C. Overall, and L.A. Glasgow, *Synergistic effect on mortality in mice with murine cytomegalovirus and Pseudomonas aeruginosa, Staphylococcus aureus, or Candida albicans infections*. Infect Immun, 1976. **14**(4): p. 982-9.
190. Hamilton, J.R., J.C. Overall, Jr., and L.A. Glasgow, *Synergistic infection with murine cytomegalovirus and Candida albicans in mice*. J Infect Dis, 1977. **135**(6): p. 918-24.
191. Yong, M.K., M.A. Slavin, and D.P. Kontoyiannis, *Invasive fungal disease and cytomegalovirus infection: is there an association?* Curr Opin Infect Dis, 2018. **31**(6): p. 481-489.
192. Miyake, K. and H. Karasuyama, *The Role of Trogocytosis in the Modulation of Immune Cell Functions*. Cells, 2021. **10**(5).
193. Mercer, F., et al., *Neutrophils kill the parasite Trichomonas vaginalis using trogocytosis*. PLoS Biol, 2018. **16**(2): p. e2003885.
194. Matlung, H.L., et al., *Neutrophils Kill Antibody-Opsonized Cancer Cells by Trogocytosis*. Cell Rep, 2018. **23**(13): p. 3946-3959 e6.
195. Wakim, L.M. and M.J. Bevan, *Cross-dressed dendritic cells drive memory CD8+ T-cell activation after viral infection*. Nature, 2011. **471**(7340): p. 629-32.
196. Yamanaka, N., et al., *Bone marrow transplantation results in human donor blood cells acquiring and displaying mouse recipient class I MHC and CD45 antigens on their surface*. PLoS One, 2009. **4**(12): p. e8489.
197. Rosenits, K., et al., *T cells acquire cell surface determinants of APC via in vivo trogocytosis during viral infections*. Eur J Immunol, 2010. **40**(12): p. 3450-7.
198. Steele, S., et al., *Trogocytosis-associated cell to cell spread of intracellular bacterial pathogens*. Elife, 2016. **5**.

199. Kongsomros, S., et al., *Trogocytosis with monocytes associated with increased alpha2,3 sialic acid expression on B cells during H5N1 influenza virus infection*. PLoS One, 2020. **15**(9): p. e0239488.
200. Aucher, A., et al., *Could CD4 capture by CD8+ T cells play a role in HIV spreading?* J Biomed Biotechnol, 2010. **2010**: p. 907371.
201. Hind, L.E. and A. Huttenlocher, *Neutrophil Reverse Migration and a Chemokinetic Resolution*. Dev Cell, 2018. **47**(4): p. 404-405.
202. Colom, B., et al., *Leukotriene B4-Neutrophil Elastase Axis Drives Neutrophil Reverse Transendothelial Cell Migration In Vivo*. Immunity, 2015. **42**(6): p. 1075-86.
203. Buckley, C.D., et al., *Identification of a phenotypically and functionally distinct population of long-lived neutrophils in a model of reverse endothelial migration*. J Leukoc Biol, 2006. **79**(2): p. 303-11.
204. Wu, D., et al., *Reverse-migrated neutrophils regulated by JAM-C are involved in acute pancreatitis-associated lung injury*. Sci Rep, 2016. **6**: p. 20545.
205. Wang, J., et al., *Visualizing the function and fate of neutrophils in sterile injury and repair*. Science, 2017. **358**(6359): p. 111-116.
206. van Zandbergen, G., et al., *Cutting edge: neutrophil granulocyte serves as a vector for Leishmania entry into macrophages*. J Immunol, 2004. **173**(11): p. 6521-5.
207. Christiaansen, A., S.M. Varga, and J.V. Spencer, *Viral manipulation of the host immune response*. Curr Opin Immunol, 2015. **36**: p. 54-60.
208. Pocock, J.M., et al., *Human Cytomegalovirus Delays Neutrophil Apoptosis and Stimulates the Release of a Prosurvival Secretome*. Front Immunol, 2017. **8**: p. 1185.
209. Sinclair, J., *Human cytomegalovirus: Latency and reactivation in the myeloid lineage*. J Clin Virol, 2008. **41**(3): p. 180-5.
210. Gabali, A.M., et al., *Activation by inflammatory stimuli increases neutrophil binding of human immunodeficiency virus type 1 and subsequent infection of lymphocytes*. J Virol, 2004. **78**(19): p. 10833-6.

211. Bonecchi, R., et al., *Induction of functional IL-8 receptors by IL-4 and IL-13 in human monocytes*. J Immunol, 2000. **164**(7): p. 3862-9.
212. Farrell, H.E., et al., *Murine Cytomegalovirus Spreads by Dendritic Cell Recirculation*. mBio, 2017. **8**(5).
213. Farrell, H.E., et al., *Murine Cytomegalovirus Spread Depends on the Infected Myeloid Cell Type*. J Virol, 2019. **93**(15).
214. Alter, A., et al., *Determinants of human B cell migration across brain endothelial cells*. J Immunol, 2003. **170**(9): p. 4497-505.
215. Compton, T., D.M. Nowlin, and N.R. Cooper, *Initiation of Human Cytomegalovirus-Infection Requires Initial Interaction with Cell-Surface Heparan-Sulfate*. Virology, 1993. **193**(2): p. 834-841.

**CHAPTER 2 - IMMUNOPHENTYPING CXCR2 EXPRESSION  
ACROSS A VARIETY OF IMMUNE CELLS DERIVED FROM  
VARIOUS TISSUES**

This work was performed by: Trevor J. Hancock, Sean Callahan, Jeremiah G. Johnson, Joseph W. Jackson, and Tim E. Sparer

Author Contributions: Conceptualization, T.E.S., J.W.J., and T.J.H.; Methodology, T.J.H.; Formal analysis, T.J.H.; Investigation, S.C. and T.J.H.; Writing—original draft preparation, J.W.J. and T.J.H.; Writing—review and editing, T.E.S., J.W.J., and T.J.H.; Visualization, T.J.H.; Funding Acquisition, J.G.J and T.E.S.

### **Abstract:**

Chemokine receptor expression is a tightly controlled process to ensure proper immune cell recruitment and activation. The chemokine receptor CXCR2 is important for many inflammatory responses. CXCR2 is associated with granulocytes where it plays a role in maturation and regulation of neutrophils. It is expressed on a variety of other, non-neutrophil immune cells in healthy and diseased individuals. However, CXCR2 expression has not been simultaneously profiled across multiple immune cell types in naïve humans or mice. We performed immunophenotyping to examine the distribution of CXCR2 on various cell types in human peripheral blood, as well as across three murine tissues (i.e., bone marrow, peripheral blood, and spleen). We show species differences in distribution of CXCR2 among human and mouse peripheral blood leukocytes, and varied CXCR2 expression among different mouse tissues. Overall, we found major leukocyte subsets widely express CXCR2 providing a more complete picture of possible targets of CXCR2-ligands in mice and humans.

### **Introduction:**

How cells within the body communicate with each other locally within tissues and across longer distances is an important immunological concept. Most cell types in the body express cytokines and their cognate receptors to some degree as a method for intercellular communication [1]. Within the broader classification of cytokines are small, soluble molecules known as chemokines which are primarily involved in trafficking and migration of cells [1]. Cytokine and chemokine receptors are important for the activation and

recruitment of immune cells from bone marrow or peripheral blood to distal tissues to mediate inflammation, pathogen clearance, wound repair, and tissue homeostasis [1, 2]. There are four broad classes of chemokines (and respective receptors) divided by the spacing of their N-terminal cysteines (i.e., CC, CXC, CX3C, C) [2]. Chemokines interact with select chemokine receptors (which are divided by their recognition of the four chemokine classes) [2]. These receptors fall under the umbrella of seven transmembrane, G-protein coupled receptors. While chemokines are selective for a specific-class of receptors, chemokines can interact with more than one receptor (and inversely one receptor can recognize multiple different chemokines) which can induce cell-specific responses [2]. Due to their important roles in immune responses and physiological development, expression of chemokines and their cognate receptor(s) is a tightly regulated process.

Binding and activation of a chemokine receptor can vary based on the chemokine interacting with it [3]. Two chemokines that bind to and activate the same receptor may activate the receptor differently, causing varying functional outcomes even on the same cell type [3]. This differential activation or “biased agonism” may be due to several factors including chemokine/receptor interface bindings. One of the most important motifs on a chemokine is its N-terminus. Differences in the length and amino acid composition of the N-terminus may determine the outcome of receptor activation [4]. Chemokine receptor and ligand may also interact at one or more extracellular loops of the G-protein coupled receptor [4, 5]. These interactions appear to play a role in the overall binding and positioning of the N-terminus of the chemokine and receptor [4, 5]. Further complicating the issue is that for some chemokine receptors expression is cell type specific.

Cells derived from the hematopoietic lineage are a major cell type expressing and influenced by chemokines. However, chemokine signaling within this population is not homogeneous. Some receptors and chemokines are ubiquitously expressed on immune cells, but not all cells express the same set of receptors/chemokines [2]. A prime example is the broadly expressed CXCR4 receptor and its ligand, CXCL12 (SDF-1). CXCR4 expression and stimulation by CXCL12 (SDF-1, secreted from stromal cells) is important for the proper retention and maturation of many immune cells in the bone marrow [6-8]. Analogously, the expression of the chemokine receptor CCR7 is tightly regulated and

found predominantly on cells capable of residing within the lymphatic system [9]. Cells expressing CCR7 migrate to lymph nodes towards gradients of CCL19/CCL21, which is released by multiple cell types found in secondary lymphoid organs [9]. Chemokine stimulation of cells such as neutrophils serves to “prime” them for subsequent antimicrobial functions as well as recruitment to tissues following infection or inflammation [10]. CXCL1 or CXCL8 stimulated neutrophils more readily produce ROS, perform phagocytosis, release cytotoxic granules, or release neutrophil extracellular traps (NETs), *via* a process termed NETosis [10]. Chemokines thus serve two important roles, both homing and activating/priming immune cells for effector functions.

CXCR2 is a pleiotropic chemokine receptor which is involved in varied diseases such as cancer, atherosclerosis/heart disease, and bacterial, viral, and fungal infections [11-13]. CXCR2 recognizes at least 7 CXC chemokines in humans (CXCL1-3 and CXCL5-8) with several homologs reported for mice [14]. One notable exception is human CXCL8 (IL-8), which lacks a homolog in mice [14]. However, murine CXCR2 is capable of recognizing and responding to human CXCL8 stimulation, highlighting the similarities in receptor function among diverse species [15]. Studies inhibiting or deleting CXCR2 lead to a compromised immune response and susceptibility to microbial infection [16-18]. In contrast, tumor cells expressing CXCR2 and secretion of CXCR2 ligands points to a more insidious role for CXCR2 in cancer, where this chemokine-receptor axis promotes tumor progression and metastasis [19-21]. Regardless of its role in diseases, activation of cells through the CXCR2 signaling axis can have important and wide-ranging immunological impacts.

However, only a scattering of cell types and subsets have been reported to be CXCR2 positive. Neutrophils represent the most prominent CXCR2-expressing cells owing to their uniformly high expression levels and relative abundance [2]. As such, studies on the receptor and its chemokine ligands typically utilize them. Many monocytes are also generally regarded as being CXCR2 positive, and their role in CXCR2-mediated responses is often reported [22-24]. Additional CXCR2 subsets such as T cells [25, 26], B cells [27, 28], NK cells [29, 30], and DCs [31] have also been published. However, many of these reports were individual immune cell types under specific conditions with little to

no correlation made back to the overall immune cell population. As such, there is a need to profile steady-state CXCR2 expression across prominent immune cell types in the commonly utilized C57BL/6 mouse strain, and peripheral blood of healthy human donors. Our goal was to determine not just what cells express CXCR2, but also their relative abundance within the overall CXCR2-positive and total population. Using multiparameter, spectral flowcytometry we broadly characterized CXCR2 expression in murine leukocytes from three distinct tissues (bone marrow, peripheral blood, and spleen) of naïve mice, and human peripheral blood.

### **Results:**

We performed multiparameter flowcytometry to broadly immunophenotype CXCR2 expression in murine leukocytes. Bone marrow, spleen, and peripheral blood were harvested from C57BL/6J mice and stained for flow cytometric analysis. Isolated and stained immune cells were stratified into the following classifications based on surface protein expression: T cells (CD3<sup>+</sup>, CD49b<sup>-</sup>), natural killer T cells (NKT cells) (CD3<sup>+</sup>, CD49b<sup>+</sup>) [32], B cells (CD3<sup>-</sup>, B220<sup>+</sup>, CD11b/c<sup>-</sup>) [33], pre-mature natural killer cells (pre-mNK cells) (CD49<sup>+</sup>, B220<sup>+</sup>, CD11c<sup>+</sup>) [34-37], mature natural killer cells (mNK cells) (CD3<sup>-</sup>, B220<sup>-</sup>, CD49b<sup>+</sup>) [38], plasmacytoid dendritic cells (pDC) (B220<sup>+</sup>, Ly6C<sup>+</sup>, CD11c<sup>+</sup>, CD11b<sup>-</sup>) [39, 40], conventional dendritic cells (cDC) (Ly6G<sup>-</sup>, Ly6C<sup>+</sup>, CD11c<sup>+</sup>) [40], monocytes (Ly6G<sup>-</sup>, Ly6C<sup>+</sup>, CD11c<sup>-</sup>, CD49b<sup>-</sup>) [40], neutrophils (Ly6G<sup>+</sup>, Ly6C<sup>+</sup>) [40]. The mouse immunophenotyping panel does not dive into specific T cell subsets, instead broadly classifying them based on CD3 expression. Similarly, B cells are broadly identified by B220 expression, and not subdivided into plasma cells, follicular cells, etc. We were able to stratify dendritic cells (DCs) into plasmacytoid and conventional DC subsets to examine CXCR2 expression and occurrence. Similarly, NKT's (natural killer T cells) were separated from other CD3-expressing T cells and CXCR2 expression characterized for this subset.

In Figure 1A, histograms show the cell types with each color representing a specific tissue. A large portion of neutrophils in all tissues are CXCR2-positive, but neutrophils within the bone marrow have more variable CXCR2 expression (Fig. 2.1 A). CXCR2-

positive cells can be seen within the monocyte, pDC, and NK cell populations (both pre-mNK and mNK cells) (Fig. 2.1 A). Monocytes from the bone marrow have the greatest relative abundance of CXCR2-positive cells, and for the splenic compartment, pDCs (Fig. 2.1 A). CXCR2-expressing NK cells are readily observed in both the spleen and bone marrow of mice (Fig. 2.1 A). The NKT CXCR2-expressing populations are found in all tissues assessed, but with a slight decrease in relative expression in the spleen (Fig. 2.1 A).

When murine bone marrow CXCR2-positive cells are stratified into their respective cell types, the population is dominated by neutrophils (72%) and monocytes (13%), followed by smaller numbers of the other assessed cell types (Fig. 2.1 B). Along with comprising the majority of CXCR2-positive cells, ~50% of bone marrow neutrophils express CXCR2 (Fig. 2.1 C). However, many cell types within the bone marrow had similar levels of CXCR2 expression in their cell populations (Fig 2.1 C). Large portions of bone marrow resident monocytes, cDCs, NKT cells, and mNK cells express CXCR2 as well (all >20%) (Fig. 2.1 C), but their lower abundance led to a lower percentage of total CXCR2-positive cells (Fig. 2.1 B). Among peripheral blood CXCR2<sup>+</sup> cells, neutrophils are the largest fraction at ~36%, followed surprisingly by B cells (26%), and CD3<sup>+</sup> T cells (12%) (Fig. 2.1 B). Despite being the second most numerous CXCR2-positive cells in peripheral blood, CXCR2-positive B cells are a lower percent of their total population (~10%), representing a subset of B cells in circulation (Fig. 2.1 C). Within the spleen, B cells (51%), DCs (~19%, combined pDC and cDC), and NK cells (12%, combined pre-mature and mature NK cells) are the three most abundant CXCR2-expressing cell types (Fig. 2.1 B). Splenic neutrophils are relatively rare (~0.4% of CD45<sup>+</sup> events) which explains why despite having >95% CXCR2 positive they represent only 5% of CXCR2-positive cells within the spleen (Fig. 2.1 B,C). Like the bone marrow, myeloid cells (i.e., monocytes, DCs, and NK cells) in other tissues represent abundant CXCR2-positive cells in both the overall CXCR2 population and among their respective cell type (Fig. 2.1 B,C). Outside of the bone marrow, CD3<sup>+</sup> T cells and NKT cells make up a large portion of the overall CXCR2-positive population. Combined they make up ~19% in peripheral blood, ~9% in the spleen (Fig. 2.1 B). In all, CXCR2-positive cells were found for all cell types

and their distribution/relative abundance even within the same animal appears to vary based on the tissue.

CXCR2 positivity was compared for each cell type across the three tissues isolated from the same animal (Fig. 2.1 D). For CD3<sup>+</sup> T cells, CXCR2 was expressed most often in the bone marrow with lower numbers in blood and spleen (Fig. 2.1 D). The increased contribution of CD3<sup>+</sup> T cells in the blood and spleen can be explained by their higher overall abundance in those tissues (Fig. 2.1 B). For NKT cells, B cells, and monocytes the percent of the population that is CXCR2-positive was not significantly different based on tissue type (Fig. 2.1 D). Pre-mNK cells and pDCs showed similar trends of CXCR2 percentage difference depending on tissue type (spleen>peripheral blood>bone marrow) (Fig. 2.1 D). mNK cells and cDCs had peak CXCR2 levels in the bone marrow (Fig. 2.1 D). Neutrophils found outside of the bone marrow are >95% positive for CXCR2 (Fig. 2.1 D), whereas neutrophils retained within the bone marrow are significantly lower at ~50% positive for CXCR2 (Fig. 2.1 D). Mature neutrophils and splenic pDCs have the highest percentage of CXCR2-positivity (Fig. 2.1 D).

Relative expression levels of CXCR2 were inferred by the mean fluorescent intensity (MFI) of CXCR2 staining. The MFI of the CXCR2-positive populations for each cell type is shown in Figure 2.1 E by tissue. PMNs have historically been associated with high expression and prevalence of CXCR2 [2]. We see this with high expression in bone marrow and spleen, with somewhat lowered CXCR2 levels in circulation (Fig. 2.1 E). However, subsets of other CXCR2<sup>+</sup> cells appear to be on par with murine neutrophils. For instance, pDCs are among the highest CXCR2 expressing cells in all three tissues. This expression is even higher than PMNs in bone marrow and peripheral blood (Fig. 2.1 E).

To assess species differences in CXCR2 expression, human peripheral blood was stained and cell type CXCR2 expression characterized. Immune subsets were identified by surface marker expression [41]. T cells were initially separated from CD3 expressing NKT cells by expression of CD56. CD56<sup>-</sup> T cells were then stratified based on expression of CD4 and CD8: helper T cells (CD4<sup>+</sup>, CD8<sup>-</sup>), cytotoxic T cells (CD4<sup>-</sup>, CD8<sup>+</sup>), double-positive T cells (CD4<sup>+</sup>, CD8<sup>+</sup>), and double-negative T cells (CD4<sup>-</sup>, CD8<sup>-</sup>). B cells (CD20<sup>+</sup>) and NK cells (CD3<sup>-</sup>, CD20<sup>-</sup>, CD56<sup>+</sup>) were separated from myeloid cells. Myeloid cells

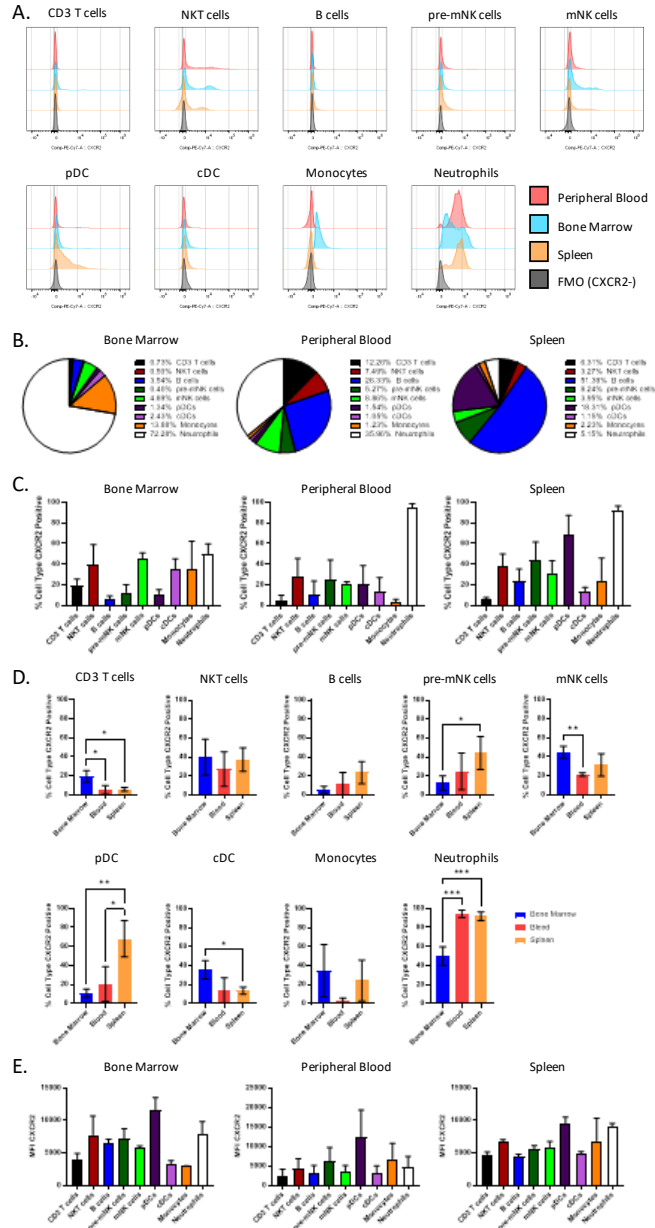


**Figure 2.1:** CXCR2 expression in various mouse tissues.

(A) Representative histograms of CXCR2 expression of various immune cell types. Histograms from each tissue for each identified cell type were overlaid. Each color represents a different tissue or fluorescence minus one (FMO) control lacking the CXCR2 antibody. Histograms were normalized to mode. (B) CXCR2 parts of whole. Total CXCR2 population in each tissue was broken down by contributing cell type. Colors correspond to each cell type and percent of whole is shown in each tissue's legend. (C) Percent of cell type CXCR2-positive. For each tissue, percent of each cell type positive for CXCR2 is shown. Comparison of the same cell type across each tissue was performed. Percent of the total population that is CXCR2 positive (D), mean fluorescent intensity (MFI) of the CXCR2-only (E) population were graphed for each cell type across all three tissues examined. (B-F)  $n \geq 2$  with 2-3 mice per group. Mean  $\pm$  standard deviation shown. Significance was determined by Welch's ANOVA with Dunnett's multiple comparisons. \* =  $p < 0.05$ , \*\* =  $p < 0.01$ , \*\*\* =  $p < 0.001$ , \*\*\*\* =  $p < 0.0001$ .

(CD3<sup>-</sup>, CD20<sup>-</sup>, CD56<sup>-</sup>, CD11b<sup>+/-</sup>) were examined for monocyte and dendritic cell populations: non-classical monocytes (CD16<sup>+</sup>, CD14<sup>-</sup>), intermediate monocytes (CD16<sup>+</sup>, CD14<sup>+</sup>), classical monocytes (CD16<sup>-</sup>, CD14<sup>+</sup>), pDCs (CD16/14<sup>-</sup>, CD123<sup>+</sup>, CD11c<sup>+/-</sup>) cDCs (CD16/14<sup>-</sup>, CD123<sup>-</sup>, CD11c<sup>+</sup>). Neutrophils in the peripheral blood mononuclear (PBMCs) and granulocytic fraction were identified as CD16<sup>+</sup> and CD66b<sup>+</sup> [42].

CXCR2 expression levels for each identified cell type are shown (Fig. 2.2 A). Neutrophils have abundant and high expression of CXCR2, followed by peripheral monocytes and NK cells (Fig. 2.2 A). CXCR2-positive cells were broken down by cell type with (Fig. 2.2 B) and without the inclusion of peripheral neutrophils (Fig. 2.2 C). Neutrophils represent 65% of circulating CXCR2<sup>+</sup> cells, followed by NK cells (10%), classical Monocytes (8%), and pDCs (6%) (Fig. 2.2 C). When neutrophils are excluded, almost 75% of circulating CXCR2 expressing cells are NK cells, classical monocytes, and pDCs (Fig. 2.2 B). The number of circulating CXCR2<sup>+</sup> cells per mL of whole blood is shown for each cell type (Fig. 2.2 D). Additionally, the percentage of each cell type that is CXCR2<sup>+</sup> is shown in Fig. 2.2 E. Myeloid cells were  $\geq 20\%$  CXCR2<sup>+</sup>, with the three highest  $>50\%$  (neutrophils, NK cells, classical monocytes) (Fig. 2.2 E). Relative expression of CXCR2 on positive cells was examined (Fig. 2.2 F), and unsurprisingly neutrophils are the highest CXCR2 expressors. Among the other CXCR2<sup>+</sup> peripheral leukocytes, expression levels were similar (Fig. 2.2 F).

### **Discussion:**

Based on the results of the immunophenotyping panel, CXCR2 is expressed on almost all murine immune cell types examined (albeit only on a smaller subset of T and B cells) (Fig. 2.1 C). The composition of CXCR2 positive cells appears to vary based on the tissue type. Where neutrophils compromise a larger percent of the total population such as bone marrow and peripheral blood, they dominate the CXCR2-positive population (Fig. 1.2B). Monocytes, DCs, NK, and NKT cells represent the next most abundant CXCR2 expressing cells. Next to neutrophils, they have the highest percentage of CXCR2-positivity and contribute accordingly to the overall CXCR2 positive population. We were

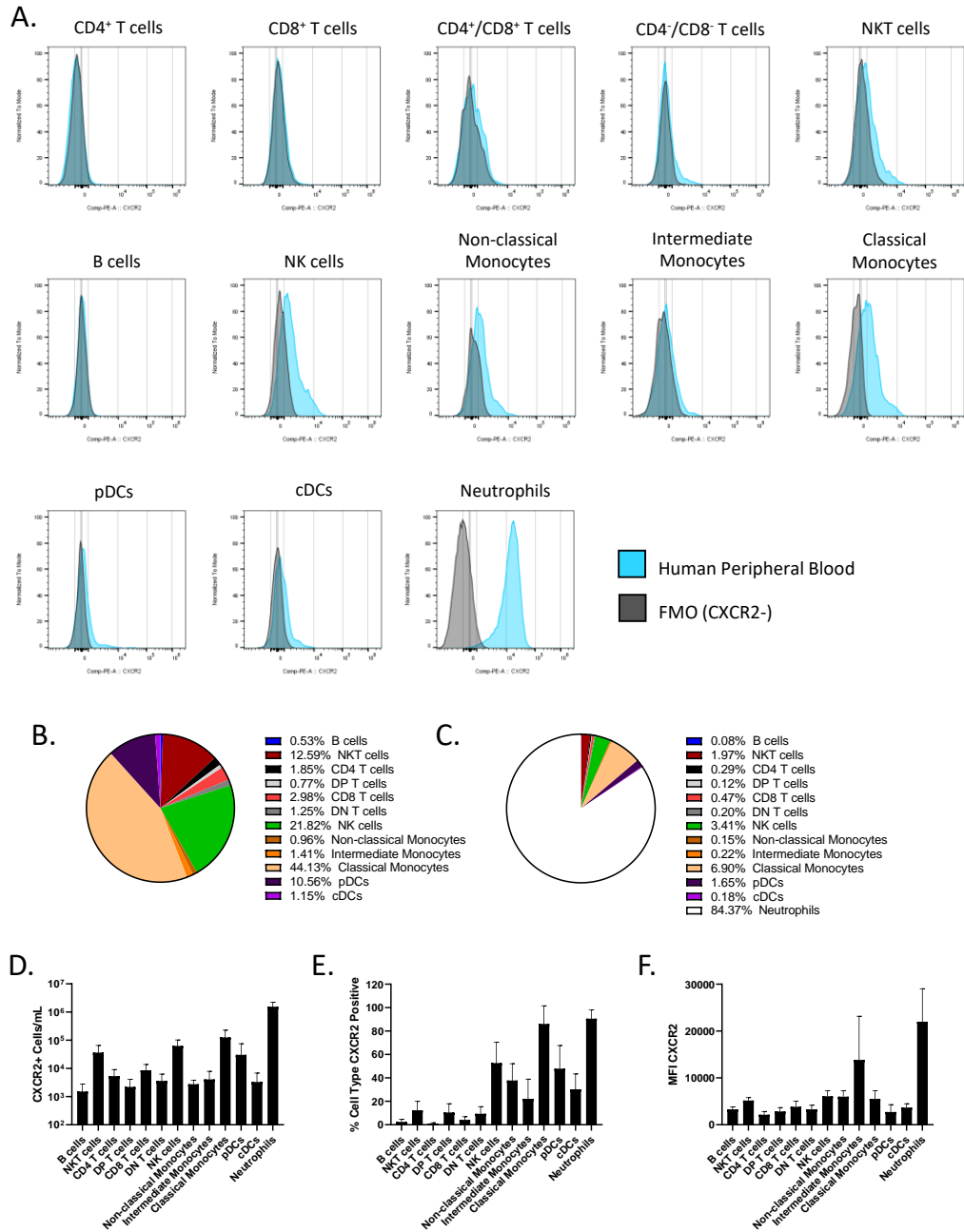


**Figure 2.2:** CXCR2 expression in human peripheral blood.

(A) Histograms of CXCR2 expression of various immune cell types. Histograms from peripheral blood and fluorescence minus one (FMO) control were overlaid. Histograms were normalized to mode. CXCR2 parts of whole of circulating leukocytes, exclusive (B) or inclusive (C) of peripheral neutrophils. Total CXCR2 population was broken down by contributing cell type. Colors correspond to each cell type and percent of whole is shown in the legend. (D) Levels of CXCR2-expressing cells in circulation. Cells per milliliter of peripheral blood was calculated for each cell type and graphed. (E) Percent of cell type CXCR2-positive. For each cell type, percent positive for CXCR2 is shown. (F) Mean fluorescent intensity (MFI) of the CXCR2 expressing population was graphed for each cell type examined. (B-F)  $\geq 1$ . Mean  $\pm$  standard deviation shown.

surprised by both the presence and relative abundance of CXCR2 positive B cells in multiple murine tissues. While CXCR2-positive B cells represent a smaller subset of the B cell population, their high numbers in the spleen and peripheral blood results in a greater relative abundance of CXCR2 expressing B cells in those tissues. Similarly, CXCR2-positive CD3 T cells represent a smaller proportion of the overall T cell population, but constitute a substantial portion of CXCR2-positive cells in peripheral blood because of their sheer numbers.

Similar immunophenotyping panels were utilized to allow for comparison between murine and human leukocyte expression of CXCR2. In both human and murine peripheral blood, neutrophils are the most abundant CXCR2 expressing cell type, with high levels of surface chemokine receptor expression. Human peripheral neutrophils constitute a larger proportion of peripheral blood (50-70%) than in mice (10-25%) [14], so they contribute more to the overall CXCR2 positive cell population. Interestingly, in humans CXCR2<sup>+</sup> B cells are relatively rare (0.26% of circulating leukocytes). This contrasts with mouse peripheral blood where B cells are the second most abundant CXCR2<sup>+</sup> cell type (26%). This raises a question of translational relevance of CXCR2<sup>+</sup> B cells given the differences in numbers of CXCR2<sup>+</sup> cells among humans and mice. In humans, monocytes have a greater contribution to the CXCR2 population than in mice (~9% vs ~1%). Similarly, human DCs are a greater proportion CXCR2<sup>+</sup> cells than mice. In mice, CXCR2<sup>+</sup> cells have fairly similar expression levels regardless of cell type. Humans mirror this, with the exception of peripheral neutrophils. The CXCR2 MFI of human neutrophils is ~3x that of other CXCR2<sup>+</sup> cell types, indicating increased relative surface expression of CXCR2<sup>+</sup> on neutrophils vs other cells. There appears to be to species-specific differences in CXCR2 expression between humans and mice. This is perhaps unsurprising, as mice do not contain CXCL8 or CXCL7 homologs, highlighting differences in immune biology between the two [14]. CXCR2 may play a slightly different role in murine responses with broader expression and functional consequences. However, murine neutrophils expressing human CXCR2 have similar responsiveness *in vitro* and *in vivo* to chemokines and inflammatory stimuli (such as LPS and thioglycolate) [43, 44] questioning this possibility.

For neutrophils, CXCR2 expression and stimulation is crucial for proper activation and release from bone marrow. Increased CXCR2 signaling over CXCR4 signals neutrophils to leave the bone marrow and traffic to sites of inflammation [6, 8, 45]. Senescent neutrophils decrease CXCR2 levels, upon which CXCR4 signaling drives their migration back to bone marrow for clearance [6, 8, 45]. That other hematopoietic cells express CXCR2 may point to a similar function for maturation and release for CXCR2-expressing subsets. CXCR2 is increased on mouse mature circulating or splenic neutrophils, monocytes, and DCs. Circulating human myeloid cells echo the high percentages of CXCR2 expressing cells. Similar decreases in CXCR4 expression on B cells allow for signaling through other receptors such as CCR7, and their migration to resident tissues such as the spleen and other secondary lymphoid organs [7, 46]. In support of CXCR2's involvement in B cell maturation, a whole body knockout of CXCR2 was reported to result in increased numbers of extramedullary neutrophils and B cells [47]. Alternatively, high CXCR2 abundance in B cells may help with rapid mobilization of B cells to sites of inflammation. Secretion of CXCL8 and other CXCR2-stimulating chemokines is common during the early stages of the immune response to recruit neutrophils and other CXCR2 expressing cells [2, 6, 11]. By expressing CXCR2, B cells (and others such as T cells) may be poised to migrate into these sites for antigen recognition or antigen uptake for presentation to T cells. Indeed, stimulation of CXCR2-positive human B cells with CXCL1 or CXCL8 results in their migration demonstrating presence of functional CXCR2 [27, 28]. Previous reports on CXCR2 expression in T cells implied that CXCR2<sup>+</sup> cells are typically non-activated helper or cytotoxic T cells, with activation via anti-CD3 antibodies blocking migration of cells towards CXCR2 ligands [25, 26]. Thus, CXCR2 signaling may help mediate the interface/interaction between antigen presenting cells and T cells within inflamed tissues. Increased CXCR2 on these cell types could also represent a broadening of inflammatory signals/responses. Tissue infiltrated neutrophils have been shown to upregulate and express non-canonical chemokine receptors enhancing their ability to respond to stimuli [48].

Along with migration out of the bone marrow and chemotaxis to sites of inflammation [6, 8], CXCR2 stimulation plays important roles in modifying immune cell

function [10]. CXCR2-bound ligands prime neutrophils, increasing and altering their metabolic state and increasing antimicrobial responses with a more rapid response following stimulation [10]. Tumor derived CXCL8 functions to retain infiltrating DCs within the mass, rather than migration back to lymphatics for antigen presentation [31]. Alternatively, CXCR2-CXCL8 inhibition within mice receiving colorectal cancer xenografts worsened tumor progression by reducing the migration of DCs to the local tumor environment [49]. For NK cells, overexpression of CXCL8 recruits murine NK cells *in vivo* [50]. Genetic modification of NK cells to express CXCR2 results in functional migration with the aim of increased tumoral homing [51]. However, the efficacy of such an approach may be in question. Tumor secreted IL-6/CXCL8 stimulation of NK cells impairs their anti-tumor function, indicating CXCR2 stimulation inhibits typical NK cell functions [29]. CXCR2 plays a role in monocyte/macrophage immune responses. Monocyte CXCR2 expression leads to their arrest in inflamed tissues, which develops/exacerbates atherosclerosis [22, 24, 52-54]. Additionally, what functions CXCR2 plays on T and B cells is largely unknown. Whether CXCR2 stimulation is merely involved in migration of CXCR2 positive T and B cells, or whether it plays a functional role in enhancing or suppressing adaptive responses is yet to be determined.

Due to its role in a variety of diseases, knowledge of CXCR2 expressing cell types and their role in homeostasis can help us understand the immunological response to various stimuli. In this study, we have generated a more complete profile of the CXCR2 expressing immune landscape in multiple different mouse tissues and human peripheral blood. Expression of CXCR2 differed between analogous human and murine tissues, potentially highlighting species divergence in chemokine receptor expression and function. CXCR2 expression is found on almost all major leukocytes with high prevalence on myeloid cells (i.e., neutrophils, monocytes, DCs, NK cells) and murine B cells. CXCR2-positive T cells were also identified on subset of cells. What role(s) CXCR2 plays on these noncanonically expressing cell types is yet to be discovered, but highlights the complexity of chemokine and receptor biology in immunology and the utility of system-wide immunophenotyping.

## **Materials and Methods:**

### ***IACUC and IRB approval***

All animal experiments were approved by the Institutional Animal Use and Care Committee (IACUC) at the University of Tennessee (IACUC #1250). C57BL/6 mice were purchased from Jackson Laboratory (Bar Harbor, ME, USA) and housed under specific pathogen free conditions. Both male and female mice >6-weeks of age were used for experiments.

Human subjects research was approved by the University of Tennessee's Institutional Review Board (Protocol: UTK IRB-14-06476-XP). All subjects gave informed consent before study participation.

### ***Isolation of cells from murine tissues***

Mice peripheral blood was isolated *via* cardiac puncture (~500-800uL per mouse) and placed in an EDTA-treated tube. 250uL of blood was then depleted of RBCs by 2x ACK (ammonium-chloride-potassium) lysis treatment. The remaining leukocytes were stained as described below. Spleens were harvested post-mortem, and a single cell suspension was achieved by homogenizing tissue through a 70um filter. Cells were collected, counted, and  $1 \times 10^6$  cells stained. Bone marrow was isolated by removing femurs, excess tissue was removed, and marrow flushed out using a 27G needle and 3mL of cell culture media. Bone marrow cells were pelleted at 400x g's for 5 minutes, resuspended, and passed through a 70um filter to yield a single cell suspension. Cells were counted and  $1 \times 10^6$  cells stained.

### ***Isolation of human peripheral blood cells***

Human peripheral blood was collected by venous draw into lithium-heparin treated vacutainers. Isolation of PBMCs and PMNs has been previously described [55]. Briefly, blood was diluted in PBS and underlaid with lymphocyte separation media (Lonza, Basel, Switzerland) Cells were spun at 400x g's for 30 minutes in a swing bucket centrifuge with the brake off. The upper buffy coat containing PBMCs was collected, diluted in PBS, centrifuged, washed with PBS, and centrifuged again. The PBMC pellet was counted and

stained for flow cytometry. Granulocytes and RBCs were resuspended in 20mL HBSS, 20mL 3% dextran, and 20mL 0.9% NaCl. After 30 minutes the upper layer was transferred, pelleted, and RBC lysis was performed using two washes of 0.2% NaCl and 1.6% NaCl. Final pellet was resuspended in PBS, counted, and stained for flow cytometry. Peripheral neutrophils were >95% pure as assessed by flow cytometry (CD16<sup>+</sup>, CD66b<sup>+</sup>, CD11b<sup>+</sup>).

### ***Staining cells and flow cytometry***

Isolated mouse leukocytes were stained with the following antibodies: CD11b (BV421, clone M1/70), CD317 (mPDCA-1, BV605, clone 927), CD11c (BV785, clone N418), Ly6G (FITC, 1A8), CD182 (CXCR2, PE-Cy7, clone SA044G4), CD34 (PE-Dazzle594, clone HM34), Ly6C (PerCP-Cy5.5, clone HK1.4), CD49b (PE, clone DX5), CD45 (AlexaFluor 532, clone 30-F11), CD3 (BV510, clone 17A2), CD45R (BV570, clone RA3-6B2). Antibodies were titrated and single stain controls generated for each. Fluorescent minus one (FMO) controls were performed with CXCR2 (PE-Cy7). Isolated human peripheral blood cells were stained with the following antibodies: CD11b (BV421, clone M1/70), CD16 (BV480, clone 3G8), Zombie Aqua viability dye, CD123 (BV650, clone 6H6), HLA-DR (BV711, clone L243), CD34 (BV785, clone 651), CD11c (BB515, clone B-ly6), CD3 (Spark Blue 550, clone SK7), CD182 (CXCR2) (PE, clone 5E8), CD14 (PE/Fire 640, clone 63D3), CD66b (PerCP-Cy5.5, clone QA17A51), CD8a (PerCP-eFluor 710, clone SK1), CD56 (PE-Cy7, clone 5.1H11), CD20 (cFluor V450, clone 2H7), CD45 (cFluor V547, clone HI30), CD4 (cFluor V610, clone SK3). Samples were run on a 2-laser (Violet-405nm, Blue-488nm) Cytex Northern Lights spectral cytometer (Cytex Biosciences, Fremont, CA), and data was analyzed using FlowJo (FlowJo, Becton, Dickinson and Company, Ashland, OR).

### ***Statistics***

Each experiment consisted of 2 or more experiments with 3 replicates/mice per group. Averaged data points are shown for each graph with mean and standard deviation graphed where appropriate. Significance was determined by Welch's ANOVA with Dunnett's multiple comparisons. Statistical analyses were performed using GraphPad

Prism (GraphPad Software, La Jolla, CA). Significance values are shown as: \* =  $p < 0.05$ , \*\* =  $p < 0.01$ , \*\*\* =  $p < 0.001$ , \*\*\*\* =  $p < 0.0001$ , ns = not significant.

## References

1. Turner, M.D., et al., *Cytokines and chemokines: At the crossroads of cell signalling and inflammatory disease*. Biochim Biophys Acta, 2014. **1843**(11): p. 2563-2582.
2. Hughes, C.E. and R.J.B. Nibbs, *A guide to chemokines and their receptors*. FEBS J, 2018. **285**(16): p. 2944-2971.
3. Eiger, D.S., et al., *Biased agonism at chemokine receptors*. Cell Signal, 2021. **78**: p. 109862.
4. Kufareva, I., C.L. Salanga, and T.M. Handel, *Chemokine and chemokine receptor structure and interactions: implications for therapeutic strategies*. Immunol Cell Biol, 2015. **93**(4): p. 372-83.
5. Jorgensen, A.S., et al., *Biased Signaling of CCL21 and CCL19 Does Not Rely on N-Terminal Differences, but Markedly on the Chemokine Core Domains and Extracellular Loop 2 of CCR7*. Front Immunol, 2019. **10**: p. 2156.
6. Martin, C., et al., *Chemokines acting via CXCR2 and CXCR4 control the release of neutrophils from the bone marrow and their return following senescence*. Immunity, 2003. **19**(4): p. 583-93.
7. Nie, Y., et al., *The role of CXCR4 in maintaining peripheral B cell compartments and humoral immunity*. J Exp Med, 2004. **200**(9): p. 1145-56.
8. Suratt, B.T., et al., *Role of the CXCR4/SDF-1 chemokine axis in circulating neutrophil homeostasis*. Blood, 2004. **104**(2): p. 565-71.
9. Raju, R., et al., *Differential ligand-signaling network of CCL19/CCL21-CCR7 system*. Database (Oxford), 2015. **2015**.
10. Miralda, I., S.M. Uriarte, and K.R. McLeish, *Multiple Phenotypic Changes Define Neutrophil Priming*. Front Cell Infect Microbiol, 2017. **7**: p. 217.
11. Stadtmann, A. and A. Zarbock, *CXCR2: From Bench to Bedside*. Front Immunol, 2012. **3**: p. 263.
12. Korbecki, J., et al., *CXCR2 Receptor: Regulation of Expression, Signal Transduction, and Involvement in Cancer*. Int J Mol Sci, 2022. **23**(4).
13. Boisvert, W.A., L.K. Curtiss, and R.A. Terkeltaub, *Interleukin-8 and its receptor CXCR2 in atherosclerosis*. Immunol Res, 2000. **21**(2-3): p. 129-37.

14. Mestas, J. and C.C. Hughes, *Of mice and not men: differences between mouse and human immunology*. J Immunol, 2004. **172**(5): p. 2731-8.
15. Bozic, C.R., et al., *The murine interleukin 8 type B receptor homologue and its ligands. Expression and biological characterization*. J Biol Chem, 1994. **269**(47): p. 29355-8.
16. Del Rio, L., et al., *CXCR2 deficiency confers impaired neutrophil recruitment and increased susceptibility during Toxoplasma gondii infection*. J Immunol, 2001. **167**(11): p. 6503-9.
17. Herbold, W., et al., *Importance of CXC chemokine receptor 2 in alveolar neutrophil and exudate macrophage recruitment in response to pneumococcal lung infection*. Infect Immun, 2010. **78**(6): p. 2620-30.
18. Khan, S., et al., *The role of CXC chemokine receptor 2 in Pseudomonas aeruginosa corneal infection*. J Leukoc Biol, 2007. **81**(1): p. 315-8.
19. Romero-Moreno, R., et al., *The CXCL5/CXCR2 axis is sufficient to promote breast cancer colonization during bone metastasis*. Nat Commun, 2019. **10**(1): p. 4404.
20. Sharma, B., et al., *CXCR2: A Novel Mediator of Mammary Tumor Bone Metastasis*. Int J Mol Sci, 2019. **20**(5).
21. Steele, C.W., et al., *CXCR2 Inhibition Profoundly Suppresses Metastases and Augments Immunotherapy in Pancreatic Ductal Adenocarcinoma*. Cancer Cell, 2016. **29**(6): p. 832-845.
22. Gerszten, R.E., et al., *MCP-1 and IL-8 trigger firm adhesion of monocytes to vascular endothelium under flow conditions*. Nature, 1999. **398**(6729): p. 718-23.
23. Bonecchi, R., et al., *Induction of functional IL-8 receptors by IL-4 and IL-13 in human monocytes*. J Immunol, 2000. **164**(7): p. 3862-9.
24. Wang, L., et al., *CXCL1-CXCR2 axis mediates angiotensin II-induced cardiac hypertrophy and remodelling through regulation of monocyte infiltration*. Eur Heart J, 2018. **39**(20): p. 1818-1831.

25. Jinquan, T., et al., *Recombinant human growth-regulated oncogene-alpha induces T lymphocyte chemotaxis. A process regulated via IL-8 receptors by IFN-gamma, TNF-alpha, IL-4, IL-10, and IL-13.* J Immunol, 1995. **155**(11): p. 5359-68.
26. Qin, S., et al., *Expression of monocyte chemoattractant protein-1 and interleukin-8 receptors on subsets of T cells: correlation with transendothelial chemotactic potential.* Eur J Immunol, 1996. **26**(3): p. 640-7.
27. Jinquan, T., et al., *Chemotaxis and IL-8 receptor expression in B cells from normal and HIV-infected subjects.* J Immunol, 1997. **158**(1): p. 475-84.
28. Alter, A., et al., *Determinants of human B cell migration across brain endothelial cells.* J Immunol, 2003. **170**(9): p. 4497-505.
29. Wu, J., et al., *IL-6 and IL-8 secreted by tumour cells impair the function of NK cells via the STAT3 pathway in oesophageal squamous cell carcinoma.* J Exp Clin Cancer Res, 2019. **38**(1): p. 321.
30. Yamin, R., et al., *HCMV vCXCL1 Binds Several Chemokine Receptors and Preferentially Attracts Neutrophils over NK Cells by Interacting with CXCR2.* Cell Reports, 2016. **15**(7): p. 1542-1553.
31. Alfaro, C., et al., *Carcinoma-derived interleukin-8 disorients dendritic cell migration without impairing T-cell stimulation.* PLoS One, 2011. **6**(3): p. e17922.
32. Stenstrom, M., et al., *Natural killer T-cell populations in C57BL/6 and NK1.1 congenic BALB.NK mice-a novel thymic subset defined in BALB.NK mice.* Immunology, 2005. **114**(3): p. 336-45.
33. Nikolic, T., et al., *A subfraction of B220(+) cells in murine bone marrow and spleen does not belong to the B cell lineage but has dendritic cell characteristics.* Eur J Immunol, 2002. **32**(3): p. 686-92.
34. Blasius, A.L., et al., *Development and function of murine B220+CD11c+NK1.1+ cells identify them as a subset of NK cells.* J Exp Med, 2007. **204**(11): p. 2561-8.
35. Guimont-Desrochers, F., et al., *Redefining interferon-producing killer dendritic cells as a novel intermediate in NK-cell differentiation.* Blood, 2012. **119**(19): p. 4349-57.

36. Zitvogel, L. and F. Housseau, *IKDCs or B220+ NK cells are pre-mNK cells*. Blood, 2012. **119**(19): p. 4345-6.
37. Vosshenrich, C.A., et al., *CD11cIcloB220+ interferon-producing killer dendritic cells are activated natural killer cells*. J Exp Med, 2007. **204**(11): p. 2569-78.
38. Arase, H., et al., *Cutting edge: the mouse NK cell-associated antigen recognized by DX5 monoclonal antibody is CD49b (alpha 2 integrin, very late antigen-2)*. J Immunol, 2001. **167**(3): p. 1141-4.
39. Asselin-Paturel, C., et al., *Mouse strain differences in plasmacytoid dendritic cell frequency and function revealed by a novel monoclonal antibody*. J Immunol, 2003. **171**(12): p. 6466-77.
40. Rose, S., A. Misharin, and H. Perlman, *A novel Ly6C/Ly6G-based strategy to analyze the mouse splenic myeloid compartment*. Cytometry A, 2012. **81**(4): p. 343-50.
41. Maecker, H.T., J.P. McCoy, and R. Nussenblatt, *Standardizing immunophenotyping for the Human Immunology Project*. Nat Rev Immunol, 2012. **12**(3): p. 191-200.
42. Lakschevitz, F.S., et al., *Identification of neutrophil surface marker changes in health and inflammation using high-throughput screening flow cytometry*. Exp Cell Res, 2016. **342**(2): p. 200-9.
43. Sparer, T.E., et al., *Expression of human CXCR2 in murine neutrophils as a model for assessing cytomegalovirus chemokine vCXCL-1 function in vivo*. J Interferon Cytokine Res, 2004. **24**(10): p. 611-20.
44. Mihara, K., et al., *Human CXCR2 (hCXCR2) takes over functionalities of its murine homolog in hCXCR2 knockin mice*. Eur J Immunol, 2005. **35**(9): p. 2573-82.
45. Eash, K.J., et al., *CXCR2 and CXCR4 antagonistically regulate neutrophil trafficking from murine bone marrow*. J Clin Invest, 2010. **120**(7): p. 2423-31.
46. McHeik, S., et al., *Coexpression of CCR7 and CXCR4 During B Cell Development Controls CXCR4 Responsiveness and Bone Marrow Homing*. Front Immunol, 2019. **10**: p. 2970.

47. Cacalano, G., et al., *Neutrophil and B cell expansion in mice that lack the murine IL-8 receptor homolog*. Science, 1994. **265**(5172): p. 682-4.
48. Rudd, J.M., et al., *Neutrophils Induce a Novel Chemokine Receptors Repertoire During Influenza Pneumonia*. Front Cell Infect Microbiol, 2019. **9**: p. 108.
49. Li, E., et al., *CXCL8 Associated Dendritic Cell Activation Marker Expression and Recruitment as Indicators of Favorable Outcomes in Colorectal Cancer*. Front Immunol, 2021. **12**: p. 667177.
50. Vujanovic, L., et al., *Adenovirus-engineered human dendritic cells induce natural killer cell chemotaxis via CXCL8/IL-8 and CXCL10/IP-10*. Oncoimmunology, 2012. **1**(4): p. 448-457.
51. Kremer, V., et al., *Genetic engineering of human NK cells to express CXCR2 improves migration to renal cell carcinoma*. J Immunother Cancer, 2017. **5**(1): p. 73.
52. Huo, Y., et al., *The chemokine KC, but not monocyte chemoattractant protein-1, triggers monocyte arrest on early atherosclerotic endothelium*. J Clin Invest, 2001. **108**(9): p. 1307-14.
53. Phillips, R.J., M. Lutz, and B. Premack, *Differential signaling mechanisms regulate expression of CC chemokine receptor-2 during monocyte maturation*. J Inflamm (Lond), 2005. **2**: p. 14.
54. Wang, L., et al., *Genetic and Pharmacologic Inhibition of the Chemokine Receptor CXCR2 Prevents Experimental Hypertension and Vascular Dysfunction*. Circulation, 2016. **134**(18): p. 1353-1368.
55. Markert, M., P.C. Andrews, and B.M. Babior, *Measurement of O<sub>2</sub>- production by human neutrophils. The preparation and assay of NADPH oxidase-containing particles from human neutrophils*. Methods Enzymol, 1984. **105**: p. 358-65.

**CHAPTER 3 - FUNCTIONAL AND STRUCTURAL  
CHARACTERISTICS OF *UL146* FROM DISTINCT HUMAN CMV  
STRAINS**

This work was performed by: Trevor J. Hancock, Joseph W. Jackson, Madison Keely, Tom Masi, and Tim E. Sparer

Author Contributions: Conceptualization, T.E.S. and T.J.H.; Methodology, T.M. and T.J.H.; Formal analysis, T.J.H.; Investigation, M.E., J.W.J., T.M., and T.J.H.; Writing—original draft preparation, T.J.H.; Writing—review and editing, J.W.J., T.E.S., and T.J.H.; Visualization, T.J.H.; Funding Acquisition, T.E.S.

### Abstract

CMV is a clinically important human pathogen causing significant disease among immunocompromised populations. CMVs encode a variety of immunomodulatory proteins to manipulate the immune system into a pro-viral state. One such immunomodulatory protein is the viral gene product of the *UL146* gene, a potent alpha-chemokine capable of stimulating and inducing chemotaxis of CXCR2-expressing neutrophils. vCXCL-1, the *UL146* encoded protein is a proposed virulence factor increasing dissemination and disease in mouse models of CMV. However, multiple isoforms of vCXCL-1 exist with differences described for *in vitro* activation and chemotaxis. How these isoforms differentially contribute to CMV disease is unknown, as well as the *in vivo* molecular mechanism by which they do so. Using recombinant MCMV expressing two isoforms of vCXCL-1, we examined the impact of differential vCXCL-1 on CMV infection. We found potential trends for increased virulence and mortality for vCXCL-1 with high affinity for CXCR2 while lower for weaker CXCR2 stimulators. Additionally, we performed *in vitro* and *in silico* experiments to identify the mechanism which induces differential stimulation. Using *in silico* comparisons, we identified a unique region on the C-terminus of vCXCL-1 isoforms absent on host CXCR2-interacting chemokines. This region could potentially inhibit glycosaminoglycan binding of viral chemokines and alter their interaction with host chemokine receptors. This provides rationale for further investigation of the molecular mechanisms by which vCXCL-1 functions and its *in vivo* consequences.

## Introduction

Cytomegalovirus (CMV) is a clinically relevant human pathogen found in roughly 40-90% of adults worldwide [1]. Like many herpesviruses it is spread *via* contact with infected bodily secretions whereupon the virus establishes a lifelong infection in its host [1]. Primary infection or reactivation is typically asymptomatic in healthy individuals [1]. However, within immunocompromised populations CMV represents a pathogen of significant concern. Susceptible persons (i.e., HIV/AIDS, organ transplant recipients, cancer patients and others undergoing immunosuppressive treatment, etc.) develop a myriad of clinical symptoms ranging from gastroenteritis, retinitis, transplant rejection, and rarely mortality [1-3]. Along with immunocompromised individuals, CMV represents the most common cause of infectious congenital disorders including microcephaly, intellectual disability, and sensorineural hearing loss [4, 5]. CMV's broad range of symptoms and organs affected is due in part to the systemic circulation of virus [6] and broad tropism [7]. Viral dissemination causes clinical disease and subsequent inflammation within the infected tissues [8]. Immune cells, primarily of myeloid origin, mediate both inflammation and dissemination *in vivo* [6, 9-11].

At the interface of both inflammation and dissemination is the human cytomegalovirus (HCMV) viral chemokine vCXCL-1, encoded by the *UL146* gene [12, 13]. Chemokines are small, soluble chemotactic molecules secreted to recruit immune cells to sites of inflammation, damage, or infection [14]. Alpha chemokines, those that contain an ELR- motif immediately prior to the CXC sequence, are important in shaping the initial immune response to infection or inflammation [14-16]. Chemokine binding to a cognate receptor can induce calcium flux, intracellular signaling cascades, chemotaxis, and prime immune cells for subsequent inflammation (or anti-inflammatory) responses [15, 17, 18]. As a chemokine, vCXCL-1 has the potential to play a major role in shaping the initial immune response to CMV infection, alter the inflammatory influx, and promote a pro-viral state. Expression of HCMV's vCXCL-1 in a mouse model of CMV disease resulted in increased viral burden and dissemination within immunocompetent hosts [11]. This provided some of the first direct, *in vivo* evidence of its role as a virulence factor. Infections of immunocompromised mice with MCMV expressing vCXCL-1 resulted in almost

complete mortality within a few days of infection [11]. This points to the role of vCXCL-1 in dissemination and pathogenesis.

Chemokine receptors belong to the G protein coupled receptor family (GPCRs) which consist of seven transmembrane regions, three extracellular loops, and an extracellular N-terminal domain involved in chemokine recognition and binding [14, 19]. Chemokine receptor binding is highly influenced by the structure of the N-terminus of both chemokine and receptor [14]. Differences for some chemokines in N-terminus length and composition have been shown to alter receptor binding and functional outcomes [14]. Multiple different chemokines engage the same receptor causing differential outcomes. This concept is alternatively called functional selectivity or biased agonism, where in spite of interacting with the same receptor, ligands induce different/biased signaling or functional outcomes. A prime example is the chemokine receptor CCR7 which binds the ligands CCL19 and CCL21 [20, 21]. Binding may also involve more than interactions between the N-terminus of chemokine or receptor. There are potentially 2-3 points of contact between receptor and ligand, and these additional contacts may serve as another layer of complexity leading to the functional selectivity of the chemokine system [20, 22-24].

*UL146* is a polymorphic gene which is currently divided into 14 separate genotypes [25]. These distinct proteins differentially stimulate CXCR2-expressing cells [12, 13, 17]. Chemotaxis, calcium flux, and binding potentials differ between the separate genotypes of vCXCL-1 [17]. Some vCXCL-1's such as one from the Toledo strain of HCMV can interact with both CXCR2 and CXCR1 [12, 17]. This is akin to that of the host chemokine CXCL8 [12, 17]. Most vCXCL-1's fail to stimulate or bind the receptor to the same affinity as host CXCL8 or CXCL1 [17], but vCXCL-1<sub>Toledo</sub> can bind, induce calcium flux, and chemotaxis highly effectively [17]. There is conflicting *in vivo* data within humans for an association of some vCXCL-1 genotypes with more disease severity [26-29]. However, based on *in vitro* differences and vCXCL-1's proposed role as a virulence factor, we propose that isoforms of vCXCL-1 will translate into differences in virulence/dissemination *in vivo*. Viral CXCL-1 from the Towne and Toledo strains of HCMV differently stimulate human peripheral neutrophils *in vitro* [17]. Utilizing a

recombinant MCMV expressing vCXCL-1 from the Toledo strain of HCMV, our lab previously demonstrated that vCXCL-1 expression during MCMV infection increased viral burden, altered the composition of immune infiltrate, and increased mortality in immunocompromised mice [11]. To examine how *in vitro* differences in chemokine activity impacts *in vivo* infections/disease outcomes, we performed infections with recombinant MCMVs expressing vCXCL-1 from Toledo or Towne strains. We additionally produced and purified recombinant viral chemokines to determine a biochemical mechanism underlying previous differences in immune cell binding, chemotaxis, and activation using protein structural prediction models and isothermal titration calorimetry to determine chemokine-heparin binding affinity.

## Results

We previously developed a recombinant MCMV capable of expressing HCMV vCXCL-1<sub>Toledo</sub> under the control of a murine viral chemokine (MCK-2) promoter [11]. Recombinant MCMV expressing vCXCL-1<sub>Toledo</sub> was previously characterized and compared to its parental (Smith) strain [11]. Using this same system, we generated a recombinant virus expressing vCXCL-1<sub>Towne</sub> (RMvCXCL-1<sub>Towne</sub>). Restriction digest (Fig. 3.1 A) and targeted sequencing (data not shown) confirmed correct insertion of vCXCL-1 in RMvCXCL-1<sub>Towne</sub>. Single and multi-step growth curves were performed and compared to parental virus (Fig. 3.1 B,C). Recombinant virus statistically differed at later timepoints for the single-step growth curve, but those differences were less than half a log (Fig. 3.1 C). Western blots in Fig. 3.1 D show expression of both 6His-tagged vCXCL-1<sub>Towne</sub> and Flag-tagged MCK2. For MCK2, both low (monomer) and high (oligomer) molecular weight forms are seen as reported previously [13, 30]. Mice were then infected with recombinant vCXCL-1 expressing viruses (vCXCL-1<sub>Toledo</sub> and vCXCL-1<sub>Towne</sub>) to compare immune responses between the two (Fig. 3.1 E). Footpad swelling was measured for 3 days post infection (dpi). RMvCXCL-1<sub>Toledo</sub> showed the most swelling/inflammation (Fig. 3.1 E). However, it was not significant (Fig. 3.1 E). RMvCXCL-1<sub>Towne</sub> and Smith (i.e., wild-type virus) showed overlapping footpad swelling levels at all timepoints.

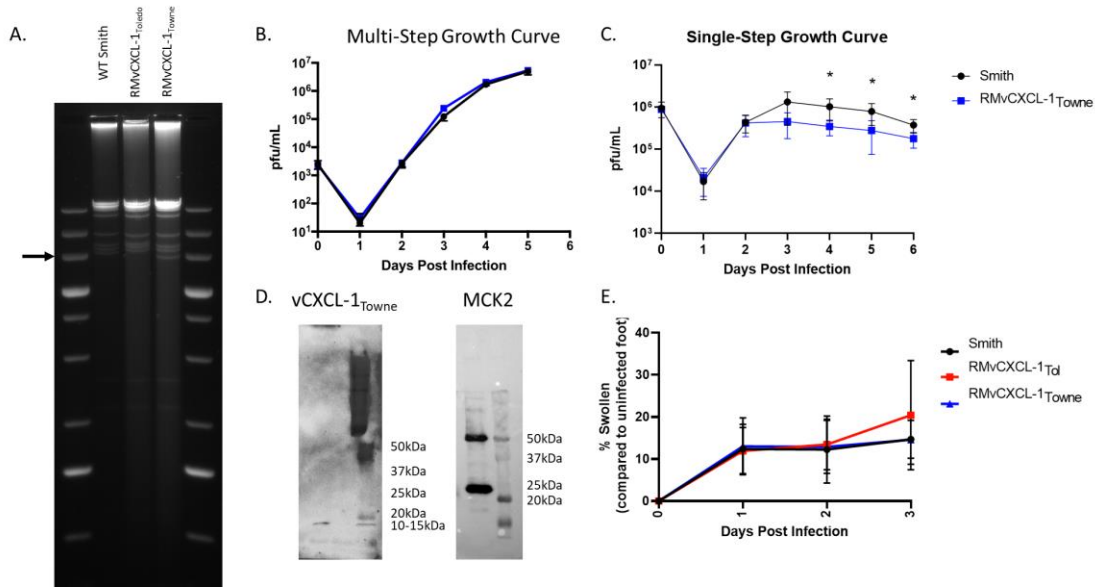


**Figure 3.1:** Characterization of a recombinant MCMV expressing vCXCL-1 from the Towne strain of HCMV.

(A) HindIII restriction fragment length polymorphism (RFLP) analysis of recombinant Smith (MCMV) bacterial artificial chromosome (BAC). BAC DNA was digested with HindIII and run on an agarose gel to visualize genome wide changes. WT Smith triplet (indicated by arrow), with recombinant viruses expressing Toledo and Towne shown adjacent. (B) Multi-step (MOI 0.01), (C) Single-step (MOI 5) growth curves of RMvCXCL-1<sub>Towne</sub> and WT virus. (D) Western blot of supernatant from RMvCXCL-1<sub>Towne</sub> infected MEF 10.1 fibroblasts. vCXCL-1<sub>Towne</sub> was isolated by Ni-NTA resin, and MCK-2 by anti-Flag beads. Beads were boiled in SDS-buffer, run on a 12% PAGE gel, and blotted onto nitrocellulose. White light and chemiluminescent images were overlaid, and blots represent supernatants on left and ladders on the right. Sizes are indicated to the right of ladder. (E) Footpad swelling of f.p. inoculated mice at different days post infection (dpi). Mice were infected and swelling measured by calipers. Swelling was normalized to infected foot and shown as percent increase in footpad size. Mean +/- standard deviation shown. For all, n≥3. For (E), 5 mice per group were used. Multiple T-tests were performed for (B), (C), (E). \* = p<0.05.

As no differences were observed in footpad swelling of immune-competent mice based on the genotype of vCXCL-1 expressed, we wanted to examine the effects of vCXCL-1<sub>Towne</sub> on virulence in a mouse model of immunosuppression. Using cyclophosphamide, mice were immunosuppressed and infected with parental and vCXCL-1 expressing MCMVs (Fig. 3.2 A). Again, footpad swelling at the site of infection was non-invasively measured (Fig. 3.2 B). Cyclophosphamide treatment delayed inflammation, taking RMvCXCL-1<sub>Toledo</sub> 9-10 days to reach levels previously reached by 3 dpi. Interestingly, RMvCXCL-1<sub>Towne</sub> did not appear to greatly increase footpad swelling compared with both Smith and RMvCXCL-1<sub>Toledo</sub> ~4 and 7-fold higher, respectively. Cyclophosphamide-treated animals had their weight and condition monitored everyday (Fig. 3.2 C). RMvCXCL-1<sub>Toledo</sub> reached 100% lethality at 10 dpi, with both RMvCXCL-1<sub>Towne</sub> and Smith having a 33% chance of survival at 14 dpi (Fig. 3.2 D). While there was no difference in footpad swelling based on vCXCL-1 genotype (Fig. 3.1 E, 3.2 B), RMvCXCL-1<sub>Towne</sub> was less virulent than, and on par with WT MCMV (Fig. 3.2 D). Viruses expressing vCXCL-1<sub>Toledo</sub> (RMvCXCL-1<sub>Toledo</sub>) were previously shown to be more virulent in immunocompromised mice [11], matching our data (Fig. 3.2 D).

*UL146* is highly polymorphic [25]. We compared the amino acid sequences of various vCXCL-1 isoforms and host CXCL8 in an attempt to identify important residues for chemokine signaling along with conserved residues and ones unique to viral chemokines (Fig. 3.3). Sequences were trimmed to the first amino acid preceding the ELR motif and aligned using ClustalW. While there were regions of conservation between CXCL8 and vCXCL-1s, there were significant differences throughout the rest of the protein. One of the most striking differences was the length of viral chemokine versus host. All vCXCL-1s shown were >90 amino acids compared to the ~70 amino acids for human CXCL8. These extra residues for the viral chemokines were located primarily within the C-terminus, just after the GAG-binding domain. Alignments with other CXCR2-engaging host chemokines demonstrated an extended C-terminus present in vCXCL-1, but not host chemokines (data not shown). Like the GAG binding domain for host chemokines, this extended C-terminus contains a high density of positively charged amino acids (i.e., arginine and lysine). Other host chemokines with extended positively charged C-termini

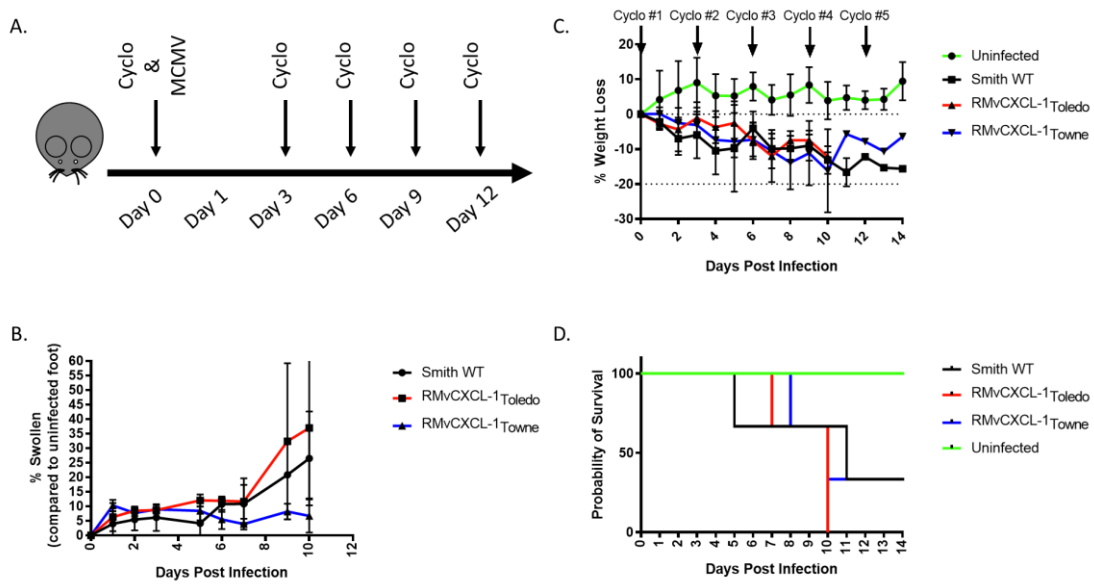


**Figure 3.2:** Recombinant MCMV's expressing vCXCL-1's differentially affect virulence in immunocompromised mice.

(A) Schematic overview of cyclophosphamide (cyclo) and MCMV injections. Mice were injected with 0.15mg/kg cyclophosphamide on days 0, 3, 6; and 0.1mg/kg on days 9 and 12. Mice were infected f.p. with  $\sim 1 \times 10^6$  pfu. (B) Footpad swelling of immunocompromised mice is delayed. Mice were infected as in (A), and footpad swelling measured over several days. (C) Weight loss of treated/infected mice over the experiment term. (D) Survival curve of immunocompromised mice infected with recombinant and WT MCMV. Mean  $\pm$  standard deviation shown.  $n=1$  with 3 mice per group.

show greater GAG binding, and truncation or domain swaps ablate or enhance GAG binding, respectively [20, 31]. Based on this, we posited that the extended terminus of vCXCL-1's serves to enhance GAG binding potentially enhancing the formation of chemotactic gradients and receptor engagement *in vivo*.

To study vCXCL-1's specific effects on immune cells *in vitro* and *in vivo*, the yeast expression system *Pichia pastoris* was used to produce recombinant host and viral chemokines. FPLC-purified chemokines were checked for purity by PAGE and silver stained gel (Fig. 3.4 A, B). Purified chemokines were the appropriate size with no extraneous bands, demonstrating high purity. *Pichia*-produced vCXCL-1<sub>Toledo</sub> has glycosylated forms analogous to cell culture generated vCXCL-1<sub>Toledo</sub> [13]. PNGase F removal of N-linked glycosylations resulted in both bands collapsing into a single form indicating the presence of glycosylations (Fig. 3.4 C). Western blots of CXCL8 and vCXCL-1<sub>Toledo</sub> demonstrate purification of the correct protein (Fig. 3.4 D, E). Anti-CXCL8 (Fig. 3.4 F) and anti-vCXCL-1<sub>Toledo</sub> (Fig. 3.4 G) ELISAs further confirmed protein identity. Antibodies against each chemokine recognize their specific antigen with no cross reactivity against the other (data not shown), and naïve serum failed to react demonstrating the specificity of the positive reactions (Fig. 3.4 F, G).

While soluble chemokine is commonly used to study chemotaxis and receptor stimulation *in vitro*, chemokines *in vivo* are likely found anchored to the extracellular matrix or cell surface [32, 33]. Glycosaminoglycans (GAGs) such as heparan sulfate proteoglycans (HSPGs) bind and establish chemotactic gradients to give directionality to the stimulus [32-34]. GAG binding is mediated by clusters of positively charged amino acids within the typically helical C-terminus [20, 35]. Binding of chemokines to cognate receptor or GAG scaffold allows for chemokines to form oligomers [18, 34]. GAG binding and retention of several chemokines including human CXCL8 decreases stimulation of their cognate receptor, despite increasing local concentrations of chemokine [33, 36]. Additionally, mutant chemokines incapable of GAG-binding display defects on *in vivo* chemotaxis [18, 33]. GAGs then play important roles for chemokine function *in vivo* affecting local concentrations and receptor binding capacity.

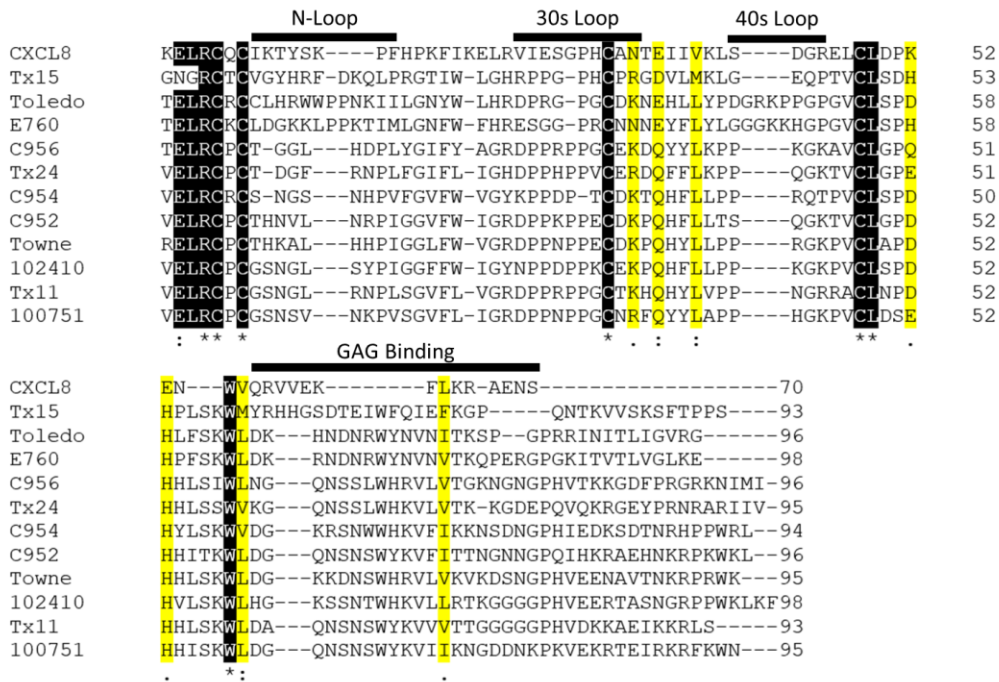


**Figure 3.3:** Alignments of HCMV vCXCL-1's reveals extended C-terminus. ClustalW amino acid alignments of various vCXCL-1's were performed with human CXCL8. For some, N-terminus was shortened to show just ELR motif and preceding residue. Conserved residues are shown in black with \* below. Highlights (with : or . below) represent conservation of strongly or weakly similar residues, respectively. Annotations shown above sequences are based on those for CXCL8.

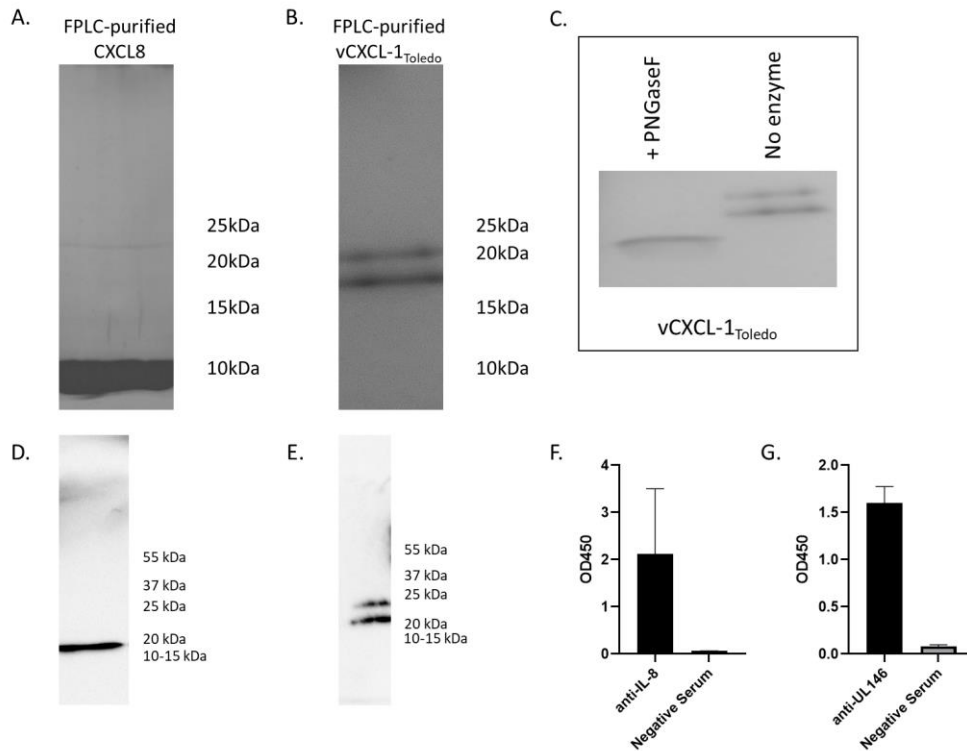


**Figure 3.4:** Expression of recombinant chemokines using *Pichia pastoris*.

Recombinant CXCL8 (A) and vCXCL-1<sub>Toledo</sub> (B) was produced in *Pichia* and purified by anionic exchange in an FPLC (fast protein liquid chromatography). Chemokine-containing fractions were collected, combined, and checked for purity by SDS-PAGE gel and silver staining. Size markers are shown to the right of gel images. (C) Identity of upper vCXCL-1<sub>Toledo</sub> band was determined by PNGase F enzymatic deglycosylation. Western blot of *Pichia* produced CXCL8 (D) and vCXCL-1<sub>Toledo</sub> (E) probed with anti-CXCL8 and anti-vCXCL-1 antibodies. Protein size shown next to blot images. Purified chemokines were confirmed by ELISA (F) CXCL8 and (G) vCXCL-1<sub>Toledo</sub>. OD<sub>450</sub> values are shown for anti-CXCL8 and anti-vCXCL-1<sub>Toledo</sub> serum and normal mouse serum (Negative Serum). For (D) and (E), n=1. Mean +/- standard deviation is shown.

Protein alignments identified a conserved, extended C-terminus within numerous vCXCL-1 isoforms (Fig. 3.3). This extended region is downstream of the GAG-binding domain annotated for CXCL8, and has a high density of positively charged amino acids. This mirrors some host chemokines such as CCL21, for which the extended C-terminus enhances GAG-binding [20]. Based on the extended C-terminal tail of vCXCL-1<sub>Toledo</sub>, we anticipated it to have increased GAG interactions. Isothermal Titration Calorimetry (ITC) allows for detecting small-scale changes in heat due to interactions. From these measured heat changes, binding affinity ( $K_d$ ) and stoichiometric ratios can be determined. CXCL8 and vCXCL-1<sub>Toledo</sub> were examined for their binding affinity to soluble heparin. Heparin is a soluble, highly sulfated analog for HSPGs [36, 37], and various concentrations were titrated into recombinant *Pichia* produced chemokines (Fig. 3.5 A, B). Thermograms representing changes in temperature versus concentration of heparin are shown for CXCL8 (Fig. 3.5 A) and vCXCL-1<sub>Toledo</sub> (Fig. 3.5 B). Host and viral chemokine appear to interact with heparin in opposing fashion. CXCL8 binding to heparin is an exothermic process, whereas vCXCL-1<sub>Toledo</sub> binds in an endothermic manner. Both chemokines bind energetically favorably, as evidenced by the negative Gibbs free energy value ( $\Delta G$ ) (Fig. 3.5 C). CXCL8-heparin binding is driven primarily by favorable enthalpy values ( $\Delta H$ ) indicating electrostatic interactions behind CXCL8 binding (Fig. 3.5 C). In contrast, vCXCL-1<sub>Toledo</sub> binding to heparin is driven by favorable entropy ( $-T\Delta S$ ) indicating hydrophobic interactions and potential conformational changes (Fig. 3.5 C). The apparent  $K_d$  (binding/dissociation) of CXCL8 to heparin is ~129nM. This is similar to values previously reported using other methods [38]. vCXCL-1<sub>Toledo</sub> has a much lower affinity for heparin binding in the micromolar range (~37.8uM). This supports the increased heparin concentration required for vCXCL-1<sub>Toledo</sub> to generate binding signatures (~62uM for CXCL8 vs. ~2mM vCXCL-1<sub>Toledo</sub>). Along with differences in affinity, CXCL8 binds at a higher ratio than vCXCL-1<sub>Toledo</sub> (i.e., ~6 CXCL8 bind per heparin chain, while only 1/18 heparin chains are bound by vCXCL-1<sub>Toledo</sub>). This is surprising as we initially suspected vCXCL-1<sub>Toledo</sub> to have increased GAG binding due to the extended, positively charged C-terminus.

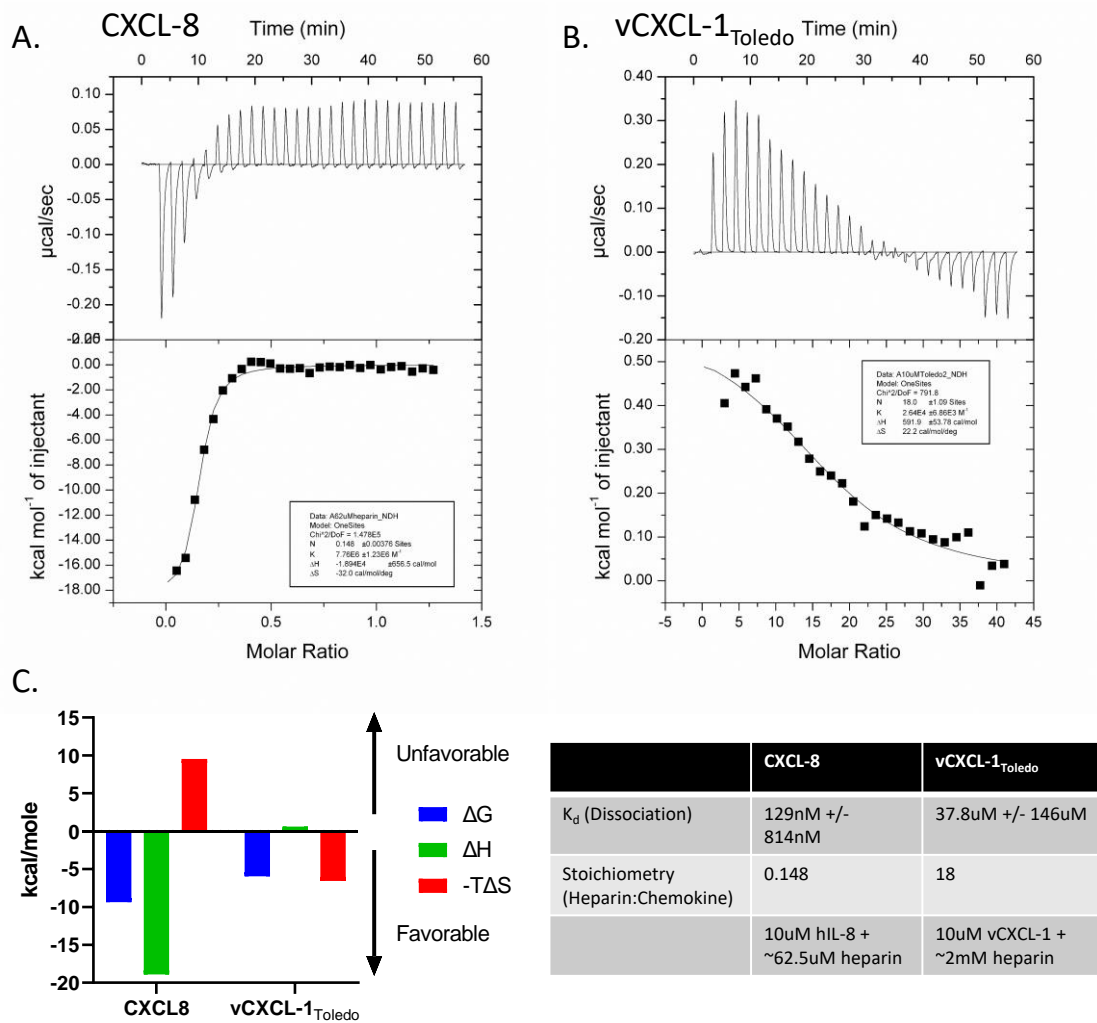


**Figure 3.5:** vCXCL-1<sub>Toledo</sub> has diminished heparin binding. Isothermal titration calorimetry (ITC) was performed to measure chemokine binding to heparin. (A) CXCL8 binding isotherm (top) with curve fitting using single set of sites (bottom). (B) vCXCL-1<sub>Toledo</sub> binding isotherm (top) with curve fitting using single set of sites (bottom). (C) Thermodynamic signatures for CXCL8 and vCXCL-1<sub>Toledo</sub> to heparin sulfate. Gibbs free energy, enthalpy, and entropy of heparin chemokine binding was determined by ITC and graphed. Table below displays calculated dissociation/binding constant, stoichiometry, and concentration of chemokine and heparin used to generate each graph. Heparin was titrated into chemokine-deficient buffer and background subtracted from both. For both,  $n > 2$ . Representative data shown.

As vCXCL-1<sub>Toledo</sub>'s GAG binding is diminished, the role of the extended C-terminus in vCXCL-1's function was questioned. Side-by-side comparisons of protein models can identify unique structures and allow inferences about structure-function of conserved or unique regions. Structural prediction software was used to generate models of vCXCL-1<sub>Toledo</sub> and vCXCL-1<sub>Towne</sub> to better identify the role of the C-terminal chemokine region [39]. The top 5 predicted structures for each were overlaid (Fig. 3.6 A & B). In regards to overall structure, the modeled chemokines appear to adopt the classic "Greek key" chemokine structure with three beta-sheets and an alpha helix towards the C-terminus. vCXCL-1<sub>Toledo</sub> models all have similar structures, with lower overlap in the extended C-terminal "tail" (Fig. 3.6 A). Unlike vCXCL-1<sub>Toledo</sub>, vCXCL-1<sub>Towne</sub> has significant divergence in the C-terminus (Fig. 3.6 B). For vCXCL-1<sub>Towne</sub>, one predicted structure has the C-terminus forming a fourth beta sheet and folding back across the chemokine core. This region is important for dimerization of host chemokines CXCL1 and CXCL8 [40, 41], while the C-terminus of vCXCL-1<sub>Towne</sub> could potentially block this dimerization. Models of both viral chemokines (i.e., vCXCL-1<sub>Toledo</sub> and vCXCL-1<sub>Towne</sub>) were compared (Fig. 3.6C). The viral chemokines are predicted to have similar N-terminal and chemokine core structures with marked differences in the C-terminal region. vCXCL-1<sub>Towne</sub> has a shorter alpha-helix than vCXCL-1<sub>Toledo</sub>, forming a longer C-terminal loop protruding from the core of the chemokine. The extended C-terminus of vCXCL-1<sub>Towne</sub> also appears to fold back towards the core of the chemokine. For many host chemokines, extended C-termini enhance binding to GAGs, but not for vCXCL-1<sub>Toledo</sub>. The implications/consequences of the extended C-terminus is unknown.

The extended C-terminus on vCXCL-1s may be interfering with normal GAG binding (Fig. 3.5). Human CXCL8 GAG-binding is mediated by basic residues within the C-terminal alpha-helix forming a putative binding groove (shown by red line/arrow in Fig. 3.7) [42]. Visualization of both CXCL8 and vCXCL-1<sub>Toledo</sub> (Fig. 3.7A) and CXCL8 and vCXCL-1<sub>Towne</sub> (Fig. 3.7B) monomers are shown in three orientations. Overlay of CXCL8 and vCXCL-1<sub>Toledo</sub> shows high structural similarity in the core of the chemokine. However, for both viral chemokines, the extended C-terminus is predicted to loop back across the face of the chemokine. This may block the interface used for heparin binding. The extended

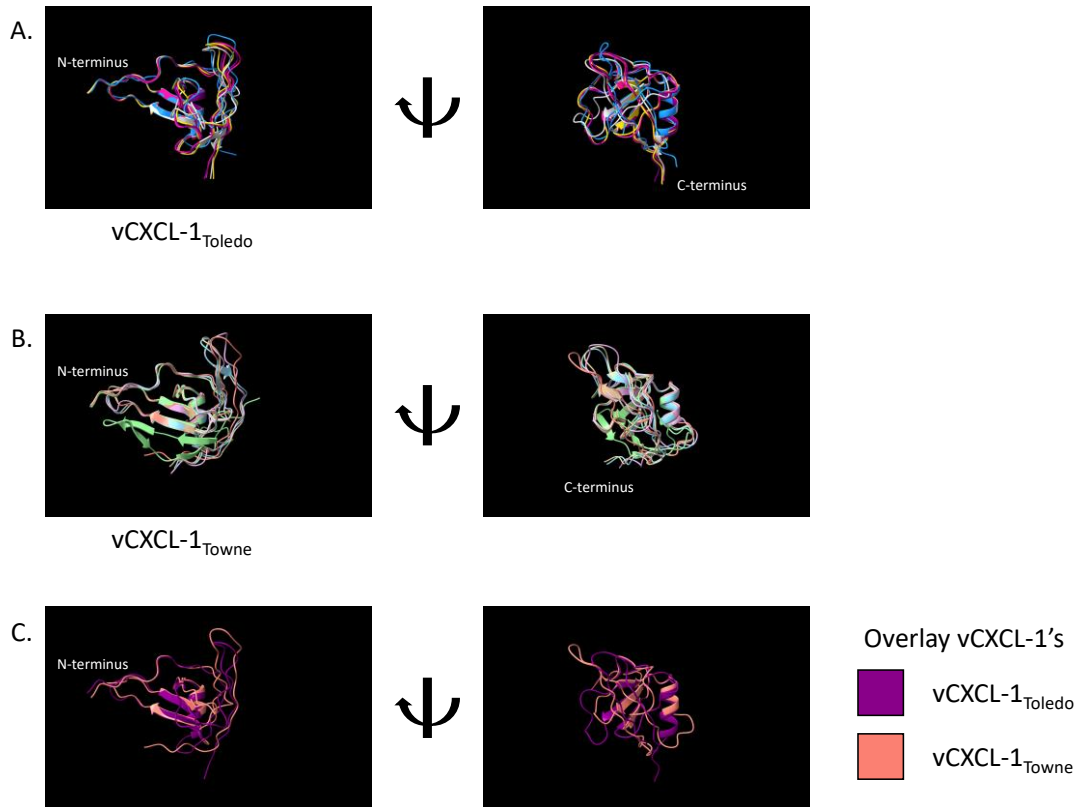


**Figure 3.6:** *Ab initio* modeling of vCXCL-1 from Toledo and Towne strains of HCMV. Top 5 structures of (A) vCXCL-1<sub>Toledo</sub> and (B) vCXCL-1<sub>Towne</sub> were overlaid. (C) Overlay of anticipated structures of vCXCL-1 from Toledo and Towne strains. Models of vCXCL-1's were generated by Phyre2 *ab initio* modeling. Visualization of individual and overlaid models was performed in ChimeraX.

“tail” of vCXCL-1’s may sterically hinder this process and explain the lower affinity for heparin (Fig. 3.5). Functionally, GAG-binding plays important roles in chemokine function [18, 33, 34, 36], and conservation of an extended C-terminus among one of the most polymorphic genes in HCMV points to it playing an important role *in vivo*. Whether GAG-binding of vCXCL-1 enhances or inhibits receptor stimulation is unknown, but truncation of the extended C-terminus of vCXCL-1 may restore heparin binding by exposing residues capable of forming the necessary electrostatic interactions.

Along with GAG-binding, structural differences in the C-terminus may impact receptor binding and stimulation of CXCR2. Insertion of a FLAG epitope within the C-terminus of *UL146* prevented migration of human peripheral blood neutrophils in response to supernatants from infected cells [13]. To examine this interaction, a previously solved structure of CXCR2 with bound CXCL8 [42] was utilized to model the two predicted isoforms of vCXCL-1 (Toledo and Towne) in place of CXCL8 (Fig. 3.8). The N-terminus of both vCXCL-1s appears to be shallower in the binding region of CXCR2 than CXCL8. vCXCL-1<sub>Toledo</sub> is the deeper of the two vCXCL-1’s. Additionally, the N-terminus of CXCR2 likely interacts with the vCXCL-1s differently than CXCL8, because there are different charges and significant steric hindrance of the CXCR2 N-terminus. Along with N-terminal interactions, for some chemokines, the extracellular loops of the receptor, such as extracellular loop 2 (ECL2), play important roles in receptor activation and biased signaling [20]. Again, vCXCL-1s appear to have a different occupation of the binding pocket and interaction with ECL2, with Towne potentially sterically hindered as evidenced by clashes/overlap between the 30S loop and ECL-2. This could result in vCXCL-1<sub>Towne</sub> actually sitting even further out of CXCR2’s binding pocket than shown, further limiting or altering the stimulation of the receptor. These structural differences could further contribute to functional selectivity and *in vivo* differences in CXCR2 activity.

### **Discussion**

*UL146* appears to encode for an HCMV virulence factor, increasing dissemination of virus and mortality *in vivo* [11]. The molecular mechanism by which vCXCL-1<sub>Toledo</sub> functions as a virulence factor was unclear. That it functions through a CXCR2-positive

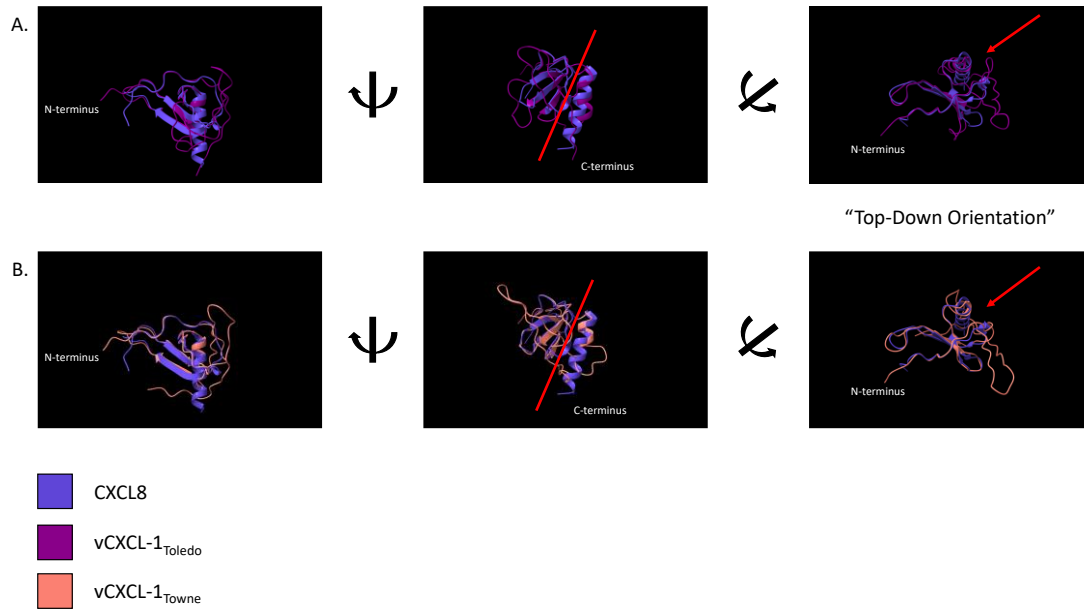


**Figure 3.7:** Extended C-terminus of vCXCL-1<sub>Toledo</sub> and vCXCL-1<sub>Towne</sub> is not present in host CXCL8. Structures of (A) CXCL8 and vCXCL-1<sub>Toledo</sub>, (B) CXCL8 and vCXCL-1<sub>Towne</sub> were overlaid. CXCL8's GAG-chemokine interface is highlighted by either a red line or arrow. CXCL8 structure was previously determined by x-ray crystallography. Model of vCXCL-1<sub>Toledo</sub> was generated by Phyre2 *ab initio* modeling. Visualization of individual and overlaid models was performed in ChimeraX.

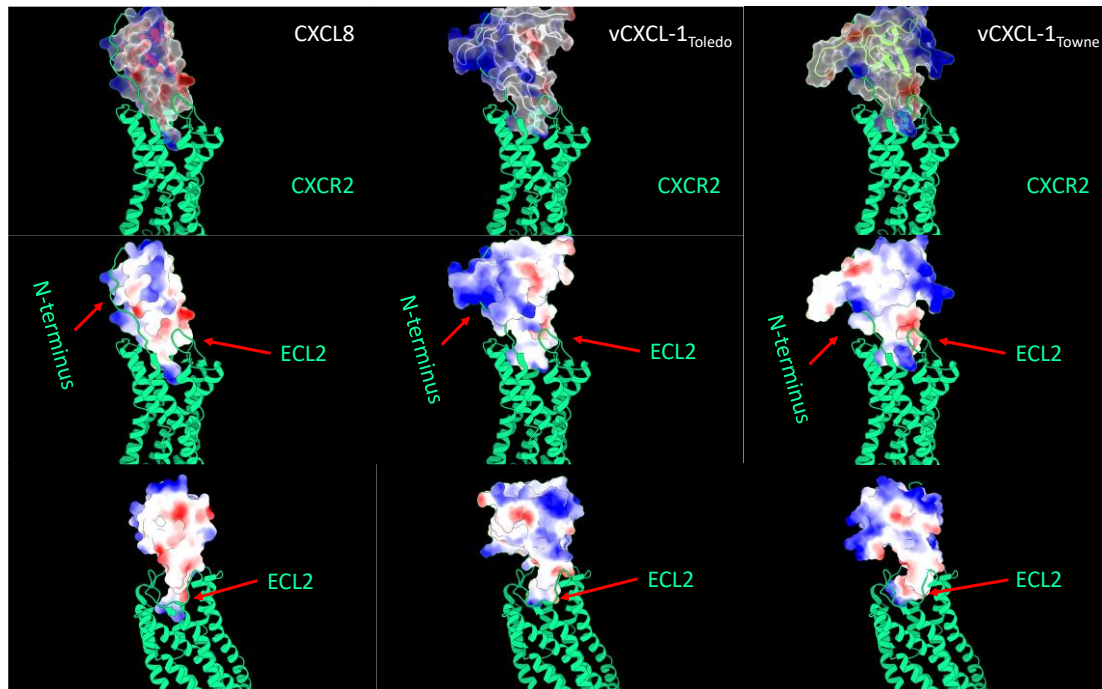


**Figure 3.8:** CXCR2 chemokine ligand models.

The solved structure of a CXCR2-CXCL8 complex is shown on the left with key annotations for receptor N-terminus and ECL2 highlighted. vCXCL-1<sub>Toledo</sub> (center) and vCXCL-1<sub>Towne</sub> (right) were overlaid in the place of CXCL8 to identify similarities and differences in receptor occupancy and interaction.

immune cells is likely, but the functional consequences or viral strategy is still elusive. We present further characterization of two distinct vCXCL-1s *in vivo*, *in vitro*, and *in silico*. HCMV vCXCL-1s do not significantly induce differential inflammation (Fig. 3.1 E, 3.2 B). This is likely due to significant variability in footpad swelling among infected animals making it difficult to ascertain differences in inflammation among the viruses. However, there are trends of increased inflammation and mortality for vCXCL-1<sub>Toledo</sub> expressing viruses (Fig. 3.2 D), further supporting functional selectivity amongst viral chemokines. Herein, we provide preliminary *in vivo* evidence of differences in virulence and disease outcomes based on the genotype of vCXCL-1 present. Why vCXCL-1<sub>Towne</sub> fails to generate a strong immune response at the site of infection or increased mortality versus a non-vCXCL-1 containing virus is an interesting question. Whether this is a function of vCXCL-1<sub>Towne</sub> to escape antiviral clearance or a byproduct of specific immune cell recruitment, the biological function of different vCXCL-1s remains an open question. *In vitro*, isoforms of vCXCL-1 were shown to differentially induce chemotaxis and calcium flux [17], but whether these chemokines activate different intracellular signaling pathways or similar pathways to differing degrees is an area requiring further investigation. Thus, despite similar CXCR2 interactions and stimulation *in vitro*, the exact *in vivo* role/function of vCXCL-1's still needs to be fully ascertained.

Sequence analysis of multiple vCXCL-1's versus other human CXCR2-binding chemokines, such as CXCL8, identified a region unique to HCMV vCXCL-1 (Fig. 3.3, data not shown). The overall positively charged, extended C-terminus was found in all examined vCXCL-1 isoforms (Fig. 3.3). Initially, based on observations of host chemokines, we thought that this extended region would be unstructured and enhance GAG-binding similar to CXCL13 or CCL21 [20, 31]. This does not appear to be the case, however. Full-length vCXCL-1<sub>Toledo</sub> has low affinity for heparin (Fig. 3.5 B). In contrast, host CXCL8 bound with high affinity and with multiple chemokines binding per chain (Fig. 3.5 A). CXCL8's heparin binding appears to be due to electrostatic interactions, with vCXCL-1<sub>Toledo</sub> undergoing entropically favorable conformational changes or protein solvation for binding. Host chemokines are able to bind GAGs modulating stimulation of host chemokine receptors. For CXCR2-interacting chemokines such as CXCL8, mCXCL1,

CXCL2, binding to GAGs can prevent receptor stimulation [33, 36, 38]. Recruitment of circulating immune cells varies based not just on concentration but also the steepness of the established chemokine gradient [43]. GAG-binding is coupled to the formation of chemotactic gradients and oligomerization of chemokines [18, 34, 38, 43]. CXCL8 is able to form both monomers and dimers based on local concentrations, and GAG-interaction with monomer and dimer are essential for proper immune stimulation and recruitment [36, 38, 43, 44]. Failure of viral chemokines to associate with GAGs could be a mechanism to tweak the receptor to a desired, specific level. Indeed, differences in GAG binding between mCXCL1 and mCXCL2 are thought to influence and contribute to their differences in neutrophil recruitment [37]. Additionally, truncation of the C-terminal GAG-binding domain from CXCL8 impaired neutrophil recruitment despite intact N-terminus and overall structure [45]. This carried over to *in vivo* experiments where mutations in GAG-binding residues of CXCL8 reduced leukocyte accumulation within the peritoneum [34]. Interestingly, GAG-deficient CXCL8 showed increased recruitment of leukocytes within the lungs potentially highlighting a tissue-specific response to chemokine release [34]. vCXCL-1<sup>Toledo</sup> appears to have lower affinity for HS than CXCL8 (Fig. 3.5) which may affect subsequent receptor stimulation, chemokine oligomerization, and *in vivo* potency. This could be due to occlusion of the alpha-helix by an extended C-terminus (Fig. 3.7). By preventing or reducing dimerization and GAG-binding, vCXCL-1 may spread over further distances *in vivo*, recruiting CXCR2 positive cells from distal sites. vCXCL-1 distribution may also serve to prime recipient cells, altering their functions for pro-viral outcomes. Although this is a conserved region among *UL146* genotypes, *in vivo* cathepsins may process it similar to CXCL13 [31]. Cathepsin B cleavage of CXCL13's extended C-terminus prevents GAG-binding and potentiates receptor signaling and chemotaxis *in vivo* [31]. Similar cleavage of vCXCL-1 may play a role to "activate" or "inactivate" vCXCL-1 by altering HS-binding, dimerization, and chemokine activity *in vivo*. Altogether, GAG-chemokine interactions play important roles in the regulation of chemokine function *in vivo*, and the consequences of GAG-impairment for viral chemokines presents further complications to determining their biological function. Why this extended C-terminal region is conserved across all the polymorphic vCXCL-1s forms is currently unclear, but

it represents a novel area for further investigation towards understanding the role of vCXCL-1 in HCMV infections.

Along with the effect of GAG-binding on chemokine receptor interactions, vCXCL-1s may interface with CXCR2 differently than host CXCL8 (Fig. 3.8). Receptor-binding models suggest differential interaction with CXCR2 for vCXCL-1<sub>Toledo</sub> and vCXCL-1<sub>Towne</sub> (Fig. 3.8). The differences in receptor binding and interface residues could explain *in vitro* observed differences in receptor affinity and stimulation [17]. The full downstream signaling cascades induced by stimulation with different vCXCL-1 isoforms still need to be determined, however. The C-terminus of vCXCL-1 may also be involved in CXCR2 interactions (Fig. 3.8) [13]. A FLAG epitope inserted into vCXCL-1 reduced the migration of neutrophils towards infected supernatants to the same degree as deletion of genes spanning *UL138-UL148* [13]. That, vCXCL-1 FLAG tag impaired the chemotaxis of PBNs *in vitro* points to the C-terminus playing a functional role in receptor binding. This provides further evidence for a role of the extended C-terminus of vCXCL-1 in receptor stimulation. Future work should further focus on the function of vCXCL-1s C-terminus and how it plays a role during *in vitro* CXCR2 stimulation as well as the *in vivo* role of different isoforms of vCXCL-1 with and without their extended C-terminus.

## Materials and Methods

### *Cells and Viruses*

Murine embryonic fibroblast (MEF 10.1) cells were used at <20 passages [46]. Cells were maintained at 37°C with 5% CO<sub>2</sub> in DMEM with 1% penicillin, 1% streptomycin, 1% L-glutamine, and 10% FetalClone III (Cytiva, Marlborough, MA). Wildtype Smith virus was maintained on a bacterial artificial chromosome (BAC). Generation of recombinant chemokine expressing viruses using recombineering and GalK selection has been described previously [11]. Briefly, a recombination cassette containing the galactokinase (GalK) gene was transformed into SW105 *E. coli* strain containing the MCMV BAC. Transformants are then selected for on MacConkey agar plates containing galactose. Successful transformants are then recombined with a cassette to replace the GalK gene which restores the WT genome and introduces a Flag tag on the end of MCK2,

followed by a 2A cleavage peptide, and the HCMV viral chemokine (vCXCL-1, encoded by UL146) tagged with a 6x histidine tag. Recombinant BACs were screened by growth on 2-deoxygalactose plates. Successful transformants were further screened by RFLP genome analysis and targeted sequencing across the MCK2 gene locus.

### ***Animals***

All procedures were reviewed and approved by the Institutional Animal Care and Use Committee at the University of Tennessee. BALB/cJ mice were obtained from Jackson Laboratory (Bar Harbor, ME) and housed in a specific-pathogen free environment at the University of Tennessee. Mice >6 weeks of age were injected in the footpad with  $\sim 1 \times 10^6$  pfu. Footpad swelling was measured using digital calipers and normalized as percent swelling greater than uninfected foot. Cyclophosphamide treated mice were injected intraperitoneally three separate times with 150mg/kg (days 0, 3, 6) and then twice with 100mg/kg (days 9, 12). Survival of cyclophosphamide treated mice was determined by body conditioning score. Mouse weights were taken daily as an additional indicator of condition.

### ***Production and Purification of Recombinant Chemokines***

Chemokine sequences were codon optimized and cloned into the *Pichia* expression vector pPic $\alpha$  with the alpha leader sequence replacing the native chemokine signal sequence (i.e., first chemokine amino acid just downstream of the kex2 cleavage sequence). Plasmids were transformed into *Pichia* and screened on YPD-zeocin plates. Expression induced by growth in methanol containing media for 3 days and chemokine production determined and compared by SDS-PAGE gel and silver stain. High expressing clones were then scaled up to 1 liter, induced for 3 days, centrifuged to collect supernatant, and 0.2 $\mu$ m filtered. Filtered supernatant was dialyzed (3000 mwco) against 5mM sodium phosphate buffer to remove salts and lower conductivity. Dialyzed supernatant was further diluted  $\sim 10$ -fold to reduce salts sufficiently for cationic exchange. Supernatant was then loaded onto a 5mL SP Sepharose fast flow column (Cytiva, Marlborough, MA). Protein was eluted using a linear salt gradient (0 – 1M sodium chloride in 5mM sodium phosphate buffer)

over 20 fractions. Protein was quantified by  $A_{230}$  measurement and protein containing fractions checked by SDS-PAGE/silver stain. Chemokine containing fractions were combined and filtered through a 0.2 $\mu$ m filter and stored at 4°C. vCXCL-1<sub>Toledo</sub> was treated with PNGase F (New England Biolabs, Ipswich, MA) prior to running on a SDS PAGE gel and silver staining.

### ***Anti-Chemokine ELISAs***

Indirect ELISAs were performed by addition of respective chemokine (50 $\mu$ L of ~1 $\mu$ g/mL) to a well of a high-binding 96-well plate and incubated overnight at 4°C. Unbound chemokine was removed and wells washed 3x with PBS-T (PBS with 0.1% Tween-20). Blocking buffer (5% milk in PBS) was added to wells and incubated for 2 hours at room temperature. Excess block was removed and washed 1x with PBS-T. Primary (anti-chemokine) antibody anti-UL146 (R & D Systems, Minneapolis, MN) or anti-CXCL8 (Becton, Dickinson and Company, Franklin Lakes, NJ) was added at 1:500 dilution and incubated for 1 hour. Excess was removed and washed 3x with PBS-T. HRP-conjugated anti-mouse was added at 1:10,000 and incubated for 1 hour. Excess removed, washed 3x with PBS-T, and wells developed using 1-step TMB (Thermo Fisher Scientific, Waltham, MA). Colorimetric reaction was stopped by the addition of 2M sulfuric acid and absorbance read at 450nm using a BioTek Synergy H1 plate reader (BioTek, Winooski, VT).

### ***Western Blots***

Western blots were performed against *Pichia* produced and purified CXCL8 and vCXCL-1<sub>Toledo</sub>. Chemokines were boiled in Laemmli buffer and run under denaturing conditions on a 12% SDS PAGE gel. Proteins were transferred onto nitrocellulose and probed with anti-chemokine primary antibodies (1:500). Anti-mouse IgG HRP conjugated secondaries were added (1:10,000), and blots developed with chemiluminescent substrate (Thermo Fisher Scientific, Waltham, MA). Blots were imaged on a BioRad ChemiDoc, and luminescent and white light overlaid.

### ***Isothermal Titration Calorimetry***

Isothermal titration calorimetry was performed using a MicroCal VP-ITC calorimeter (Malvern Panalytical, Malvern, United Kingdom). Chemokines were diluted to ~10uM in sterile filtered PBS. Heparin sodium salt (from porcine mucosal tissue) was resuspended in PBS and titrated into the chemokines. Unfractionated heparin concentration was approximated based on the manufacturer's reported average molecular weight (~18kDa). Background titrations were performed by titration of heparin at experimental concentrations and subtracted from the final data. Data analysis was performed and thermograms visualized using Origin software (Malvern Panalytical, Malvern, United Kingdom).

### ***Protein Structural Prediction***

Secondary structure of vCXCL-1<sub>Toledo</sub> was estimated using Phyre2's intensive settings [39]. Structural models of vCXCL-1<sub>Toledo</sub> and x-ray crystallography of CXCL8 (PDB: 5d14) were visualized using Chimera X [47]. Individual and overlaid images were recorded and presented here. For CXCR2-binding analysis, a previously determined CXCR2-CXCL8 complex (PDB: 6lfo) [42] was used as a scaffold for superimposing/matching viral chemokines onto CXCL8.

### ***Protein Alignments***

Protein sequences for human CXCL8, and vCXCL-1's from the following HCMV strains (Tx15, Toledo, E760, C956, Tx24, C954, C952, Towne, 102410, Tx11, 100751) were N-terminally truncated at the amino acid preceding the ELR motif (NGR for Tx15). Truncated sequences were then aligned using Clustal Omega [48] alignment. Aligned sequences were then highlighted at conserved residues. Annotations were added based on the known CXCL8 sequence and structure.

### ***Statistics***

Individual or averaged data points are shown for all graphs with mean and standard deviation graphed. Significance was determined by multiple T-tests. Relevant statistical

analyses were performed in GraphPad Prism (GraphPad Software, La Jolla, CA, USA) and described in figure legends. Significance values are shown as: \* =  $p < 0.05$ , \*\* =  $p < 0.01$ , \*\*\* =  $p < 0.001$ , \*\*\*\* =  $p < 0.0001$ , ns = not significant.

### ***Acknowledgements***

We would like to thank Dr. Ed Wright for his help and insight.

## References

1. Liu, L., *Fields Virology, 6th Edition*. Clinical Infectious Diseases, 2014. **59**(4): p. 613-613.
2. Ramanan, P. and R.R. Razonable, *Cytomegalovirus infections in solid organ transplantation: a review*. Infect Chemother, 2013. **45**(3): p. 260-71.
3. Cheung, T.W. and S.A. Teich, *Cytomegalovirus infection in patients with HIV infection*. Mt Sinai J Med, 1999. **66**(2): p. 113-24.
4. Demmler, G.J., *Congenital cytomegalovirus infection*. Semin Pediatr Neurol, 1994. **1**(1): p. 36-42.
5. Stagno, S., et al., *Congenital and perinatal cytomegalovirus infections: clinical characteristics and pathogenic factors*. Birth Defects Orig Artic Ser, 1984. **20**(1): p. 65-85.
6. Rinaldo, C.R., Jr., P.H. Black, and M.S. Hirsch, *Interaction of cytomegalovirus with leukocytes from patients with mononucleosis due to cytomegalovirus*. J Infect Dis, 1977. **136**(5): p. 667-78.
7. Sinzger, C., M. Digel, and G. Jahn, *Cytomegalovirus cell tropism*. Curr Top Microbiol Immunol, 2008. **325**: p. 63-83.
8. Jackson, J.W. and T. Sparer, *There Is Always Another Way! Cytomegalovirus' Multifaceted Dissemination Schemes*. Viruses, 2018. **10**(7).
9. Daley-Bauer, L.P., et al., *Cytomegalovirus hijacks CX3CR1(hi) patrolling monocytes as immune-privileged vehicles for dissemination in mice*. Cell Host Microbe, 2014. **15**(3): p. 351-62.
10. Saederup, N., et al., *Murine cytomegalovirus CC chemokine homolog MCK-2 (m131-129) is a determinant of dissemination that increases inflammation at initial sites of infection*. Journal of Virology, 2001. **75**(20): p. 9966-9976.
11. Jackson, J.W., et al., *The Human Cytomegalovirus Chemokine vCXCL-1 Modulates Normal Dissemination Kinetics of Murine Cytomegalovirus In Vivo*. MBio, 2019. **10**(3).
12. Luttichau, H.R., *The Cytomegalovirus UL146 Gene Product vCXCL1 Targets Both CXCR1 and CXCR2 as an Agonist*. Journal of Biological Chemistry, 2010. **285**(12): p. 9137-9146.

13. Penfold, M.E.T., et al., *Cytomegalovirus encodes a potent alpha chemokine*. Proceedings of the National Academy of Sciences of the United States of America, 1999. **96**(17): p. 9839-9844.
14. Bhusal, R.P., S.R. Foster, and M.J. Stone, *Structural basis of chemokine and receptor interactions: Key regulators of leukocyte recruitment in inflammatory responses*. Protein Sci, 2020. **29**(2): p. 420-432.
15. Sokol, C.L. and A.D. Luster, *The chemokine system in innate immunity*. Cold Spring Harb Perspect Biol, 2015. **7**(5).
16. Thiele, S. and M.M. Rosenkilde, *Interaction of chemokines with their receptors--from initial chemokine binding to receptor activating steps*. Curr Med Chem, 2014. **21**(31): p. 3594-614.
17. Heo, J., et al., *Novel Human Cytomegalovirus Viral Chemokines, vCXCL-1s, Display Functional Selectivity for Neutrophil Signaling and Function*. J Immunol, 2015. **195**(1): p. 227-36.
18. Proudfoot, A.E., et al., *Glycosaminoglycan binding and oligomerization are essential for the in vivo activity of certain chemokines*. Proc Natl Acad Sci U S A, 2003. **100**(4): p. 1885-90.
19. Monteclaro, F.S. and I.F. Charo, *The amino-terminal extracellular domain of the MCP-1 receptor, but not the RANTES/MIP-1alpha receptor, confers chemokine selectivity. Evidence for a two-step mechanism for MCP-1 receptor activation*. J Biol Chem, 1996. **271**(32): p. 19084-92.
20. Jorgensen, A.S., et al., *Biased Signaling of CCL21 and CCL19 Does Not Rely on N-Terminal Differences, but Markedly on the Chemokine Core Domains and Extracellular Loop 2 of CCR7*. Front Immunol, 2019. **10**: p. 2156.
21. Yan, Y., et al., *CCL19 and CCR7 Expression, Signaling Pathways, and Adjuvant Functions in Viral Infection and Prevention*. Front Cell Dev Biol, 2019. **7**: p. 212.
22. Ottersbach, K., et al., *A310 helical turn is essential for the proliferation-inhibiting properties of macrophage inflammatory protein-1 alpha (CCL3)*. Blood, 2006. **107**(4): p. 1284-91.

23. Joseph, P.R., et al., *Dynamic conformational switching in the chemokine ligand is essential for G-protein-coupled receptor activation*. *Biochem J*, 2013. **456**(2): p. 241-51.
24. Katancik, J.A., et al., *Mapping of the extracellular binding regions of the human interleukin-8 type B receptor*. *Biochem Biophys Res Commun*, 1997. **232**(3): p. 663-8.
25. Lurain, N.S., et al., *Analysis of the human cytomegalovirus genomic region from UL146 through UL147A reveals sequence hypervariability, genotypic stability, and overlapping transcripts*. *Virology Journal*, 2006. **3**.
26. Berg, C., et al., *The frequency of cytomegalovirus non-ELR UL146 genotypes in neonates with congenital CMV disease is comparable to strains in the background population*. *BMC Infect Dis*, 2021. **21**(1): p. 386.
27. Guo, G., et al., *Polymorphisms and features of cytomegalovirus UL144 and UL146 in congenitally infected neonates with hepatic involvement*. *PLoS One*, 2017. **12**(2): p. e0171959.
28. Heo, J., et al., *Polymorphisms within human cytomegalovirus chemokine (UL146/UL147) and cytokine receptor genes (UL144) are not predictive of sequelae in congenitally infected children*. *Virology*, 2008. **378**(1): p. 86-96.
29. Paradowska, E., et al., *Cytomegalovirus alpha-chemokine genotypes are associated with clinical manifestations in children with congenital or postnatal infections*. *Virology*, 2014. **462-463**: p. 207-17.
30. MacDonald, M.R., et al., *Spliced mRNA encoding the murine cytomegalovirus chemokine homolog predicts a beta chemokine of novel structure*. *J Virol*, 1999. **73**(5): p. 3682-91.
31. Cosgrove, J., et al., *B cell zone reticular cell microenvironments shape CXCL13 gradient formation*. *Nat Commun*, 2020. **11**(1): p. 3677.
32. Thompson, S., et al., *Regulation of Chemokine Function: The Roles of GAG-Binding and Post-Translational Nitration*. *International Journal of Molecular Sciences*, 2017. **18**(8).

33. Crijs, H., V. Vanheule, and P. Proost, *Targeting Chemokine-Glycosaminoglycan Interactions to Inhibit Inflammation*. Front Immunol, 2020. **11**: p. 483.
34. Gangavarapu, P., et al., *The monomer-dimer equilibrium and glycosaminoglycan interactions of chemokine CXCL8 regulate tissue-specific neutrophil recruitment*. J Leukoc Biol, 2012. **91**(2): p. 259-65.
35. Webb, L.M., et al., *Binding to heparan sulfate or heparin enhances neutrophil responses to interleukin 8*. Proc Natl Acad Sci U S A, 1993. **90**(15): p. 7158-62.
36. Joseph, P.R.B., K.V. Sawant, and K. Rajarathnam, *Heparin-bound chemokine CXCL8 monomer and dimer are impaired for CXCR1 and CXCR2 activation: implications for gradients and neutrophil trafficking*. Open Biol, 2017. **7**(11).
37. Sepuru, K.M., et al., *Structural basis, stoichiometry, and thermodynamics of binding of the chemokines KC and MIP2 to the glycosaminoglycan heparin*. J Biol Chem, 2018. **293**(46): p. 17817-17828.
38. Kuschert, G.S., et al., *Glycosaminoglycans interact selectively with chemokines and modulate receptor binding and cellular responses*. Biochemistry, 1999. **38**(39): p. 12959-68.
39. Kelley, L.A., et al., *The Phyre2 web portal for protein modeling, prediction and analysis*. Nat Protoc, 2015. **10**(6): p. 845-58.
40. Fairbrother, W.J., et al., *The solution structure of melanoma growth stimulating activity*. J Mol Biol, 1994. **242**(3): p. 252-70.
41. Clore, G.M., et al., *Three-dimensional structure of interleukin 8 in solution*. Biochemistry, 1990. **29**(7): p. 1689-96.
42. Liu, K., et al., *Structural basis of CXC chemokine receptor 2 activation and signalling*. Nature, 2020. **585**(7823): p. 135-140.
43. Das, S.T., et al., *Monomeric and dimeric CXCL8 are both essential for in vivo neutrophil recruitment*. PLoS One, 2010. **5**(7): p. e11754.
44. Fernando, H., et al., *Dimer dissociation is essential for interleukin-8 (IL-8) binding to CXCR1 receptor*. J Biol Chem, 2004. **279**(35): p. 36175-8.

45. Goldblatt, J., et al., *A Requirement for Neutrophil Glycosaminoglycans in Chemokine:Receptor Interactions Is Revealed by the Streptococcal Protease SpyCEP*. J Immunol, 2019. **202**(11): p. 3246-3255.
46. Harvey, D.M. and A.J. Levine, *P53 Alteration Is a Common Event in the Spontaneous immortalization of Primary Balb/C Murine Embryo Fibroblasts*. Genes & Development, 1991. **5**(12b): p. 2375-2385.
47. Pettersen, E.F., et al., *UCSF ChimeraX: Structure visualization for researchers, educators, and developers*. Protein Sci, 2021. **30**(1): p. 70-82.
48. Madeira, F., et al., *The EMBL-EBI search and sequence analysis tools APIs in 2019*. Nucleic Acids Res, 2019. **47**(W1): p. W636-W641.

**CHAPTER 4 - HEPARAN SULFATE UTILIZATION DIFFERS  
BETWEEN *IN VIVO* AND *IN VITRO* DERIVED MCMV**

This work was performed by: Trevor J. Hancock, Joseph W. Jackson, Yue Zhou, Madison Keelty, Andrea Ramirez, and Tim E. Sparer

Author Contributions: Conceptualization, T.E.S., J.W.J., and T.J.H.; Methodology, J.W.J. and T.J.H.; Formal analysis, T.J.H.; Investigation, T.J.H., J.W.J., Y.Z., M.E., and A.R.; Writing—original draft preparation, T.J.H.; Writing—review and editing, J.W.J., T.E.S. and T.J.H.; Visualization, T.J.H.; Funding Acquisition, T.E.S.

### **Abstract:**

Cytomegaloviruses (CMVs) represent a group of clinically important herpesviruses. Because these viruses are highly prevalent and are a significant disease burden in susceptible immunocompromised populations, the development of new therapeutic treatment options is a priority. Previous efforts to develop and assess the applicability of heparan sulfate (HS) binding peptides as anti-CMV drugs discovered subtle differences in host cell infection between *in vivo* and *in vitro* derived CMV (both human and murine). Here, we attempt to further characterize the HS-CMV interactions by analyzing cell culture derived virus and salivary gland derived virus in finer detail with the aims of developing more specific therapeutics capable of inhibiting both types of viruses and furthering our understanding of the differences between *in vivo* and *in vitro* viruses. Using HS mutant cells lines, we show that MCMV infection is related to the level of sulfation/negative charge present on the surface of cells and identify differential utilization of HS by cell culture and salivary gland viruses.

### **Introduction:**

Found in most adults, CMV is a significant pathogen for many immunocompromised individuals [1]. Infection is spread by contact with infected bodily secretions, vertically from infected mothers, or during organ transplantation and hematopoietic stem cell transfer [2-5]. CMVs establish a lifelong infection likely within hematopoietic progenitor cells [1, 6], with sporadic periods of reactivation and shedding [7]. Disease is typically mild. However, immunocompromised persons may suffer severe symptoms such as: graft versus host disease, retinitis, gastroenteritis, and transplant

rejection [4, 5]. Congenital CMV is the leading infectious cause of congenital disorders potentially resulting in microcephaly, sensorineural hearing loss, and developmental disorders [2, 3].

Following recruitment of a target cell or cell-free inoculation of CMV, infection is likely dependent on heparan sulfate proteoglycan (HS) interactions [8]. HS is an O-linked glycosaminoglycan (GAG) expressed on the surface of mammalian cells [8]. It consists of a long, unbranched sugar chains attached to either surface (heparan sulfate) or secreted (heparin sulfate) proteins [9, 10]. A core tetrasaccharide attached to a serine/threonine is followed by alternating N-acetylglucosamine/glucuronic acid to form a chain several hundred saccharides in length [9, 10]. The fully extended chain is then modified by a series of enzymes sequentially adding negatively charged sulfate groups in a cell type dependent level and pattern (i.e., sugars are not sulfated in equal levels or positions) [9, 10]. There are four families of sulfotransferases responsible for the modification of the initial chain [9, 10]. The activity/pattern of sulfation by a family of enzymes is thought to be determined by the upstream enzymatic activity, with loss of earlier enzyme families/sulfation having a greater overall impact versus later downstream enzymes [9, 10]. Early studies on HS-deficient cell types demonstrated that loss of HS renders cell types resistant to CMV infection [11]. CMVs have also been found to express several glycoproteins with potential HS interactions, which allow for the tethering of CMV to the host cell surface [12-15]. Recent efforts have highlighted the importance of HS chain polymerization to MCMV infection [16]. However, the exact HS pattern or sulfation required for cell entry has yet to be determined. Identification of the exact pattern that CMVs utilize for viral entry would allow for targeted development of anti-CMV drugs with potentially greater efficacy and specificity.

Following adsorption, CMVs interact with cellular receptors on the host cell surface to trigger two distinct entry processes which are dependent on cell type/receptor expression [17, 18]. Entry into fibroblast cell lines occurs *via* fusion/macropinocytosis at the cell membrane and is mediated primarily by platelet derived growth factor receptor  $\alpha$  (PDGFR $\alpha$ ) bound by an HCMV glycoprotein trimer of gO, gH, gL [17, 19, 20]. For entry into hematopoietic cells, endothelial cells, epithelial cells, and others, endocytosis occurs

following engagement of neuropilin 2 to a pentameric complex of gH, gL, UL128, UL129, UL131 [21-23]. Following cellular engagement by viral entry complexes, the fusion peptide of CMV (gB) can interact with the host cell membrane and trigger the introduction of viral nucleocapsid and tegument proteins into the host cell [24-26]. Whether the same host cellular receptors are conserved in the entry of MCMV or other animal models of CMV is unknown. However, different viral proteins are responsible for the entry processes of MCMV. Murine viral homologs of gO, gH, gL drive fibroblastic entry [27], but a trimer of gH, gL, and MCK2 carries out endocytic entry [28]. Tropism of CMV is determined, in part, by the presence/absence of these proteins responsible [21, 22, 29]. The cell type in which the virus replicates also influences viral tropism by retaining self-tropic viruses or affecting the relative production of viral complexes responsible for fusion or endocytosis [29, 30]. Susceptibility to infection is influenced by the presence/ratio of GAGs on the cell surface, with infection of macrophages (*via* MCK2 and an endocytic pathway) more reliant upon non-HS GAGs [31]. This is further complicated by strain differences during production of entry complexes even within the same cell type [32, 33].

Our lab has previously shown viruses derived *in vivo* and *in vitro* differ in their susceptibility to HS-blocking peptides [34]. For *in vitro*, cell culture virus (TCV) we demonstrated robust inhibition of infection following addition of HS-binding peptides, soluble heparin, and desulfation of the HS chain [34]. Viruses derived *in vivo* (i.e., derived from salivary glands, footpad, or spleen) were resistant to those same treatments [34]. This may be due to the predominant virus-producing cell type (i.e., acinar epithelial cells in salivary gland, hematopoietic cells in spleen) producing progeny viruses distinct from cell culture fibroblasts [30]. Viruses derived from epithelial cells typically display a reduced ability to infect other cells through the endocytic pathway but retains full tropism for fibroblasts [30]. Other differences have been reported previously for *in vivo* and *in vitro* derived viruses. Virus isolated from infected salivary glands (SGV) is more lethal in neonatal mice, resistant to neutralization, and interacts with host cell carbohydrates differently than cell culture virus [35-37]. While differences between MCMV source have been known since the 1960's, a full characterization and mechanism behind TCV and SGV is lacking. Based on our previous findings of HS-binding peptides' differential inhibition

of MCMV infection based on derivation source, we sought to further characterize and understand the specific MCMV-HS interactions driving infection for TCV and SGV viruses.

### **Results:**

MCMV infection of Chinese hamster ovary (CHO) cells with mutations in key HS-production genes [38-40] demonstrated the importance of HS to MCMV susceptibility [8, 11, 34]. Using a fluorescent reporting MCMV, we infected parental and HS mutant CHO cells at an MOI of 1 overnight and measured GFP expression by flow cytometry (Figure 4.1). Infection with cell culture derived WT MCMV expressing GFP (Fig. 4.1A) and mutant-MCK2 MCMV expressing GFP (Fig. 4.1B) was normalized to WT CHO cells. Complete loss of HS chains ( $\Delta$ HSPG) resulted in the least infection (Fig. 4.1A,B). Presence of a full-length chain that drastically reduced sulfation ( $\Delta$ NDST1), increased infection compared to HS-deficiency, but without statistical significance (Fig. 4.1A,B). Similarly,  $\Delta$ HS2ST further restored the HS chain to parental levels, and correspondingly increased infection (Fig. 4.1A,B). The presence or absence of functional MCK2 had no impact on infection, despite CHO cells being epithelial in origin. This is potentially due to a species-specific endocytic entry pathway not present or impaired in CHO cells or that MCMV enters epithelial cells using fusion/trimer as reported by some [41].

As CMV's are species-specific, CHO cells do not support productive infection, require large amounts of virus for quantifying infection, limit assays, and restrict infections to reporter viruses [1]. A potential solution to this technical challenge is the use of CRISPR-Cas9 to generate bulk-HS mutations in permissive murine fibroblasts (MEF 10.1). Because HS is essential for CMV infection of fibroblasts [31, 34, 42] (Fig 4.1A,B), we sought to profile HS dependency by targeting genes responsible for sulfotransferase enzymes. Using our bulk mutant cell lines, plaque assays were performed using virus derived from cell culture (TCV) and salivary gland homogenate (SGV) (Fig. 4.2). Similar to Fig. 4.1, the level of HS-sulfation impacted TCV infection. Cas9 targeting of enzymes that impact sulfation more significantly causes greater reduction in plaque formation ( $\Delta$ NDST1 >  $\Delta$ HS2ST >>  $\Delta$ NDST2) [9, 10]. Surprisingly, for the highly reduced sulfation mutants ( $\Delta$ NDST1

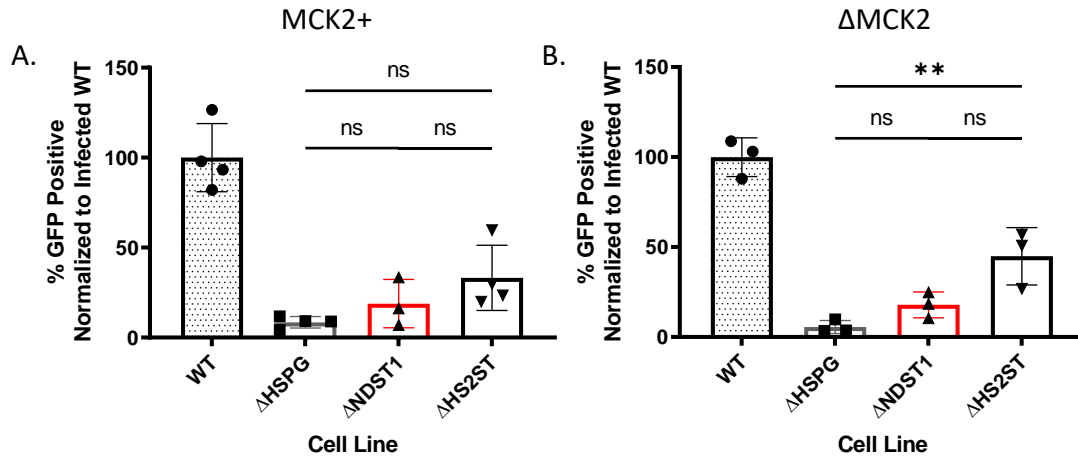


**Figure 4.1:** MCMV Entry is HS-dependent, irrespective of viral MCK2 status. HS levels influence MCMV infection of HS-mutants. CHO HS-mutants were infected overnight at an MOI of 1 with wildtype (A) or MCK2-mutant (B) MCMVs. GFP-expression was measured by flow cytometry and normalized to wildtype CHO cells. Statistical significance was determined by Tukey's one-way ANOVA. \*\* =  $p < 0.01$  ; ns = not significant.

and HS2ST), TCV and SGV infection was equally impacted. Infection of the NDST2 mutant fibroblasts identified a significant difference between TCV and SGV, with SGV infecting at parental fibroblast levels (i.e., NDST2-SG vs MEF 10.1) and TCV decreased ~25% compared to WT cells ( $p < 0.0001$ ).

HS binding in some cases is dependent upon specific sulfate positions and patterns. For instance, binding of thrombin/antithrombin and HSV-1 to HS is influenced by a specific sulfate sequence on the HS chain [43, 44]. A question is whether the decreased infection is due to a decrease in overall sulfation or removal of specific sulfations patterns on the HS chain [16]. One thought is that CMV's binding to host cells is specifically mediated by 3-O-sulfation [16, 45]. This was initially described for herpes simplex virus, a related alpha-herpesvirus, with subsequent examination in CMV [43, 45]. Evidence against CMV's dependence on a specific 3-O-sulfation is infection of CHO cells (Fig. 4.1) [11]. Wildtype and HS-mutant CHO cells fail to produce 3-O-sulfation [44]. As such, we hypothesize that CMV's binding to HS is largely mediated through a charged interaction with the negative sulfations overall. To test the theory that HS infection is dependent on the overall HS sulfation, we performed chemical desulfation of parental fibroblasts and our NDST1-mutant cell line (Fig. 4.3A). Sodium chlorate is a chemical method of selective desulfation capable of removing 2-O and 6-O-sulfations based on concentration [46]. Chlorate removal of 2-O and 6-O-sulfations from the WT cells decreased infection on par with an NDST1 mutant line (~35%) (Fig. 4.3A). Further removal of sulfates from the NDST1 cells decreased infection vs WT (~15%). Along with depletion of sulfates from HS, heparinase I digestion was utilized to truncate HS chains (Fig. 4.3B). Heparinase I cleaves HS chains to yield disaccharides, cleaving between N- and 2-O-sulfated hexosamines. This would remove highly N-sulfated regions from parental fibroblasts and remove any similarly remaining regions from the NDST1 mutants. Heparinase I treatment of WT cells reduced infection to NDST1 mutant levels (~25% vs ~37%, respectively) (Fig. 4.3B). Heparinase treatment of NDST1 lead to infection at ~12% of WT infection, on par with sodium chlorate treatment (Fig. 4.3A,B). Further establishing that the level of HS likely determines the infection of host cells.

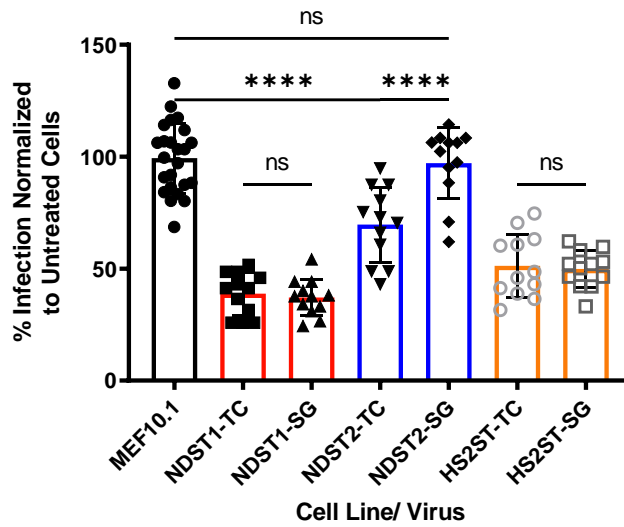


**Figure 4.2:** Fibroblasts with HS mutations point to variable HS utilization by TCV and SGV. Fibroblasts with HS sulfotransferase genes targeted by CRISPR-Cas9 were infected with TCV and SGV MCMV. Plaque formation was measured and normalized to infected WT, parental MEF 10.1 cells. Statistical significance was determined by Tukey's one-way ANOVA. \*\*\*\* =  $p < 0.0001$  ; ns = not significant.

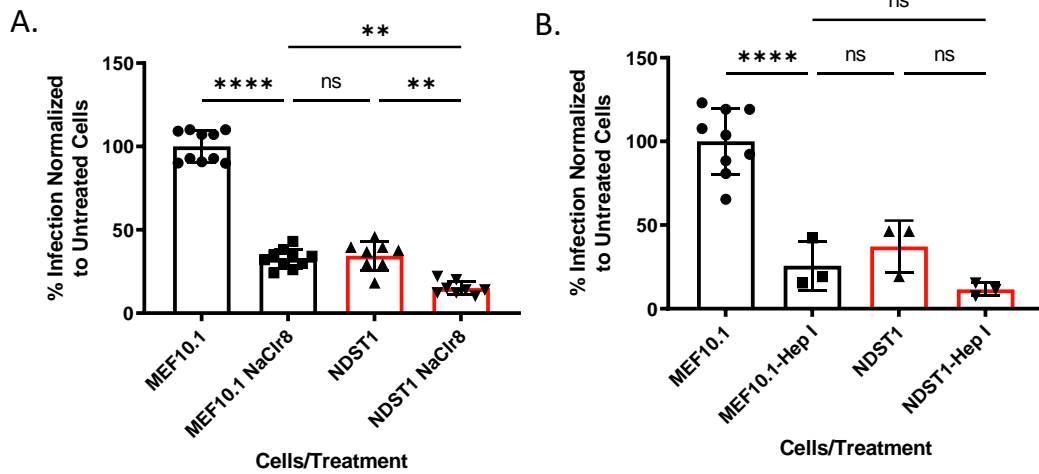


**Figure 4.3:** Sulfation and negative charge on HS chains are responsible for MCMV infection. WT and NDST1 fibroblasts were treated with either sodium chlorate (NaClr8) (A), or Heparinase I (Hep I) (B) and infected with TCV MCMV. Plaque formation was measured and normalized to WT, untreated MEF 10.1 cells 5 dpi. Statistical significance was determined by Tukey's one-way ANOVA. \*\* =  $p < 0.01$  ; \*\*\*\* =  $p < 0.0001$  ; ns = not significant.

To test the entry kinetics of TCV and SGV on HS mutant fibroblasts, infections were carried out at 37°C and 4°C. Infections at 37°C allows for both viral attachment to the cell surface and subsequent entry to occur. Performing incubations at 4°C allows the initial host-virus attachment to occur but subsequent viral entry is delayed until cells are returned to 37°C. Removal of inoculum prior to incubation at 37°C results in decreased infection (MEF 10.1 vs MEF 10.1 at 4°C) (Fig. 4.4A,B). For TCV, incubation temperature did not affect infection of HS-mutant lines (Fig. 4.4A), with all showing infections on a similar level regardless of the temperature. There was a slight trend of decreasing infection when incubations were performed at 4°C, but it failed to reach statistical significance. With SGV, a similar trend was observed, except for the NDST2 infection (Fig. 4.4B). Infection of NDST2 mutant cells was significantly diminished when performed at 4°C (~50%,  $p < 0.0001$ ). At 4°C, there was no difference between TCV and SGV on the same HS mutant cell lines (Fig. 4.4C). Because we see similar levels of infection for HS mutants at 37°C and 4°C, there is likely a defect in the entry process. This is likely upstream of the actual fusion or endocytosis event. The exception of SGV and NDST2 further highlights differences in HS utilization for infection.

We now suspected a disconnect between viral attachment and entry for viruses on HS mutants, with TCV and SGV appearing to differ in their HS utilization. This follows recent observations demonstrating a difference in surface retention between TCV and SGV [42]. Wildtype fibroblasts were infected with MCMV for 30 minutes, after which cells were washed with PBS to remove loosely associated virions. TCV showed a decrease of ~30% when washed with PBS versus ~50% reduction in the SGV infected (Fig. 4.5). This demonstrates SGV has a lowered attachment/retention to parental fibroblast cells. Similar infections and washes were performed on WT and HS mutant fibroblasts to look for differences in host cell attachment between TCV and SGV (Fig. 4.6). PBS washes significantly decreased infection on all cell types regardless of virus type, demonstrating a reduced retention on the cell surface (Fig. 4.6A,B). This contrasts Figure 4.4 where delaying viral entry had no impact on overall infection of HS mutants. When residual post-PBS wash infection is compared between TCV and SGV there are no differences for HS mutants (Fig. 4.6C). We find that equal amounts of infection are retained by HS mutants,

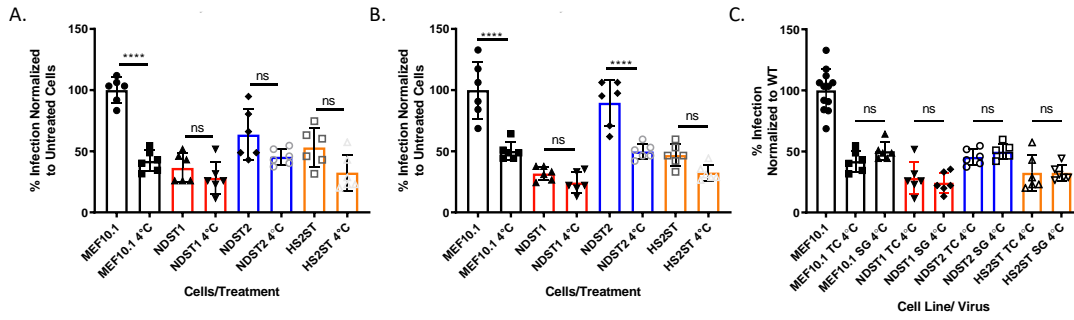


**Figure 4.4:** HS mutants alter entry kinetics.

WT and HS mutant fibroblasts were infected with either TCV (A) or SGV (B). Infections with each virus/cell combination were incubated at 37°C or 4°C for 30 minutes. Inoculum was removed and CMC overlays added after 30 minutes. Plaque formation was measured and normalized to WT, 37°C infected cells 5 dpi. In (C), TCV and SGV infections at 4°C are shown together. Statistical significance was determined by Tukey's one-way ANOVA. \*\*\*\* =  $p < 0.0001$  ; ns = not significant.

but SGV is more susceptible to washes on WT cells or cells it infects at WT levels (NDST2).

### **Discussion:**

We present evidence that the level of sulfation of host cells affects susceptibility to MCMV infection. MCMV cannot infect CHO HS mutants yet can infect WT CHO cells (Fig. 4.1), despite CHO cells lacking 3-O-sulfotransferase activity [44]. This was independent of functional MCK2 (i.e., RM4503 vs RM4511) (Fig. 4.1). MCK2 enables entry *via* endocytosis in some cell types and has previously been shown to be dispensable for infection and attachment to fibroblasts [28, 31, 42]. While we cannot discount that a specific sulfation pattern may be required for infection, we would argue that 3-O-sulfation is not indispensable as previously reported [16, 45]. CHO HS mutants display decreased sulfated HS on the cell surface and infection follows the relative sulfation status (Fig. 4.1). Similarly, HS mutant murine fibroblasts display the same phenotype of decreased sulfation, decreased infection (Fig. 4.2). Selective ablation of 2-O and 6-O-sulfations by sodium chlorate and heparinase I cleavage of highly sulfated HS chains further decreased infection of the already reduced NDST1 fibroblast mutants (Fig. 4.3). This demonstrates that despite targeting of a major driver of HS sulfotransferase activity the residual sulfation activity can be further removed by treatment. This is not surprising as HS production and modification is a highly complex process with numerous overlapping enzymes potentially able to, at least partially, restore function [47].

TCV and SGV appear to interact with host cells differently. SGV is not impacted by the NDST2 HS mutants, while TCV infection is reduced ~30% (Fig. 4.2). Likewise, retention of TCV on WT fibroblast cells is greater and less susceptible to a PBS wash than SGV (Fig. 4.5). We suspected differing affinity for HS between the two viruses and potentially a difference in the sulfation pattern necessary for infection. HS mutant infections at 4°C and infections performed with PBS washes demonstrate the disconnect between viral attachment when HS sulfation is impacted (Fig. 4.4, 4.6). Infections of NDST2 cells shows that SGV interacts with host cells and HS differently than TCV (Fig. 4.6). This mirrors a previous study which reported differences between the two in terms of

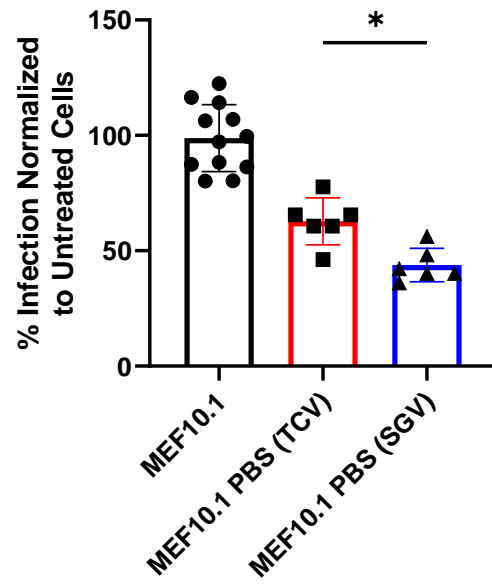


**Figure 4.5:** SGV has lowered affinity/attachment to fibroblasts. MEF 10.1 fibroblasts were infected with either TCV or SGV MCMV for 30 minutes prior to PBS washes. Plaque formation was measured and normalized to untreated, infected cells 5 dpi. Statistical significance was determined by Tukey's one-way ANOVA. \* =  $p < 0.05$ .

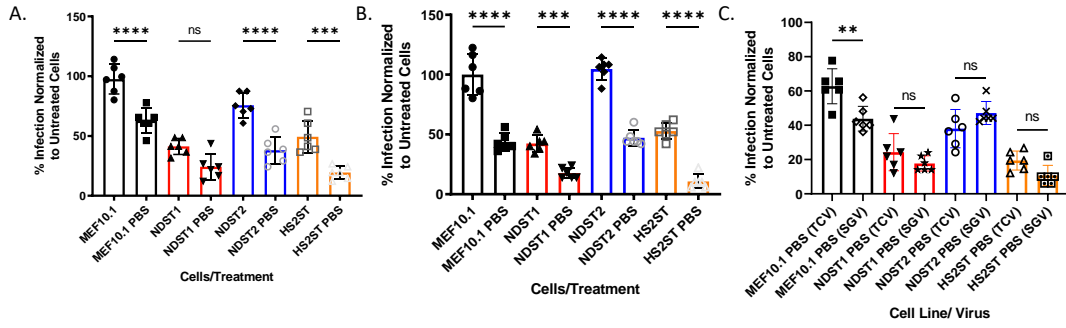


**Figure 4.6:** Loss of HS leads to equal attachment for TCV and SGV.

WT and HS mutant fibroblasts were infected with either TCV (A) or SGV (B). Infections with each virus/cell combination were incubated for 30 minutes. Inoculum was removed and cells washed twice with PBS prior to addition of CMC overlays. Plaque formation was measured and normalized to WT untreated infected cells 5 dpi. In (C), PBS washed TCV and SGV infections are shown together. Statistical significance was determined by Tukey's one-way ANOVA. \*\* =  $p < 0.01$  ; \*\*\*\* =  $p < 0.0001$  ; ns = not significant.

lectin inhibition, where SGV was more inhibited by sialidases and sialic acid binding lectins than TCV, whereas TCV was more impacted by lectins binding N-acetylglucosamine, a component of HS [36]. Together, this potentially points to an alternative attachment strategy for SGV. Cell culture HCMV that has developed reduced dependence/interaction with cell surface HS typically displays increased neutralization and a mutation within the major HS-binding glycoprotein (i.e., gM) [48]. This contrasts SG-derived MCMV, which is more resistant to neutralization and considered to be genetically identical to its parental cell culture virus [49, 50]. It is possible that due to older sequencing techniques and read coverage that minor species or point mutations in surface glycoproteins could have gone unnoticed. However, this would not explain the differences in neutralization. An additional possibility is the involvement of other GAGs for SGV entry. Fibroblast and epithelial cell entry is typically driven by surface HS [31], but entry into macrophage lines involves alternative GAGs such as Chondroitin Sulfate (CS) [31]. SGV could have shifted to be more dependent on CS for attachment. However, SGV displays reduced tropism for monocytes/macrophages calling this into question [51].

Further understanding of the SGV vs TCV phenotype is necessary. *In vitro* assays with HCMV have informed the design of many therapeutics and entry inhibitors but the relevance of *in vitro* to *in vivo* virus is poorly documented. Additional efforts should generate viruses more reflective of their *in vivo* counterparts both in terms of genetics and phenotypes, of which animal models of CMV can greatly contribute. MCMV represents a model system where generation of large quantities of genetically tractable virus both *in vivo* and *in vitro* is possible. We have further characterized the interaction of MCMV for HS based on virus derivation source, demonstrating altered affinity and utilization of surface glycosaminoglycans for SGV. This is relevant to entry inhibitor design as virus *in vivo* may be interacting with cells through alternative mechanisms not targeted by current proposed treatments. However, more work is needed to fully capture the differences between TCV and SGV, as well as recapitulate the *in vivo* phenotype *ex vivo/in vitro*.

## **Materials and Methods:**

### ***Cells and viruses:***

Murine embryonic fibroblast (MEF 10.1) cells were used at <20 passages [52]. Cells were maintained at 37°C with 5% CO<sub>2</sub> in DMEM with 1% penicillin, 1% streptomycin, 1% L-glutamine, and 10% FetalClone III (Cytiva, Marlborough, MA). Chinese hamster ovary (CHO) cells were graciously supplied by J.D. Esko (University of California San Diego). Wildtype K1 cells, pgsA ( $\Delta$ HS), pgsE ( $\Delta$ NDST1), pgsF ( $\Delta$ HS2ST) [38, 40, 53] were maintained in Ham's F12 with 1% penicillin, 1% streptomycin, 1% L-glutamine, and 10% FetalClone III (Cytiva, Marlborough, MA). Wildtype GFP-expressing MCMV (RM4503) and MCK2 mutated (RM4511) were utilized for all infections [54]. Production of TCV and SGV viruses has been described previously [34, 42]. Briefly, to generate TCV, a 2 liter roller bottle was seeded with MEF10.1 cells and infected at an MOI of 0.01. Virus and cells were harvested once 100% cytopathic effect was reached, and virus was purified by sequential centrifugation. Virus pelleted at 20,000x g was resuspended in cell culture media and sonicated. For SGV, 14 mice >6 weeks old were infected intraperitoneal with  $1 \times 10^6$  pfu. Infected salivary glands were harvested 14 days post infection and homogenized in a dounce homogenizer. SG virus was then centrifuged and prepared as above for TCV.

### ***Flow cytometry detection of infection***

WT or HS-mutant CHO cells were seeded into a 24-well dish and allowed to reach confluency. Cells were inoculated with GFP-expressing MCMV at an MOI of 1 and incubated overnight. Following overnight infection, cells were trypsinized and collected for flow cytometry analysis. GFP expression was examined using a 3 laser (405 nm, 488 nm, and 633 nm) LSR-II (Becton, Dickinson and Company, Franklin Lakes, NJ). Analysis was performed using FlowJo (FlowJo, Becton, Dickinson and Company, Ashland, OR). GFP expression/infection was normalized to infected, WT CHO K1 cells.

### ***Plaque assays***

Plaque assays were performed on permissive murine fibroblasts (WT or HS mutants). Cells were seeded sub-confluent into 24-well plates and allowed to reach confluency overnight. Confluent monolayers were infected with RM4503 derived from cell culture (TCV) or salivary gland homogenates (SGV). Infection was allowed to proceed for 30 minutes to 1 hour based on assay. Following incubation, virus was removed and replaced with a CMC overlay. Infected cells were incubated for 5 days after which plaques were counted. For sodium chlorate treated infections, cells were treated with sodium chlorate (150 mM) overnight prior to infection. Media was removed and virus inoculum added as in standard infection. Heparinase treated cells were incubated with heparinase I (1 U/mL) (New England Biolabs, Ipswich, MA) for 1 hour prior to infection. Heparinase media was removed and virus added.

Duplicate infections performed at 4°C and 37°C were incubated for 30 minutes at their respective temperatures. After 30 minutes, virus was removed and CMC overlay added. Similarly, for PBS wash experiments, cells were incubated with MCMV for 30 minutes. After incubation, 2x cold PBS washes were performed to remove loosely associated virus. CMC overlay was added to both washed and untreated infections.

### ***CRISPR-Cas9 generation of HS mutants***

A LentiCRISPR-V<sub>2</sub> plasmid encoding CRISPR-Cas9 was used to generate HS mutants in MEF 10.1 cells. Targeting gRNAs were designed, annealed together, and ligated into the plasmid backbone. Each CRISPR plasmid was separately transfected into MEF 10.1 cells, which then underwent puromycin selection. Resistant cell lines were allowed to proliferate in the presence of antibiotic selection until confluent. Genes responsible for sulfotransferase enzymes were targeted at the following regions: NDST1 - 5' CGATGCCTTTGTGATAGTTG ; NDST2 - 5' CAGCTAGCACAGAGCGGTTG ; HS2ST - 5' ATGTGTCCGTGATAGAAGCC .

### *Animals*

All procedures were reviewed and approved by the Institutional Animal Care and Use Committee at the University of Tennessee. BALB/cJ mice were obtained from Jackson Laboratory (Bar Harbor, ME) and housed in a specific-pathogen free environment at the University of Tennessee.

### *Statistics*

Each experiment consisted of 2 or more experiments with 3 replicates per group. Individual or averaged data points are shown for all graphs with mean and standard deviation graphed. Significance was determined by Tukey's one-way ANOVA with multiple comparisons. Relevant statistical analyses were performed in GraphPad Prism (GraphPad Software, La Jolla, CA, USA) and described in figure legends. Significance values are shown as: \* =  $p < 0.05$ , \*\* =  $p < 0.01$ , \*\*\* =  $p < 0.001$ , \*\*\*\* =  $p < 0.0001$ , ns = not significant.

## References

1. Liu, L., *Fields Virology, 6th Edition*. Clinical Infectious Diseases, 2014. **59**(4): p. 613-613.
2. Stagno, S., et al., *Congenital and perinatal cytomegalovirus infections: clinical characteristics and pathogenic factors*. Birth Defects Orig Artic Ser, 1984. **20**(1): p. 65-85.
3. Demmler, G.J., *Congenital cytomegalovirus infection*. Semin Pediatr Neurol, 1994. **1**(1): p. 36-42.
4. Cheung, T.W. and S.A. Teich, *Cytomegalovirus infection in patients with HIV infection*. Mt Sinai J Med, 1999. **66**(2): p. 113-24.
5. Ramanan, P. and R.R. Razonable, *Cytomegalovirus infections in solid organ transplantation: a review*. Infect Chemother, 2013. **45**(3): p. 260-71.
6. Sinclair, J., *Human cytomegalovirus: Latency and reactivation in the myeloid lineage*. J Clin Virol, 2008. **41**(3): p. 180-5.
7. Heilingloh, C.S., et al., *L Particles Transmit Viral Proteins from Herpes Simplex Virus 1-Infected Mature Dendritic Cells to Uninfected Bystander Cells, Inducing CD83 Downmodulation*. J Virol, 2015. **89**(21): p. 11046-55.
8. Compton, T., D.M. Nowlin, and N.R. Cooper, *Initiation of Human Cytomegalovirus-Infection Requires Initial Interaction with Cell-Surface Heparan-Sulfate*. Virology, 1993. **193**(2): p. 834-841.
9. Kreuger, J. and L. Kjellen, *Heparan Sulfate Biosynthesis: Regulation and Variability*. Journal of Histochemistry & Cytochemistry, 2012. **60**(12): p. 898-907.
10. Li, J.P. and M. Kusche-Gullberg, *Heparan Sulfate: Biosynthesis, Structure, and Function*. Int Rev Cell Mol Biol, 2016. **325**: p. 215-73.
11. Neyts, J., et al., *Sulfated polymers inhibit the interaction of human cytomegalovirus with cell surface heparan sulfate*. Virology, 1992. **189**(1): p. 48-58.
12. Boyle, K.A. and T. Compton, *Receptor-binding properties of a soluble form of human cytomegalovirus glycoprotein B*. Journal of Virology, 1998. **72**(3): p. 1826-1833.

13. Carlson, C., W.J. Britt, and T. Compton, *Expression, purification, and characterization of a soluble form of human cytomegalovirus glycoprotein B*. *Virology*, 1997. **239**(1): p. 198-205.
14. Pontejo, S.M. and P.M. Murphy, *Two glycosaminoglycan-binding domains of the mouse cytomegalovirus-encoded chemokine MCK-2 are critical for oligomerization of the full-length protein*. *Journal of Biological Chemistry*, 2017. **292**(23): p. 9613-9626.
15. Kari, B. and R. Gehrz, *A Human Cytomegalovirus Glycoprotein Complex Designated Gc-Ii Is a Major Heparin-Binding Component of the Envelope*. *Journal of Virology*, 1992. **66**(3): p. 1761-1764.
16. Mitra, D., et al., *The degree of polymerization and sulfation patterns in heparan sulfate are critical determinants of cytomegalovirus entry into host cells*. *PLoS Pathog*, 2021. **17**(8): p. e1009803.
17. Hetzenecker, S., A. Helenius, and M.A. Krzyzaniak, *HCMV Induces Macropinocytosis for Host Cell Entry in Fibroblasts*. *Traffic*, 2016. **17**(4): p. 351-68.
18. Bodaghi, B., et al., *Entry of human cytomegalovirus into retinal pigment epithelial and endothelial cells by endocytosis*. *Invest Ophthalmol Vis Sci*, 1999. **40**(11): p. 2598-607.
19. Huber, M.T. and T. Compton, *The human cytomegalovirus UL74 gene encodes the third component of the glycoprotein H-glycoprotein L-containing envelope complex*. *Journal of Virology*, 1998. **72**(10): p. 8191-8197.
20. Wu, Y.Q., et al., *Human cytomegalovirus glycoprotein complex gH/gL/gO uses PDGFR-alpha as a key for entry*. *Plos Pathogens*, 2017. **13**(4).
21. Ryckman, B.J., et al., *Human cytomegalovirus entry into epithelial and endothelial cells depends on genes UL128 to UL150 and occurs by endocytosis and low-pH fusion*. *J Virol*, 2006. **80**(2): p. 710-22.
22. Wang, D. and T. Shenk, *Human cytomegalovirus virion protein complex required for epithelial and endothelial cell tropism*. *Proc Natl Acad Sci U S A*, 2005. **102**(50): p. 18153-8.

23. Martinez-Martin, N., et al., *An Unbiased Screen for Human Cytomegalovirus Identifies Neuropilin-2 as a Central Viral Receptor*. *Cell*, 2018. **174**(5): p. 1158-+.
24. Kinzler, E.R. and T. Compton, *Characterization of human cytomegalovirus glycoprotein-induced cell-cell fusion*. *Journal of Virology*, 2005. **79**(12): p. 7827-7837.
25. Isaacson, M.K. and T. Compton, *Human Cytomegalovirus Glycoprotein B Is Required for Virus Entry and Cell-to-Cell Spread but Not for Virion Attachment, Assembly, or Egress*. *Journal of Virology*, 2009. **83**(8): p. 3891-3903.
26. Feire, A.L., et al., *The Glycoprotein B Disintegrin-Like Domain Binds Beta 1 Integrin To Mediate Cytomegalovirus Entry*. *Journal of Virology*, 2010. **84**(19): p. 10026-10037.
27. Scrivano, L., et al., *The m74 gene product of murine cytomegalovirus (MCMV) is a functional homolog of human CMV gO and determines the entry pathway of MCMV*. *J Virol*, 2010. **84**(9): p. 4469-80.
28. Wagner, F.M., et al., *The viral chemokine MCK-2 of murine cytomegalovirus promotes infection as part of a gH/gL/MCK-2 complex*. *PLoS Pathog*, 2013. **9**(7): p. e1003493.
29. Adler, B., *A Viral Pilot for HCMV Navigation?* *Viruses-Basel*, 2015. **7**(7): p. 3857-3862.
30. Scrivano, L., et al., *HCMV spread and cell tropism are determined by distinct virus populations*. *PLoS Pathog*, 2011. **7**(1): p. e1001256.
31. Pontejo, S.M. and P.M. Murphy, *Mouse Cytomegalovirus Differentially Exploits Cell Surface Glycosaminoglycans in a Cell Type-Dependent and MCK-2-Independent Manner*. *Viruses*, 2019. **12**(1).
32. Wilkinson, G.W.G., et al., *Human cytomegalovirus: taking the strain*. *Medical Microbiology and Immunology*, 2015. **204**(3): p. 273-284.
33. Zhou, M.M., et al., *Comparative Analysis of gO Isoforms Reveals that Strains of Human Cytomegalovirus Differ in the Ratio of gH/gL/gO and gH/gL/UL128-131 in the Virion Envelope*. *Journal of Virology*, 2013. **87**(17): p. 9680-9690.

34. Jackson, J.W., et al., *Anticytomegalovirus Peptides Point to New Insights for CMV Entry Mechanisms and the Limitations of In Vitro Screenings*. mSphere, 2019. **4**(1).
35. Osborn, J.E. and D.L. Walker, *Virulence and attenuation of murine cytomegalovirus*. Infect Immun, 1971. **3**(2): p. 228-36.
36. Ravindranath, R.M. and M.C. Graves, *Attenuated murine cytomegalovirus binds to N-acetylglucosamine, and shift to virulence may involve recognition of sialic acids*. J Virol, 1990. **64**(11): p. 5430-40.
37. Chong, K.T., J.J. Gould, and C.A. Mims, *Neutralization of different strains of murine cytomegalovirus (MCMV)-effect of in vitro passage*. Arch Virol, 1981. **69**(2): p. 95-104.
38. Bame, K.J. and J.D. Esko, *Undersulfated Heparan-Sulfate in a Chinese-Hamster Ovary Cell Mutant Defective in Heparan-Sulfate N-Sulfotransferase*. Journal of Biological Chemistry, 1989. **264**(14): p. 8059-8065.
39. Lidholt, K., et al., *A Single Mutation Affects Both N-Acetylglucosaminyltransferase and Glucuronosyltransferase Activities in a Chinese-Hamster Ovary Cell Mutant Defective in Heparan-Sulfate Biosynthesis*. Proceedings of the National Academy of Sciences of the United States of America, 1992. **89**(6): p. 2267-2271.
40. Bai, X.M. and J.D. Esko, *An animal cell mutant defective in heparan sulfate hexuronic acid 2-O-sulfation*. Journal of Biological Chemistry, 1996. **271**(30): p. 17711-17717.
41. Yunis, J., et al., *Murine Cytomegalovirus Glycoprotein O Promotes Epithelial Cell Infection In Vivo*. J Virol, 2019. **93**(3).
42. Hancock, T.J., et al., *MCMV Centrifugal Enhancement: A New Spin on an Old Topic*. Pathogens, 2021. **10**(12).
43. Shukla, D., et al., *A Novel Role for 3-O-Sulfated Heparan Sulfate in Herpes Simplex Virus 1 Entry*. Cell, 1999. **99**(1): p. 13-22.
44. Thacker, B.E., et al., *Heparan sulfate 3-O-sulfation: A rare modification in search of a function*. Matrix Biology, 2014. **35**: p. 60-72.

45. Baldwin, J., et al., *A Role for 3-O-Sulfated Heparan Sulfate in Promoting Human Cytomegalovirus Infection in Human Iris Cells*. Journal of Virology, 2015. **89**(9): p. 5185-5192.
46. Safaiyan, F., et al., *Selective effects of sodium chlorate treatment on the sulfation of heparan sulfate*. J Biol Chem, 1999. **274**(51): p. 36267-73.
47. Qiu, H., et al., *A mutant-cell library for systematic analysis of heparan sulfate structure-function relationships*. Nat Methods, 2018. **15**(11): p. 889-899.
48. Murray, M.J., et al., *Evasion of a Human Cytomegalovirus Entry Inhibitor with Potent Cysteine Reactivity Is Concomitant with the Utilization of a Heparan Sulfate Proteoglycan-Independent Route of Entry*. J Virol, 2020. **94**(7).
49. Cheng, T.P., et al., *Stability of Murine Cytomegalovirus Genome after In Vitro and In Vivo Passage*. Journal of Virology, 2010. **84**(5): p. 2623-2628.
50. Chong, K.T., J.J. Gould, and C.A. Mims, *Neutralization of Different Strains of Murine Cytomegalo-Virus (Mcmv)-Effect of Invitro Passage*. Archives of Virology, 1981. **69**(2): p. 95-104.
51. Daley-Bauer, L.P., et al., *Cytomegalovirus hijacks CX3CR1(hi) patrolling monocytes as immune-privileged vehicles for dissemination in mice*. Cell Host Microbe, 2014. **15**(3): p. 351-62.
52. Harvey, D.M. and A.J. Levine, *P53 Alteration Is a Common Event in the Spontaneous Immortalization of Primary Balb/C Murine Embryo Fibroblasts*. Genes & Development, 1991. **5**(12b): p. 2375-2385.
53. Esko, J.D., T.E. Stewart, and W.H. Taylor, *Animal-Cell Mutants Defective in Glycosaminoglycan Biosynthesis*. Proceedings of the National Academy of Sciences of the United States of America, 1985. **82**(10): p. 3197-3201.
54. Saederup, N., et al., *Murine cytomegalovirus CC chemokine homolog MCK-2 (m131-129) is a determinant of dissemination that increases inflammation at initial sites of infection*. Journal of Virology, 2001. **75**(20): p. 9966-9976.

**CHAPTER 5 - MCMV CENTRIFUGAL ENHANCEMENT: A NEW  
SPIN ON AN OLD TOPIC.**

A version of this chapter was initially published by: Trevor J. Hancock, Morgan Lynn Hetzel, Andrea Ramirez, and Tim E. Sparer

Hancock TJ, Hetzel ML, Ramirez A, Sparer TE. MCMV Centrifugal Enhancement: A New Spin on an Old Topic. *Pathogens*. 2021; 10(12):1577.

Author Contributions: Conceptualization, T.E.S. and T.J.H.; Methodology, T.J.H.; Formal analysis, T.J.H.; Investigation, T.J.H., M.L.H. and A.R.; Writing—original draft preparation, T.E.S. and T.J.H.; Writing—review and editing, T.E.S. and T.J.H.; Visualization, T.J.H.; Funding Acquisition, T.E.S.

### **Abstract:**

Human cytomegalovirus (HCMV) is a ubiquitous pathogen infecting a majority of people worldwide, with diseases ranging from mild to life-threatening. Its clinical relevance in immunocompromised people and congenital infections have made treatment and vaccine development a top priority. Because of cytomegaloviruses' species specificity, murine cytomegalovirus (MCMV) models have historically informed and advanced translational CMV therapies. Using the phenomenon of centrifugal enhancement, we explored differences between MCMVs derived *in vitro* and *in vivo*. We found centrifugal enhancement on tissue culture-derived virus (TCV) was  $\sim 3\times$  greater compared with salivary gland derived virus (SGV). Using novel “flow virometry,” we found that TCV contained a distinct submicron particle composition compared to SGV. Using an inhibitor of exosome production, we show these submicron particles are not extracellular vesicles that contribute to centrifugal enhancement. We examined how these differences in submicron particles potentially contribute to differing centrifugal enhancement phenotypes, as well as broader *in vivo* vs. *in vitro* MCMV differences.

### **Introduction:**

Human cytomegalovirus (HCMV) is a highly pervasive  $\beta$ -herpesvirus infecting approximately 40–90% of adults worldwide [1]. HCMV is spread through contact with

infected bodily secretions or vertically from infected mothers [1]. Once exposed, typical infection is asymptomatic causing mild disease after which CMV establishes a lifelong infection of their host [1, 2]. Primary infection or reactivation of HCMV in an immunocompromised individual (i.e., HIV/AIDS, cancer patients and organ transplant recipients) is associated with significant morbidity and mortality [3-6]. Additionally, in utero infections can be associated with significant neurological sequelae (i.e., sensorineural hearing loss, mental retardation, and microencephaly) [4, 6]. Due to the high prevalence and potential disease in vulnerable populations, identification and development of safe and effective treatments and vaccine targets for HCMV are a high priority.

An important characteristic of the  $\beta$ -herpesvirus family is the strict species-specificity of its members. Murine cytomegalovirus (MCMV) is commonly used as an *in vivo* model system for studying CMV pathogenesis and dissemination [7]. While MCMV and HCMV diverge genetically, disease characteristics and progression mirror each other, making it a valuable system for studying CMV *in vivo* [7]. Within the HCMV field, inter-strain differences between lab and clinical isolates have furthered the understanding of genetic changes upon serial passage *in vitro* [8]. For example, HCMV adaptation to cell culture leads to RL13 mutating immediately upon passage while others like UL128 mutate after a handful of passages [8, 9]. As such, there is a heightened focus on ensuring genomic integrity and minimizing passages of clinically derived viruses to generate more “*in vivo*-like” virus strains. While important in HCMV research, re-derivation of “clinical” strains of MCMV is relatively rare. Many labs still use derivatives of the initial Smith and K181 strains from 1954 and ~1980, respectively [10, 11]. Significant divergence may exist between commonly used research strains, even those preserved in bacterial artificial chromosomes and environmental isolates [12]. Despite the potential laboratory adaptation of MCMV, the mouse model of CMV allows for the comparison between *in vivo* vs. *in vitro* derived viruses, especially with the ability to easily generate large amounts of *in vivo* virus. These differences would be difficult to study in HCMV and direct clinical isolates.

Previously, differences between *in vivo* and *in vitro* CMVs have been documented. *In vivo* derived MCMVs are more virulent/lethal to neonates compared with viruses grown in tissue culture [13, 14]. Similarly, *in vivo* derived MCMV is more resistant to entry

inhibitors such as heparan sulfate proteoglycan (HSPG) binding peptides and is highly resistant to antibody neutralization. This parallels findings with HCMV where direct clinical isolates are resistant to HSPG-entry inhibitors [15, 16]. The viral source was also shown to impact their entry mechanism, modifying cell-surface carbohydrate attachment and cellular tropism [17, 18]. These differences may be related to *in vivo* and *in vitro* differences in the composition of their virus particle [19]. *In vivo* derived viruses are more homogenous in size, with cell-culture viruses having both individual virions and multicapsid clusters [19]. These differences in the source for MCMV can affect virulence. Salivary derived virus is attenuated in neonatal mice. However, immunosuppression with cyclophosphamide is capable of restoring virulence [14]. This may be due to reactivation of acute infection or a broadening of SG tropism. For example, immune depletion of CD4+ and CD8+ T cells results in salivary gland infection of both acinar epithelial cells and fibroblasts, potentially altering the virus composition/tropism [20]. Depending on where the virion obtains its membrane can also affect particle composition. MCMV that derives its envelope from the inner nuclear membrane consists of a single capsid per virion, whereas those that derive their envelope from cytoplasmic vacuoles can be either single or multi-capsid virions [21]. Additionally the infected cell type determines the production of single vs. multi-capsid virions. Infection of fibroblasts *in vitro* or lung fibroblasts *in vivo* results in the production of single and multicapsid viruses [21, 22], while salivary gland acinar cells (epithelial cells) produce single capsid virions *in vivo* pointing to different maturation processes [19]. How these differences in size and shape affect infection could indicate important limitations of *in vitro* models and hamper subsequent anti-CMV drug development.

In the late 1960s low speed (<2000× *g*) centrifugation was shown to significantly increase the effective titer of MCMV [23]. This spin enhancement was speculated to be due to a decrease in virus dissociation from the cell surface, thus leading to more efficient attachment to the cell [24]. Observations in other systems such as *Toxoplasma* and *Trachoma* showed that the increase in infectious titer was related to their size and the speed at which they were centrifuged [25, 26]. This enhancement of infection was termed “spinoculation” or “centrifugal enhancement”. With MCMV, centrifugal enhancement was

observed for both viruses derived *in vivo* and *in vitro* with similar levels of enhancement reported [23]. Both virus clusters and individual virions were infectious and enhanceable with centrifugation [19]. Enhancement occurs for multiple herpesviruses such as: HCMV, guinea pig CMV, KSHV, etc. and other non-herpesviruses as well (like HIV, hantavirus, etc.) and can occur on multiple cell types [27-31]. Interestingly this enhancement was absent in the similarly-sized alpha-herpesvirus, HSV [23]. For HSV and some other viruses, enhancement was eventually achieved using ultracentrifugation and speeds well in excess of those required for MCMV [29, 30, 32-35]. Because CMV infections are enhanced following slow speed centrifugation, this may point to entry differences observed for viruses derived *in vivo* and *in vitro*. In order to explore these differences, we carried out a series of experiments with *in vitro* and *in vivo* grown MCMVs to measure physical characteristics related to our observed entry differences.

Sedimentation of a particle during centrifugation is related to its size. Based on the ~150–200 nm size of CMV, we would anticipate much greater speeds for enhancement if it were due to sedimentation of the virus [19, 36]. One possible explanation of the differences between TCV and SGV stocks is the induction of extracellular vesicles (EVs). EVs are small membranous particles secreted by cells that are capable of transferring proteins and nucleic acids among neighboring cells [37]. Released under homeostatic conditions, EVs are divided into different categories based on their size/biogenesis ranging from small exosomes (<200 nm), microvesicles (~200–500 nm), and ectosomes ( $\geq$ 500 nm) [38, 39]. These intercellular shuttles represent an emerging area of research, with their roles in viral infections recently being explored [38, 40-43]. In CMV infections, EVs purified with HCMV were found to contain viral proteins on their surface and interior [37, 44, 45]. These EVs increase the spread rate of HCMV during focal expansion, potentially due to increased delivery of viral proteins [37]. For HSV, viral-EVs impact infection by enhancing plaque formation, delivery of viral proteins, or manipulation of host immune cells [42, 43, 46, 47]. The size, types, and contents of EVs varies based upon the secreting cell/tissue type [48, 49]. *In vitro* and *in vivo* tissue/cell types could differ following MCMV infection as well as their secreted EVs. We examined the submicron particle composition

of MCMVs from cell culture versus salivary gland and whether these particles could be responsible for the centrifugal enhancement that we observed.

### **Results:**

In an effort to better understand centrifugal enhancement, two lower speeds were used to measure enhancement, with significant enhancement of MCMV still occurring (Fig. 5.1A). An ~5-fold increase in plaque formation was observed following a 400× *g* spin and a >15-fold enhancement upon increasing to 800× *g* spin ( $p < 0.0001$ ) (Fig. 5.1A). Previous studies examined significantly higher centrifugation speeds (1000–2000× *g*'s) and found ~20–50 fold increases in plaque formation demonstrating a direct relationship between centrifugal force and spin enhancement [23]. To investigate the mechanism of centrifugal enhancement, cells were “pretreated” with centrifugation prior to infection. This pretreatment tests whether the act of centrifugation alters the cell’s susceptibility to infection. Enhancement only occurs when virus is present during the centrifugation step [24]. To measure whether adsorption time alters centrifugal enhancement, cells were preincubated with virus for differing times to allow for more adsorption prior to spin enhancement (Fig. 5.1B). Pre-incubation of virus for 10-min intervals up to 30 min prior to centrifugation did not impact enhancement, agreeing with previous findings (Fig. 5.1B) [24, 50]. Having established our experimental system, the impact of MCMV source was examined. We suspected potential differences based on our findings that tissue culture, salivary gland, and bone marrow derived macrophage-derived viruses (TCV, SGV, and BMDMV) have subtle differences in their entry process and susceptibility to peptide-based entry inhibitors [15]. Centrifugal enhancement of *in vitro*-derived viruses (i.e., TCV and BMDMV) had similar increases in infection following enhancement (~5-fold), whereas SGV had only a modest increase in plaque formation (~1.8-fold) ( $p < 0.0001$  and  $p < 0.05$ , respectively) (Fig. 5.1C). To ensure that the SGV prep did not mask the enhancement process, TCV was “spiked” into uninfected salivary glands and its impact on enhancement was assessed (Fig. 5.1D). Despite the addition of salivary gland homogenate to the TCV prep, centrifugal enhancement levels were similar to TCV alone and much greater than the 1.8-fold enhancement observed for SGV alone ( $p < 0.0001$ ). Interestingly, our lab has

previously found that BMDMV and TCV had different susceptibilities to anti-CMV peptides pointing to differences in HSPG-dependent entry, with BMDMV conferring an *in vivo*-like resistance, a phenotype shared by viruses derived from infected mouse salivary gland, spleen, and footpad [15]. If those entry differences correlated with centrifugal enhancement, we would have expected BMDMV to have the lower enhancement seen for SGV.

As TCV and SGV differed in their susceptibility to HSPG-binding entry inhibitors [15] and there are differences in centrifugal enhancement based on virus source (Fig. 5.1D), one possible explanation of centrifugal enhancement could be the entry process. MCMV entry into fibroblasts is dependent upon host surface HSPGs and occurs through fusion/macropinocytosis at the cell membrane [51, 52]. Using TCV due to its unrestricted tropism and large fold change following centrifugal enhancement, cells were treated with sodium chlorate, a chemical inhibitor of heparan sulfate sulfation and centrifugal enhancement measured. Entry was impacted as expected. However, the sodium chlorate treated group still showed an ~5-fold enhancement over their control wells although it was not statistically significant, probably due to the low level of virus infection (Fig. 5.2A). To further demonstrate the importance of HSPGs in the entry and centrifugal enhancement process, cells were pre-incubated with heparin sodium salt, a known blocker of HSPG entry (Fig. 5.2B). As expected, the treated groups had decreased infection but still showed enhancement following centrifugation ( $p < 0.0001$ ). Endocytosis of MCMV occurs in select cell types and is mediated *via* the viral protein MCK2 [53]. To rule out endocytosis as a mechanism contributing to centrifugal enhancement, ammonium chloride was administered to block the endocytic entry pathway of MCMV [27, 51]. Treatment with ammonium chloride did not impact infection in the control group and enhancement still occurred in the centrifuged group ( $p < 0.0001$ ) (Fig. 5.2C). Similarly, an MCK2-deficient strain of MCMV (RM461) [54], which would limit its endocytosis [53], was still enhanced with a low-speed centrifugation ( $p < 0.0001$ ) (Fig. 5.2D).

Without a difference in entry mechanisms to explain the differences in enhancement, size could be another possible explanation. Previous MCMV reports noted the presence of >200 nm “multicapsid clusters” containing multiple viral capsids inside a single membrane

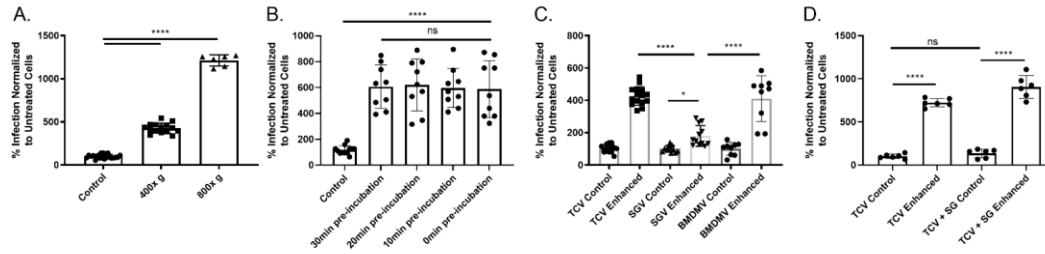


**Figure 5.1:** Centrifugal enhancement is predominantly an in vitro phenotype.

For all experiments, infection was normalized to a non-centrifuged control. (A) Speed determines the level of murine cytomegalovirus (MCMV) enhancement. MCMV adsorbed cells were spun at either 400× or 800× *g* ( $n \geq 3$ ). (B) Pre-incubation does not affect enhancement. Virus was incubated with cells for the indicated times prior, removed, and centrifuged ( $n = 3$ ). (C) Virus source determines enhancement. Virus derived from tissue culture (TCV), salivary gland (SGV), or bone marrow-derived macrophages (BMDMV) was centrifugally enhanced (400× *g*) ( $n \geq 3$ ). (D) Salivary gland homogenate does not impact enhancement. Homogenized salivary glands from uninfected mice were mixed with TCV and centrifugally enhanced or not ( $n = 2$ ). Mean and standard deviation shown for all graphs. For all experiments Tukey's one-way analysis of variance (ANOVA) with multiple comparisons was performed. Significance: \*  $p < 0.05$ , \*\*\*\*  $p < 0.0001$ , ns = not significant

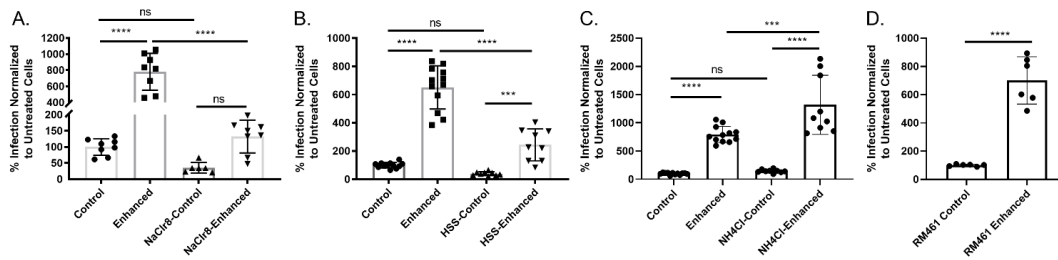


**Figure 5.2:** Centrifugal enhancement relies upon heparan sulfate proteoglycans and is MCK2/endocytosis independent.

For all experiments, MCMV was either added prior to centrifugation (enhanced) or post-centrifugation (control). (A) Enhancement still occurs when heparan sulfate proteoglycan (HSPGs) are reduced with sodium chlorate. Cells were treated overnight with sodium chlorate to reduce sulfation of HSPGs and viral entry (n = 3). (B) Enhancement still occurs despite heparin sodium salt (HSS) inhibition. Cells were treated with HSS prior to addition of virus (n = 3). (C) Endocytosis does not prevent entry or enhancement in fibroblasts. Cells were treated with ammonium chloride prior to infection (n = 3). (D) MCK2 deficient virus still undergoes enhancement. Cell-culture derived RM461 strain of MCMV was used to infect MEF 10.1 fibroblasts (n = 2). In all experiments infection is normalized to untreated, non-enhanced infection. Mean and standard deviation shown for all graphs. For A, B, C Tukey's one-way ANOVA with multiple comparisons was used. For D, a Student's one-tailed t-test was used for statistical analysis. Significance: \*\*\* = p < 0.001, \*\*\*\* = p < 0.0001, ns = not significant.

[19]. These larger particles sedimented with a different density than individual virions, but were similarly infectious [19]. To eliminate these larger clusters, TCV was filtered through a 0.2  $\mu\text{m}$  filter and centrifuged. Despite the absence of particles  $>200$  nm, centrifugal enhancement still occurred when normalized to the non-enhanced filtered control ( $p < 0.0001$ ) (Fig. 5.3). Because enhancement still occurs, the presence/differences in  $\leq 200$  nm particles between *in vitro* and *in vivo* derived viruses were measured.

To examine the heterogeneity of submicron MCMV particles between TCV and SGV, flow virometry was used to examine virus particle sizes. Thanks to recent advances in flow cytometry detectors and technology, minimum detectable particle size of violet side scatter equipped machines has dropped precipitously [55, 56]. Using a Cytex Northern Lights cytometer equipped with a violet (405 nm) laser with violet side scatter set as the trigger, particles as small as 100 nm can be discriminated from noise. Using those settings, particles were gated into 100 nm, 200 nm, and 500 nm approximate size groups (Fig. 5.4A). We utilized the nucleic acid stain acridine orange to stain TCV and SGV derived MCMV and analyzed each *via* flow cytometry (Fig. 5.4B). Due to the membrane-permeable nature of acridine orange, positive events could constitute enveloped virions, naked capsids, or nucleic acid containing EVs. Virus preparations were first treated with DNase/RNase to remove extracellular DNA/RNA and prevent false staining of damaged particles. In Figure 5.4B, TCV and SGV plots are shown at equivalent dilutions and titers. When the flow virometry graphs are overlaid, there is a notable difference in their particle size distributions (Fig. 5.4C). TCV has a broader distribution of particle sizes, whereas SGV is predominantly within the 200 nm gate (Fig. 5.4C,E). The event rate for equivalent titered TCV and SGV stocks ( $\sim 34,000$  and  $37,000$ , respectively) was not significantly different at the same dilution (Fig. 5.4D). Additionally, the events detected were significantly greater than the event rate of the FBS-containing media (Media Only  $\sim 500$ ) or uninfected media concentrated and resuspended as for TCV (Concentrated Media  $\sim 500$ ) (Fig. 5.4D). When plotted together in Figure 5.4E, the number of nucleic acid positive events illustrates the differences in sizes of these particles depending on their source. TCV has a nearly 50/50 distribution of particles in the 100 nm and 200 nm gates. Approximately 90% of the SGV stock is within the 200 nm gate with the remainder closely split between 100 nm and 500

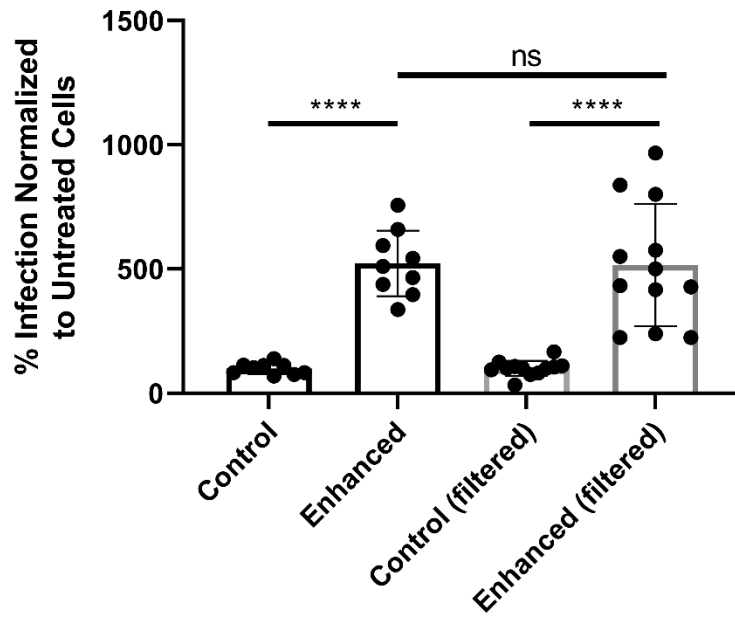


**Figure 5.3:** Enhancement is not due to >200 nm particles. 0.2  $\mu\text{m}$  filtration of MCMV does not prevent enhancement. TCV was filtered through a 0.2  $\mu\text{m}$  Millipore filter. Filtered stock was then centrifugally enhanced and normalized to control, non-centrifuged (but still filtered) virus ( $n \geq 3$ ). Mean and standard deviation are shown. One-way ANOVA was performed with multiple comparisons. Significance: \*\*\*\*  $p < 0.0001$ , ns = not significant.

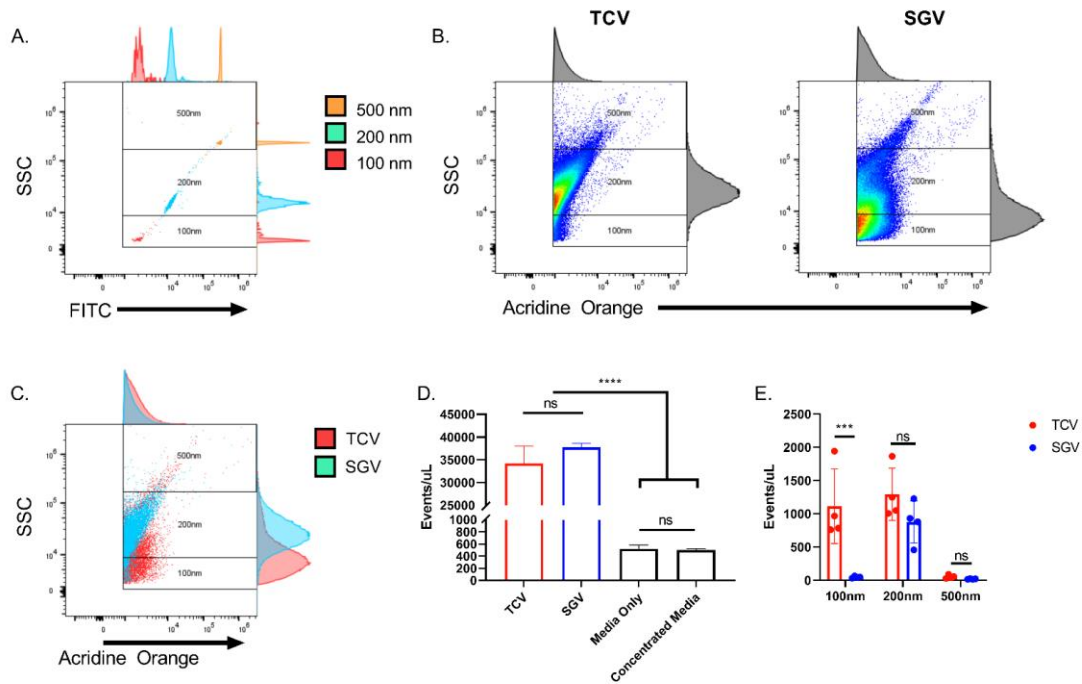


**Figure 5.4:** Flow virometry of MCMV identifies distinct TCV vs. SGV particle distributions. (A) Sub-micron particle reference standards and gates. 100 nm, 200 nm, and 500 nm beads were run separately and overlaid. (B) Flow virometry of tissue culture and salivary gland viruses. Viruses were stained with acridine orange. Nucleic acid positive events were graphed vs. side-scatter and gates corresponding to different sub-micron sizes overlaid. Representative data shown. (C) Overlay of TCV and SGV acridine orange-stained viruses. Nucleic acid positive populations in (B) were overlaid and distributions compared. For (A–C) histograms on top and right-hand side show location and distribution of each population. (D) Events per microliter of each sample type at equivalent dilutions/viral titers. (E) Distribution of nucleic acid-positive events. TCV and SGV nucleic acid positive events are graphed with separate colors representing percentage of events that coincided within each gate (100 nm, 200 nm, and 500 nm). For all,  $n \geq 2$  and mean  $\pm$  standard deviation are shown. For D, one-way ANOVA was performed with multiple comparisons. Two-way ANOVA was performed in (E), \*\*\*  $p < 0.001$ , \*\*\*\*  $p < 0.0001$ , ns = not significant.

nm (Fig. 5.4E). This size distribution of SGV matches electron microscopy observations from the early 1970s stating that SGV has a very homogenous composition [19]. Based on acridine orange staining, TCV and SGV only differ significantly in the 100 nm nucleic acid positive events ( $p < 0.001$ ) (Fig. 5.4E).

Differences in the production of EVs could explain the differences in particle sizes contained within the TCV and SGV stocks. HCMV infected cells alter their EV production, skewing particle size downwards and increasing their production [37], whereas MCMV's effect on EV production is unknown. To investigate submicron particle production *in vitro* and within excised salivary glands, TCV/SGV and supernatants from uninfected cells/tissue were stained with acridine orange and anti-CD63 antibody, which recognizes a Type III lysosomal protein found on EVs [38]. CD63 is also potentially found on HCMV virions due to a similar egress pathway as many EVs [45]. Based on this, CD63+/acridine orange (AO)+ events in  $\geq 200$  nm gates could represent either EVs or MCMV. In Figure 5.5A flow virometry plots show differences in similarly prepared stocks from infected and uninfected fibroblasts (TCV and conditioned media (CM), respectively). As expected, MCMV infection increased total submicron events/ $\mu\text{L}$   $\sim 3$ – $4$ -fold ( $p < 0.05$ ) (Fig. 5.5B). CM and TCV had similar numbers of CD63+ and CD63+/AO+ (Fig. 5.5C). Infection drastically increased the number of AO+ only events ( $\sim 20$ -fold) versus CM ( $p < 0.0001$ ) (Fig. 5.5C). Along with having similar numbers of events for CD63+ and CD63+/AO+ groups (Fig. 5.5C), the size of those particles was not significantly different between TCV and CM (Fig. 5.5D). There were trends of decreasing CD63+ and CD63+/AO+ event rates in infected cells, but they failed to reach significance despite CM showing  $\sim 2$ -fold greater events (Fig. 5.5C), driven by 100 nm and 200 nm sizes (Fig. 5.5D). Size distributions of AO+ events shown in Figure 5.5D demonstrate that TCV produced significantly more particles (both 100 nm and 200 nm sizes ( $p < 0.0001$ )) than uninfected cells. Most likely these are virus particles. For SGV, equivalent numbers of salivary glands from infected and uninfected mice (SGV and uninfected SG, respectively) were harvested and stained as in Figure 5.5 (Fig. 5.6A). Similar numbers of total submicron events were detected for both infected and uninfected salivary glands (Fig. 5.6B). Uninfected salivary gland tissue had

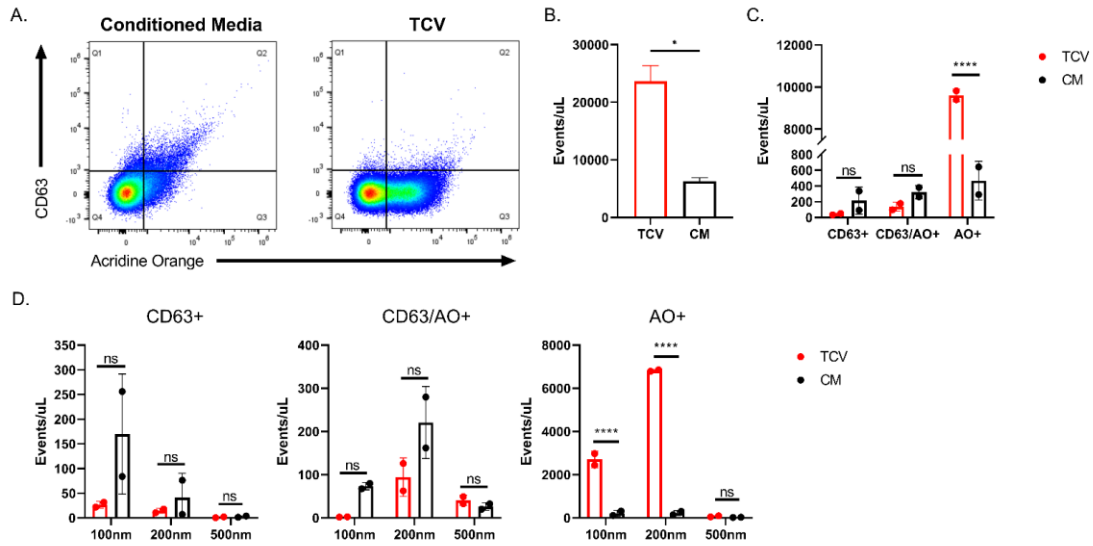


**Figure 5.5:** MCMV infection alters MEF 10.1-secreted extracellular vesicles (EVs).

(A) Comparison of CD63+ and AO+ positive events from uninfected (conditioned media) and infected cells (TCV). Representative FACS plots are shown. (B) Event rate of similarly produced conditioned media (CM) and TCV. (C) Quantification of events per microliter that were positive in each gate of (A). (D) Particle size comparison of single and double positive CD63+ and AO+ events for conditioned media and TCV. Representative plots shown. For all,  $n \geq 2$  and mean  $\pm$  standard deviation shown. Student's two-tailed t-test was performed for B. For C and D, two-way ANOVA was performed with multiple comparisons. \*  $p < 0.05$ , \*\*\*\*  $p < 0.0001$ , ns = not significant.

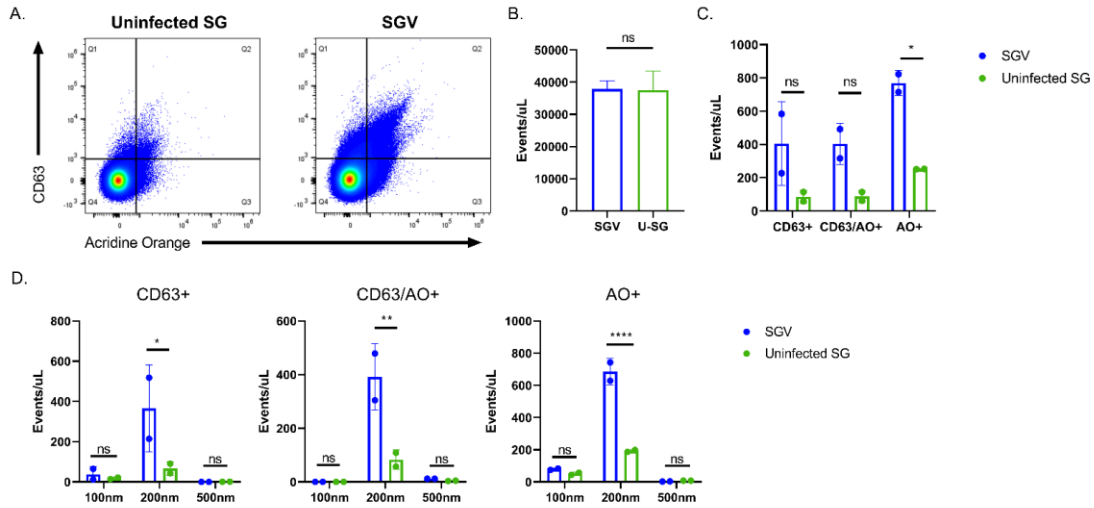


**Figure 5.6:** In vivo MCMV infection alters EV composition within the salivary gland.

(A) Comparison of CD63+ and AO+ positive events for salivary gland homogenate from uninfected (uninfected SG) and infected animals (SGV). Representative FACS plots are shown. (B) Event rate of similarly produced uninfected salivary glands (U-SG or Uninfected SG) and SGV. (C) Quantification of events per microliter that were positive in each gate of (A). (D) Particle size comparison of single and double positive CD63 and AO events for uninfected SG and SGV. Representative plots shown. For all,  $n \geq 2$  and mean  $\pm$  standard deviation shown. A Student's two-tailed  $t$ -test was performed for (B). For (C,D), two-way ANOVA was performed with multiple comparisons. \*  $p < 0.05$ , \*\*  $p < 0.01$ , \*\*\*\*  $p < 0.0001$ , ns = not significant.

noticeably fewer CD63+ or CD63+/AO+ events than infected salivary glands (~20% SGV events/ $\mu$ L), but only AO+ single positive events showed statistical significance ( $p < 0.05$ ) with ~3-fold increase when salivary glands were infected (Fig. 5.6C). The increased events in SGV were driven by 200 nm particles in every quadrant (Fig. 5.6D). There was no statistical difference between SGV and uninfected salivary glands positive events in the 100 nm and 500 nm sizes.

Nucleic acid positive events and size distributions differ between TCV and SGV (Fig. 5.4) and uninfected cells or SG tissue (Fig. 5.5 and 5.6). To directly compare CD63+ and AO+ positive events between TCV and SGV stocks, equivalent titer virus stocks were stained as in Figures 5.5 and 6.5 (Fig. 5.7A,B). For TCV, CD63 and AO rarely co-stain, with most events being positive for either CD63 or AO (~500 and 2200 events/ $\mu$ L, respectively) and few double positives (~90 events/ $\mu$ L) (Fig. 5.7A,C). This contrasts SGV where there was more equal distribution among positive events (~400 events/ $\mu$ L CD63+ and CD63+/AO+ and ~760 AO+) (Fig. 5.7A,C). TCV and SGV have similar levels of CD63+ events, but TCV has considerably more AO+ than SGV (~2200 vs. 760) ( $p < 0.0001$ ) (Fig. 5.7A,B). In comparing the sizes of these different events, CD63+ events in TCV are predominantly below 200 nm in size (>80%), with CD63/AO+ double positives split more equitably among all three submicron sizes and AO+ single positive events almost evenly divided between 100 nm and 200 nm (49% vs. 50%) (Fig. 5.7D). Because SGV has a highly homogenous particle size, CD63+ and CD63+/AO+ had >90% of events within the 200 nm size (Fig. 5.7D). Only the AO+ events had <90% (88%) of events in 200 nm with ~12% in the smaller 100 nm gate (Fig. 5.7D). These data point to the differences in particle sizes from SGV and TCV, with SGV generating a predominance of 200 nm particles and TCV often a balanced production of 100 nm and 200 nm particles.

Due to the potential presence of EVs in isolated viral stocks, we sought to examine the impact of small EVs (exosomes) on centrifugal enhancement. Using the sphingomyelinase inhibitor, GW4869, we treated infected and uninfected cells to characterize the resulting viruses following exosomal diminution. The results of GW4869 treatment on submicron particles concentrated from uninfected flasks is shown in Figure 5.8. Virus stocks treated



with vehicle (DMSO) or exosome inhibitor (GW4869) were stained and analyzed *via* flow virometry (Fig. 5.9A). Exosomal inhibition decreased total submicron particle event rate but failed to reach significance (Fig. 5.9B). Further, GW4869 treatment failed to significantly alter submicron particle composition (Fig. 5.9C) or the sizes of those particles (Fig. 5.9D). Exosome inhibition was demonstrated on uninfected flasks in Figure 5.8. Treatment did slightly decrease the amount of extracellular virus released by infected cells, but not significantly ( $p = 0.06$ ) (Fig. 5.9E). Also, despite inhibition of the exosome biogenesis pathway, the exosome-depleted virus still underwent enhancement to the same degree (~5-fold) as vehicle control and previous TCV stocks (Fig. 5.1A and 5.9F).

### Discussion

Our results further contribute to our understanding of *in vivo* and *in vitro* MCMV, as well as the phenomenon of centrifugal enhancement. Speeds  $<800\times g$  are still sufficient for enhancement to occur, and the centrifugal speed determines the degree of enhancement (Fig. 5.1A). However, there was one point of difference versus previous observations. The initial description of enhancement of MCMV found that virus source (i.e., SGV and TCV) did not impact centrifugal enhancement [23]. In contrast, we found that *in vivo* derived virus was not enhanced to the same degree as *in vitro* derived virus (Fig. 5.1C). This may be due to differences in the enhancement process as our centrifugation was performed at  $400\times g$  vs. their  $2000\times g$ . As our enhancement was performed at a slower speed, the fold change was significantly less (~50-fold vs. ~5-fold), and this may allow finer discrimination/differentiation of phenotypes between the two virus preparations. In support of our findings, the virulent strain of MCMV (K181), which was maintained by serial propagation through mouse salivary glands, was also reported to not enhance to the same degree as the cell-culture maintained Smith strain [28]. Several passages of K181 through cell culture were sufficient to reverse the phenotype and allow for centrifugal enhancement [28]. Our K181-derived viruses were differentially enhanced based upon passage *in vivo* or *in vitro*. This difference between virus sources was not due to a component within the salivary gland environment that directly inhibits enhancement as addition of uninfected

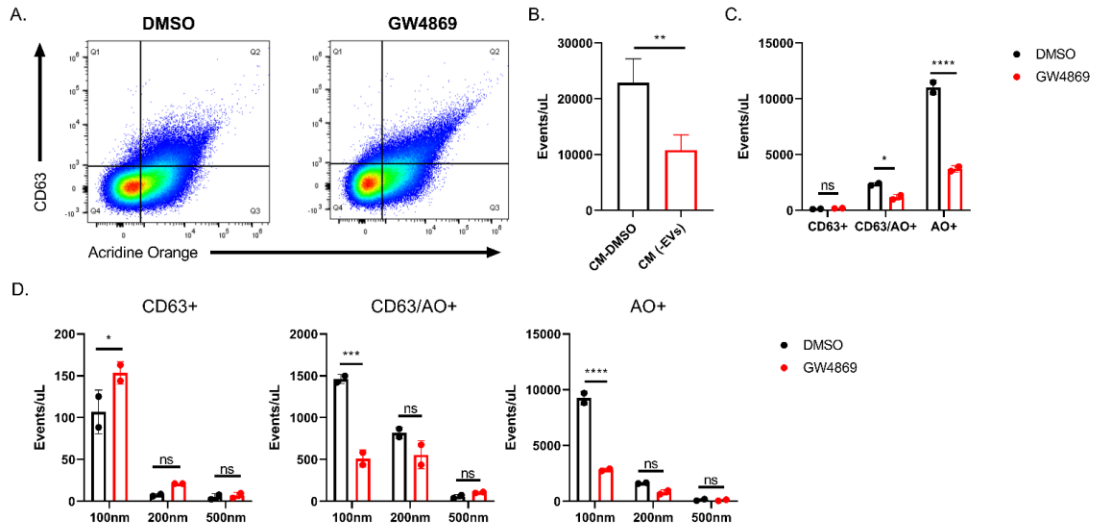


**Figure 5.8:** Exosome inhibition alters EVs produced by uninfected MEF 10.1 cells. (A) Comparison of CD63+ and AO+ events for conditioned media treated with EV inhibitor (GW4869) or vehicle control (DMSO). Representative FACS plots are shown. (B) Event rate of similarly produced conditioned media depleted of EVs (CM (-EVs)) or control (CM-DMSO). (C) Quantification of events per microliter that were positive in each gate of (A). (D) Particle size comparison of single and double positive CD63+ and AO+ events for treated and untreated conditioned media. Representative plots shown. For all,  $n \geq 2$  and mean  $\pm$  standard deviation shown. Student's two-tailed *t*-test was performed for (B). For (C,D), two-way ANOVA was performed with multiple comparisons. \*  $p < 0.05$ , \*\*  $p < 0.01$ , \*\*\*  $p < 0.001$ , \*\*\*\*  $p < 0.0001$ , ns = not significant.

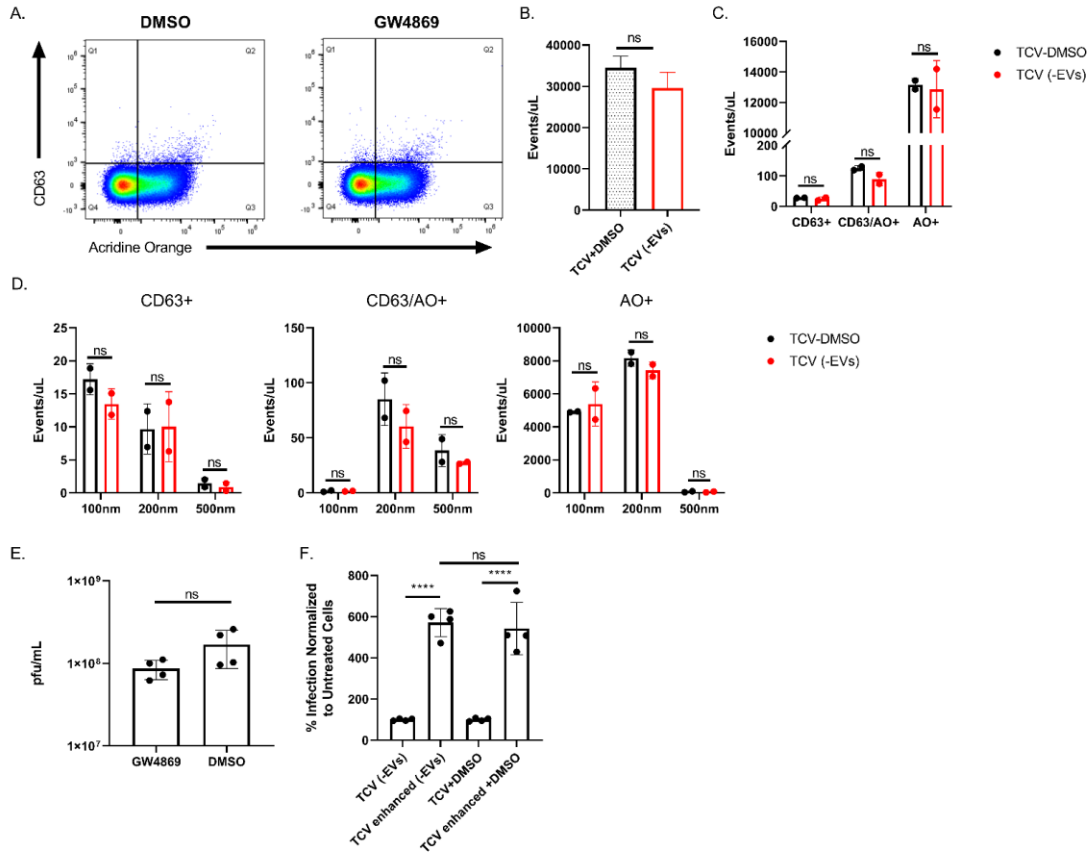


**Figure 5.9:** Exosome inhibition does not impact centrifugal enhancement.

(A) Flow virometry comparison of CD63<sup>+</sup> and AO<sup>+</sup> events of virus produced from GW4869 and DMSO treated cells. Representative FACS plots are shown. (B) Event rate of TCV produced when treated with exosome inhibitor GW4869 (TCV (-EVs)) or DMSO control (TCV-DMSO). (C) Quantification of events per microliter that were positive in each gate of (A). (D) Particle size comparison of single and double positive CD63<sup>+</sup> and AO<sup>+</sup> events for DMSO treated TCV (TCV-DMSO) or EV-depleted TCV (TCV (-EVs)). (E) Viral titer of MCMV produced when incubated with EV-inhibitor (GW4869) or vehicle control (DMSO). (F) Centrifugal enhancement of viruses produced with or without EV-inhibitor. Virus was enhanced by centrifugation at 400 $\times$  *g* and normalized to unenhanced, treated control. Representative plots shown. For all,  $n \geq 2$  and mean  $\pm$  standard deviation is shown. Student's two-tailed *t*-test was performed for (B,E). For (C,D), two-way ANOVA was performed with multiple comparisons. One-way ANOVA with multiple comparisons was performed for (F). \*\*\*\*  $p < 0.0001$ , ns = not significant.

salivary gland to TCV had no impact on unenhanced infection (i.e., control) or centrifugal enhancement groups (Figure 5.1D). We also found that the enhancement process occurs *via* the typical MCMV entry process as enhancement was impacted and unable to fully restore infection for sodium chlorate or heparin treated cells (Fig. 5.2A,B). Enhancement was unaffected by the blockade of the endocytosis pathway (either chemically or by deletion of MCK2) (Fig. 5.2C,D). This points to centrifugal enhancement utilizing the same entry process as typical infection (i.e., attachment to HSPGs), but with greater efficiency following a low-speed spin. This is in line with the increased adsorption mechanism hypothesized previously [23, 24], whereby application of a centrifugal field during the infection process increases the retention of virus on the surface and leads to increased plaque formation. One explanation of why SGV does not enhance to the same degree as TCV, could be due to its lowered dependence on HSPGs for entry [15]. However, we also demonstrated that *ex vivo* generated BMDMV has a similar lowered dependence on HSPGs as SGV [15], yet its enhancement was similar to TCV. Failure of this correlation between HSPG usage and centrifugal enhancement, points to potentially another mechanism at play.

Since the discovery of centrifugal enhancement, cellular tropism and viral/host factors involved in entry into different cell types have been reported [51, 53, 57]. Tropism for MCMVs is determined based on the presence/absence of viral glycoproteins responsible for entry. Complexes containing either gO or MCK2 are responsible for entry by fusion or endocytosis, respectively [51, 53]. These different entry processes allow for infection of fibroblasts *via* fusion and viral gO while viral MCK2 contributes to entry into epithelial/endothelial/monocytic cells *via* endocytosis [51, 53]. The infected cell type likely determines the relative abundance/composition of these entry complexes [58]. SGV displays some restrictions in tropism when compared to the equivalent TCV [17]. If the lack of SGV enhancement is due to a restriction in tropism or alteration of tropism, we would expect a comparably tropism-restricted cell culture-derived virus to have lowered enhancement (Fig. 5.1C). The less centrifugally enhanced SGV does not have tropism for macrophages/monocytes despite having an intact MCK2 [17]. Cell culture derived RM461 similarly does not have tropism for cell types requiring endocytosis, which includes

monocytes/macrophages, and still shows enhancement on par with fully tropic TCV (Fig. 5.2D) despite the loss of MCK2 [54, 59]. RM461's enhancement and SGV's lack of enhancement eliminates tropism differences as the mechanism for centrifugal enhancement. Similarly, the HCMV strain AD169, which lacks a functional pentameric complex responsible for entry into non-fibroblast cell types, is still enhanced on human fibroblast cell lines [25]. Taken together, centrifugal enhancement is not due to changes in tropism of CMV, as viruses with full or restricted tropism are still capable of enhancement. This points to another component of the virus as being responsible for enhancement.

MCMV derived from cell culture and salivary glands are reported to differ in their composition of particles [19]. Infectious TCV consists of individual virions (~200 nm), non-infectious naked capsids (~200 nm), and infectious "multicapsid clusters" ( $\geq 500$  nm) [19]. In contrast, the viral component of SGV is composed almost entirely of individual virions (~200 nm) [19]. We and others postulated that the larger clusters of viruses were responsible for the enhancement of TCV. Based on their size, they are more likely to be sedimented with slow speed centrifugation. Their entry into cells would also represent the delivery of multiple genomes in a single fusion event. However, when the multicapsid clusters are separated either by gradient [19] or filtration (Fig. 5.3), enhancement still occurs. Because enhancement still occurred even when filtered through a 0.2  $\mu\text{m}$  filter, particle sizes at 200 nm and below in TCV and SGV could be responsible for centrifugal enhancement.

The supernatant of infected (or uninfected cells) consists of a mixture of host-derived extracellular vesicles, many of which would easily pass through a 0.2  $\mu\text{m}$  filter. EVs are known to deliver protein and RNA between cells, with DNA transfer more recently described [60, 61]. Transfer of EVs between cells could serve to prime immune responses [62, 63], alter host physiology [64-66], transfer infectious genomes [67, 68], and reprogram host physiology to pro-viral states [47, 69, 70]. While still a burgeoning area of research, EVs from HCMV infected cells are known to package viral proteins intra-vesicularly and on their surface [44, 45], and exosomes isolated from infected cells increase the rate of viral spread [37]. Up to now studies on the presence, composition, and impact of EVs from MCMV infected cells have been lacking. We found that MCMV alters the submicron

composition of infected cells from tissue culture, increasing the number of submicron events (Fig. 5.5B), nucleic acid positive events (Fig. 5.5C,D), and globally decreasing CD63+ events (Fig. 5.5C,D) for TCV vs. conditioned media. The increasing event rate in TCV is driven significantly by increased nucleic acid positive events (in 100 nm and 200 nm gates) (Fig. 5.5C,D). For *in vivo* derived virus, there were no drastic differences in the types of particles secreted versus uninfected tissue homogenate, but infection globally increased the number of CD63+ and/or nucleic acid positive events (Fig. 5.6A,C). This increase was only significant for nucleic acid positive events, but 200 nm events were significantly elevated in each stain (Fig. 5.6C,D). With regard to TCV and SGV differences, nucleic acid single positive events in TCV greatly outnumber their SGV counterpart (Fig. 5.7C). Within the CD63+ and AO+ portions, the TCV stock contains more <200 nm particles, but SGV generates few of these particles (<10%) (Fig. 5.4 and 5.7). This lack of smaller particles could be due to the rapid absorption of small EVs *in vivo*, low production *in vivo*, an increased production of naked capsids in cell culture, or a result of the salivary gland isolation process. CD63+ single-positive events likely represent EVs (not naked capsids or infectious virus). The relative abundance of TCV EVs below 200 nm in size may represent the “enhanceable element” not present in SGV stocks (Fig. 5.7D). These EVs could increase the delivery of pro-viral products (i.e., host or viral protein, RNA, and/or DNA) to allow centrifugal enhancement. EVs utilize many of the same entry pathways as viruses, including fusion at cellular membranes and dependence upon HSPG-binding [38]. Centrifugation could be responsible for the increased retention of EVs on the cell surface much as was hypothesized for viral enhancement.

Pan or targeted inhibition of EVs is currently a technical challenge. Specific blockade of exosome release is possible and commonly performed using the drug GW4869 [37, 46, 71]. Exosomes have been implicated in the increased focal spread of HCMV, post-initial infection [37]. We provide evidence that an EV inhibitor (GW4869) does not significantly impact the generation of cell culture virus stocks (Fig. 5.9A–D). Virus produced with and without inhibitor is dominated by nucleic acid positive events (Fig. 5.9A,C). EV inhibition was performed at similar concentrations and timepoints as previously reported, and differences were observed in submicron particles of uninfected

cells following GW4869 treatment (Fig 5.8). We found a slight but non-significant decrease in viral titer (Fig. 5.9E), again matching a previous report [37]. Finally, EV-depletion failed to prevent centrifugal enhancement (Fig. 5.9F). Based on these results, we would discount the involvement of exosomes in the process of centrifugal enhancement. Unfortunately, we cannot rule out the contribution of other, larger EV types. Similarly, while CD63 is a prominent marker of EVs, understanding of the full EV complexity has yet to be resolved, and the contribution of other EV types may be significant.

We present further evidence for the distinction of *in vivo* and *in vitro* MCMVs. MCMV derived from infected salivary glands undergoes enhancement to a lesser degree than cell culture viruses. While this could be driven by differences in HSPG interactions, MCMVs resistant to HSPG-binding inhibitors still displayed enhancement [15]. Consequently, we sought to determine the differences in EVs and submicron composition of virus preparations and their impact on centrifugal enhancement. Following MCMV infection, the secretion of extracellular vesicles and submicron particles by host cells are altered. Despite these alterations and the presence of CD63+ submicron particles, exosomal inhibition had no noticeable impact on centrifugal enhancement. GW4869 treatment did slightly (but not significantly) lower the production of submicron particles and extracellular viral titer of infected cells. Thus, despite likely containing EVs of varying origins with potential pro-and anti-viral roles, the exosomes contained within MCMV viral stocks are not responsible for spin enhancement of CMV. Although we were not able to identify the factor responsible for enhancement, we were able to demonstrate further differences between MCMVs derived *in vivo* and *in vitro*. The host or viral factors contained within EVs represent an important puzzle piece for further dissecting differences between TCV and SGV viruses. Although EVs may not play a role in centrifugal enhancement, we have shown differences in their generation between *in vivo* vs. *in vitro* grown MCMVs. The translatability of tissue culture EVs to *in vivo* disease is an important question going forward, and one that the murine model of CMV is uniquely suited to address.

## Methods:

### *Cells and Viruses*

Low passage (<20) MEF 10.1 cells [72] were used to generate and titer viral stocks. Cells were maintained in Dulbecco's modified Eagle medium (DMEM) with 10% triple 0.1  $\mu\text{m}$  filtered Fetalclone III serum (Cytiva, Marlborough, MA, USA), and 1% penicillin/streptomycin and L-glutamine, each. Viral strains RM 4503, RM 461, and K181 were used for infections and plaque assays [54, 73]. Once 100% cytopathic effect was observed, viral supernatants were clarified by  $2\times 400\times g$  spins at 4 °C for 20 min. Virus was then pelleted by centrifugation at  $20,000\times g$  for 2 h at 4 °C. Viral pellets were resuspended in cell culture media and sonicated  $2\times$  at 20% amplitude for 30 s, aliquoted, and stored at  $-80$  °C until use. Generation of both salivary gland and bone marrow-derived macrophage virus stocks has been previously reported [15]. Briefly, salivary gland (SG) virus stocks were first homogenized in a dounce homogenizer before being centrifuged and sonicated as above. Bone marrow-derived macrophages (BMDM) were generated by plating bone marrow collected from mouse femurs in RPMI 1640 in non-treated sterile dishes. Non-adherent cells were removed 3 h later by aspiration. Cells were stimulated for 7 days in the presence of 10 ng/mL of M-CSF (Peprotech, Cranbury, NJ, USA).  $\sim 3.5$  days post-isolation cells were washed  $2\times$  with cold PBS and replaced with fresh media supplemented with M-CSF. Cells were  $>95\%$  pure as assessed by flow cytometry. BMDMs were infected with virus and once 100% CPE reached ( $\sim 14$  days post infection (dpi)), virus was isolated as described above for tissue culture virus. "Concentrated media" or "conditioned media" was obtained by centrifuging fresh cell culture media or spent media as above for tissue culture virus.

### *Animals*

BALB/cJ mice were obtained from Jackson Laboratory (Bar Harbor, ME, USA) and housed in specific-pathogen free environment at the University of Tennessee. For SG-derived viruses, mice were infected with  $\sim 1 \times 10^6$  PFU intraperitoneally (i.p.) and salivary

glands harvested 14 days post-infection. All procedures were reviewed and approved by the Institutional Animal Care and Use Committee at the University of Tennessee.

### ***Plaque Assays and Centrifugal Enhancement***

Plaque assays were performed in 12-well tissue culture treated plates. MEF 10.1 cells were seeded at  $\sim 1 \times 10^5$  cells per well and allowed to reach confluency overnight. Spent media was aspirated and viral inoculum was added to “enhanced” wells, and plates were centrifuged at 400–800 $\times$  *g* for 10 min at 4 °C. Virus was added to control/non-enhanced wells and plates placed in 37 °C CO incubator for 1 h. After 1 h, viral inoculums were removed and replaced with a carboxymethylcellulose (CMC) overlay. Plates were incubated for a further 5 days, fixed and stained with Coomassie blue, and plaques counted. Slight modifications were made for experiments involving entry inhibitors (i.e., sodium chlorate, ammonium chloride, and heparin sodium salts). Sodium chlorate was added at 50 mM, and incubated with cells overnight at 37 °C. Ammonium chloride was added at 50 mM, and incubated with cells for 2 h. Heparin sodium salt was added at 50  $\mu$ g/mL and incubated with cells for 30 min at 4 °C.

### ***Flow Virometry***

Virus preparations were diluted 1:10 in 0.2  $\mu$ m filtered ddH<sub>2</sub>O. Extracellular DNA and RNA was removed by addition of DNase/RNase (DNase I,  $\sim 10$  U/mL) (MilliporeSigma, Burlington, MA, USA) (RNase A, 100  $\mu$ g/mL) (Thermo Fisher Scientific, Waltham, MA, USA) and incubated at 37 °C for 30 min. Following DNase/RNase treatment, virus was fixed by mixing 1:1 with BioLegend fixation buffer (BioLegend, San Diego, CA, USA) (4% paraformaldehyde) and incubating at 4 °C for 10 min. After fixation, virus was stained with anti-EV antibodies (anti-CD63, PE-Cy7, NVG-2 clone) (BioLegend, San Diego, CA, USA) and/or nucleic acid stain acridine orange (1  $\mu$ g/mL). Stained and unstained virus was diluted 1:10 and serially diluted 1:2 generating 5–6 dilutions for flow cytometric analysis. In addition to unstained controls, antibody and dye only controls were generated at equivalent dilutions to samples to determine potential for dye/antibody aggregates and false positives. To analyze samples, a Cytex Northern

Light flow cytometer (Cytex Biosciences, Fremont, CA, USA) equipped with 488 and 405 nm lasers was used. Violet SSC was used to trigger the threshold. Sub-micron particle size reference beads were used to establish approximate size gates (Thermo Fisher Scientific, Waltham, MA, USA) with SSC vs. fluorescence. Sample event rate vs. dilution was used to determine linearity and minimize the possibility of “swarms.” Additional 1:2 dilutions were performed as necessary to reach event rate linearity. All flow analysis was performed in FlowJo ver. 10.8 (FlowJo, Becton, Dickinson and Company, Ashland, OR, USA).

### ***Exosome Inhibition***

Exosome inhibition was performed as in [37]. MEF 10.1 cells were grown to confluency in a T-175 flask. Two days before infection, cells were pre-treated with either GW4869 (8  $\mu$ m) (Tocris Biosciences, Bristol, UK) or DMSO (dimethylsulfoxide, vehicle control). Prior to infection, media was replaced, and cells were infected at ~0.1 MOI. Three hours after infection, GW4869 or DMSO was added back to the flasks at 2.5  $\mu$ m. GW4869 was replenished (2.5  $\mu$ m) every other day until 100% CPE was reached (6–7 dpi), at which point virus was harvested as above.

### ***Statistics***

Each experiment consisted of two or more independent experiments with 3 replicates per group, unless indicated otherwise. Individual data points are shown for all graphs, with mean and standard deviation error bars. Statistical significance was determined by one or two-way ANOVA with multiple comparisons or one-tailed Student’s *t*-test where appropriate. All graphs and statistical analyses were performed in GraphPad Prism ver. 9 (GraphPad Software, La Jolla, CA, USA). Significance: \* =  $p < 0.05$ , \*\* =  $p < 0.01$ , \*\*\* =  $p < 0.001$ , \*\*\*\* =  $p < 0.0001$ , ns = not significant.

## References

1. Liu, L., *Fields Virology, 6th Edition*. Clinical Infectious Diseases, 2014. **59**(4): p. 613-613.
2. Sinclair, J., *Human cytomegalovirus: Latency and reactivation in the myeloid lineage*. J Clin Virol, 2008. **41**(3): p. 180-5.
3. Cheung, T.W. and S.A. Teich, *Cytomegalovirus infection in patients with HIV infection*. Mt Sinai J Med, 1999. **66**(2): p. 113-24.
4. Demmler, G.J., *Congenital cytomegalovirus infection*. Semin Pediatr Neurol, 1994. **1**(1): p. 36-42.
5. Ramanan, P. and R.R. Razonable, *Cytomegalovirus infections in solid organ transplantation: a review*. Infect Chemother, 2013. **45**(3): p. 260-71.
6. Stagno, S., et al., *Congenital and perinatal cytomegalovirus infections: clinical characteristics and pathogenic factors*. Birth Defects Orig Artic Ser, 1984. **20**(1): p. 65-85.
7. Reddehase, M.J. and N.A.W. Lemmermann, *Mouse Model of Cytomegalovirus Disease and Immunotherapy in the Immunocompromised Host: Predictions for Medical Translation that Survived the "Test of Time"*. Viruses, 2018. **10**(12).
8. Wilkinson, G.W., et al., *Human cytomegalovirus: taking the strain*. Med Microbiol Immunol, 2015. **204**(3): p. 273-84.
9. Stanton, R.J., et al., *Reconstruction of the complete human cytomegalovirus genome in a BAC reveals RL13 to be a potent inhibitor of replication*. J Clin Invest, 2010. **120**(9): p. 3191-208.
10. Smith, M.G., *Propagation of salivary gland virus of the mouse in tissue cultures*. Proc Soc Exp Biol Med, 1954. **86**(3): p. 435-40.
11. Misra, V. and J.B. Hudson, *Minor base sequence differences between the genomes of two strains of murine cytomegalovirus differing in virulence*. Arch Virol, 1980. **64**(1): p. 1-8.
12. Smith, L.M., et al., *Laboratory strains of murine cytomegalovirus are genetically similar to but phenotypically distinct from wild strains of virus*. J Virol, 2008. **82**(13): p. 6689-96.

13. Osborn, J.E. and D.L. Walker, *Virulence and attenuation of murine cytomegalovirus*. *Infect Immun*, 1971. **3**(2): p. 228-36.
14. Selgrade, M.K., et al., *Effects of cell source, mouse strain, and immunosuppressive treatment on production of virulent and attenuated murine cytomegalovirus*. *Infect Immun*, 1981. **33**(3): p. 840-7.
15. Jackson, J.W., et al., *Anticytomegalovirus Peptides Point to New Insights for CMV Entry Mechanisms and the Limitations of In Vitro Screenings*. *mSphere*, 2019. **4**(1).
16. Chong, K.T., J.J. Gould, and C.A. Mims, *Neutralization of different strains of murine cytomegalovirus (MCMV)-effect of in vitro passage*. *Arch Virol*, 1981. **69**(2): p. 95-104.
17. Daley-Bauer, L.P., et al., *Cytomegalovirus hijacks CX3CR1(hi) patrolling monocytes as immune-privileged vehicles for dissemination in mice*. *Cell Host Microbe*, 2014. **15**(3): p. 351-62.
18. Ravindranath, R.M. and M.C. Graves, *Attenuated murine cytomegalovirus binds to N-acetylglucosamine, and shift to virulence may involve recognition of sialic acids*. *J Virol*, 1990. **64**(11): p. 5430-40.
19. Hudson, J.B., V. Misra, and T.R. Mosmann, *Properties of the multicapsid virions of murine cytomegalovirus*. *Virology*, 1976. **72**(1): p. 224-34.
20. Jonjic, S., et al., *Site-restricted persistent cytomegalovirus infection after selective long-term depletion of CD4+ T lymphocytes*. *J Exp Med*, 1989. **169**(4): p. 1199-212.
21. Weiland, F., et al., *Studies on the morphogenesis of murine cytomegalovirus*. *Intervirology*, 1986. **26**(4): p. 192-201.
22. Reddehase, M.J., et al., *Interstitial murine cytomegalovirus pneumonia after irradiation: characterization of cells that limit viral replication during established infection of the lungs*. *J Virol*, 1985. **55**(2): p. 264-73.
23. Osborn, J.E. and D.L. Walker, *Enhancement of infectivity of murine cytomegalovirus in vitro by centrifugal inoculation*. *J Virol*, 1968. **2**(9): p. 853-8.

24. Hodgkin, P.D., et al., *Murine cytomegalovirus binds reversibly to mouse embryo fibroblasts: implications for quantitation and explanation of centrifugal enhancement*. J Virol Methods, 1988. **22**(2-3): p. 215-30.
25. Chaparas, S.D. and R.W. Schlesinger, *Plaque assay of Toxoplasma on monolayers of chick embryo fibroblasts*. Proc Soc Exp Biol Med, 1959. **102**: p. 431-7.
26. Gordon, F.B., A.L. Quan, and R.W. Trimmer, *Morphologic observations on trachoma virus in cell cultures*. Science, 1960. **131**(3402): p. 733-4.
27. Ryckman, B.J., et al., *Human cytomegalovirus entry into epithelial and endothelial cells depends on genes ULI28 to ULI50 and occurs by endocytosis and low-pH fusion*. J Virol, 2006. **80**(2): p. 710-22.
28. Hudson, J.B., V. Misra, and T.R. Mosmann, *Cytomegalovirus infectivity: analysis of the phenomenon of centrifugal enhancement of infectivity*. Virology, 1976. **72**(1): p. 235-43.
29. Kariwa, H., et al., *Enhancement of infectivity of hantavirus in cell culture by centrifugation*. J Virol Methods, 1994. **49**(2): p. 235-44.
30. O'Doherty, U., W.J. Swiggard, and M.H. Malim, *Human immunodeficiency virus type 1 spinoculation enhances infection through virus binding*. J Virol, 2000. **74**(21): p. 10074-80.
31. Bodaghi, B., et al., *Entry of human cytomegalovirus into retinal pigment epithelial and endothelial cells by endocytosis*. Invest Ophthalmol Vis Sci, 1999. **40**(11): p. 2598-607.
32. Tenser, R.B., *Ultracentrifugal inoculation of herpes simplex virus*. Infect Immun, 1978. **21**(1): p. 281-5.
33. Tenser, R.B. and M.E. Dunstan, *Mechanisms of herpes simplex virus infectivity enhanced by ultracentrifugal inoculation*. Infect Immun, 1980. **30**(1): p. 193-7.
34. Hohdatsu, T., T. Tatekawa, and H. Koyama, *Enhancement of feline infectious peritonitis virus type I infection in cell cultures using low-speed centrifugation*. J Virol Methods, 1995. **51**(2-3): p. 357-62.

35. Yan, R., et al., *Spinoculation Enhances HBV Infection in NTCP-Reconstituted Hepatocytes*. PLoS One, 2015. **10**(6): p. e0129889.
36. Wright, H.T., Jr., C.R. Goodheart, and A. Lielausis, *Human Cytomegalovirus. Morphology by Negative Staining*. Virology, 1964. **23**: p. 419-24.
37. Streck, N.T., et al., *Human Cytomegalovirus Utilizes Extracellular Vesicles To Enhance Virus Spread*. J Virol, 2020. **94**(16).
38. Raab-Traub, N. and D.P. Dittmer, *Viral effects on the content and function of extracellular vesicles*. Nat Rev Microbiol, 2017. **15**(9): p. 559-572.
39. Urbanelli, L., et al., *The Role of Extracellular Vesicles in Viral Infection and Transmission*. Vaccines (Basel), 2019. **7**(3).
40. Meckes, D.G., Jr. and N. Raab-Traub, *Microvesicles and viral infection*. J Virol, 2011. **85**(24): p. 12844-54.
41. Meckes, D.G., Jr., *Exosomal communication goes viral*. J Virol, 2015. **89**(10): p. 5200-3.
42. Bello-Morales, R., et al., *Role of Microvesicles in the Spread of Herpes Simplex Virus 1 in Oligodendrocytic Cells*. J Virol, 2018. **92**(10).
43. Bello-Morales, R. and J.A. Lopez-Guerrero, *Extracellular Vesicles in Herpes Viral Spread and Immune Evasion*. Front Microbiol, 2018. **9**: p. 2572.
44. Zicari, S., et al., *Human cytomegalovirus-infected cells release extracellular vesicles that carry viral surface proteins*. Virology, 2018. **524**: p. 97-105.
45. Turner, D.L., et al., *The host exosome pathway underpins biogenesis of the human cytomegalovirus virion*. Elife, 2020. **9**.
46. Deschamps, T. and M. Kalamvoki, *Extracellular Vesicles Released by Herpes Simplex Virus 1-Infected Cells Block Virus Replication in Recipient Cells in a STING-Dependent Manner*. J Virol, 2018. **92**(18).
47. Dargan, D.J. and J.H. Subak-Sharpe, *The effect of herpes simplex virus type 1 L-particles on virus entry, replication, and the infectivity of naked herpesvirus DNA*. Virology, 1997. **239**(2): p. 378-88.

48. Cai, J., et al., *Extracellular vesicles derived from different sources of mesenchymal stem cells: therapeutic effects and translational potential*. Cell Biosci, 2020. **10**: p. 69.
49. Yeung, C.C., et al., *Proteomics identifies differences in fibrotic potential of extracellular vesicles from human tendon and muscle fibroblasts*. Cell Commun Signal, 2020. **18**(1): p. 177.
50. Hudson, J.B., *Further studies on the mechanism of centrifugal enhancement of cytomegalovirus infectivity*. J Virol Methods, 1988. **19**(2): p. 97-108.
51. Scrivano, L., et al., *The m74 gene product of murine cytomegalovirus (MCMV) is a functional homolog of human CMV gO and determines the entry pathway of MCMV*. J Virol, 2010. **84**(9): p. 4469-80.
52. Hetzenecker, S., A. Helenius, and M.A. Krzyzaniak, *HCMV Induces Macropinocytosis for Host Cell Entry in Fibroblasts*. Traffic, 2016. **17**(4): p. 351-68.
53. Wagner, F.M., et al., *The viral chemokine MCK-2 of murine cytomegalovirus promotes infection as part of a gH/gL/MCK-2 complex*. PLoS Pathog, 2013. **9**(7): p. e1003493.
54. Noda, S., et al., *Cytomegalovirus MCK-2 controls mobilization and recruitment of myeloid progenitor cells to facilitate dissemination*. Blood, 2006. **107**(1): p. 30-8.
55. Lippe, R., *Flow Virometry: a Powerful Tool To Functionally Characterize Viruses*. J Virol, 2018. **92**(3).
56. Ricci, G., et al., *Flow virometry for process monitoring of live virus vaccines- lessons learned from ERVEBO*. Sci Rep, 2021. **11**(1): p. 7432.
57. Compton, T., D.M. Nowlin, and N.R. Cooper, *Initiation of human cytomegalovirus infection requires initial interaction with cell surface heparan sulfate*. Virology, 1993. **193**(2): p. 834-41.
58. Scrivano, L., et al., *HCMV spread and cell tropism are determined by distinct virus populations*. PLoS Pathog, 2011. **7**(1): p. e1001256.
59. Stoddart, C.A., et al., *Peripheral blood mononuclear phagocytes mediate dissemination of murine cytomegalovirus*. J Virol, 1994. **68**(10): p. 6243-53.

60. Malkin, E.Z. and S.V. Bratman, *Bioactive DNA from extracellular vesicles and particles*. Cell Death Dis, 2020. **11**(7): p. 584.
61. O'Brien, K., et al., *RNA delivery by extracellular vesicles in mammalian cells and its applications*. Nat Rev Mol Cell Biol, 2020. **21**(10): p. 585-606.
62. Torralba, D., et al., *Priming of dendritic cells by DNA-containing extracellular vesicles from activated T cells through antigen-driven contacts*. Nat Commun, 2018. **9**(1): p. 2658.
63. Kitai, Y., et al., *DNA-Containing Exosomes Derived from Cancer Cells Treated with Topotecan Activate a STING-Dependent Pathway and Reinforce Antitumor Immunity*. J Immunol, 2017. **198**(4): p. 1649-1659.
64. Skog, J., et al., *Glioblastoma microvesicles transport RNA and proteins that promote tumour growth and provide diagnostic biomarkers*. Nat Cell Biol, 2008. **10**(12): p. 1470-6.
65. Lian, Q., et al., *Chemotherapy-induced intestinal inflammatory responses are mediated by exosome secretion of double-strand DNA via AIM2 inflammasome activation*. Cell Res, 2017. **27**(6): p. 784-800.
66. Danielson, K.M., et al., *Plasma Circulating Extracellular RNAs in Left Ventricular Remodeling Post-Myocardial Infarction*. EBioMedicine, 2018. **32**: p. 172-181.
67. Feng, Z., et al., *A pathogenic picornavirus acquires an envelope by hijacking cellular membranes*. Nature, 2013. **496**(7445): p. 367-71.
68. Ramakrishnaiah, V., et al., *Exosome-mediated transmission of hepatitis C virus between human hepatoma Huh7.5 cells*. Proc Natl Acad Sci U S A, 2013. **110**(32): p. 13109-13.
69. McLauchlan, J., et al., *Noninfectious L-particles supply functions which can facilitate infection by HSV-1*. Virology, 1992. **190**(2): p. 682-8.
70. Heilingloh, C.S., et al., *L Particles Transmit Viral Proteins from Herpes Simplex Virus 1-Infected Mature Dendritic Cells to Uninfected Bystander Cells, Inducing CD83 Downmodulation*. J Virol, 2015. **89**(21): p. 11046-55.

71. Kosaka, N., et al., *Secretory mechanisms and intercellular transfer of microRNAs in living cells*. J Biol Chem, 2010. **285**(23): p. 17442-52.
72. Harvey, D.M. and A.J. Levine, *p53 alteration is a common event in the spontaneous immortalization of primary BALB/c murine embryo fibroblasts*. Genes Dev, 1991. **5**(12B): p. 2375-85.
73. Saederup, N., et al., *Murine cytomegalovirus CC chemokine homolog MCK-2 (m131-129) is a determinant of dissemination that increases inflammation at initial sites of infection*. J Virol, 2001. **75**(20): p. 9966-76.

**CHAPTER 6 - CONCLUSIONS AND RECOMMENDATIONS**

## Conclusions

### *Chapter 2*

Using a broad immunophenotyping panel, we determined that a myriad of immune cell types in mice and humans express CXCR2. This work highlights additional cell types that are CXCR2<sup>+</sup> and for the first time looks at their relative levels in relationship to each other. For mice, CXCR2 expression varies by tissue, with some cell types having higher CXCR2 levels both in percentages of CXCR2<sup>+</sup> cells and surface expression levels in one tissue versus another. CXCR2 also is more broadly distributed in mice. This may be due to differences in chemokine biology between mice and humans [1], but human CXCR2 expression in peripheral blood is dominated by neutrophils. Murine neutrophils abundantly express CXCR2, but they are a smaller proportion of mature circulating cells than in human blood and express CXCR2 at relatively similar levels as other positive cell types. In contrast, human neutrophils dominate the CXCR2<sup>+</sup> cell types and express the receptor at a high level. Along with the distribution of CXCR2 expression *in vivo* for mice and humans, we identified species differences as a potential point of complication when utilizing murine models involving CXCR2. What impact this has upon clinical translation of CXCR2 driven mouse models is unclear.

### *Chapter 3*

The viral chemokine vCXCL-1 is a polymorphic protein recently shown to enhance virulence *in vivo* [2]. We performed further *in vivo*, *in vitro*, and *in silico* analysis of vCXCL-1 isoforms to identify differences in function. *In vivo* pilot studies failed to yield significance but trended towards differences in inflammation and virulence between viruses expressing high and low stimulatory viral chemokines. We identified a unique region in the C-terminus of vCXCL-1 isoforms that alters GAG-binding potentially impacting its function *in vivo*. *In silico* analysis of vCXCL-1 models provided insight into potential receptor binding, informing future experiments. The consequences of vCXCL-1 biased agonism *in vivo*, as well as how the extended C-terminus of vCXCL-1 affects activity *in vitro* and *in vivo* is yet to be determined.

## **Chapter 4 & 5**

Viral entry of CMV represents an attractive target for the development of novel antivirals. *In vitro* and *in vivo* derived MCMVs display different entry phenotypes with *in vivo* derived viruses resistant to inhibitors [3]. We examined the dependence of TCV (*in vitro*) and SGV (*in vivo*) viruses on heparan sulfate proteoglycans (HSPGs) for entry. SGV appears to be less reliant upon HSPGs for entry than TCV. This makes targeting HSPGs problematic. Despite their effectiveness *in vitro*, *in vivo* virus is less dependent on the traditional entry mechanism. SGV's decreased HSPG affinity was supported by the lack of centrifugal enhancement of SGV. This mechanism increases virus retention on the cell surface, thus increasing infectivity. We additionally explored the differences between TCV and SGV viruses and identified differences in particle composition between the two. The submicron particles in each virus preparation were initially suspected to represent different extracellular vesicles (EVs). However, inhibition of EV production failed to impact the enhancement of TCV eliminating EVs as the mechanism driving centrifugal enhancement. Altogether, we characterized the differences in HSPG-utilization between *in vivo* and *in vitro* derived viruses, as well as the submicron particles in the viral preparations. This can potentially inform the design of entry inhibitors targeted towards HSPGs involved in both TCV and SGV infection. While EVs are not responsible for the phenomenon of centrifugal enhancement, they do appear to represent an additional area of difference between *in vivo* and *in vitro* viruses with functions and contributions *in vivo* uncharacterized.

### **Future Directions**

#### ***CXCR2 Expression***

We generated a profile of CXCR2 expression in naïve, resting murine and human leukocytes. However, we have not investigated the impacts of inflammation on CXCR2 expression in these systems and across tissues. While neutrophils are the predominant CXCR2-expressing cell type, the presence of additional CXCR2<sup>+</sup> cells raises the question of their contribution to CXCR2-driven immune responses. Additionally, murine B cells were identified as a prominent source of CXCR2<sup>+</sup> cells *in vivo*, but their functional role is

unclear. Future work needs to be done to further subdivide B cells into major divisions such as naïve B cells, plasma cells, follicular B cells, marginal zone B cells, and determine if CXCR2 is restricted to certain subtypes and what role it plays in B cell responses. There appears to be species-specific differences in CXCR2 distribution and relative expression between human and mouse peripheral blood. This is potentially due to the lack of a true hCXCR1 homolog [4]. Whether CXCR2 plays the same role in mice and humans and is a good homolog for human CXCR2 *in vivo* remains to be seen.

### ***vCXCL-1's Role in CMV Infection***

Functional selectivity is not a foreign concept for chemokines and chemokine receptors [5]. As such, that the slight structural differences between viral vCXCL-1s induce differential activation was perhaps unsurprising [6]. While we present preliminary evidence for differences in vCXCL1 virulence *in vivo*, further experiments are needed to determine the mechanism by which lethality is caused in immunocompromised animals. vCXCL-1 isoforms differentially induce chemotaxis *in vitro* [6], but how that translates to *in vivo* immune cell recruitment is unknown. Intranasal chemokine administration to measure *in vivo* chemotaxis has been performed in other systems [7], and may provide a non-infectious model to study *in vivo* differences in immune cell recruitment among vCXCL-1 isoforms. Along with the levels of chemotaxis induced by the different isoforms of vCXCL-1, further information is needed on the dominant immune cell types recruited *in vivo*. Based on CXCR2 expression, we would expect large numbers of neutrophils, but whether other CXCR2<sup>+</sup> cell types respond is unknown. Further work is needed to investigate the functional consequences of vCXCL-1 stimulation. vCXCL-1 signaling could play a role in CXCR2<sup>+</sup> cells (i.e., neutrophils or other cell types) to produce a pro-viral environment by limiting MHC levels and antigen presentation, T cell proliferation, generation of anti-CMV T and B cell responses, and inhibiting antiviral functions of effector cells such as CXCR2<sup>+</sup> NK and NKT cells. Future work should focus on levels of CMV-specific T cells and anti-CMV serum following infection in murine models of vCXCL-1. This will allow a broad determination of vCXCL-1's adaptive immune response modulation. Additionally, *in vitro* stimulation of CXCR2<sup>+</sup> cells can provide insight into the

functional impacts on purified cell populations, allowing measurements of things such as: secondary chemokine release, impairment of antiviral effector functions, and antigen presentation.

### ***vCXCL-1 C-terminus function and CXCR2 interaction***

The extended C-terminus of vCXCL-1 represents a conserved motif with potential impacts on glycosaminoglycan (GAG) binding. Impairment of GAG binding may represent a viral strategy to control receptor stimulation. *In vivo*, GAG-binding association (and dissociation) are vital for proper chemokine function [8, 9]. As such, *in vitro* assays may not accurately reflect *in vivo* activity. Truncations of vCXCL-1 should be performed to assess the impact of the C-terminus on GAG-binding, *in vitro* activation, and *in vivo* recruitment of immune cells. Furthermore, *in silico* analysis predicted altered CXCR2-vCXCL-1 interactions. Predictive models should be followed up by crystal structures of both vCXCL-1 alone and vCXCL-1 bound to CXCR2. Along with confirming predicted structures, crystal structures will allow for better understanding of interactions and rational design of vCXCL-1 inhibitors. Until then, small molecule library screens for vCXCL-1/CXCR2 inhibitors may prove fruitful for finding potential therapeutics to limit CMV disease in animal models.

### ***Viral Entry of TCV and SGV***

Viral entry is an attractive target for development of novel therapeutics. Currently, licensed anti-CMV therapeutics center around viral replication and packaging [10]. CMV transmission to new cells and propagation of infection occurs via initial interactions with the aid of HS [11]. Previous work with HS-blocking peptides decreased initial infection *in vivo* [12], but failed to provide protection at later time points [3]. We demonstrated differences in HS utilization between viruses derived in cell culture or *in vivo* salivary glands. Using CRISPR-Cas9 to target genes for key HS-generation enzymes, we found that cell culture virus and salivary gland virus were equally impacted by the loss of some HS genes, with salivary gland virus less reliant on HS for infection overall. However, we have yet to fully characterize the HS mutant cell lines to confirm depletion or diminution of our

suspected sulfations. The HS levels and modifications on these HSPG mutants should be characterized using mass spectrometry. Fine scale differences in HS usage may also exist. Utilizing synthetic HS of defined length and sulfation, a virus binding ELISA can possibly identify differences in HS binding based on viral source. Knowledge of HS-binding moieties will allow for better design of targeting molecules, minimizing host toxicity and conferring protection *in vivo*.

## References

1. Miyake, K. and H. Karasuyama, *The Role of Trogocytosis in the Modulation of Immune Cell Functions*. *Cells*, 2021. **10**(5).
2. Jackson, J.W., et al., *The Human Cytomegalovirus Chemokine vCXCL-1 Modulates Normal Dissemination Kinetics of Murine Cytomegalovirus In Vivo*. *MBio*, 2019. **10**(3).
3. Jackson, J.W., et al., *Anticytomegalovirus Peptides Point to New Insights for CMV Entry Mechanisms and the Limitations of In Vitro Screenings*. *mSphere*, 2019. **4**(1).
4. Mestas, J. and C.C. Hughes, *Of mice and not men: differences between mouse and human immunology*. *J Immunol*, 2004. **172**(5): p. 2731-8.
5. Jorgensen, A.S., et al., *Biased Signaling of CCL21 and CCL19 Does Not Rely on N-Terminal Differences, but Markedly on the Chemokine Core Domains and Extracellular Loop 2 of CCR7*. *Front Immunol*, 2019. **10**: p. 2156.
6. Heo, J., et al., *Novel Human Cytomegalovirus Viral Chemokines, vCXCL-1s, Display Functional Selectivity for Neutrophil Signaling and Function*. *J Immunol*, 2015. **195**(1): p. 227-36.
7. Das, S.T., et al., *Monomeric and dimeric CXCL8 are both essential for in vivo neutrophil recruitment*. *PLoS One*, 2010. **5**(7): p. e11754.
8. Gangavarapu, P., et al., *The monomer-dimer equilibrium and glycosaminoglycan interactions of chemokine CXCL8 regulate tissue-specific neutrophil recruitment*. *J Leukoc Biol*, 2012. **91**(2): p. 259-65.
9. Joseph, P.R.B., K.V. Sawant, and K. Rajarathnam, *Heparin-bound chemokine CXCL8 monomer and dimer are impaired for CXCR1 and CXCR2 activation: implications for gradients and neutrophil trafficking*. *Open Biol*, 2017. **7**(11).
10. Chen, S.J., S.C. Wang, and Y.C. Chen, *Antiviral Agents as Therapeutic Strategies Against Cytomegalovirus Infections*. *Viruses*, 2019. **12**(1).
11. Compton, T., D.M. Nowlin, and N.R. Cooper, *Initiation of Human Cytomegalovirus-Infection Requires Initial Interaction with Cell-Surface Heparan-Sulfate*. *Virology*, 1993. **193**(2): p. 834-841.

12. Pitt, E.A., et al., *The D-form of a novel heparan binding peptide decreases cytomegalovirus infection in vivo and in vitro*. Antiviral Research, 2016. **135**: p. 15-23.

**APPENDIX - POSSIBLE CROSS REACTIVITY OF FELINE AND WHITE-  
TAILED DEER SAMPLES TOWARDS THE RBD OF SARS-COV-2**

This work was performed by: Trevor J. Hancock<sup>1</sup>, Peyton Hickman<sup>1</sup>, Niloo Kazerooni<sup>2</sup>, Melissa Kennedy<sup>2</sup>, Stephen A. Kania<sup>2</sup>, Michelle Dennis<sup>2</sup>, Nicole Szafranski<sup>2</sup>, Richard Gerhold<sup>2</sup>, Chunlei Su<sup>1</sup>, Tom Masi<sup>3</sup>, Stephen Smith<sup>4</sup>, Tim E. Sparer<sup>1\*</sup>

<sup>1</sup> Department of Microbiology, University of Tennessee, Knoxville, Tennessee, USA

<sup>2</sup> Department of Biomedical and Diagnostic Sciences, University of Tennessee, Knoxville, Tennessee, USA

<sup>3</sup> Graduate School of Medicine, University of Tennessee Medical Center, Knoxville, Tennessee, USA

<sup>4</sup> MEDIC Regional Blood Center, Knoxville, Tennessee, USA

Author Contributions: Conceptualization, T.E.S. and T.J.H.; Methodology, T.J.H.; Formal analysis, T.J.H.; Investigation, T.J.H., P.H., N.K., M.K., and T.M.; Resources, N.K., M.K., S.A.K., M.D., N.S., R.G., C.S., and S.S.; Writing—original draft preparation, T.E.S. and T.J.H.; Writing—review and editing, T.E.S. and T.J.H.; Visualization, T.J.H.; Funding Acquisition, T.E.S. and T.J.H.

### **Abstract**

In late 2019, a novel coronavirus began circulating within humans in central China. It was designated SARS-CoV-2 because of its genetic similarities to the 2003 SARS coronavirus (SARS-CoV). Now that SARS-CoV-2 has spread worldwide, there is a risk of it establishing new animal reservoirs and recombination with native circulating coronaviruses. To screen local animal populations in the United States for exposure to SARS-like coronaviruses, we developed a serological assay using the receptor binding domain (RBD) from SARS-CoV-2. SARS-CoV-2's RBD is antigenically distinct from common human and animal coronaviruses allowing us to identify animals previously infected with SARS-CoV or SARS-CoV-2. Using an indirect ELISA for SARS-CoV-2's RBD, we screened serum from wild and domestic animals for the presence of antibodies against SARS-CoV-2's RBD. Surprisingly pre-pandemic feline serum samples submitted to the University of Tennessee Veterinary Hospital were ~50% positive for anti-SARS RBD antibodies. Some of these samples were serologically negative for feline coronavirus

(FCoV), raising the question of the etiological agent generating anti-SARS-CoV-2 RBD cross-reactivity. We also identified several white-tailed deer from South Carolina with anti-SARS-CoV-2 antibodies. These results are intriguing as cross-reactive antibodies towards SARS-CoV-2 RBD have not been reported to date. The etiological agent responsible for seropositivity was not readily apparent, but finding seropositive cats prior to the current SARS-CoV-2 pandemic highlights our lack of information about circulating coronaviruses in other species.

### **Importance**

We report on the existence of cross-reactive antibodies from pre-pandemic cats and post-pandemic South Carolina white-tailed deer that are specific for SARS-CoV receptor binding domain. Cross-reactive antibodies against SARS-CoV-2's RBD independent of infection has not been shown previously. There are several potential causes for this cross-reactivity, each with important implications to coronavirus disease surveillance. Perhaps the most intriguing possibility is the existence and transmission of an etiological agent (such as another coronavirus) with similarity to SARS-CoV-2's RBD region. However, conclusive pre-pandemic transmission of a SARS-like virus is still lacking. This does provide additional impetus for adoption of a One Health Initiative style goal of infectious disease surveillance of multiple animal species to predict the next zoonotic transmission to humans.

### **Introduction**

Severe acute respiratory syndrome coronavirus 2 (SARS-CoV-2) is an emergent zoonotic beta-coronavirus initially identified in late 2019 after human-to-human transmission within central China [1]. By early 2020, the virus had caused a pandemic infecting millions of people and continues to circulate throughout the world. Like other human coronaviruses it is spread *via* aerosolized particles, leading to respiratory infections [1, 2]. Infected individuals develop a range of symptoms from mild/asymptomatic infection to severe pneumonia-like disease (i.e., coronavirus disease (COVID)) [2]. Sequence analysis of known SARS coronaviruses points to a bat origin with probable intermediate

hosts prior to human adaptation [3-5]. However, the exact intermediate host and factors that led to its zoonosis and establishment within humans are under investigation.

Secretion of SARS-CoV-2 is thought to be primarily *via* aerosolized particles with high viral loads in the lungs and nasopharyngeal secretions of infected individuals [6, 7]. However, both viral RNA and infectious particles have been detected in fecal samples of acutely infected individuals. In the original SARS-CoV outbreak, there was documented fecal-oral transmission of infection [6, 8-12]. Fecal to oral spread and shedding is a common route of transmission of other animal coronaviruses. Oropharyngeal viral RNA shedding of SARS-CoV-2 in humans lasts for ~17 days on average but persists up to 60-120 days in the respiratory tract and stool [13]. Similarly, oropharyngeal secretion of infectious SARS-CoV-2 in cats appears to cease by 5-10 days post infection (dpi) [14]. Infected felids shed SARS-CoV-2 viral RNA in their feces for at least 5 dpi, but whether that represents infectious virus, or a potential route of transmission is yet to be demonstrated [15].

Due to the multiple routes of spread and close contact with other species, transmission of SARS-CoV-2 from humans to animals is plausible [16]. Human-to-animal and animal-to-animal transmission of SARS-CoV-2 has been documented or experimentally demonstrated. Companion animals such as cats and dogs are susceptible to experimental as well as natural infection from COVID-positive owners [14, 17-21]. In addition, susceptible animals are capable of transmitting infection to cohoused animals [14, 22]. In the case of minks, transmission from humans-to-minks and back to humans was demonstrated [23]. This is similar to a situation at the Amoy Garden complex during the original SARS-CoV outbreak where animal-to-human transmission occurred when an animal vector potentially contracted and spread SARS-CoV throughout the complex [24-26]. Human transmission of SARS-CoV-2 to companion animals opens up the potential for spillover into wild animal populations. Indeed, transmission from humans to deer within North America has been proposed, as post-pandemic deer have been demonstrated seropositive in multiple states and SARS-CoV-2 genome sequenced from lymph nodes [27-29]. Human to animal transmission could contribute to the spread of SARS-like

coronaviruses and the establishment of new reservoirs for recombination and the generation of future novel coronavirus outbreaks.

Infected humans and animals mount humoral responses to SARS-CoV-2 [13, 14, 30-32]. In humans, SARS-CoV-2 antibodies arise within 5-14 days post-infection/symptom onset and peak around 17-20 dpi [13, 31, 33]. For cats experimentally inoculated or naturally exposed to SARS-CoV-2, detectable antibody titers appeared by 7-14 days post-infection peaking ~21 dpi [14]. This matches anti-FCoV responses where high antibody levels can arise within ~9 dpi [34-36]. Immunity to coronaviruses in cats is typically short-lived, with the average FCoV humoral responses lasting several months to 2 years [37]. Anti-SARS-CoV-2 RBD responses in seropositive cats had similar declines in antibody titers only lasting around 4-5 months [38]. However, humans infected with the initial SARS-CoV mounted robust responses detectable 1-2 years post exposure [39-41]. The duration of anti-SARS-CoV-2 antibody responses is the subject ongoing research, but natural exposure is unlikely to induce long-term or lifelong immunity/seropositivity [42].

Major antigenic targets for SARS-CoV-2 infected individuals are the nucleocapsid, which is one of the most abundantly produced viral proteins [43], and spike protein, which is responsible for viral entry [44]. The spike has high immunogenicity and diverges from other coronaviruses [32, 44, 45]. Spike is composed of two subunits (S1/S2). The S1 subunit contains the receptor binding domain (RBD) responsible for binding to host ACE-2 and determining tropism/entry, while the S2 domain contains the fusogenic region of the spike [44, 45]. SARS coronaviruses share very low similarity to other coronaviruses within the spike protein [32], but antibodies against the S2 subunit can cross-react with common human coronaviruses [46-48]. Cross-reactivity of the S1 subunit occurs at very low rates. Within the S1 region, the RBD is highly immunogenic and unique to SARS-CoV-2 [32, 49]. Serum from humans infected with common human coronaviruses such as OC43, NL63, and 229E failed to recognize the RBD from SARS-CoV-2 [32, 46, 49]. Animals infected or immunized with other coronaviruses similarly fail to generate cross-reactive antibodies against SARS-CoV-2's RBD [32]. For infected cats, SARS-CoV-2 seroconversion was not impacted by pre-existing immunity against feline coronavirus (FCoV), an alpha-coronavirus with limited similarity to SARS-CoV-2 [38]. Collectively,

seropositivity against the RBD of SARS-CoV-2 is a specific marker of SARS-CoV-2 exposure and has led several groups to create highly specific indirect ELISAs against SARS-CoV-2's RBD to screen for SARS-CoV-2 exposure [30, 32, 33]. A final consideration of antibodies targeting the RBD is they could be either neutralizing or non-neutralizing [33, 50-53]. This may explain why serum from humans and animals exposed to the original SARS-CoV were able to recognize the spike and RBD of SARS-CoV-2 while their cross-neutralization potential was variable [54, 55].

Despite limited similarity in the spike protein of SARS-CoV-2 vs common circulating coronaviruses, there are reports of pre-pandemic, pre-existing SARS-CoV-2 reactive serum in humans [48, 49, 54]. These cross-reactive antibodies represent a rare response to common human coronaviruses within conserved epitopes of SARS-CoV-2's spike protein (usually in the S2 region) with reports of ~0.6% prevalence of pre-existing anti-RBD responses [46, 48, 49]. Although there is increasing evidence for earlier timelines of SARS-CoV-2 spread among humans, pre-existing seropositivity among other species has not been reported [38, 56-58]. Indeed, even within central China, researchers failed to find evidence of SARS-CoV-2 exposure prior to the pandemic [38, 56, 58].

As SARS-CoV-2 spreads and encounter's new species, there is a need for monitoring local populations for SARS-CoV-2 transmission and the potential establishment of local reservoirs. Currently, we have a limited understanding of coronavirus reservoirs, spread, and recombination among diverse species. The original SARS outbreak in 2003 was a harbinger of the potential risk of crossover coronaviruses. At that time, animal coronavirus surveillance was a high priority. Unfortunately, this investment was not sustained. Our aim was to address whether SARS-CoV-2 is being introduced into companion animals of North America by tracking seroconversion using an in-house indirect ELISA against the RBD of SARS-CoV-2. We chose to focus on companion animals (i.e., cats and dogs) as they represent a significant source of human-animal interactions with potential for contact and further spillover into wild animal populations. Surprisingly, we found evidence of anti-RBD seropositive animals pre-dating the pandemic by several months to years. Our study provides evidence for the existence and prevalence of SARS-CoV-2 serum reactivity prior to the current pandemic.

## Materials and methods

### *Recombinant RBD production and purification*

Recombinant RBD production has been previously published [56]. Our lab deviated from the prior published method to utilize equipment readily available. Briefly, the plasmid containing the RBD of SARS-CoV-2 was produced under federal contract HHSN272201400008C and obtained through BEI Resources, NIAID, NIH. Vector pCAGGS contains the SARS-related coronavirus 2, Wuhan-Hu-1 spike glycoprotein RBD, NR-52309. To produce recombinant RBD, the pCAGGS-RBD plasmid was transfected into  $\sim 5 \times 10^7$  adherent HEK-293/T17 cells (ATCC CRL-11268) in a T-175 using PEI (Polyethylenimine, linear 25,000 m.w.(Polysciences, Warrington, PA, USA). Plasmid was mixed at a 1:3 ratio with PEI (20ug of plasmid : 60ug PEI for a T-175 transfection) in 1 mL serum-free DMEM for 30 minutes at room temperature. Media was aspirated and the transfection mixture was added to 14mL fresh growth media and placed onto cells. Three to four hours post-transfection, media was changed and replaced with DMEM containing either 2% or 5% Fetal Bovine Serum (Hyclone FetalClone III, Cytiva Life Sciences, USA). Maintenance in a lower serum prevents overgrowth. However, we found higher protein yields when supplemented with 5% FBS. Transfection efficiency was nearly 100% as assessed by GFP-positive transfected cells in a control flask.

Supernatants from transfected HEK-293 T17 cells were collected into 50mL conical tubes and frozen at days 3 and 6 post-transfection. Pooled supernatants were thawed and incubated with Ni-NTA (Ni-NTA Agarose, Qiagen, Germany) resin with gentle rocking overnight. The resin was spun down at  $>3400 \times g$  in a swing-bucket Sorvall RT centrifuge for 10 minutes at  $4^{\circ}\text{C}$ . Ni-NTA resin was resuspended in 1mL wash buffer (20mM imidazole, 5mM  $\text{NaH}_2\text{PO}_4 \cdot \text{H}_2\text{O}$ , 0.3M NaCl in  $\text{H}_2\text{O}$ ), transferred to a 2mL microcentrifuge tube, gently rocked for 10 minutes at room temperature, spun, and resuspended in fresh buffer. Resin was washed between 3-7 times until  $\text{OD}_{230}$  was  $\leq$  wash buffer. Once the supernatant OD dropped sufficiently, 1mL elution buffer (235mM Imidazole, 5mM  $\text{NaH}_2\text{PO}_4 \cdot \text{H}_2\text{O}$ , 0.3M NaCl in  $\text{H}_2\text{O}$ ) was added to elute the RBD from the nickel resin. Eluate was rocked for 10 minutes at room temp and then centrifuged. Two elution steps were performed with a third final elution using 0.5M imidazole. Protein

concentration was determined by standard curve analysis of a silver-stained (Pierce Silver Stain Kit, Thermo Scientific, USA) 12% SDS-PAGE gel using a standard curve of BSA (bovine serum albumin). Analysis was performed using Image Studio Lite ver. 5.3 (Li-Cor Biosciences, Lincoln, NE, USA).

### ***Serum and Plasma samples***

Previously collected pre-SARS-CoV-2 de-identified human serum samples were kindly donated by Dr. Jon Wall and Steve Foster (University of Tennessee Medical Center, Knoxville, Tennessee, USA). De-identified COVID-positive plasma samples were donated from: MEDIC Regional Blood Center (Knoxville, Tennessee, USA) and Dr. Mark Slifka (Oregon Health Sciences University, Portland, Oregon, USA). The following reagents were obtained through BEI Resources, NIAID, NIH: Human Plasma, Sample ID WU353-073, NR-53643; WU353-074, NR-53644; WU353-075, NR-53645; WU353-076, NR-53646; WU353-076, NR-53647, were contributed by Ali Ellebedy, Ph.D., Washington University School of Medicine, St. Louis, Missouri, USA. The following reagents were obtained through BEI Resources, NIAID, NIH: polyclonal anti-feline infectious peritonitis virus, 79-1146 (antiserum, guinea pig), NR-2518; polyclonal anti-canine coronavirus, UCD1 (antiserum, guinea pig), NR-2727; polyclonal anti-bovine coronavirus, Mebus (antiserum, guinea pig), NR-455; polyclonal anti-porcine respiratory coronavirus, ISU-1 (antiserum, guinea pig), NR-459; polyclonal anti-turkey coronavirus, Indiana (antiserum, guinea pig), NR-9465. Client-owned canine and feline serum samples were submitted to the University of Tennessee Veterinary Hospital for routine animal testing. Canine samples (n=36) were collected post-pandemic from local, East Tennessee animals. All feline samples were pre-pandemic. Samples from East Tennessee feral cats (n=36) were collected from 2007-2012. Client-owned feline samples (n=92) were collected nationwide as part of clinical diagnostic testing (see Table 1.7). Twenty cat samples were grouped into FCoV positive and negative groups based on feline infectious peritonitis (FIP) serology using an immunofluorescence assay (IFA) against FIP serotypes I and II, as well as TGEV (transmissible gastroenteritis virus) (VMRD, Pullman, WA, USA). Normal cat serum was purchased from Jackson ImmunoResearch (West Grove, PA, USA). Tennessee-resident

cows (n=33) and tigers (n=9) were collected pre-pandemic for routine diagnostic testing. Post-mortem, post-pandemic samples were collected from East Tennessee elk (n=12) and South Carolina white-tailed deer (n=22).

### ***Anti-RBD ELISA***

Anti-RBD ELISA was based on the published protocol by Amanat et al. and Stadlbauer et al. [30, 59]. Purified RBD was diluted to 2ug/mL in PBS and 50uL was placed into each well of a 96 well plate (Immulon 4HBX, Thermo Fisher, USA) and allowed to incubate overnight at 4<sup>0</sup>C. Unbound RBD was removed and wells were washed 3x with PBS-T (PBS with 0.1% Tween-20). Rinsed wells were blocked with 5% milk in PBS for 2 hours at room temp. Block was removed and serum or plasma samples were added at 1:50 dilution for the initial screen in PBS with 1% milk and incubated at room temp for 1 hour. After 1 hour, wells were washed 3x with PBS-T and a secondary antibody for that species was added (i.e., HRP goat-anti-human IgG, Rockland Immunochemicals, Pottstown, PA, USA; HRP goat-anti-dog IgG, Bethyl Laboratories, Montgomery, TX, USA; HRP goat-anti-cat IgG, Invitrogen, Waltham, MA, USA; HRP goat-anti-guinea pig IgG, Life Technologies Corp, Carlsbad, CA, USA; HRP rabbit-anti-deer IgG, KPL, Gaithersburg, MD, USA; HRP sheep-anti-cow IgG, Bethyl Laboratories, Montgomery, TX, USA) at dilutions of 1:10,000 (anti-human, cat, dog, tiger) or 1:250 (anti-cow, deer, elk) in PBS with 1% milk. Optimal secondary antibody concentrations were determined by titration on either 5% milk (negative control) or 1:50 dilution of that species serum (positive control). Secondary antibodies were allowed to incubate for 1 hour at room temperature before being washed 3x with PBS-T. ELISA was developed with 50uL TMB (1-Step Ultra TMB-ELISA, Thermo Fisher, Waltham, MA, USA) for 10 minutes. Reactions were stopped by the addition of 2M sulfuric acid and read using a BioTek Synergy 2 or Synergy H1 plate reader set at 450nm (BioTek, Winooski, VT, USA). Receiver operator curve (ROC) analysis was performed to determine the appropriate threshold to yield 100% specificity of ELISAs performed at a 1:50 dilution. For titrations of seropositive and seronegative samples, threshold values for each dilution were calculated as the average of negative samples plus 3 times the standard deviation. Titrated samples were initially diluted 1:100

and then serially diluted 1:3 (final dilution of 1:8100). Serum dilutions were made in PBS with 1% milk and added to RBD-coated and blocked wells. OD<sub>450</sub> values for each species and titrations were graphed in GraphPad Prism ver. 8 (GraphPad Software, San Diego, CA, USA).

### ***Western and dot blots***

For dot blots, 5-10uL of sample was applied directly onto nitrocellulose membranes and allowed to dry. Western blots were loaded with 30uL (~3ug) of purified recombinant RBD, resolved in a 12% SDS-PAGE gel and transferred to a nitrocellulose membrane. Blots were blocked overnight at 4<sup>0</sup>C with 5% milk in PBS. Mouse anti-6His-HRP conjugated antibody (1:5,000) (Proteintech, Rosemont, IL, USA) or polyclonal serum samples (1:20) were incubated with the blots at room temperature for 2 hours and subsequently washed 2x with TBS-T (tris buffered saline with 0.1% Tween-20). For polyclonal serum, species specific HRP anti-IgG antibodies (1:5,000 dilution) were incubated for an additional 2 hours and washed 2x as above. Chemiluminescent substrate (Pierce SuperSignal West Pico PLUS, Thermo Fisher, USA) was added and luminescence was detected using BioRad ChemiDoc (Bio-Rad, Hercules, CA, USA).

### ***Neutralization assays***

Serum samples were screened for neutralization using LEGENDplex SARS-CoV-2 neutralizing antibody assay (BioLegend, San Diego, CA, USA) following manufacturer recommendations. Briefly, serum was diluted 1:100 and incubated with biotinylated SARS-CoV-2 S1 subunit containing the RBD and human ACE-2 (hACE-2) conjugated to fluorescent beads. Streptavidin-PE (phycoerythrin) was added to detect SARS-CoV-2 S1 subunit bound to beads/hACE-2. Binding/PE levels were detected *via* a BD LSR-II equipped with 488 and 633nm lasers (Becton Dickinson, Franklin Lakes, NJ, USA). Data was analyzed using BioLegend LEGENDplex Data Analysis Software. Mean fluorescent intensity (MFI) was normalized and graphed in GraphPad prism v9 (GraphPad Software, San Diego, CA, USA).

### ***Fecal coronavirus PCR screen and sequence alignments***

De-identified fecal samples from thirty healthy East Tennessee cats were collected and stored at -80°C. Samples were resuspended in PBS to yield a 10% solution and centrifuged to clarify. Fecal RNA was extracted using a Qiagen viral RNA extraction kit (Qiagen, Hilden, Germany) and RNA was reverse transcribed using Verso cDNA kit with random hexamers and RT enhancer (Thermo Fisher, Waltham, MA, USA). PCR amplification of conserved coronavirus regions using previously reported primer pairs was used to screen the cDNA [60]. PCR amplicons were visualized on a 1% agarose gel and positive PCR samples were Sanger dideoxy sequenced. Sequences were viewed using 4Peaks software (Nucleobytes, Amsterdam, Netherlands). Sequences from fecal samples were Clustal W aligned to common coronaviruses, trimmed and phylogenetic trees were generated using Maximum-Likelihood method for each positive loci using MEGA X [61, 62]. For phylogenetic trees using multiple loci, aligned and trimmed sequences for each loci were concatenated together prior to Maximum-Likelihood tree construction. Phylogenetic trees were tested by bootstrap testing with 1000 iterations. Common coronavirus sequences for ORF1ab (RdRp and helicase loci) and spike were obtained from the following: porcine coronavirus HKU15 (NC039208), SARS-CoV-2 (MN988668), SARS-CoV (NC004718), porcine respiratory coronavirus/PRCoV (KY406735), human coronavirus OC43 (NC006213), MERS-CoV (NC038294), feline coronavirus/FCoV (NC002306), canine respiratory coronavirus/CRCoV (KX432213), canine coronavirus/CCoV (JQ404410), bovine coronavirus/BCoV (NC003045), avian coronavirus (NC048214), human coronavirus 229E (NC002645), transmissible gastroenteritis virus/TGEV (NC038861), murine hepatitis virus/MHV (NC048217), human coronavirus NL63 (NC005831), feline coronavirus strain UU8 (FJ938055), feline coronavirus strain UU19 (HQ392470), feline coronavirus strain Black (EU186072), feline coronavirus strain RM (FJ938051), feline coronavirus strain Felix (MG893511). All generated sequences were deposited in GenBank under accession numbers: MZ220722 through MZ220762 (sample ID, positive loci, animal location, and accession numbers are shown in Table 2.7).

### *Statistics*

All graphs and statistical analysis were performed in GraphPad Prism ver. 9 (GraphPad Software, San Diego, CA, USA). ELISA OD<sub>450</sub> results were normalized to an inter-plate replicate run with all assays. Student's one-tailed t-tests with Welch's correction and one-way ANOVA with multiple comparisons tests were performed on ELISA results and documented in the respective figure legends. Descriptive statistics were provided for each ELISA group (mean, median, and quartiles). Receiver operator curve (ROC) analysis was performed to determine appropriate threshold values for human, cat, and deer serum samples. Area under the curve was calculated for each titrated ELISA sample and graphed. Neutralization data was normalized with negative control group (normal cat serum) representing 100% MFI.

Data will be made publicly available upon publication and upon request for peer review.

### **Results**

We developed an in-house ELISA to serologically screen companion animals based on a protocol developed at Mt. Sinai [30, 59]. To examine cross-reactivity of our in-house anti-SARS-CoV-2 RBD indirect ELISA, we used polyclonal guinea pig serum raised against different animal coronaviruses (Fig A.1). Consistent with previous reports, no cross-reactive antibodies for any of the common coronaviruses were found [18, 32, 38, 56]. Only antibodies from SARS-CoV or SARS-CoV-2 infected individuals reacted (Fig A.1 A,B). Human serum collected from individuals prior to the SARS-CoV-2 pandemic or plasma from recovered SARS-CoV-2 donors were used to validate our ELISA screen (Fig A.1 B). ROC analysis determined the positive cutoff threshold, using a value that gave highest specificity and sensitivity with pre-pandemic human serum and serum from confirmed SARS-CoV-2 infected individuals. ROC analysis was in agreement with the commonly used threshold determination method of three standard deviations above the mean negative value. Our assay based on RBD screening showed high sensitivity (96.96%) and specificity (95.45%) with 66 SARS-CoV-2 samples and 22 pre-SARS-CoV-2 samples (Fig A.1 B). While Stadlbauer et al. performed two diagnostic ELISAs, one with RBD and

the other with full-length spike, our results using only the RBD-based screen are in good agreement with their published data. Others have also demonstrated the accuracy of an RBD-only based ELISA [33, 38]. A western blot using an anti-6His antibody (Fig A.1 C) shows the expected size of purified RBD with a single band ~32kDa. This shows that our isolated RBD is the correct size and runs as a monomer. Silver stain of the same affinity-purified SARS-CoV-2 RBD demonstrates relative purity (Fig A.1 D). However, there are co-purified proteins present at lower levels.

To establish a baseline for future SARS-CoV-2 screening of companion animals, 128 pre-pandemic feline serum samples collected prior to December 2019 were retrospectively screened using our in-house ELISA. Nineteen samples were of a known FCoV serological status, with the remaining 109 of unknown FCoV status. Following the same protocol used for screening human serum samples (Fig A.1), feline samples were tested for antibodies against SARS-CoV-2's RBD (Fig A.2 A). There were two batches tested. Serum samples from feral cats in East Tennessee collected from 2007 to 2012 (2007-2012) (n=36) and convenience samples from client-owned cats undergoing routine blood work (listed as Pre-pandemic) (n=92) (Fig A.2 A). As expected, SARS-CoV-2 experimentally infected cats [14] tested positive with high relative OD<sub>450</sub>, and normal cat serum (i.e., negative control) with very low relative OD<sub>450</sub> (Fig A.2 A). Despite pre-dating the pandemic, 52% (67/128) of the cat samples tested positive for antibodies against SARS-CoV-2 RBD. This is surprising as there was a lack of high cross-reactivity in guinea pigs immunized with FCoV in Fig A.1 A. Several reports also showed a lack of similarity and cross reactivity between alpha coronaviruses and SARS-CoVs [18, 32, 38, 56]. Indeed, two other groups found that pre-existing immunity to FCoV had no impact on seropositivity of feline samples [38, 58]. To ensure that the positive ELISA results were specific to the RBD and not to a co-purified protein, a western blot was carried out using serum from a positive sample (Fig A.2 B). Positive cat serum bound a ~32 kDa protein, the size of the RBD protein (Fig A.1 C). Notably, normal cat serum did not react with any other protein despite the presence of co-purified proteins. To further show the specificity of the anti-RBD response, we titrated seropositive and seronegative samples. Starting with serum from cats experimentally infected with SARS-CoV-2 (Fig A.2 A) and normal cat serum, saw a

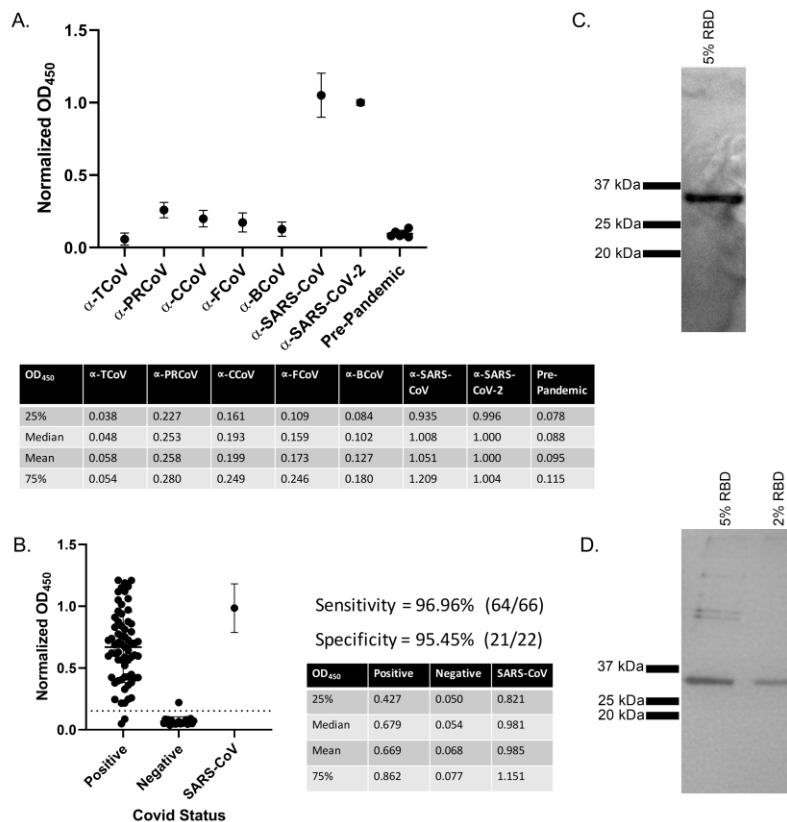


**Figure A.1: Anti-SARS-CoV-2 ELISA Sensitivity and Specificity.**

(A) Cross reactivity of anti-CoV antibodies against SARS-CoV-2 RBD. Polyclonal sera from guinea pigs immunized with common animal coronaviruses (turkey coronavirus, TCoV; porcine respiratory coronavirus, PRCoV; canine coronavirus, CCoV; feline coronavirus, FCoV; bovine coronavirus, BCoV) was used in a SARS-CoV-2 RBD indirect ELISA. Positive samples consisted of polyclonal serum from a SARS-CoV-2 infected patient and a monoclonal antibody to SARS-CoV (CR3022). The negative control group was comprised of pre-pandemic human serum. Secondary antibodies were either anti-human IgG (1:10,000) (Rockland Immunochemicals, USA) or anti-guinea pig IgG (1:10,000) (Life Technologies Corp, USA). Bars represent mean and standard deviation ( $n > 3$  for all samples). (B) ELISA validation using 66 human Covid-positive plasma and 22 negative serum samples. Human antibodies against the SARS-CoV-2 RBD were detected with an indirect RBD-specific ELISA. Secondary antibody was the anti-human IgG (1:10,000) (Rockland Immunochemicals, USA). ROC analysis determined the positive OD<sub>450</sub> cutoff value (dashed line). Positive plasma samples were donated COVID recovered patients and pre-pandemic serum samples were the negative controls. Based on the experimentally determined cutoff value, 64 of the 66 positive samples were anti-RBD positive, giving a sensitivity value of 96.96%. All but one of the negative samples were below the cutoff value for a specificity of 95.45%. Adjacent tables list first and third quartiles along with mean and median OD<sub>450</sub> values of COVID-positive and negative human samples. Bars represent mean and standard deviation ( $n > 3$ ). (C) Anti-6His western blot on HEK-293T17 purified RBD from 5% serum conditions. Samples were run on a 12% denaturing SDS-PAGE gel. Protein was transferred to nitrocellulose and probed with anti-6His antibody at 1:10,000 (Proteintech, USA). White light and chemiluminescent images were overlaid and from left to right, ladder (lane 1) and purified RBD (lane 2). (D) Silver stain of purified recombinant SARS-Cov-2 RBD produced in HEK-293T17. From left to right: Ladder, HEK-RBD under 5% serum conditions, HEK-RBD from 2% serum conditions. Samples were denatured and run on a 12% SDS-PAGE gel and Silver Stained (Thermo Fisher Scientific, USA). For B and C, representative data shown.

normalized OD<sub>450</sub> >3 standard deviations above the negative control (i.e., normal cat serum) at all dilutions. This gives a titer >8100 (Fig A.2 C). 17 seropositive and 10 seronegative pre-2020 cat samples were titrated and assayed in our ELISA (Fig A.2 D). Titers ranged from 900 to 8100, with a median titer of 2700 demonstrating both a high anti-SARS RBD prevalence and titer. Titrations of these earlier seropositive and seronegative feral cat samples have a similarly high titer (Fig A.2 E) (median titer 8100) which is on par with the pre-pandemic samples. AUC for all groups is shown to the right side of their respective titration. AUC analysis of the titrated samples showed a significant difference between all positive and negative samples.

Following the surprising presence and prevalence of anti-RBD responses in pre-pandemic cats, we explored the epidemiological characteristics of our samples. Pre-pandemic convenience samples were submitted to the University of Tennessee for diagnostic testing of feline herpesvirus, feline calicivirus, and FCoV. Age, sex, and location of seropositive and seronegative samples are shown in Table A.1. Both seropositive and seronegative samples had a mean age of >3 years with no difference between the groups and contained similar ratios of male: female animals (Table A.1). Seropositive samples were found in disparate geographic locations from opposite coasts of the United States (i.e., New York to California (Table A.1)). This observation indicates that seropositivity is not confined to a single geographic region (e.g., East Tennessee). Based on our limited sampling, we were unable to identify any unique characteristic or identifier for seropositive vs seronegative samples.

With our discovery of pre-existing antibodies against SARS-CoV-2's RBD, it was pertinent to examine samples from dogs, another companion animal with high human contact. Serum samples from dogs (n=36) were collected and retrospectively screened as part of a tick study during a 7-month period beginning in Jan 2020 and extending into July 2020. These samples are considered post-pandemic because the timeframe straddles the arrival of SARS-CoV-2 in East Tennessee (~March 2020). The initial ELISA screen identified 97% seropositivity in the dog samples (Fig A.3 A) with only 1 sample falling below the cutoff established on human serum. Surprisingly, serum from purpose-bred research animals housed at the University of Tennessee also showed high levels of

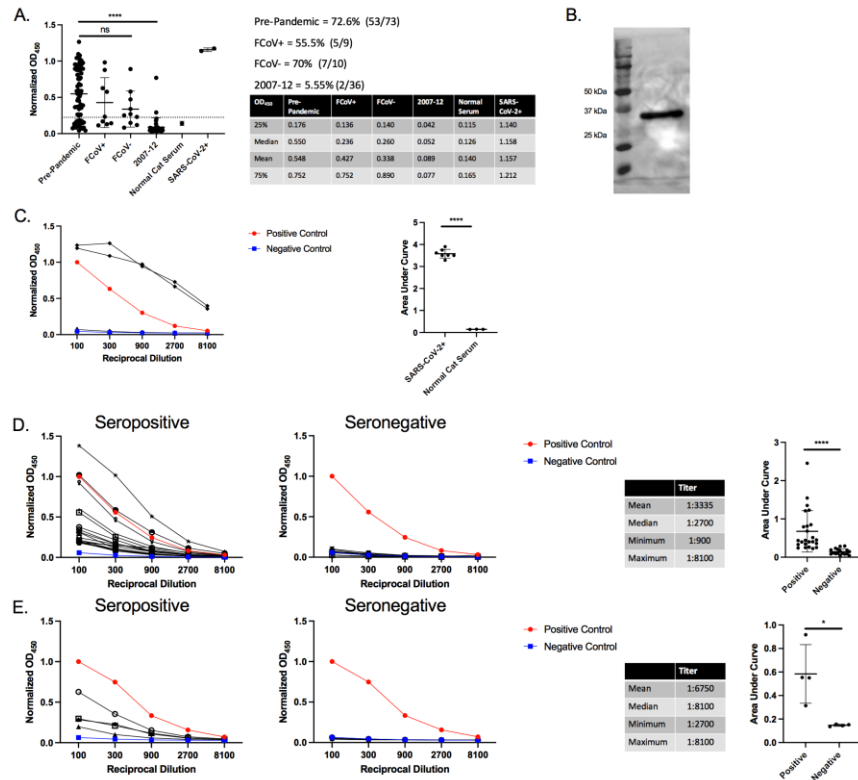


**Figure A.3: Pre-Pandemic Feline Antibodies Cross-React with SARS-CoV-2 RBD.**

(A) ELISA results of cat serum RBD reactivity. 93 pre-pandemic feline serum samples were tested for reactivity in our anti-RBD ELISA with anti-felid IgG secondary (1:10,000) (Invitrogen, USA). Cutoff values were determined by receiver operator curve (ROC) analysis. OD<sub>450</sub> for samples in each group were plotted with the dotted line representing the positive threshold. Two sets of pre-pandemic cat samples were collected. Pre-pandemic cat convenience samples (n=73) were collected in local clinics and sent to the University of Tennessee for diagnostic testing or during feral cat studies (2007-2012) (n=36). Pre-pandemic convenience samples were subdivided into feline coronavirus positive (FCoV+) and negative (FCoV-) subgroups. Normal cat serum (Jackson ImmunoResearch Laboratories, USA) serves as the negative control and SARS-CoV-2+ serum from two cats experimentally inoculated with SARS-CoV-2 as positive controls. Side table lists first and third quartiles and mean and median OD<sub>450</sub> values for all samples. Bars represent mean +/- standard deviation (n>3 for all samples). (B) Western blot of purified RBD using serum from a single positive cat sample. Purified RBD was run under denaturing conditions and blotted onto nitrocellulose. The RBD blot was first probed with cat serum from an ELISA positive sample (1:20 dilution) followed by anti-felid IgG-HRP conjugated (1:10,000 dilution) (Invitrogen, USA). White light and chemiluminescent images were overlaid. Lane 1 is the molecular weight ladder and lane 2 is purified RBD. (C, D, E) Titration of seropositive and seronegative serums assessed *via* RBD ELISA. OD<sub>450</sub> values were plotted against the reciprocal dilution. Samples were considered positive if they were 3 standard deviations above the negative average for each dilution. Anti-RBD titer was designated as the last dilution above the negative cutoff. Positive controls were human COVID-positive serum and negative controls were normal human and cat serum (Jackson ImmunoResearch Laboratories, USA). Statistics for the positive sample titrations are included in the table along with AUC analysis. (C) Serum from two SARS-CoV-2 infected cats (●) and normal cat serum (■) were titrated in an anti-RBD ELISA. (D) Titration of 17 seropositive and 10 seronegative, pre-pandemic cat samples. (E) Titration of four seropositive and seronegative cat samples collected from 2007-12. For A and B, representative data shown. For A, Tukey's one-way ANOVA with multiple comparisons was performed. For C, D, E AUC analysis and Student's one-tailed t-test with Welch's correction was performed. p< 0.05 = \*, p< 0.01 = \*\*, p< 0.001 = \*\*\*.

**Table A.2:** Characteristics of Feline Samples.

| Characteristic                   | No. seropositive | %     | No. seronegative | %     |
|----------------------------------|------------------|-------|------------------|-------|
| <b>Age</b>                       |                  |       |                  |       |
| Total no. of samples             | 58               |       | 15               |       |
| Avg age of feline (yrs $\pm$ SD) | 3.56 $\pm$ 3.67  |       | 3.87 $\pm$ 4.37  |       |
| <1 yr                            | 15               | 25.86 | 5                | 33.33 |
| 1-3 yrs                          | 22               | 37.93 | 4                | 26.67 |
| 4-6 yrs                          | 10               | 17.24 | 2                | 13.33 |
| >6 yrs                           | 11               | 18.97 | 4                | 26.67 |
| <b>Sex</b>                       |                  |       |                  |       |
| Total no. of samples             | 56               |       | 19               |       |
| Male                             | 30               | 53.57 | 12               | 63.16 |
| Female                           | 26               | 46.43 | 7                | 36.84 |
| <b>Location</b>                  |                  |       |                  |       |
| Total no. of samples             | 62               |       | 21               |       |
| TN                               | 10               | 16.12 | 7                | 33.33 |
| NY                               | 19               | 30.64 | 9                | 42.85 |
| CA                               | 27               | 43.54 | 5                | 23.8  |
| MA                               | 4                | 6.45  | 0                | 0     |
| SC                               | 1                | 1.61  | 0                | 0     |
| WI                               | 1                | 1.61  | 0                | 0     |

Cats were grouped based on the seronegative/positive status from the ELISA from Fig 2A. Student's t-test was used to determine significance (ns = not significant).

reactivity (Fig A.3 A). This raised suspicion about the specificity of the response. To address this, western blot analysis with canine serum (Fig A.3 B) identified a protein other than the RBD (see the ~32 kDa protein in Fig A.1 C and A.2 B). The canine serum recognized a ~60 kDa protein which is likely a co-purified protein present after RBD purification and is faintly seen in the silver-stained gel in Fig A.1 D. This co-purified protein was not detected in the blots performed for Fig. A.1 C and A.2 B using anti-6His monoclonal antibody and cat serum, respectively. Although there is a possibility that canine serum recognizes an oligomer of RBD [63], based on Fig A.1 C the anti-6His antibody does not detect any protein >32kDa, eliminating this possibility.

Following our observation of high levels of anti-SARS-CoV-2 RBD antibodies in North American cats, we began examining other regional animals. Serum from Tennessee resident, pre-pandemic cows (n=33) and tigers (n=9), post-pandemic East Tennessee elk (n=12), and post-pandemic South Carolina white-tailed deer (n=22) were tested for anti-SARS-CoV-2 RBD antibodies (Fig A.4 A). Of the four species tested, only the deer from South Carolina showed any seropositive samples (2/22). Serum titrations show the two seropositive samples have a high titer >8100 (Fig A.4 B), and AUC of the titrations show a significant difference between seropositive and negative deer samples (Fig A.4 C). Unfortunately, due to limited sample volume, we were unable to run western blots to demonstrate the specificity for the RBD protein. The deer are post-pandemic and could represent recent transmission of SARS-CoV-2 into the deer population. Although these animals probably have had limited contact with humans, white-tailed deer are susceptible to and capable of transmitting SARS-CoV-2 [64]. Another possibility is that this species was exposed to the same etiological agent as our pre-pandemic seropositive cats.

To address whether our ELISA-positive animal samples can neutralize SARS-CoV-2 infections, we measured the ability of cat serum to block the interaction of the spike protein with the human ACE-2 (hACE-2) receptor using a commercially available flow cytometry-based bead assay. In this assay, neutralization is characterized as the decrease in fluorescence when antibodies block the fluorescently labeled SARS-CoV-2 S1 subunit from binding to hACE-2 conjugated beads (Fig A.5 A). Because this assay is not species specific or immunoglobulin type dependent, it is applicable for assessing both human and

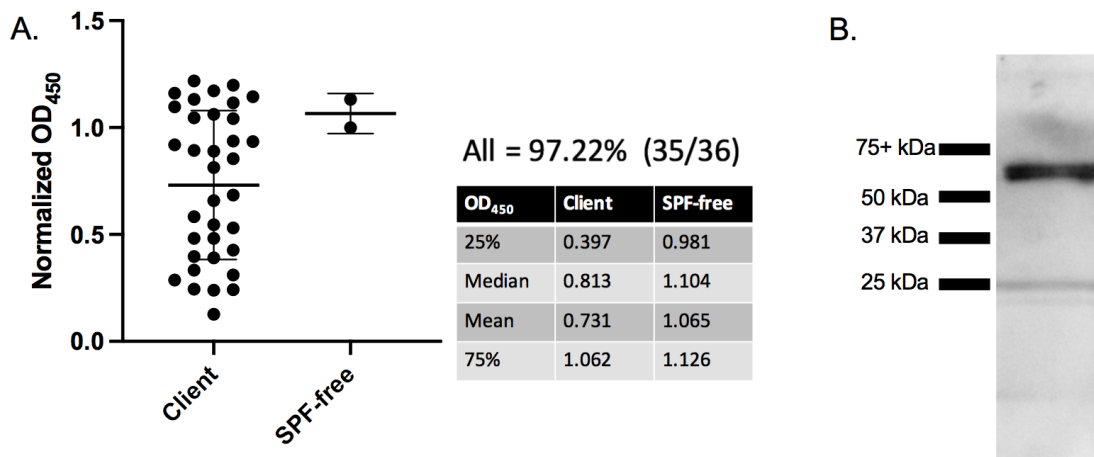


**Figure A.5:** Dog Serum Cross-reacts to a Co-Purified Protein.

(A) Anti-SARS-CoV-2 RBD ELISA with dog serum. Serum from thirty-six client-owned and two purpose-bred research dogs were tested in an anti-RBD ELISA with anti-canine IgG secondary HRP (1:10,000) (Bethyl Laboratories, USA). Table to the right lists the first and third quartiles, median, and mean OD<sub>450</sub> values for all samples. Bars represent mean +/- standard deviation (n>3). (B) Western blot of purified RBD using serum from a positive dog sample. Purified RBD was probed with dog serum from an ELISA positive sample (1:20 dilution) followed by anti-canine IgG-HRP (1:10,000 dilution) (Bethyl Laboratories, USA). White light and chemiluminescent images were overlaid. Lane 1 (from left to right) ladder and lane 2: purified RBD. For all figures, representative data shown.

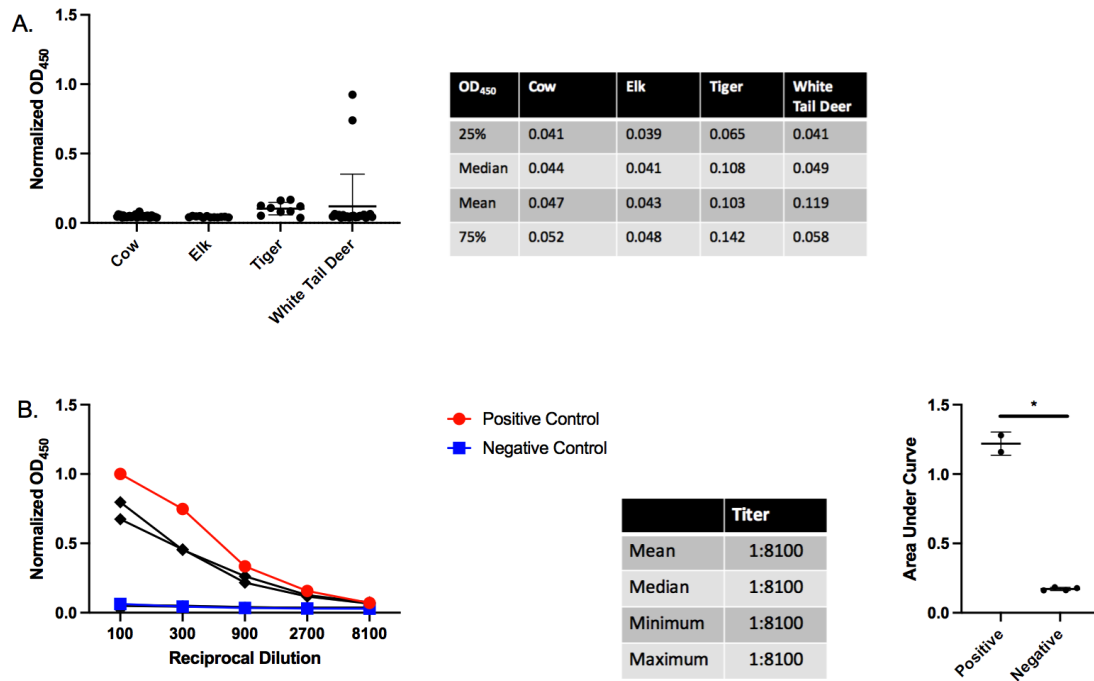


**Figure A.7:** Serological Testing of Other Regional Animals.

(A). Anti-SARS-CoV-2 RBD ELISA with bovine, elk, tiger, and deer serum. Thirty-three pre-pandemic East Tennessee cows, twelve post-pandemic East Tennessee elk, nine pre-pandemic East Tennessee tigers, and twenty-two post-pandemic South Carolina deer serum samples were tested for anti-RBD antibodies. Species-specific secondary antibodies were used at the following dilutions: anti-bovine 1:250 (Bethyl Laboratories, USA), anti-elk/deer 1:250 (KPL, USA), anti-tiger/cat 1:10,000 (Invitrogen, USA), and anti-deer 1:250 (KPL, USA). Bars represent mean  $\pm$  standard deviation ( $n > 3$  for all samples). (B) Titration of two seropositive (●) and four seronegative (■) deer samples. OD<sub>450</sub> values are plotted against the reciprocal dilution of each sample. Samples were considered positive if they were 3 standard deviations above the negative average for each dilution. Positive and negative controls were human COVID-positive and negative samples, respectively. Statistics for the positive sample titrations are included in the table. The AUC analysis for titrations of deer ELISA positive and negative samples is shown to the right. For all figures, representative data shown. For AUC analysis Student's one-tailed t-test with Welch's correction was performed.  $p < 0.05 = *$ ,  $p < 0.01 = **$ ,  $p < 0.001 = ***$ .

feline serum. The internal antibody control shows a decrease in fluorescence corresponding to levels of neutralizing monoclonal antibody against SARS-CoV-2. Serum from experimentally infected cats showed potent neutralization at 1:100 dilution. However, only one ELISA-positive, pre-pandemic cat sample showed neutralization (Fig A.5 B). One of the seropositive white-tailed deer samples, and a single serum sample from mice immunized with PRCoV also showed slight neutralization, clearing the determined ROC threshold/cutoff value (Fig A.5 B). Notably, we were unable to detect high levels of neutralization/neutralizing antibodies even in several of the human convalescent serum samples (Fig A.5 B).

Because cross-reactivity of antibodies to SARS-CoV-2 RBD independent of SARS-CoV-2 infection has not been previously reported in felines, we suspected that the etiological agent could be another coronavirus [38, 58]. Fecal samples were collected from healthy East Tennessee cats and screened for coronaviruses using pan-coronavirus primers amplifying conserved regions of the RNA-dependent RNA polymerase (RdRp), helicase (Hel), and spike (S) genes [60]. Coronavirus viral RNA, whether common animal coronavirus or SARS-like coronavirus, is potentially shed in feces [8, 9, 11, 13]. Collection of fecal samples represented a non-invasive collection method, and SARS-CoV-2 has been reported to have prolonged shedding within fecal samples of humans [8, 9, 11, 13]. Fifteen out of thirty samples (50%) tested positive for at least one loci, with most yielding positive results for multiple loci (Table A.2). Not surprisingly, sequences cluster within the alpha-coronavirus group and with high similarity to previously identified FCoV strains. When all five loci were aligned and concatenated together, the Maximum-Likelihood phylogenetic tree places the concatenated coronavirus sequences within the alpha-coronavirus lineage, closely related to FCoV (Fig A.6 A). We were unable to amplify or identify any sequences which resemble SARS-like coronaviruses or beta-coronaviruses. Partial sequencing of the S1 region was able to amplify the RBD from several coronavirus RNA positive samples. The sequenced RBDs were again highly similar to FCoV based on Maximum-Likelihood phylogenetic tree (Fig A.7 A). Along with the phylogenetic tree, a similarity matrix demonstrates high RBD similarity between previous FCoV strains and those sequenced here (~80%) (Fig A.7 B). The RBD from these fecal samples displays low similarity to

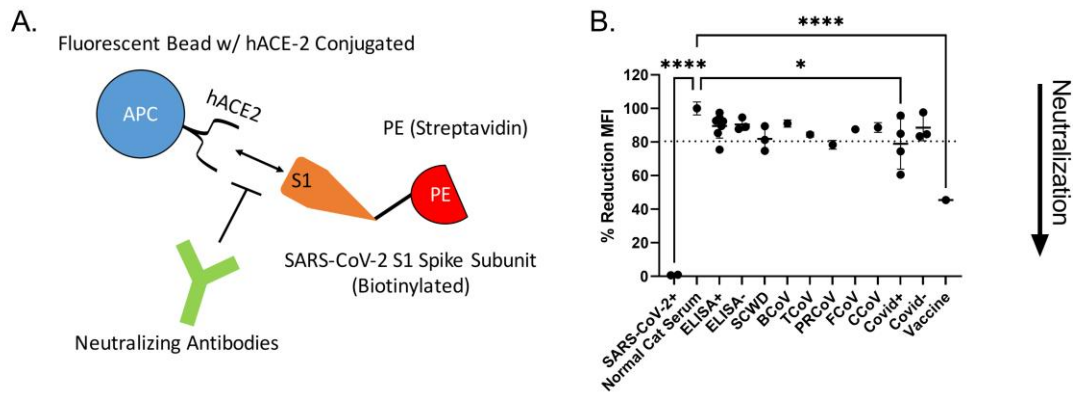


**Figure A.9:** Neutralization Assays.

(A) Schematic of the neutralization assay. Neutralization is measured as the decrease in binding of phycoerythrin (PE)-labeled SARS-CoV-2 S1 subunit to human ACE-2 conjugated beads. Addition of neutralizing antibodies results in a decreased mean fluorescent intensity (MFI) as measured by flow cytometry. (B) Neutralization of SARS-CoV-2 S1 subunit interaction with hACE2. Serum from several ELISA positive and negative cats (ELISA+ and ELISA-, respectively), serum from South Carolina white-tailed deer (SCWD, 2 ELISA-positive and 1 negative), mice immunized with other common coronaviruses (BCoV=bovine coronavirus, TCoV= Turkey coronavirus, PRCoV=porcine respiratory coronavirus, FCoV=feline coronavirus, CCoV=canine coronavirus), and human serum samples (Covid+ = convalescent plasma from Covid+ humans, Covid- = pre-SARS-CoV-2 serum samples, Vaccine = serum post vaccination against SARS-CoV-2 Spike protein). SARS-CoV-2 infected cats and normal cat serum served as positive and negative controls, respectively. Data was normalized to normal cat serum representing 100% binding of SARS-CoV-2 S1 subunit to hACE2 beads. ROC analysis was used to generate a positive reduction threshold (dotted line). Each point is an average of 2 replicates. A Tukey's one-way ANOVA with multiple comparisons was used to analyze experimental groups.  $p < 0.05 = *$ ,  $p < 0.0001 = ****$ .

betacoronaviruses such as MERS, SARS-CoV, and SARS-CoV-2 (~30%) as previously reported (Fig A.7 B).

### **Discussion**

We have employed serological screening as a method to detect potential SARS-CoV-2 exposure in animal populations. Tracking active viral spread in wild and domesticated animals in real-time *via* sequencing and RT-qPCR is expensive and low throughput. In addition, the unknown transient nature of viral shedding from different secretions/locations makes this type of surveillance prohibitively expensive with no guarantee of identifying a virus. Serological detection of antibodies against SARS-CoV-2 is comparatively high-throughput and inexpensive while still maintaining sensitivity. A downside of this methodology is the lack of an up-to-date picture of cross-species transmission, as serology trails initial infections by several days to weeks [22, 33]. On the other hand, due to the lowered cost of serological testing there is a compensatory increase in testing capability allowing a broader swath of animals and regions to be sampled with more frequent re-sampling to track spillover into new species. Our adapted protocol yields recombinant SARS-CoV-2 RBD protein allowing production of a low-cost indirect anti-RBD ELISA. The recombinant RBD was sufficient for serological screening *via* ELISA and is amenable to most labs with prior tissue culture capabilities and does not require large initial investments in cell lines, culture media, or specialized incubators. We validated our method demonstrating low cross-reactivity with other common animal coronaviruses (Fig A.1 A) and >95% sensitivity and specificity on human serum samples (Fig A.1 B).

For the seropositive samples identified in our study, mean titers for positive cat samples were relatively high at ~2700 (Fig A.2 E, G), which based on reported rapid declines in anti-RBD responses for SARS-CoV and FCoV points to exposure within the past few years [37, 38, 40]. Further, based on FCoV studies, animals with high titers typically correlate with active viral shedding and spread within a household, which highlights a potential overlap between seropositivity and viral shedding [37]. This is in stark contrast to SARS-CoV-2 serosurveys on pre- and post-pandemic feline samples from Central China. They found no evidence of exposure before the outbreak, but also positivity

**Table A.4:** Fecal Coronavirus Screening Information.

| Sample   | RdRp1 | RdRp2 | Spike1 | Spike2 | Spike3 | Helicase | Location                            | Accession #'s     |
|----------|-------|-------|--------|--------|--------|----------|-------------------------------------|-------------------|
| CP-20-01 |       |       |        |        |        |          | Jefferson County, TN, USA           | MZ220722-MZ220724 |
| CP-20-02 |       |       |        |        |        |          | Washington County, TN, USA          | MZ220725-MZ220727 |
| CP-20-03 |       |       |        |        |        |          | TN, USA                             | N/A               |
| CP-20-04 |       |       |        |        |        |          | Monroe County, TN, USA              | MZ220728-MZ220730 |
| CP-20-05 |       |       |        |        |        |          | TN, USA                             | N/A               |
| CP-20-06 |       |       |        |        |        |          | Sullivan County, TN, USA            | N/A               |
| CP-20-07 |       |       |        |        |        |          | Grainger County, TN, USA            | MZ220731-MZ220734 |
| CP-20-08 |       |       |        |        |        |          | Monroe County, TN, USA              | MZ220735          |
| CP-20-09 |       |       |        |        |        |          | Sullivan County, TN, USA            | MZ220736-MZ220738 |
| CP-20-10 |       |       |        |        |        |          | Washington County, TN, USA          | N/A               |
| CP-20-11 |       |       |        |        |        |          | Jefferson County, TN, USA           | N/A               |
| CP-20-12 |       |       |        |        |        |          | Monroe County, TN, USA              | MZ220739-MZ220742 |
| CP-20-13 |       |       |        |        |        |          | Grainger County, TN, USA            | MZ220743-MZ220745 |
| CP-20-14 |       |       |        |        |        |          | Jefferson County, TN, USA           | N/A               |
| CP-20-15 |       |       |        |        |        |          | Sullivan County, TN, USA            | N/A               |
| CP-20-16 |       |       |        |        |        |          | Sevier County, TN, USA              | N/A               |
| CP-20-17 |       |       |        |        |        |          | Cocke County, TN, USA               | N/A               |
| CP-20-18 |       |       |        |        |        |          | Hamblin County, TN, USA             | N/A               |
| CP-20-19 |       |       |        |        |        |          | Washington/Sullivan County, TN, USA | MZ220746-MZ220747 |
| CP-20-20 |       |       |        |        |        |          | Hamblin County, TN, USA             | MZ220748          |
| CP-20-21 |       |       |        |        |        |          | Washington/Sullivan County, TN, USA | N/A               |
| CP-20-22 |       |       |        |        |        |          | Grainger County, TN, USA            | N/A               |
| CP-20-23 |       |       |        |        |        |          | Jefferson County, TN, USA           | MZ220749-MZ220750 |
| CP-20-24 |       |       |        |        |        |          | Jefferson County, TN, USA           | N/A               |
| CP-20-25 |       |       |        |        |        |          | Grainger County, TN, USA            | N/A               |
| CP-20-26 |       |       |        |        |        |          | Grainger County, TN, USA            | MZ220751-MZ220755 |
| CP-20-27 |       |       |        |        |        |          | Grainger County, TN, USA            | MZ220756-MZ220759 |
| CP-20-28 |       |       |        |        |        |          | Washington/Sullivan County, TN, USA | MZ220760          |
| CP-20-29 |       |       |        |        |        |          | TN, USA                             | N/A               |
| CP-20-30 |       |       |        |        |        |          | Grainger County, TN, USA            | MZ220761-MZ220762 |

Sample IDs were assigned to de-identified fecal samples from healthy cats. RNA was extracted from each and PCR screened for amplification of 6 coronavirus loci across 3 conserved genes (RdRp, spike, and helicase). Positive amplification and sequencing is shown by a black shaded box. 15/30 samples were positive for at least one coronavirus loci. Animals originated from multiple East Tennessee counties, and, when known, exact county of origin is listed. Accession numbers for each sample are shown to the right and consist of each sequenced loci.

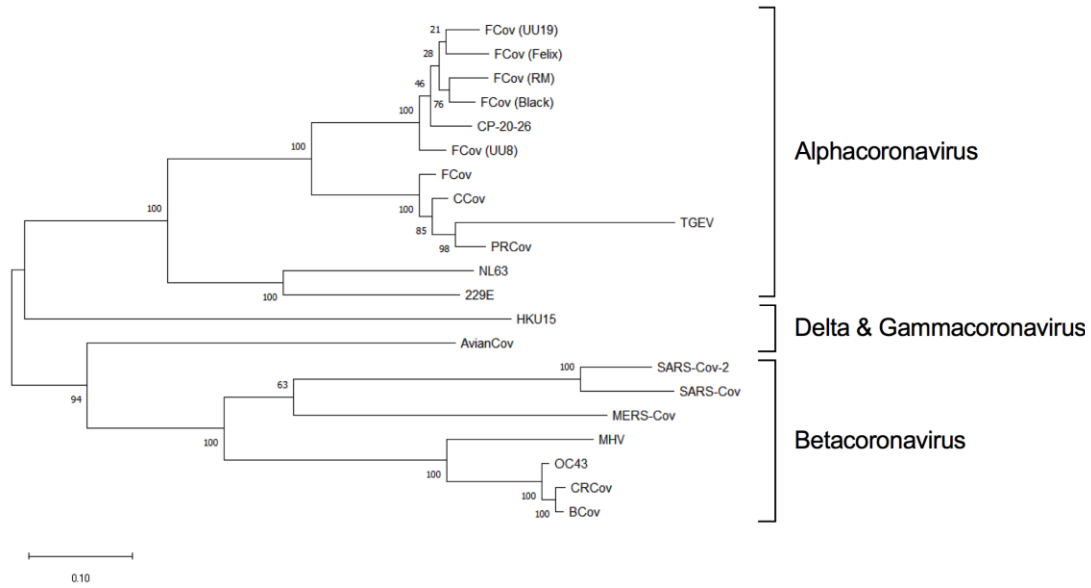
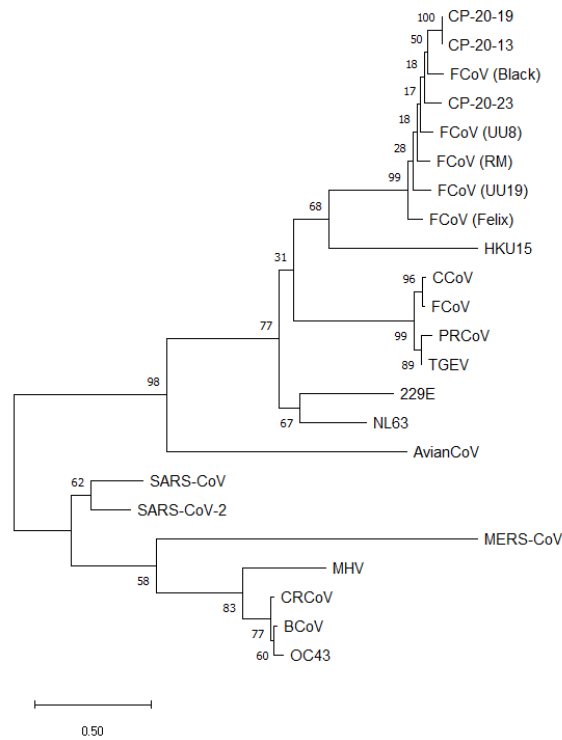


**Figure A.11:** Pan Coronavirus Screen of East Tennessee Felines.

Fecal samples from healthy cats were collected and screened for conserved coronavirus sequences. Phylogenetic trees were generated consisting of common human and animal coronaviruses: CRCoV (canine respiratory coronavirus), BCoV (bovine coronavirus), OC43 (human beta-coronavirus), MHV (murine hepatitis virus), MERS-CoV (Middle East respiratory coronavirus), SARS-CoV-2 (severe acute respiratory coronavirus-2), SARS-CoV (severe acute respiratory coronavirus), AvianCoV (duck coronavirus), NL63 (human alpha-coronavirus), 229E (human alpha-coronavirus), TGEV (transmissible gastroenteritis virus), PRCoV (porcine respiratory coronavirus), FCoV (feline coronavirus strains UU19, Felix, RM, Black, UU8), CCov (canine coronavirus), HKU15 (porcine delta-coronavirus), as well as a locally identified coronavirus (CP-20-26). Sequences from five coronavirus loci were independently aligned, trimmed, and concatenated together. Concatenated sequences were aligned, and phylogenetic trees generated with the Maximum-Likelihood method with bootstrap analysis in MEGA X. Bootstrap values for each branch are shown with lengths to scale. Coronavirus lineages are annotated on the tree.



| Percent Similarity | MERS-CoV | SARS-CoV | SARS-CoV-2 | CP-20-23 | CP-20-19 | CP-20-13 | FCoV (Black) | CCoV  | FCoV  | PRCoV | TGEV  | 229E  | NL63 |
|--------------------|----------|----------|------------|----------|----------|----------|--------------|-------|-------|-------|-------|-------|------|
| MERS-CoV           | 100      |          |            |          |          |          |              |       |       |       |       |       |      |
| SARS-CoV           | 32.2     | 100      |            |          |          |          |              |       |       |       |       |       |      |
| SARS-CoV-2         | 38.05    | 69.86    | 100        |          |          |          |              |       |       |       |       |       |      |
| CP-20-23           | 32.29    | 26.27    | 29.9       | 100      |          |          |              |       |       |       |       |       |      |
| CP-20-19           | 33.76    | 26.75    | 30.14      | 87.07    | 100      |          |              |       |       |       |       |       |      |
| CP-20-13           | 33.76    | 26.75    | 30.14      | 87.07    | 100      | 100      |              |       |       |       |       |       |      |
| FCoV (Black)       | 32.29    | 25.54    | 28.23      | 86.56    | 87.76    | 87.76    | 100          |       |       |       |       |       |      |
| CCoV               | 29.91    | 33.41    | 29.81      | 45.27    | 45.96    | 45.96    | 44.06        | 100   |       |       |       |       |      |
| FCoV               | 29.17    | 33.41    | 29.81      | 46.3     | 45.96    | 45.96    | 44.75        | 96.94 | 100   |       |       |       |      |
| PRCoV              | 30.34    | 34.14    | 30.53      | 45.61    | 46.64    | 46.64    | 44.92        | 88.1  | 88.78 | 100   |       |       |      |
| TGEV               | 31.01    | 34.14    | 31.49      | 45.96    | 46.81    | 46.81    | 45.09        | 91.67 | 91.67 | 94.9  | 100   |       |      |
| 229E               | 32.02    | 31.52    | 28.47      | 45.17    | 44.05    | 44.05    | 42.19        | 45.54 | 44.98 | 45.54 | 44.98 | 100   |      |
| NL63               | 33.27    | 31.02    | 31.03      | 52.41    | 51.48    | 51.48    | 50           | 49.91 | 49.17 | 48.8  | 48.61 | 57.55 | 100  |

**Figure A.13:** RBD Coronavirus Screen of East Tennessee Felines.

(A) Fecal samples from healthy cats were collected and screened for S1/RBD coronavirus sequences. Phylogenetic tree consisting of common human and animal coronaviruses: CRCoV (canine respiratory coronavirus), BCoV (bovine coronavirus), OC43 (human beta-coronavirus), MHV (murine hepatitis virus), MERS-CoV (Middle East respiratory coronavirus), SARS-CoV-2 (severe acute respiratory coronavirus-2), SARS-CoV (severe acute respiratory coronavirus), AvianCoV (duck coronavirus), NL63 (human alpha-coronavirus), 229E (human alpha-coronavirus), TGEV (transmissible gastroenteritis virus), PRCoV (porcine respiratory coronavirus), FCoV (feline coronavirus strains UU19, Felix, RM, Black, UU8), CCoV (canine coronavirus), HKU15 (porcine delta-coronavirus), as well as locally identified coronaviruses (CP-20-13, CP-20-19, CP-20-23). Sequences from the S1 region were aligned and trimmed. Maximum-Likelihood phylogenetic trees were generated with bootstrap analysis in MEGA X. Bootstrap values for each branch are shown with lengths to scale. (B) Percent similarity matrix of select coronaviruses. Aligned and truncated RBD regions from the shown coronaviruses were analyzed *via* Clustal Omega to determine percent identity matrix.

levels post-pandemic were significantly lower than shown here (~12% Central China vs >50% USA) (Fig A.2 A) [38, 58]. OD<sub>450</sub> and titers of pre-pandemic seropositive cat samples, while high, were lower than SARS-CoV-2 experimentally inoculated cats (6 weeks post infection) (Fig A.2 A, C, E, G). This likely represents a natural decline in titer over time for the environmental samples but could also represent lower titers of cross-reactive antibodies from another coronavirus.

Unfortunately, dog serum was shown to bind to a co-purified protein (Fig A.3 B), leaving us unable to utilize our assay for examining cross-species transmission of SARS-like coronaviruses to canines. We can show that recombinant RBDs produced and purified by groups at both Mt. Sinai and Emory contain co-purified proteins at approximately the same size as shown in Fig 1.7A [30, 33]. As such, screens for SARS-CoV-2 exposure in canines would likely require producing and purifying the RBD using a different strategy that eliminates non-RBD protein contamination. Recently both SARS-CoV-2's RBD and soluble full-length spike have been produced and purified in plants [65]. This alternative method may prove useful for animal SARS-CoV-2 screening by reducing or eliminating false positives due to co-purified proteins.

After the discovery of pre-pandemic seropositive cats, we examined other commercial (cow) and convenience samples from local wild species (deer, elk, tiger) (Fig A.4 A). Two out of twenty-two (9%) white-tailed deer from South Carolina were positive for antibodies against the RBD (Fig A.4 B). Unlike our cat samples, the two seropositive deer could represent transmission of SARS-CoV-2 into the local deer population because these samples were collected post-pandemic. Interestingly, a recent report showed that ~40% of white-tailed deer from 4 states (Illinois, Michigan, New York, and Pennsylvania) were positive for SARS-CoV-2 antibodies [29]. Seropositive animals were only observed from 2019 onward, with pre-pandemic deer testing negative on their SARS-CoV-2 neutralization assay. This information supports our finding in South Carolina deer (Fig A.4). SARS-CoV-2 sequences were also recently isolated from the retropharyngeal lymph nodes of wild and captive deer [27, 28]. The dominant genotype of deer-isolated SARS-CoV-2 genotypes closely corresponded to those circulating within humans at the time, pointing to potential rapid transmission from humans to animals [28]. This highlights the

importance of the One Health Initiative to provide information on the potential exposure and spillover into other species and whether there is recombination with native coronaviruses occurring to generate new variants or establishment of new reservoirs in North America. Further work is needed to determine the prevalence, spread, and identity of SARS and other coronaviruses circulating within North American deer and associated species.

That samples from cats experimentally infected with SARS-CoV-2 displayed potent neutralization (Fig A.5 B) is unsurprising because of their high ELISA titers (Fig A.2 C). These samples were collected at ~8 weeks post infection and likely represent peak titer and neutralization capacity [14]. Neutralization of SARS-CoV-2 S1 subunit was variable for environmental feline ELISA-positive samples (Fig A.5 B). There was no significant difference in MFI/neutralization between the anti-RBD seropositive and seronegative feline samples (Fig A.5 B). Even sera from convalescent, COVID-recovered individuals showed none to minimal neutralization (Fig A.5 B). Several groups have found that not all anti-RBD responses generate neutralizing antibodies [50-53, 66]. Indeed, even in convalescent serum, high levels of RBD recognition does not guarantee high neutralizing titers, consistent with our own observations (Fig A.5 B) [50]. Based on ELISA and neutralization results (Fig A.2 A, Fig A.5 B), we suspect that these animals contain antibodies recognizing SARS-CoV-2's RBD, but likely bind to non-neutralizing epitopes of the RBD domain.

Because ~50% of cats surveyed were seropositive, we reasoned that isolation of the suspected infectious agent or coronavirus might be possible. Based on fecal viral RNA shedding following animal coronavirus infections, PCR amplification with universal coronavirus primers was used to screen for potential causative agents of anti-RBD seropositivity. This allowed for non-invasive testing and isolation of coronavirus RNA from infected cats. In line with previous studies on other wild animals, we did not identify any non-alphacoronaviruses circulating in felines [67-70]. The coronavirus sequences that were isolated and sequenced likely represent normal circulating FCoV (Fig A.6). Due to the opportunistic nature of our sampling, we were unable to obtain any paired blood and fecal samples from the same animal. As such, we are unable to conclude whether the cats

with identified FCoV strains would produce cross-reactive antibodies against SARS-CoV-2's RBD. However, based on our ELISA results in Fig. A.1 A and A.2 A showing no correlation with SARS RBD antibodies and FCoV infection, we would suspect not. Furthermore, not knowing when the seropositive cats were exposed (i.e., cats could have been infected potentially years prior to any fecal sampling) fecal sampling and sequencing would not detect a novel coronavirus if it had been cleared. Following the identification of coronavirus positive fecal samples, we attempted to amplify and sequence the entire RBD region from positive samples to look for similarity to SARS-CoV-2 or SARS-like viruses. Large portions of the S1 region spanning the RBD were sequenced and contained RBD regions similar to previously isolated FCoV strains (Fig. A.7), with no similarity to SARS or betacoronaviruses.

The current study demonstrates cross-reactivity of pre-pandemic feline samples with the RBD of SARS-CoV-2. Our indirect ELISA screen has provided evidence for seropositivity of serum from North American cats and deer to a SARS-CoV-2 protein previously shown to be highly specific to SARS coronaviruses [32, 38, 46, 49]. This is the first study to demonstrate seropositivity of animal samples pre-pandemic. What induces this cross-reactive response was not readily apparent. However, we propose several possibilities: exposure to another infectious agent generating cross-reactive antibodies, infection with multiple common coronavirus strains (Feline coronavirus or otherwise) generating cross-reactive antibodies, or exposure of animals to a SARS-like coronavirus pre-pandemic.

There is evidence both for and against these explanations for the seropositivity observed. While we cannot discount a non-coronavirus infection generating cross-reactive antibodies, the RBD of SARS-like viruses is thought to be unique with no previous evidence of RBD cross-reactivity [32, 38, 46, 49]. A plausible explanation for seropositivity against SARS-CoV-2's RBD is infections with coronaviruses generating an atypical response. To-date, cross-reactivity against the RBD of SARS-CoV-2 has only been reported for SARS and SARS-like coronaviruses [32, 46]. The common human and animal coronaviruses (both alpha and beta coronavirus families) individually do not generate cross-reactive antibodies against this protein, presumably making it a SARS-specific

response [30, 32, 33, 38, 46, 49]. For example, prior FCoV exposure did not impact SARS-CoV-2 RBD recognition [38]. Our own observations further demonstrated that FCoV (both serotype I and II) and TGEV did not correlate with serostatus for SARS-CoV-2's RBD (Fig 2A) (FCoV+, FCoV-). Additionally, humans and animals are exposed to multiple coronaviruses throughout their lifetime, generating measurable immune responses to antigenic proteins [71, 72]. With humans, CoV infections occur on average once a year, with protective immunity appearing to wane a few months after initial exposure [71, 72]. Despite reports of cross-reactivity towards portions of SARS-CoV-2's spike protein induced by other human coronaviruses, there have been no reports of cross-reaction against the distinct RBD region [32, 46, 49]. While it does not disprove multiple CoV infections generating cross reactive antibodies, it does cast doubt on this possibility. This leads us to propose prior exposure to a SARS-like coronavirus for North American cats.

There is limited evidence to support prior transmission of a SARS-like virus within felines. However, cats are susceptible to infection and transmission of SARS-CoV-2 [14]. SARS coronaviruses evolved from bat coronaviruses and maintain a high degree of sequence similarity, even in the RBD region [32]. Conceivably, our definition of SARS-like coronavirus could also encompass bat coronaviruses due to amino acid similarity and potential cross-reactivity in the RBD region. At least within Tennessee there are numerous cave systems with several native species of bats potentially leading to an inter-species transmission. Feline and bat interactions could lead to direct transfer of a SARS-like agent, or an intermediary species could be involved. North American deer mice were recently shown to be susceptible to human SARS-CoV-2 and capable of mouse-to-mouse transmission representing another potential point of introduction into the feline population [73]. The pre-pandemic exposure of cats to a SARS-like agent does have detractors. Other groups examining pre-pandemic samples have failed to find evidence of RBD-reactive serum even within Central China [38, 56, 58]. The ELISA-positive samples from our environmental samples (i.e., feline and deer) did not neutralize to the same degree as experimentally inoculated felines (Fig A.5 B) [14]. However, significant neutralization was not observed for most samples, even convalescent serum from COVID-positive individuals (Fig A.5 B). Despite ~50% seroprevalence in our samples, we were unable to identify any

coronavirus sequences capable of eliciting an anti-SARS RBD response (Fig A.6 and A.7). Additionally, there is currently no evidence of a circulating SARS-like or bat betacoronavirus in North America [67-70]. While we cannot conclusively demonstrate the origin of the anti-RBD responses shown here, this study indicates that there could be a virus (or another infectious agent) that can generate cross reactive antibodies to the SARS-CoV-2 RBD.

### **Limitations of this study**

A major limitation of this study is the number of serum samples surveyed for all species. Due to the small sample size, we have refrained from making extrapolations from our data to larger animal populations or geographic regions. Similarly, a relatively small number of feline fecal samples were screened for coronavirus viral RNA (n=30), limiting our ability to detect coronaviruses. Our choice of sampling source may have also limited our ability to detect novel coronaviruses or SARS-like coronaviruses. We chose to utilize fecal samples for coronavirus screening because it is non-invasive, animal coronavirus shedding within feces is common, and many are transmitted fecal to oral. Additionally, SARS-CoV and SARS-CoV-2 viral RNA has been detected in stool samples of infected humans [8, 9, 11, 13]. This fecally shed RNA persists longer than nasal or oral sources [13]. However, sampling nasal/oral sources rather than fecal samples may allow for better detection of SARS-CoV-2. Indeed, isolation of SARS-CoV-2 RNA and whole genome sequencing was possible from deer retropharyngeal lymph nodes [28]. Along with sampling site limitations, infection and shedding of viral RNA is a transient process with a relatively small window to detect and sequence the causative agent. While ~20 feline samples were tested for anti-FCoV antibodies, the majority of our samples were of an unknown FCoV status. Additionally, medical histories were not available for these animals and were not screened for prior exposure to other infectious agents. As such, we cannot definitively rule out some other infectious agent conferring the anti-RBD responses.

### **Conclusion**

Our initial goal was to develop an ELISA assay for tracking the reverse zoonosis of SARS-CoV-2. However, when establishing our baseline on pre-pandemic cat samples

we discovered seropositive serum for an antigen previously reported to be SARS-specific (i.e., RBD). Seropositivity was ~50% in feline samples and could be found several years prior to the genesis of the current SARS-CoV-2 pandemic. What generated the RBD-reactive antibodies is unknown, but we proposed three possibilities: cross-reaction caused by another infectious agent, multiple coronavirus infections creating a rare cross-reactive antibody, or existence and circulation of a SARS-related virus containing the RBD sequence. Regardless, the high rate of SARS-CoV-2 RBD seropositivity within a common companion animal further highlights our need for a better understanding of the prevalence and crossover potential of wild coronaviruses. Further investigations should address shedding of viral RNA from the seropositive species (i.e., cats and deer) identified here to isolate, sequence, and identify the agent enabling cross-reactivity against the RBD of SARS-CoV-2.

### ***Acknowledgments***

We would like to thank the following for their generous contributions making this work possible:

MEDIC Regional Blood Center

Mark Slifka – Oregon Health Sciences University

Jon Wall and Steve Foster – University of Tennessee Medical Center Knoxville

Krammer Lab – Icahn School of Medicine at Mount Sinai

Wrammert Lab – Emory University

Angela Bosco-Lauth – Colorado State University

Jennifer Weisent, Rebekah DeBolt, Sarah Englebert, Jessica Thompson – University of Tennessee College of Veterinary Medicine Shelter Medicine Service

## References

1. Poon, L.L.M. and M. Peiris, *Emergence of a novel human coronavirus threatening human health*. Nat Med, 2020. **26**(3): p. 317-319.
2. Guan, W.J., et al., *Clinical Characteristics of Coronavirus Disease 2019 in China*. N Engl J Med, 2020. **382**(18): p. 1708-1720.
3. Latinne, A., et al., *Origin and cross-species transmission of bat coronaviruses in China*. Nat Commun, 2020. **11**(1): p. 4235.
4. Li, X., et al., *Emergence of SARS-CoV-2 through recombination and strong purifying selection*. Sci Adv, 2020. **6**(27).
5. Andersen, K.G., et al., *The proximal origin of SARS-CoV-2*. Nat Med, 2020. **26**(4): p. 450-452.
6. Sun, J., et al., *Prolonged Persistence of SARS-CoV-2 RNA in Body Fluids*. Emerg Infect Dis, 2020. **26**(8): p. 1834-1838.
7. Meyerowitz, E.A., et al., *Transmission of SARS-CoV-2: A Review of Viral, Host, and Environmental Factors*. Ann Intern Med, 2021. **174**(1): p. 69-79.
8. Wang, W., et al., *Detection of SARS-CoV-2 in Different Types of Clinical Specimens*. JAMA, 2020. **323**(18): p. 1843-1844.
9. Kim, J.M., et al., *Detection and Isolation of SARS-CoV-2 in Serum, Urine, and Stool Specimens of COVID-19 Patients from the Republic of Korea*. Osong Public Health Res Perspect, 2020. **11**(3): p. 112-117.
10. Kang, M., et al., *Probable Evidence of Fecal Aerosol Transmission of SARS-CoV-2 in a High-Rise Building*. Ann Intern Med, 2020. **173**(12): p. 974-980.
11. Xiao, F., et al., *Infectious SARS-CoV-2 in Feces of Patient with Severe COVID-19*. Emerg Infect Dis, 2020. **26**(8): p. 1920-1922.
12. Yu, I.T., et al., *Evidence of airborne transmission of the severe acute respiratory syndrome virus*. N Engl J Med, 2004. **350**(17): p. 1731-9.
13. Roltgen, K., et al., *Defining the features and duration of antibody responses to SARS-CoV-2 infection associated with disease severity and outcome*. Sci Immunol, 2020. **5**(54).

14. Bosco-Lauth, A.M., et al., *Experimental infection of domestic dogs and cats with SARS-CoV-2: Pathogenesis, transmission, and response to reexposure in cats*. Proc Natl Acad Sci U S A, 2020. **117**(42): p. 26382-26388.
15. Shi, J., et al., *Susceptibility of ferrets, cats, dogs, and other domesticated animals to SARS-coronavirus 2*. Science, 2020. **368**(6494): p. 1016-1020.
16. Wu, L., et al., *Broad host range of SARS-CoV-2 and the molecular basis for SARS-CoV-2 binding to cat ACE2*. Cell Discov, 2020. **6**: p. 68.
17. Segales, J., et al., *Detection of SARS-CoV-2 in a cat owned by a COVID-19-affected patient in Spain*. Proc Natl Acad Sci U S A, 2020. **117**(40): p. 24790-24793.
18. Fritz, M., et al., *High prevalence of SARS-CoV-2 antibodies in pets from COVID-19+ households*. One Health, 2021. **11**: p. 100192.
19. Sit, T.H.C., et al., *Infection of dogs with SARS-CoV-2*. Nature, 2020. **586**(7831): p. 776-778.
20. Patterson, E.I., et al., *Evidence of exposure to SARS-CoV-2 in cats and dogs from households in Italy*. Nat Commun, 2020. **11**(1): p. 6231.
21. Barrs, V.R., et al., *SARS-CoV-2 in Quarantined Domestic Cats from COVID-19 Households or Close Contacts, Hong Kong, China*. Emerg Infect Dis, 2020. **26**(12): p. 3071-3074.
22. Halfmann, P.J., et al., *Transmission of SARS-CoV-2 in Domestic Cats*. N Engl J Med, 2020. **383**(6): p. 592-594.
23. Oude Munnink, B.B., et al., *Transmission of SARS-CoV-2 on mink farms between humans and mink and back to humans*. Science, 2021. **371**(6525): p. 172-177.
24. Martina, B.E., et al., *Virology: SARS virus infection of cats and ferrets*. Nature, 2003. **425**(6961): p. 915.
25. Ng, S.K., *Possible role of an animal vector in the SARS outbreak at Amoy Gardens*. Lancet, 2003. **362**(9383): p. 570-2.
26. Lun, Z.R. and L.H. Qu, *Animal-to-human SARS-associated coronavirus transmission?* Emerg Infect Dis, 2004. **10**(5): p. 959.

27. Hale, V.L., et al., *SARS-CoV-2 infection in free-ranging white-tailed deer*. Nature, 2021.
28. Kuchipudi, S.V., et al., *Multiple spillovers from humans and onward transmission of SARS-CoV-2 in white-tailed deer*. Proc Natl Acad Sci U S A, 2022. **119**(6).
29. Chandler, J.C., et al., *SARS-CoV-2 exposure in wild white-tailed deer (*Odocoileus virginianus*)*. Proc Natl Acad Sci U S A, 2021. **118**(47).
30. Amanat, F., et al., *A serological assay to detect SARS-CoV-2 seroconversion in humans*. Nat Med, 2020. **26**(7): p. 1033-1036.
31. Long, Q.X., et al., *Antibody responses to SARS-CoV-2 in patients with COVID-19*. Nat Med, 2020. **26**(6): p. 845-848.
32. Premkumar, L., et al., *The receptor binding domain of the viral spike protein is an immunodominant and highly specific target of antibodies in SARS-CoV-2 patients*. Sci Immunol, 2020. **5**(48).
33. Suthar, M.S., et al., *Rapid Generation of Neutralizing Antibody Responses in COVID-19 Patients*. Cell Rep Med, 2020. **1**(3): p. 100040.
34. Desmarests, L.M., et al., *Experimental feline enteric coronavirus infection reveals an aberrant infection pattern and shedding of mutants with impaired infectivity in enterocyte cultures*. Sci Rep, 2016. **6**: p. 20022.
35. Vogel, L., et al., *Pathogenic characteristics of persistent feline enteric coronavirus infection in cats*. Vet Res, 2010. **41**(5): p. 71.
36. Cevik, M., et al., *SARS-CoV-2, SARS-CoV, and MERS-CoV viral load dynamics, duration of viral shedding, and infectiousness: a systematic review and meta-analysis*. The Lancet Microbe.
37. Addie, D.D. and O. Jarrett, *Use of a reverse-transcriptase polymerase chain reaction for monitoring the shedding of feline coronavirus by healthy cats*. Vet Rec, 2001. **148**(21): p. 649-53.
38. Zhang, Q., et al., *A serological survey of SARS-CoV-2 in cat in Wuhan*. Emerg Microbes Infect, 2020. **9**(1): p. 2013-2019.

39. Liu, W., et al., *Two-year prospective study of the humoral immune response of patients with severe acute respiratory syndrome*. J Infect Dis, 2006. **193**(6): p. 792-5.
40. Cao, W.C., et al., *Disappearance of antibodies to SARS-associated coronavirus after recovery*. N Engl J Med, 2007. **357**(11): p. 1162-3.
41. Lin, Q., et al., *Duration of serum neutralizing antibodies for SARS-CoV-2: Lessons from SARS-CoV infection*. J Microbiol Immunol Infect, 2020. **53**(5): p. 821-822.
42. Tang, F., et al., *Lack of peripheral memory B cell responses in recovered patients with severe acute respiratory syndrome: a six-year follow-up study*. J Immunol, 2011. **186**(12): p. 7264-8.
43. Zeng, W., et al., *Biochemical characterization of SARS-CoV-2 nucleocapsid protein*. Biochem Biophys Res Commun, 2020. **527**(3): p. 618-623.
44. Hoffmann, M., et al., *SARS-CoV-2 Cell Entry Depends on ACE2 and TMPRSS2 and Is Blocked by a Clinically Proven Protease Inhibitor*. Cell, 2020. **181**(2): p. 271-280 e8.
45. Lan, J., et al., *Structure of the SARS-CoV-2 spike receptor-binding domain bound to the ACE2 receptor*. Nature, 2020. **581**(7807): p. 215-220.
46. Ng, K.W., et al., *Preexisting and de novo humoral immunity to SARS-CoV-2 in humans*. Science, 2020. **370**(6522): p. 1339-1343.
47. Chi, X., et al., *A neutralizing human antibody binds to the N-terminal domain of the Spike protein of SARS-CoV-2*. Science, 2020. **369**(6504): p. 650-655.
48. Song, G., et al., *Cross-reactive serum and memory B-cell responses to spike protein in SARS-CoV-2 and endemic coronavirus infection*. Nat Commun, 2021. **12**(1): p. 2938.
49. Anderson, E.M., et al., *Seasonal human coronavirus antibodies are boosted upon SARS-CoV-2 infection but not associated with protection*. Cell, 2021. **184**(7): p. 1858-1864 e10.
50. Lee, W.T., et al., *Neutralizing Antibody Responses in COVID-19 Convalescent Sera*. J Infect Dis, 2021. **223**(1): p. 47-55.

51. Rogers, T.F., et al., *Isolation of potent SARS-CoV-2 neutralizing antibodies and protection from disease in a small animal model*. *Science*, 2020. **369**(6506): p. 956-963.
52. Niu, L., et al., *A Structural Landscape of Neutralizing Antibodies Against SARS-CoV-2 Receptor Binding Domain*. *Front Immunol*, 2021. **12**: p. 647934.
53. Zhou, Y., et al., *Enhancement versus neutralization by SARS-CoV-2 antibodies from a convalescent donor associates with distinct epitopes on the RBD*. *Cell Rep*, 2021. **34**(5): p. 108699.
54. Zhu, Y., et al., *Cross-reactive neutralization of SARS-CoV-2 by serum antibodies from recovered SARS patients and immunized animals*. *Sci Adv*, 2020. **6**(45).
55. Lv, H., et al., *Cross-reactive Antibody Response between SARS-CoV-2 and SARS-CoV Infections*. *Cell Rep*, 2020. **31**(9): p. 107725.
56. Zhao, S., et al., *Serological Screening for Coronavirus Infections in Cats*. *Viruses*, 2019. **11**(8).
57. Deng, J., et al., *Serological survey of SARS-CoV-2 for experimental, domestic, companion and wild animals excludes intermediate hosts of 35 different species of animals*. *Transbound Emerg Dis*, 2020. **67**(4): p. 1745-1749.
58. Deng, J., et al., *SARS-CoV-2 Serological Survey of Cats in China before and after the Pandemic*. *Viol Sin*, 2020.
59. Stadlbauer, D., et al., *SARS-CoV-2 Seroconversion in Humans: A Detailed Protocol for a Serological Assay, Antigen Production, and Test Setup*. *Curr Protoc Microbiol*, 2020. **57**(1): p. e100.
60. Poon, L.L., et al., *Identification of a novel coronavirus in bats*. *J Virol*, 2005. **79**(4): p. 2001-9.
61. Thompson, J.D., D.G. Higgins, and T.J. Gibson, *CLUSTAL W: improving the sensitivity of progressive multiple sequence alignment through sequence weighting, position-specific gap penalties and weight matrix choice*. *Nucleic Acids Res*, 1994. **22**(22): p. 4673-80.
62. Kumar, S., et al., *MEGA X: Molecular Evolutionary Genetics Analysis across Computing Platforms*. *Mol Biol Evol*, 2018. **35**(6): p. 1547-1549.

63. Johari, Y.B., et al., *Production of trimeric SARS-CoV-2 spike protein by CHO cells for serological COVID-19 testing*. Biotechnol Bioeng, 2021. **118**(2): p. 1013-1021.
64. Palmer, M.V., et al., *Susceptibility of white-tailed deer (*Odocoileus virginianus*) to SARS-CoV-2*. J Virol, 2021.
65. Rattanapisit, K., et al., *Rapid production of SARS-CoV-2 receptor binding domain (RBD) and spike specific monoclonal antibody CR3022 in *Nicotiana benthamiana**. Sci Rep, 2020. **10**(1): p. 17698.
66. Xiaojie, S., et al., *Neutralizing antibodies targeting SARS-CoV-2 spike protein*. Stem Cell Res, 2020. **50**: p. 102125.
67. Olival, K.J., et al., *Possibility for reverse zoonotic transmission of SARS-CoV-2 to free-ranging wildlife: A case study of bats*. PLoS Pathog, 2020. **16**(9): p. e1008758.
68. Dominguez, S.R., et al., *Detection of group 1 coronaviruses in bats in North America*. Emerg Infect Dis, 2007. **13**(9): p. 1295-300.
69. Misra, V., et al., *Detection of polyoma and corona viruses in bats of Canada*. J Gen Virol, 2009. **90**(Pt 8): p. 2015-2022.
70. Osborne, C., et al., *Alphacoronaviruses in New World bats: prevalence, persistence, phylogeny, and potential for interaction with humans*. PLoS One, 2011. **6**(5): p. e19156.
71. Macnaughton, M.R., *Occurrence and frequency of coronavirus infections in humans as determined by enzyme-linked immunosorbent assay*. Infect Immun, 1982. **38**(2): p. 419-23.
72. Schmidt, O.W., et al., *Rises in titers of antibody to human coronaviruses OC43 and 229E in Seattle families during 1975-1979*. Am J Epidemiol, 1986. **123**(5): p. 862-8.
73. Griffin, B.D., et al., *SARS-CoV-2 infection and transmission in the North American deer mouse*. Nat Commun, 2021. **12**(1): p. 3612.

## VITA

Trevor J. Hancock was born in Escondido, CA to Kenneth and Julia Hancock. An ex-plant, he attended high school in Murfreesboro, TN where he graduated valedictorian. He later attended the University of Tennessee at Martin where he participated in varsity cross country and graduated *summa cum laude* with a B.S. in Biology in 2013. In the spring of 2016, he graduated from Lipscomb University in Nashville, TN, earning a M.S. in Biomolecular Science. He began his Ph.D. studies in the Fall of 2017 at the University of Tennessee Knoxville in the laboratory of Tim Sparer studying cytomegalovirus pathogenesis and viral entry. In the Spring of 2022, he graduated from the University of Tennessee with a Doctor of Philosophy in Microbiology.